Optimisation of Collagen Films Produced via Pulsed Current Electrophoretic Deposition

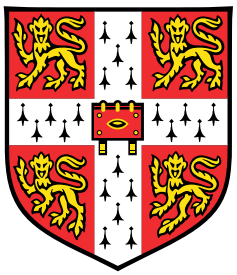

Matthew David Linley

Supervisor: **Prof. R.E. Cameron**

Prof. S.M. Best

Department of Materials Science and Metallurgy

University of Cambridge

This thesis is submitted for the degree of

Doctor of Philosophy

St John's College

November 2020

Declaration

I hereby declare that except where specific reference is made to the work of others, the contents of this report are original and have not been submitted in whole or in part for consideration for any other degree or qualification in this, or any other university. This report is my own work and contains nothing which is the outcome of work done in collaboration with others, except as specified in the text. This report contains fewer than 60,000 words including appendices, headers, figure captions, footnotes, tables, and equations, and has fewer than 150 figures.

Matthew David Linley

November 2020

Acknowledgements

First and foremost, I would like to thank my supervisors Ruth Cameron and Serena Best for their unwavering support, expertise and guidance throughout this PhD. I am grateful for their confidence in me and allowing me to find my own direction in this research. Not only have they been extremely insightful, but they have also been very supportive, particularly during difficult times.

I acknowledge the funding I have received to support this work. My project was primarily funded by a studentship from the Engineering and Physical Sciences Research Council (EPSRC), with additional funding from Geistlich Pharma AG. I am thankful for Terry Hart and everyone that I met at Geistlich for their support and giving me the opportunity to present my research at their HQ in Switzerland.

I would like to thank everyone that provided technical support throughout my PhD within the Department of Materials Science and Metallurgy. In particular, I am thankful for Dr David Barrett and Wayne Skelton-Hough for their assistance in the lab. I would also like to thank everyone in CCMM during my time there, particularly for the enjoyable tea breaks. I am extremely grateful to have made such good friends in Sheen Gurrib, Rob Murphy, and Jamie Cyr, who have made this experience infinitely more enjoyable — we have been through it all together and we made it to the other side.

My PhD at Cambridge would not have been complete without the friends and memories I gained at St John's College. I am grateful to all the staff and fellows within the college for all their hard work and support, which enriched my Cambridge experience in an unforgettable

way. The Samuel Butler Room provided a welcome retreat from my studies, while also allowing me to learn from incredible academics in other subjects. The friends I have made here are too numerous to mention, but I would particularly like to thank Phil, Pat, Jessica, Ben, and Anna (plus Danny), for all the good times.

I would like to thank my parents, Christine and David; they have been unconditionally supportive of me throughout my life, and I would not have got this far without them. Lastly, I would like to thank my wife, Gabriela, without whom none of this would be possible. She saw the potential in me and has made me the best version of myself. She has supported me both academically and emotionally, and together we make a great team. I am also grateful for her family, Salvador, Tatei, and Marcelo, for everything that they have given me throughout this time.

Abstract

Optimisation of Collagen Films Produced via Pulsed Current Electrophoretic Deposition

Matthew David Linley

Electrophoretic deposition (EPD) has been used for the deposition of insoluble collagen type I in aqueous suspensions. In this process, two electrodes are immersed in an aqueous collagen suspension and a voltage is applied. The charged particles in the suspension move towards the oppositely-charged electrode resulting in the deposition of a coating, which can be removed to create a free-standing collagen film. The aim of this project was to maximise processing efficiency and yield, and improve material properties of the collagen films produced using EPD.

The behaviour of collagen I from two different suppliers was compared when processed using pulsed current electrophoretic deposition (PC-EPD). It was found that, at voltages required for adequate yield (at least 5 V), formation of bubbles or corrosion of the electrode occurred for suspensions in aqueous media. However, dialysis of collagen suspensions against deionised water for 30 hours was shown to remove residual charge-carrying ions, notably Na^+, K^+, Cl^- and Ca^{2+}, arising from the collagen extraction process. This allowed deposition to be carried out at higher voltages (up to 10 V), leading to higher yield and the production of consistent films, avoiding the processing problems.

PC-EPD was mathematically modelled, in order to broaden understanding of the process and aid in future investigations. A pulsed current factor was developed and introduced to previously-described direct current EPD models, derived from the Hamaker equation. To validate this, collagen suspensions were characterised, and measured variables were implemented within the model. The model was compared with experimental data and was found to be accurate at applied potentials of 10 V and above. Deviations between the model and experimental values for voltages of 5 V or less were explained by factors within the pulse cycle that were not accounted for, such as molecule acceleration time.

Collagen deposits, once dried, adhered strongly to the electrode and made removal from the substrate challenging. To solve this problem, a sacrificial cellulose acetate layer was developed to assist detachment of collagen deposits from the substrate, giving free-standing films. It was also shown that more complex collagen films could be created by depositing onto shaped electrodes, and that these could also be removed successfully using a cellulose sacrificial layer. Analysis of grooved films showed that features from the substrate

were reproduced successfully onto the collagen deposits, with a resolution of 10 µm for topographical surface features, however, the larger grooved features measured approximately 100 µm (±50 µm) greater than the substrate due to the film thickness.

The density of collagen biomaterials can influence their stability and degradation properties. The densities of cast films and EPD films were compared, and deposited films were found to be at least 15% more dense. Furthermore, it was found that the density of EPD collagen films could be controlled by changing the deposition voltage, with a densities ranging from 400 $kg\,m^{-3}$ at 5 V to 700 $kg\,m^{-3}$ at 10 V. Films with a higher density were shown to have increased enzymatic degradation resistance, potentially reducing the need for chemical cross-linkers to stabilise these collagen devices, giving potential benefits for bioactivity.

Surgical application of membranes often requires the use of suturing and, therefore, the biomaterials are required to be tear-resistant. It was hypothesised that alignment of collagen fibres within the membranes would increase their ultimate tensile strength (UTS). Through optimisation of the EPD rig and processing parameters, alignment of collagen was induced during deposition by generating interfacial shear between the substrate and suspension. This was achieved using two different EPD setups, and the collagen alignment created was assessed using birefringence measurements. It was found that successful alignment was achieved (with corresponding birefringence values of 0.0025) using (1) a rotating cylindrical electrode with a tangential velocity of 0.0006 $m\,s^{-1}$ at 10 V PC-EPD, and (2) volumetric flow rate of suspension pumped through the EPD cell of 1.67 $mL\,s^{-1}$ at 40 V direct current EPD. This alignment was found to increase the UTS of cross-linked collagen films in the direction of alignment to 6.26 MPa, compared to 3.5 MPa in non-aligned films. Multilayer, cross-ply films were then produced by changing the film orientation between deposition steps. The development of the multi-orientated cross-ply collagen films could result in membranes with increased tear resistance.

This thesis has developed the capabilities of EPD processing for collagen films, providing tunability of material properties and forms, and allowing for the design of collagen membranes for a range of medical applications.

Table of contents

List of figures

List of tables

Nomenclature

Roman Symbols

C_0	initial suspension concentration (g cm^{-1})
C_s	suspension concentration (g cm^{-3})
D	diffusivity
d	distance between electrodes (cm)
E	electric field (V cm^{-1})
f	efficiency parameter
I	applied current intensity (A)
i	applied current density (A cm^{-2})
k_B	Boltzmann's constant
L_D	diffusion length
L_e	electrophoretic movement length
m	deposited mass (g)
M_0	initial solid mass in suspension (g)

R resistance (Ω)

S deposition area (cm^2)

T temperature (K)

t deposition time (s)

V voltage (V)

v volume of suspension (cm^3)

V_{eph} electrophoretic particle velocity

V_{eph} steady-state velocity of particles under an electric field

Greek Symbols

δ duty cycle

ε_0 dielectric permittivity of a vacuum

ε_1 dielectric permittivity of solvent 1

ε_2 dielectric permittivity of solvent 2

ε_3 dielectric permittivity of solvent 3

ε_m dielectric permittivity of the suspension media

η viscosity

κ pulsed current parameter

μ electrophoretic mobility ($cm^2s^{-1}V^{-1}$)

ϕ_1 volume fraction of solvent 1

ϕ_2 volume fraction of solvent 2

ϕ_3 volume fraction of solvent 3

Ψ_0 particle surface potential

Ψ_ζ potential at the surface of shear

ρ suspension resistivity (Ω cm)

ρ_0 initial resistivity of the suspension (Ω)

ρ_∞ resistivity of the suspension at infinite time (Ω)

σ suspension conductivity (S m^{-1})

τ characteristic time scale

τ_0 characteristic time scale at initial time

τ_∞ characteristic time scale at infinite time

ζ zeta potential

Acronyms / Abbreviations

AAC asymmetric alternating current

AAC-EPD asymmetric alternating current electrophoretic deposition

AC alternating current

DC direct current

dH_2O deionised water

ECM extracellular matrix

EDX energy-dispersive X-ray spectroscopy

EPD electrophoretic deposition

FTIR Fourier transform infrared

HA hydroxyapatite

PC pulsed current

PC-EPD pulsed current electrophoretic deposition

RPM revolutions per minute

SEM scanning electron microscopy

SMU source meter unit

USB universal serial bus

VDW Van der Waals

Chapter 1

Background

1.1 Introduction

Maxillofacial bone ridge augmentation surgery is needed to restore the healthy bone in the jaw, before a dental implant can be secured. Bone ridge augmentation incorporates guided bone regeneration (GBR), often through a graft [1], including autografts [2], allografts [3], and xenografts [4], but synthetic scaffolds have also been reported [5]. These grafts are held within the defect by a membrane that is sutured in place; the membrane also acts as a barrier, preventing undesired tissue migration or re-epethilialisation into the site of damaged bone. To be fit for purpose, the membrane needs to be structurally stable, and both biocompatible and occlusive to cells [6, 7]. These membranes have been made from both non-resorbable [2] and bioresorbable [4] materials. Non-resorbable membranes have been used for many years, with materials such as polytetrafluoroethylene (PTFE) possessing suitable properties for GBR [8–10]. Nowadays however, more commonly, bioresorbable membranes are desired, as there is no need for a second surgery to remove the membrane, as they can be degraded naturally within the patient [11].

Synthetic resorbable membranes have been formed from polylactic acid (PLA) and polyglycolic acid (PGA), as well as co-polymers of both (PLGA) [11]. These polymers are

naturally broken down within the body into lactic acid and glycolic acid through hydrolysis, which are then broken down into water and carbon dioxide within the liver [7]. While these membranes have shown efficacy in decreasing bone resorption [12], they have also been associated with fibrous encapsulation and local inflammation during degradation due to their acidic by-products [13].

Collagen type I has attracted interest as a biomaterial because, being a natural structural protein, it is biocompatible, bioactive, and bioresorbable [14–17]. Furthermore, as collagen I is the most abundant protein within mammals it is readily available and relatively inexpensive to extract and process [18]. Collagen has been used in a number of guided bone regeneration applications, including as a barrier membrane in bone ridge augmentation surgery [4]. Commercial collagen membranes have been formed from tendon and dermis sources from bovine, porcine and equine animals, however, these membranes can only be formed in limited sizes and forms, and offer little option for tunability, other than the amount of cross-linking [19]. Larger membranes can be formed by solvent casting collagen, however, these films are again limited in their material properties, with few processing options to improve these further [20].

Electrophoretic deposition (EPD) has presented itself as an advantageous processing technique for developing collagen films. EPD involves charged particles (in this case collagen) held within a suspension, and an electric field being passed across the suspension. The electric field drives electrophoretic movement of the charged particles towards an electrode, onto which the particles deposit, forming a film [21]. EPD is an extremely popular processing technique, due to the ability control both the suspension parameters and the process parameters, offering control over the final deposited product [22]. Furthermore, EPD does not require expensive or complex equipment and therefore represents a low cost solution [23].

It is, therefore, proposed that electrophoretic deposition be used as a processing technique to produce very controlled and reproducible collagen films quickly and inexpensively. Previous research has shown that large collagen films can be produced using EPD [24, 25], however tuning the material properties was not explored. Due to the versatility of EPD, it is anticipated that collagen films can be designed and developed with specific material properties using this technique. The work presented here seeks to further develop collagen films, via electrophoretic deposition, as membranes suitable for use in bone ridge augmentation surgery, as well as other regenerative medicine applications. This thesis aims to optimise the collagen electrophoretic deposition process to maximise yield and film quality, and to develop novel methodologies to improve and tune the material properties of these membranes for guided bone regeneration and other clinical applications.

1.2 Thesis Overview

Within this thesis, the literature is explored in Chapter 2 to understand the current state of the research into electrophoretic deposition and collagen membranes, which highlights a number of guiding and overarching questions to be addressed. The work described in the first experimental chapter (Chapter 3) looks to standardise aqueous collagen suspensions prior to EPD and improve processing efficiency. Dialysis of collagen suspensions is explored in order to remove excess charge-carrying molecules, and the effect this has on EPD processing is investigated. The work in Chapter 4 attempts to model pulsed current EPD (PC-EPD) to better understand the process and aid in future investigations. The model is built on, and advances, previously-described direct current EPD models. The investigations in Chapter 3 and Chapter 4 aim to provide a deeper fundamental understanding of PC-EPD of collagen I, allowing for further investigations.

Depositions of collagen created using EPD adhere strongly to the electrode after drying. The work described in Chapter 5 explores the development of a sacrificial layer to assist in detaching collagen deposits to give free-standing films. In this chapter, the creation of more complex shaped collagen films is also investigated, using a sacrificial layer. The material properties of EPD collagen films are investigated and manipulated in Chapters 6 and 7. In Chapter 6, the densities of EPD collagen films are studied and compared with solvent cast collagen films. Further work in this chapter investigates the effect of film density on enzymatic degradation resistance. Lastly, in Chapter 7, aligned collagen films are investigated and methods are explored to increase their ultimate tensile strength. The work in this chapter describes methods of generating an interfacial shear between the suspension and substrate to align collagen during deposition using dynamic EPD rigs. The findings of this thesis are summarised in Chapter 8, with potential future research directions indicated upon conclusion.

Chapter 2

Literature Review

2.1 Collagen

2.1.1 Collagen in Human Tissue

Collagen is the main structural protein of the extracellular matrix (ECM) in various connective tissues and is the most abundant protein in vertebrates, making up 25-35% of whole-body protein content [18]. Collagen is found in many different types of tissue, such as skin, tendons, ligaments and blood vessels [14], and plays a dominant role in maintaining the biological and structural integrity of these tissues [26]. Collagen can also be mineralised to become more rigid in hard tissues such as bone and in teeth, and a gradient of mineralisation can be seen in cartilage [27]. The importance of collagen in numerous soft and hard tissue structures make it an excellent biomaterial scaffold.

2.1.2 The Collagen Molecule and Types of Collagen

There are many different types of collagen, creating a range of structures and serving different functions in the body tissues. However, the underpinning molecular building blocks are similar. Collagen is formed of polypeptide chains, with each chain containing the amino

acid motif: Gly-X-Y, where Gly is glycine and X or Y can be any amino acid. These polypeptide molecules are called a protocollagens, and are also known as α-chains. Each α-chain forms a consistent left-handed helix with a pitch of 0.87 nm and 3.3 residues per rotation [28]. Beyond this, three α-chains intertwine into a right-handed triple helix, with a pitch of approximately 8.6 nm, the structure of which can be visualised in Figure 2.1. This tertiary peptide structure constitutes a tropocollagen molecule, with an approximate molecular weight of 300 kDa, length of 300 nm, and diameter of 1.5 nm [15]. The are several different forms of α-chain, and the triple-helical conformations of these different chains give rise to the many different types of collagen molecule. In humans there are 29 known types of collagen [16, 27, 29], the most well characterised of which can be seen in Table 2.1, along with the corresponding tissues in which they are found.

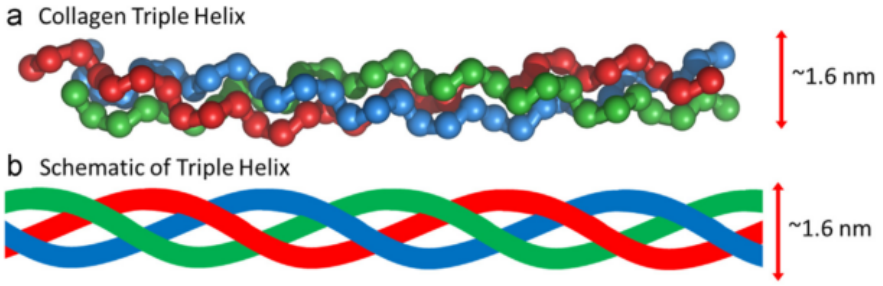

Fig. 2.1 Structure of three protocollagen chains forming a triple helical tropocollagen structure. Figure adapted from Reference [27]

The different types and composition of collagen lead to a variety of different molecular assemblies [27, 29]. These are categorised as: fibrillar collagens [31, 32], fibril associated collagens with interrupted triple helices (FACIT collagens) [33], beaded filament collagens [34], basement membrane collagens (networks) [35], short chain collagens (hexagonal networks) [34], transmembrane collagens (anchoring fibrils) [36]. The assemblies these structures are shown in Figure 2.2.

Table 2.1 Chain composition and tissue distributions of different types of collagen. Table adapted from Reference [30]

Collagen type	Chain composition	Tissue distribution
I	$(\alpha 1(I))_2\alpha 2(I)$, trimer $(\alpha 1(I))_3$	Skin, tendon, bone, cornea, dentin, fibrocartilage, large vessels, intestine, uterus, dermis, tendon
II	$(\alpha 1(II))_3$	Hyaline cartilage, vitreous, nucleus pulposus, notochord
III	$(\alpha 1(III))_3$	Large vessels, uterine wall, dermis, intestine, heart valve, gingiva
IV	$(\alpha 1(IV))_2\alpha 2(IV)$	Basement membranes
V	$\alpha 1(V)\alpha 2(V)(3(V)$ or $(\alpha 1(V))_2\alpha 2(V)$ or $(\alpha 1(V)))_3$	Cornea, placental membranes, bone, large vessels, hyaline cartilage, gingiva
VI	$\alpha 1(VI)\alpha 2(VI)\alpha 3(VI)$	Descemet's membrane, skin, nucleus pulposus, heart muscle
VII	$(\alpha 1(VII))_3$	Skin, placenta, lung, cartilage, cornea
VIII	$\alpha 1(VIII)\alpha 2(VIII)$, unknown chain organization in helix	Descemet's membrane
IX	$\alpha 1(IX)\alpha 2(IX)\alpha 3(IX)$	Cartilage
X	$(\alpha 1(X))_3$	Hypertrophic and mineralizing cartilage
XI	$\alpha 1(XI)\alpha 2(XI)\alpha 3(XI)$	Cartilage, intervertebral disc, vitreous humour

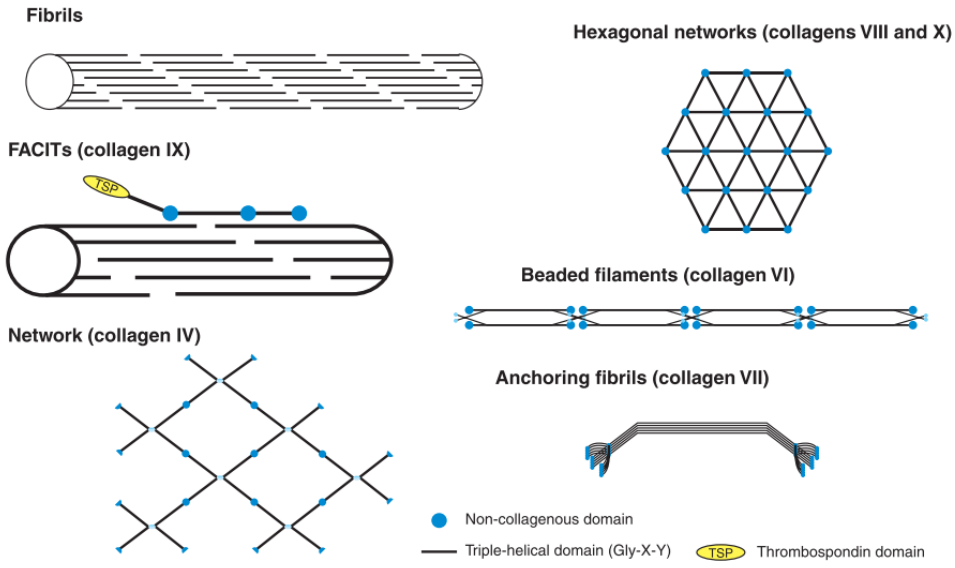

Fig. 2.2 Different assemblies of each collagen group. Figure adapted from Reference [29].

Fibrillar collagens: The most common group of collagens is the fibrillar collagens, which are highly aligned structures, normally comprising type I (which is discussed in more detail in Section 2.1.3). These highly organised and aligned collagen fibre structures have excellent mechanical strength, providing much of the structural support for many tissues. Fibrillar collagen contributes to the mechanical framework in bone, skin, cartilage, tendons, blood vessels, nerves, intestines, and fibrous encapsulation of organs [27, 37].

FACIT collagens: Fibril Associated Collagen with Interrupted Triple helices, or FACIT, collagens are named because the triple-helical domains are interrupted by non-collagenous regions. The collagens interact and associate with fibrillar collagens [33]. A hinged region allows flexibility for a terminal domain to branch out from the collagen fibril and interact with other matrix constituents [38].

Beaded filament collagens: Beaded filament collagens are only composed of collagen type VI, and comprise short triple helical regions separated by beaded filaments. These beaded regions are caused by large uncleaved N and C terminal regions on the triple helices [34].

Basement membrane collagens: Basement membrane collagens, otherwise known as network collagens, are found in the basement membrane: a fibrous matrix that lines the epithelium, mesothelium and endothelium, creating an intermediate layer to the underlying connective tissue [35]. These collagen networks form a fine mesh of triple-helical chains connected at branched junctions, with only about 20 nm between each junction. The fine network results in a relatively thin layer, approximately 40-50 nm thick, that aids with the filtration of molecules passing through it [34, 39].

Short chain collagens: Short chain collagens form hexagonal networks with short triple helical regions, about half that of fibrillar collagens. These networks act to intensify the

growth factor induced proliferation of cells, and are often found in hypertrophic regions of mineralising cartilage [34].

Transmembrane collagens: These collagens, sometimes referred to as anchoring fibrils, are found spanning cell membranes. They have several functions, namely binding, involved in both intracellular and extracellular binding, and play an important role in adhesion [35]. They can also act as matrix receptors when membrane-bound, or, when soluble, can be dissolved and serve as a signalling factor [36].

2.1.3 Collagen Type I

Collagen type I is the most abundant of all the collagen types, and is therefore also the cheapest. Furthermore, collagen I is the greatest constituent of fibrillar collagens, which form the structural support of the ECM, making it ideal for tissue engineering scaffolds. For these reasons, collagen type I is the most widely used collagen in research, and will be the collagen discussed further here.

Primary Structure

As briefly discussed, the fundamental structure of a collagen molecule consists of three polypeptide chains, each composed of approximately 1000 amino acids, arranged into a triple helix [14]. The triple helical tropocollagen molecule of type I collagen comprises three protocollagen chains: two identical α1(I) chains and one α2(I) chains with a different amino acid composition to the former [40]. The difference in chain compositions can be visualised in Table 2.2, showing the amino acid abundances in the α1(I) and α2(I) chains for type I from bovine skin. These data are fairly typical of collagen type I and there are relatively minor differences in amino acid composition between vertebrate species [41].

Table 2.2 The average amino acid compositions of type I collagen chains from bovine skin. Table adapted from reference [40]

Amino acid	α1(I)-chain	α2(I)-chain
Alanine	124	111
Arginine	53	56
Asparagine	13	23
Aspartic acid	33	24
Glutamic acid	52	46
Glutamine	27	24
Glycine	345	346
Histidine	3	8
Hydroxylysine	4	9
Hydroxyproline	114	99
Isoleucine	9	18
Leucine	22	33
Lysine	34	21
Methionine	7	4
Phenylalanine	13	15
Proline	127	108
Serine	37	35
Threonine	17	20
Tyrosine	5	4
Valine	17	34
Total	1056	1038

From Table 2.2 it can be seen that the glycine amino acid accounts for approximately one third of the total amino acids in each chain. This agrees with the Gly-X-Y structure of collagen; glycine occupies every third position within the sequence [15]. Glycine has the smallest functional group of all the amino acids and its repetition allows tight packing within the lumen of the triple-helical structure, leaving no space within the core for residues [14]. Furthermore, it can be seen that around 35% of the remaining amino acids in the non-glycine positions are occupied by either proline or hydroxyproline, predominantly found in the X and Y positions, respectively. Proline in the Y position is hydroxylated, post-translationally, by the enzyme prolylhydroxylase, into hydroxyproline [30]. A small constituent of collagen is the uncommon hydroxylysine. Derived in a similar way to hydroxyproline, lysyl hydroxylase

hydroxylates lysines within the endoplasmic reticulum. These hydroxylysines allow the attachment of sugar residues, either a single galactose or a disaccharide of galactose-glucose, to the collagen chain. These residues are a necessity for the tropocollagen to form the helical structure. Both the hydroxyproline and hydroxylysine amino acids play an important role in stabilising the triple helix structure, by forming hydrogen bonds to minimise rotation and stiffen the chains [42].

Higher Structures

It is due to collagen's complexity, compared with synthetic polymers, that it is able to form detailed and characteristic higher order structures. The third-order triple-helical tropocollagen molecules self-assemble under physiological conditions during fibrillogenesis to form fourth level of order structures (Figure 2.3, a). Type I collagen molecules align and form characteristically staggered fibrils with distinctive d-banding periodicity [43], which can be seen in Figure 2.3. The characteristic d-banding is caused by the staggered arrangement resulting in overlapping d-periods of 67 nm [27, 44]. With many tropocollagens arranged in parallel, and end-to-end, long thick fibrils can be formed. These fibrils can range from 10 to 500 nm in diameter, and several fibrils can come together to form higher order fibres [15]. It is this hierarchical order of molecules that allows collagen type I to form many tissue structures with great mechanical properties.

2.1.4 Collagen as a Biomaterial

In regenerative medicine and tissue engineering the aim is to restore functionality to tissues or organs at sites that are malformed, damaged, or diseased by means of repairing or replacing these tissues with healthy tissue [17]. The choice of scaffold material, therefore, plays a significant role in meeting these aims. To restore tissue function, biomaterial scaffolds are often designed to match the native ECM. Being the most abundant constituent of the

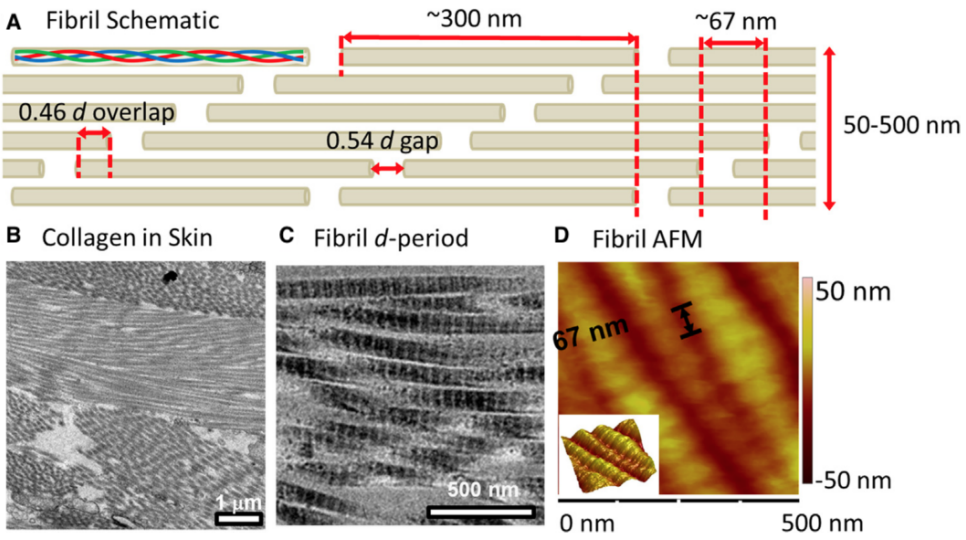

Fig. 2.3 Structural hierarchy and d-banding in fibrillar collagen. (A) staggered arrangement of tropocollagens in collagen fibril, where overlaps cause 67 nm d-periods (B) cross-section of skin showing layered collagen fibrils (C) collagen fibrils imaged with TEM (D) AFM image taken by Yang et al. 2014, showing d-banding in collagen fibrils. Figure adapted from References [27, 44].

ECM in humans, collagen type I has been proposed as an ideal candidate as an implantable biomaterial.

Isolation and Purification Processes

Before collagen can be processed for a medical purpose, it first needs to be harvested, isolated and purified. Collagen type I is often extracted from fibrous, collagen-rich tissues, such as skin and tendon [27]. It can be sourced from a variety of different species, namely bovine, porcine, and ovine [15], however additional sources have included marine species [45], human placenta [46], and recombinant human collagen from transgenic animals [47]. In the following section the different collagen extraction processes are discussed, with the forms of collagen each process is able to isolate.

Neutral salt soluble collagen: This process is effective for extracting collagens that have only recently been synthesised and are only minimally cross-linked, however most tissues

contain very little or no salt extractable collagen. These collagens are dissolved in neutral salt solutions and are then isolated using dialysis, precipitation and centrifugation [48].

Acid soluble collagen: This process is often more efficient than neutral salt extraction, using dilute acids, such as hydrochloric or acetic acid, at a pH around 2-3. Weak intermolecular cross-links between collagens are dissociated by the acid solvents [49]. Stronger cross-links found in structural tissues, such as cartilage, bone, and skin, however, are not broken, and only about 2% of collagen is extracted with this treatment, the rest is considered insoluble (see below) [42]. In order to extract this 2%, tissue is ground at low temperature and washed in saline to remove any soluble proteins or sugars, before isolating collagen with acidic solvents [49].

Alkali- and enzyme-treated collagen: A greater degree of collagen can be solubilised with alkali- and enzyme-treatment. In alkali-treatment, collagen is added to an aqueous solution of sodium hydroxide (NaOH) and sodium sulfate (Na_2SO_4) for 48 hours [50]. Any fats associated with the collagen are saponified (broken down) and the non-helical telopeptide regions at the ends of the collagen molecules are truncated, causing collagen to break up [51].

Enzymatic-treatment is effective at disintegrating collagen through selective cleavage of cross-links in the telopeptide regions, but the helical regions remain intact under the correct conditions [42]. Dilute acetic acid (0.05 M) solubilises disrupted collagen in an enzymatic aqueous solution, with a ratio of 1:10 pepsin to dry weight tissue [40]. The soluble collagen is precipitated and isolated by altering the pH, salt concentration or temperature of the solution, which can then be stored by freezing or lyophilysing it [14].

Insoluble collagen: Approximately 96–98% of extracted collagens are insoluble [52]. The majority of collagens contain cross-links that mean they will not solubilise in neutral salt or

acidic solutions. These collagens can be broken down into fine fibrils and be suspended in media to then process for biomaterial applications, but they will not be dissolved. In order to disperse fine insoluble collagen fibrils it is necessary to lower the pH, often using dilute acetic acid (0.05 M), to disrupt any intermolecular interactions, and then mechanically agitate the suspension [52]. Due to the low abundance and high processing cost of soluble collagen, insoluble collagen is often used in research and industry.

Antigenicity and Immunogenicity

Extensive use of collagen over many years has provided sufficient evidence that collagen is considered 'biocompatible'. Collagen implants often appear non-toxic, non-immunogenic, and non-antigenic. It is thought that this is attributed to the similarities in α-chain sequences between species, and the small number of aromatic amino acids present [14]. However, it has be found that both immunogenic and antigenic responses can be triggered and such reactions can depend on the source species, the host species in experiments [42] and the degree of cross-linking the collagen has undergone [53]. Extensive studies into commercial collagen implants showed that 3% of patients displayed an antibody response against the collagen, also with an increased inflammatory response [54]. Another study showed that an increased exposure to collagen injections increased the risk of an immunogenic response [55]. Despite this, collagen type I is still only mildly antigenic [56] and is regarded as a safe biomaterial for implantation [14–16].

Degradation

Degradation is an important property for medical implants as it is often desirable for the collagen scaffold to be broken down and replaced with host ECM over time [17]. However, the purpose of the scaffold needs to be considered: if it degrades too quickly it will lose its structural support and collapse before the tissue can heal, but degrading too slowly may

inhibit the host's natural production of ECM into the site. In order to tailor degradation properties, one must consider the area of implantation, collagen processing conditions, and degree of cross-linking.

The rate of degradation of collagen biomaterials is strongly dependent on the stability of the collagen scaffold, as well as the implantation site. Bonds between collagen molecules can increase the stability of the material, in particular strong covalent bonds. Native collagen type I structures have naturally occurring covalent bonds, that provide mechanical strength and degradation resistance, however, these bonds are disrupted and broken during isolation and purification processes [51]. It is possible to form strong bonds between collagen fibres within biomaterials through artificial cross-linking, which will increase the stability of the collagen, increasing resistance to degradation. Studies showed that implanted collagen films were infiltrated by fibroblasts, macrophages and neutrophils, and were broken down within 2-7 weeks when not chemically cross-linked [57–59], however cross-linked films were shown to prevent fibroblast ingrowth and the collagen remained intact [59]. Cross-linking methods are discussed further in the next section.

Cross-linking Collagen Biomaterials

Cross-linking collagen biomaterials can provide stability, to reduce the rate at which the collagen structure is broken down *in vivo*, and to increase the mechanical strength of the scaffold. Both of these properties are important considerations when developing a biomaterial scaffold, and the function and tissue type must be considered.

Chemical Cross-linking Collagen can be cross-linked using chemicals to form strong covalent bonds between molecules and improve the mechanical strength and stability of the collagen. Cross-linking agents include formaldehyde [60] glutaraldehyde [61, 62], polyepoxy compounds [63], acylazides [64], and hexamethylene diisocynate [65]. These chemical cross-linkers, however, can leave residual electrophilic reagents and compounds, which form

during degradation *in vivo*, that can be cytotoxic. Carbodiimides have also been used to successfully cross-link collagen biomaterials without associated cytotoxic by-products [66, 67]. However, while carbodiimides have been used efficaciously to strengthen and stabilise collagen structures, the process uses specific cell binding sites to bond collagen molecules together. Cross-linking with 1-ethyl-3-(3-dimethylaminopropyl)-carbodiimide hydrochloride (EDC) in the presence of N-hydroxy-succinimide (NHS) binds the glutamic acid carboxlyic acid side chain from the GFOGER motif on one collagen chain to another collagen chain (Figure 2.4). This binding motif is used for integrin-specific adhesion of cells to the collagen, and the reduction in these sites results in decreased cellular attachment, thus lowering the bioactivity of the material [68].

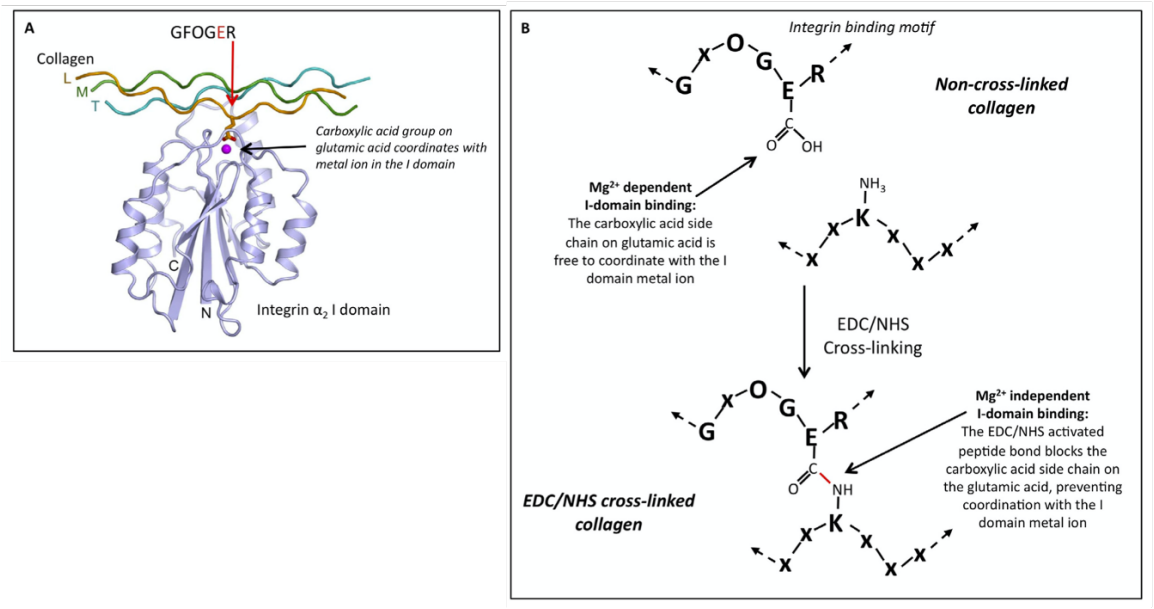

Fig. 2.4 (A) Crystal structure of the integrin α_2 I domain binding to triple-helical GFOGER collagen peptides. (B) Schematic showing the EDC/NHS mediated cross-linking of the carbolixilic acid side chain of the glutamic acid from the GFOGER motif on collagen to the amine group of lysine on an adjacent collagen chain. Figure adapted from Reference [68].

Physical Cross-linking Collagen can be physically cross-linked using ultra-violet (UV) irradiation at a wavelength of 254 nm. UV cross-linking takes just 15 minutes and can increase proteolytic resistance [69]. Dehydrothermal treatment of collagen is another cross-

linking technique, which increase the tensile strength of fibres and resistance to proteolytic degradation [70].

Enzymatic Cross-linking Transglutaminase is an enzyme that can enhance the hydrolytic resistance and tensile strength of collagen biomaterials, and does not produce any cytotoxic by-products [71]. Furthermore, transglutaminase cross-linking was found to conserve the cell binding sequences (GFOGER motif, Figure 2.4) on collagen molecules, which are used up during carbodiimide cross-linking [68], thus maintaining integrin-specific cell adhesion properties of collagen [71].

Visible light Cross-linking There are a number of cross-linking agents that will form covalent bonds between collagen molecules, and are activated by visible light sources. However, many of these have been found to be cytotoxic in the levels needed for collagen cross-linking, and are therefore unsuitable for biomaterial applications [72]. There are natural visible light cross-linkers, which are not associated with cytotoxicity, that have been used to treat keratoconus patients [73], namely riboflavin. Riboflavin in a well-characterised B vitamin that is well tolerated within the body and easily absorbed [74], and only requires a mild light source, where other photoinitiators require powerful light sources, such as lasers, halogen lamps, or UV [75]. Furthermore, studies have found that riboflavin-based cross-linking systems are significantly less cytotoxic than conventional photoinitiators [76] and that riboflavin cross-linking of collagen can lead to enhanced gene expression levels of collagen type II [77].

Biomaterial Applications of Collagen

Due to collagen's high abundance in nature, ability to self-assemble *in vitro* in relatively non-physiological environments, low toxicity, immunogenicity and antigenicity, availability of cellular attachment cites, and degradation properties it is an extremely successful bioma-

terial that has been researched extensively [78]. Here, some of the collagen structures and biomaterial applications are discussed further.

Porous Sponges Porous sponges are formed from insoluble type I collagen from animals, such as bovine, porcine and equine [26]. These are formed by lyophilising hydrated aqueous suspensions of collagen containing approximately 0.1 - 5 w/v% dry protein mass. During the freeze-drying process, ice-crystals push the suspended collagen fibres together to form the scaffold, where the ice crystals form a negative-template, which once sublimed away leave a network of interconnected pores [79]. Porous sponges have been developed over many years, and by controlling the freezing process, many of the sponge properties can be manipulated, such as porosity, interconnectivity [80], percolation diameter [81], and alignment [82] to tailor them for a variety of different tissue replacements, such as bone [83], cartilage [84], skin [85], peripheral nerves [86], cornea [87], blood vessels [88], and cardiac tissue [89].

Hydrogels Collagen hydrogels have been used extensively as injectable materials for many purposes, such as for providing subcutaneous structures and for drug delivery methods. Collagen hydrogels have been used in reconstructive surgeries, injecting collagen material subcutaneously to fill dermatological defects [90, 91]. Injectable collagen has also been used to deliver growth factors directly into sites, vastly improving tissue regeneration *in situ* [92]. Furthermore, collagen gels have been used for the slow release of drugs at the injection site. It was shown that local anaesthetic delivered with a collagen hydrogel significantly extended the effect of the drug at the site [93].

Wound Dressings Collagen materials have long been used in wound dressing applications, due to their biocompatibility and low antigenicity [94]. Wound dressings that incorporate collagen material have been shown to aid in tissue regeneration, increase the rate of epithelialisation, promote the inflammatory phase of healing, and reduce the formation of scar

tissue [95, 96]. Collagen wound dressings have also been used, alongside other materials, to reduce the risk of infection in burns victims, while also maintaining favourable air and vapour permeability [97].

Fibres Highly aligned collagen fibres have been fabricated to form structures with high tensile strengths [98, 99]. These collagen biomaterials have been developed in order to mimic the native structure of tendons and ligaments, which are primarily formed of aligned collagen type I and whose assemblies support tensile mechanical loads [100].

Films and Membranes Collagen films have been formed by casting collagen suspensions and allowing them to air-dry, leaving a dry collagen layer 10s – 100s of microns thick [101]. Films formed of collagen have been used in a variety of applications, including wound dressings, dural closures, reinforcement of compromised tissues, and barrier membranes [26]. Incorporating drugs within collagen films has been used such that the drugs can be delivered to a target site and released at a constant rate over time as the film breaks down [102]. Furthermore, films have been developed for directing and aiding cell growth, and have been used to guide tissue regeneration in dental surgery [103].

2.2 Electrophoretic Deposition

2.2.1 Introduction to EPD

Electrophoretic deposition (EPD) is an industrial process by which colloidal particles suspended in a liquid medium are deposited onto an electrode substrate [21]. EPD was first characterised into a practical technique in 1933, when a method for depositing thoria particles onto a platinum cathode was patented in the USA [104]. Since then the application of EPD has been researched and developed further, initially for use in ceramics, including enamels and porcelain, by Hamaker [105, 106], and only limited work was done on EPD processing for engineering purposes [23]. In the 1980s it was adopted for advanced ceramics [104], where more research and further understanding of the process began to be established. The process has now been well characterised, however there are still discrepancies in describing some of the underlying mechanisms and kinetics of EPD [107–109], which will be discussed later.

The process of EPD can be simply divided into two phases: electrophoresis and deposition [110, 111]. The first phase, electrophoresis, occurs when charged particles move through a medium as the result of an influencing electric current being applied through the medium. This phenomenon was first discovered in the 1740s by G.M. Bose when he created the capillary siphon effect [112]. He found that, when applying a high voltage through it, the efflux of water from the nozzle of a metal container was greatly increased. The first electric-field-induced motion of particles through a liquid medium was later discovered in 1808, when Reuss observed the effect in clay [104, 107]. The second phase of EPD is the deposition of particles onto the substrate, where they coagulate to form a desired coating, film or free-standing body [108, 113].

The great variety of different materials this method can be applied to, including metals, ceramics, polymers, glasses, and their composites [113, 110], means there is a wide range

of potential uses and outcomes. Additionally, EPD has proven advantageous due to low pollution levels, high automation, high throw power, and consistency [22]. As a result, EPD has substantiated success in many coating applications, so long as the substrate is, or can be made, conductive it is possible to deposit uniform layers to substrates of all shapes and sizes [21], and even for inaccessible porous structures [114].

The general set-up for performing EPD consists of a two-electrode cell containing a suspension liquid (Figure 2.5) [23, 113, 109]. The two electrodes, the cathode and anode, are connected to a power supply that, when turned on, applies an electric field through the suspension. This causes the charged particles within the suspension to move towards, and deposit on, either the cathode or anode, depending on their charge. Positively charged particles will deposit on the negative cathode, this process is referred to as cathodic electrophoretic deposition [115]. Anodic electrophoretic deposition is the alternative, where negatively charged particles deposit on the anode [104]. In order to effectively process materials using EPD it is essential that charged particles within a stable suspension are able to move freely when an electric field is applied. This therefore allows EPD to be applied to any solid that can be reduced to a fine powder, with particles being approximately 30 μm or less in size, or any solid that can exist as a colloidal suspension, including polymers, metals, glasses and ceramics [116, 117]. Once deposition has occurred it is usually necessary to implement a further step to finish the process. The deposited material often needs to be heat-treated, sintered or, at very least, dried to further densify the deposit and to eliminate porosity [23, 104]. This final step will vary depending on the material and desired application.

Although this thesis focuses on collagen and its processing, much of the previous work has been undertaken using metals and ceramics. The underpinning theories apply to particles in general and so the literature review will encompass the wide range of materials that have been deposited using EPD.

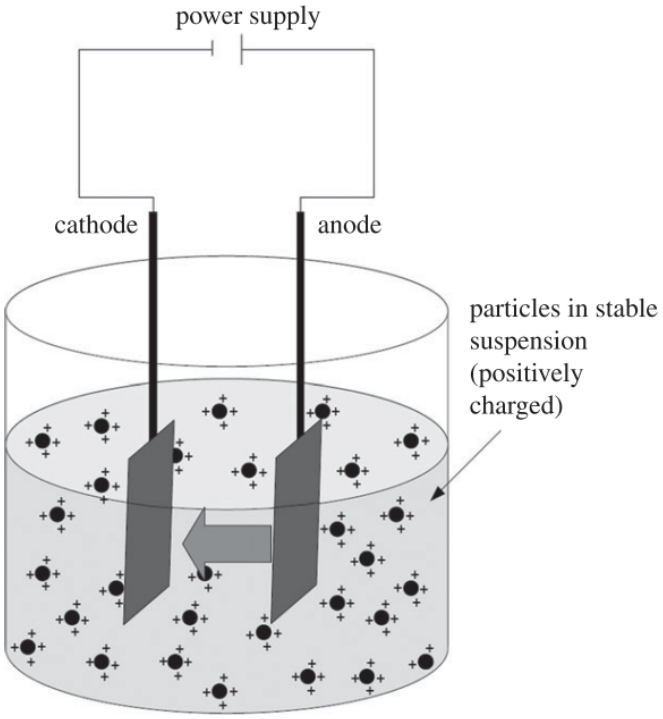

Fig. 2.5 Schematic of a standard EPD cell, in this case representing cathodic electrophoretic deposition. Figure adapted from Reference [23].

2.2.2 Particles in Suspension

For electrophoretic deposition it crucial that particles suspended in a liquid medium are sufficiently charged, well dispersed, and remain stable [118]. Most substances will develop a charge within a polar molar medium, though that does not guarantee particles will remain stable and not aggregate, and the extent of the charge depends on several factors, such as pH, and inclusion of surfactants and dispersing agents. The surface charge carried by a suspended particle can be developed by one of four mechanisms [107, 110, 116]:

1. **Dissociation of ions from solid phase into the liquid:** This is a process by which molecules split, releasing charged surface groups into the bulk solution. This is characteristic with adsorbed carboxylic acid, amine and oxide surfaces. In these cases, the pH of the solution determines the charge development on particles, because H^+ and OH^- behave as potential-determining ions.

2. **Readsorption of ions onto the solid particle from the liquid:** This process is the opposite to the previous mechanism, where ions from the solution adsorb onto the particle from the bulk solution to establish equilibrium.

3. **Adsorption of ionized surfactants:** Surfactants can be used within a suspension to stabilise certain particles that would normally aggregate.

4. **Isomorphic substitution:** This is common in minerals, where one element is substituted for another with similar ionic radii, but charge is balanced through exchangeable counter-ions.

The resulting charged particles are surrounded by ions, with an opposite charge to that of the particle's surface potential (Ψ_0), in a higher concentration to that of the bulk of the fluid [119]. This phenomenon was first modelled by Stern, which was then modified by Graham [120]; a model that has been widely accepted [104]. These ions form a layer around the particle, the Stern layer, which move with it, beyond which point a second layer of ions is formed, the diffuse layer, which does not move with the with particle [110]. Consequently, a so-called double layer is generated, as depicted in Figure 2.6. The potential at the surface of shear (Ψ_ζ), the interface between the Stern and diffuse layer, is termed the zeta potential (ζ) [121]. Under the influence of an electric field the particle and corresponding ions do not move in opposite direction, but, in fact, move together as the oppositely-charged ions enclose the particle. The particle velocity in these conditions, is therefore not determined by its surface potential, but rather the zeta potential generated by the net charge enclosed in the liquid sphere of ions [110].

Once particles have established a charge while suspended in a liquid it is essential they remain dispersed and stable during EPD [122]. Particles will aggregate if the attractive Van der Waals forces between particles exceed the repulsive electrostatic forces generated by the electric double layer [123]. The relationship between inter-atomic forces and suspension

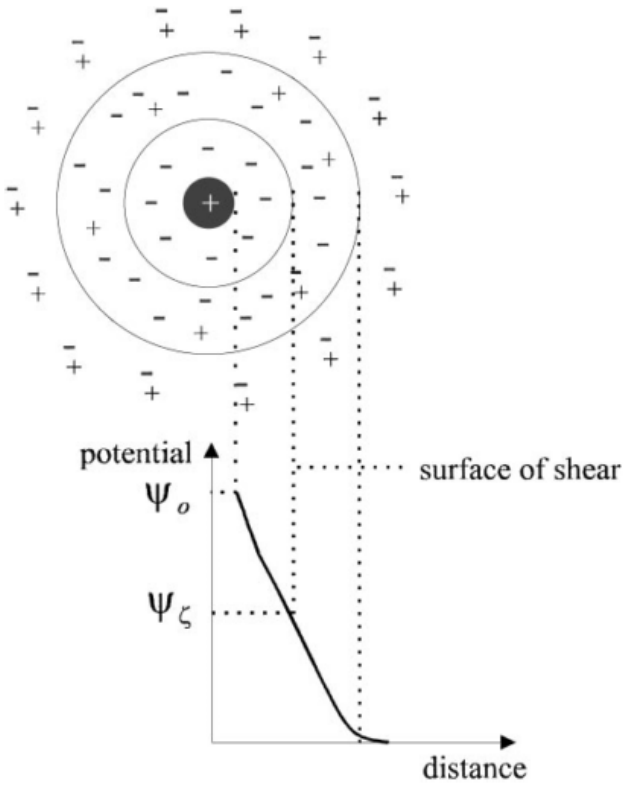

Fig. 2.6 Cross-section of the double layer effect surrounding a charged particle and corresponding graph of electric potential vs distance from the particle. Figure adapted from Reference [110].

stability can be quantitatively expressed using the DLVO theory, described by Derjaguin and Landau [124], and Verwey and Overbeek [125]. The theory is simple, stating that the total interaction energy (V_T) between particles is the summation of the repulsive forces (V_R) and the attractive forces (V_A).

$$V_T = V_R + V_A \tag{2.1}$$

Despite its simplicity, the DLVO theory can provide some insight into the stability of a suspension. Furthermore, if a suspension is likely to aggregate, due to Van der Waals attractive forces exceeding the repulsive forces, intervention is necessary if EPD is to be

successful. It is therefore of interest to note that the Van der Waals force of any given particle is constant and will remain the same despite changes to the surrounding media [126]; the electric double layer, however, can be manipulated. With this in mind, a suspension can be made more stable with the correct choice of agents, such as surfactants or polyelectrolytes.

2.2.3 Electrophoresis

The first phase of electrophoretic deposition is electrophoresis of the suspended particles. Electrophoresis is the motion of dispersed charged particles relative to the gel or fluid they are suspended in, toward an electrode of opposite charge, when a uniform electric field is applied across the suspension [127]. Stable suspended particles carry an electric surface charge that, when an electric field is applied across them, move via the electrostatic Coulomb force exerted on them [118].

The steady-state speed at which particles move toward an electrode during electrophoresis is determined by four interrelated forces acting the particles [128]. The driving force is caused by the interaction between the surface charge and the electric field exerted on the particles, accelerating them toward the electrode. The remaining forces act against this, slowing particles as they move: viscous drag from the liquid, in accordance with Stoke's Law; the opposing retardation force experienced by counter-ions within the double layer from the applied electric field; and the relaxation force caused by distortion of the double layer as the particles move [128].

2.2.4 Deposition Mechanics

Deposition is the second phase of electrophoretic deposition, though, as previously expressed, there is much ambiguity towards the underlying mechanisms controlling it [23, 107–109]. Currently, many EPD studies are being performed with a trial-and-error approach, because of the lack of agreement in the relationship between changing parameters and the final deposit

[129]. Many theories to describe the fundamental deposition mechanisms of EPD have been developed based on the framework of the DLVO theory [23], including: particle charge neutralisation [130], electrochemical coagulation of particles [131], flocculation by particle accumulation [106], and the idea of the particle double layer being distorted under a DC electric field [107], each of which will also be discussed below.

Particle Charge Neutralisation

It was suggested by Grillon et al. [130] that once particles had deposited on the electrode their charge would be neutralised. This is an important mechanism for describing single particles and monolayers, and it explains the deposition of powders that charge when salt is added to the suspension, such as in the study by Brown and Salt [132]. This mechanism is also valid for the initial stage deposition from diluted suspensions, but is invalid under a number of conditions: when EPD runs for longer times creating thick deposits; when deposition occurs across a semi-permeable membranes, preventing particle-electrode interactions; and when reactions that occur at the electrode alter the pH [108].

Electrochemical Coagulation of Particles

This mechanism suggests that repulsive forces between the particles are reduced at the electrode. Koelmans and Overbeek [131] proposed that the increase of electrolyte concentration near the depositing electrode lowers the zeta potential of particles, which in turn causes flocculation to occur. In this case it is assumed that a finite amount of time is necessary for electrolyte concentration to increase enough for deposition to occur. This was in fact observed by Koelmans and Overbeek: they showed that particles collected at the depositing electrode immediately, but there was a short delay before deposition occurred [131]. It was found that the critical time needed to pass for $MgCO_3$ to deposit was inversely proportional

to the applied voltage to the second power, hence critical time can be extremely small and is often not observed.

This mechanism is plausible for aqueous solutions where electrolytic reactions occur at the electrode, generating OH^-. Cathodic reactions that involve the generation of OH^- are listed by Zhitomirsky [133]. For solutions where there is no increase in electrolyte concentration at the electrode, however, this mechanism is invalid [104].

Flocculation by Particle Accumulation

Hamaker and Verwey [106] first attempted to describe the mechanism of EPD as flocculation by accumulation. They proposed that the deposition formation by electrophoresis is akin to sedimentation of particles due to gravity when a suspension is left to stand for long periods of time. Therefore, particles accumulate and deposit on the electrode due to the pressure exerted on them from other incoming particles, overcoming the interparticle repulsion they usually experience. This mechanism is also compatible with deposits that do not occur on the electrode but instead on semi-permeable membranes [107, 116].

Electrical Double Layer (EDL) Distortion and Thinning

Sarkar and Nicholson [107] proposed that as a particle-lyosphere system approaches the depositing electrode their electric double layer distorts and thins (Figure 2.7). A combination of fluid dynamics and the applied field act on the double-layer, distorting it so that it is thinner ahead of the particle and wider behind. This means that the zeta potential varies with position, being greater in the leading hemisphere of the particle and lesser in the trailing hemisphere. The cations in the liquid will move with the positively charged particle towards the cathode. These cations, in high concentration, will tend to react with the counter ions in the trailing ‘tail’ of the lyosphere. As a result, the distorted double layer then thins around the ‘tail’ of the particle. As the next particle approaches the cathode, which has a thin leading

lyosphere, it can easily get close enough to the thin 'tail' of the previous particle for Van der Waals (VDW) attractive force to dominate and induce coagulation [107].

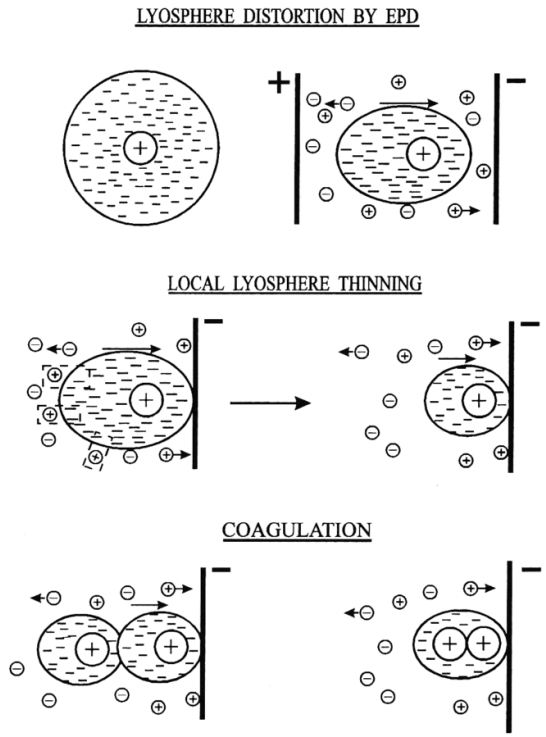

Fig. 2.7 Deposition mechanism by lyosphere distortion and thinning. Figure adapted from Reference [107]

2.2.5 Factors Influencing EPD

The mechanisms of EPD have been discussed previously in Sections 2.2.2, 2.2.3, and 2.2.4, but the parameters that govern these mechanisms can be broadly separated into two groups: the suspension parameters and the process parameters. The suspension parameters include composition and the physical and electric properties, whereas the process parameters are given by the electrical properties of the electrodes, the applied electric field and electrical regime, and deposition time [104].

The first attempt to correlate these factors and describe deposited mass was by Hamaker [105] in 1940. The Hamaker Equation, which will be explored further in Chapter 4, relates

deposit yield to applied electric field strength, electrophoretic mobility of particle in suspension, solids concentration, and deposition surface area, in planar EPD cells. Many more modern EPD models are still based on the original Hamaker Equation [134], however, since its conception, several other factors have been shown to influence the mechanics of EPD. Here we look further into the parameters influencing the electrophoretic deposition process.

Suspension Parameters

Particle Size There is no specified optimum particle size, as other factors are often more influential, though a good range has been reported to be between 1-20 μm in ceramics [116], however, this does not necessarily rule out particles out of this range. For a satisfactory deposit it is necessary for particles to remain well dispersed during EPD; larger particles, however, may have the tendency to fall due to gravity, resulting in a thicker deposit toward the bottom of the film compared with the top [104]. Furthermore, a study into the effect of particle size by Sato et al. [135] found that films formed of sub-micron particles showed significantly less cracks upon drying than films with much larger particles, therefore, suggesting films with smaller particles produce better quality films.

Dielectric Constant of Liquid The dielectric constant, sometimes referred to as the relative dielectric permittivity, of a liquid is the ratio of that liquid's permittivity with respect to the dielectric permittivity of a vacuum, which is constant. The permittivity is a measure to describe how an electric field through a media affects, or is affected by, that media; more simply, it is a measure of resistance, that describes how much flux (i.e. electric field) is present per unit charge [136]. The dielectric constant of a medium varies with temperature.

A study by Powers [137] sought to find a relationship between dielectric constant of the media and deposition yield, using beta-alumina suspensions in organic solvents. It was found that there is an optimum range for dielectric constants in EPD, where if it is too low there is insufficient dissociative power for deposition to occur, and if it is too high the electrophoretic

mobility of particles is decreased due to particle electric double layer being reduced by increased ionic concentration. As such, the ionic concentration in suspensions should remain low. The viscosity and dielectric constants of some solvents used in EPD can be seen in Table 2.3.

Table 2.3 The viscosity and dielectric constants of different organic solvents [138]

Solvents	Viscosity	Relative Dielectric Constant
Methanol	0.557	32.63
Ethanol	1.0885	24.55
n-propanol	1.9365	20.33
Iso-propanol	2.0439	19.92
n-butanol	2.5875	17.51
Ethylene glycol	16.265	37.7
Acetone	0.3087	20.7
Acetylacetone	1.09	25.7

Conductivity of the Suspension The importance of suspension conductivity was proposed by Ferrari and Moreno [139], who found that particle movement was very slow when conductivity was too high, but at increased resistance particles become less stable in suspension. Furthermore, they saw that an increase in polyelectrolye concentration and temperature lead to an increase in conductivity, for which not all values were advantageous for EPD. They concluded that there exists an optimal range for conductivity. Another study by Ferrari and Moreno [140] stated that this optimal range can be increased by increasing the applied current during EPD. Biesheuvel et al. [141] went on to observe that solids concentration had a direct affect on suspension conductivity.

Despite the apparent importance of suspension conductivity on EPD kinetics, predictive models failed to include it as a key parameter. Ferrari et al. [142] hypothesised that for long deposition times, as suspension concentration decreases, so too does the suspension conductivity. With this in mind they developed a more accurate resistivity model for EPD, based on the Hamaker Equation [105].

Viscosity of Suspension Ferrari et al. [139, 140] also noted that viscosity can play a role in deposition mechanics, intuitively that viscosity should remain low in order to maximise yield. Often in EPD of ceramics, viscosity is sufficiently low not to present an issue, though with polymers, such as collagen for example, increasing concentration can significantly increase the viscosity, so care must be taken. Furthermore, it is important to find the balance between solid loading and viscosity, lowering the concentration will also minimise the deposited mass.

Zeta Potential The zeta potential of a suspension is essentially a measure of the electric Stern layer of the colloidal particles within that suspension, which can be visualised in Figure 2.6. It is, therefore, a very important factor in EPD kinetics. As previously mentioned, it is important to achieve a high and uniform surface charge around suspended particles. It plays a role in: stabilization of suspended particles; determining direction and velocity of migration for particles during EPD; and determining the density of the deposit [143].

As well as increasing suspension stability and particle velocity, optimising the zeta potential also increases the deposit density during EPD. As the deposit forms charged particles begin to pack together with increasing attraction forces. Particles with low surface charge (i.e. low zeta potential) coagulate more readily, even at relatively large inter-particle distances, often resulting in gaps in the deposit, leading to porous depositions. Particles with an increased surface charge, however, have greater repulsive forces as they pack together. As a result, particles will be pushed to occupy all available free space, leading to a greater deposit density [144].

It is is necessary, therefore, to optimise the zeta potential of a given suspension in order to realise increased deposition quality and yield. The zeta potential can be manipulated by changing the suspension pH, using either acids or bases, or with the addition of polyelectrolytes [145]. Chen et al. [146] showed how the zeta potential of Al_2O_3 varied with respect

to pH, as shown in Figure 2.8. Furthermore, they noted that Al_2O_3 had a maximum zeta potential at pH 2.2, and thus this pH provided optimal conditions for EPD [146].

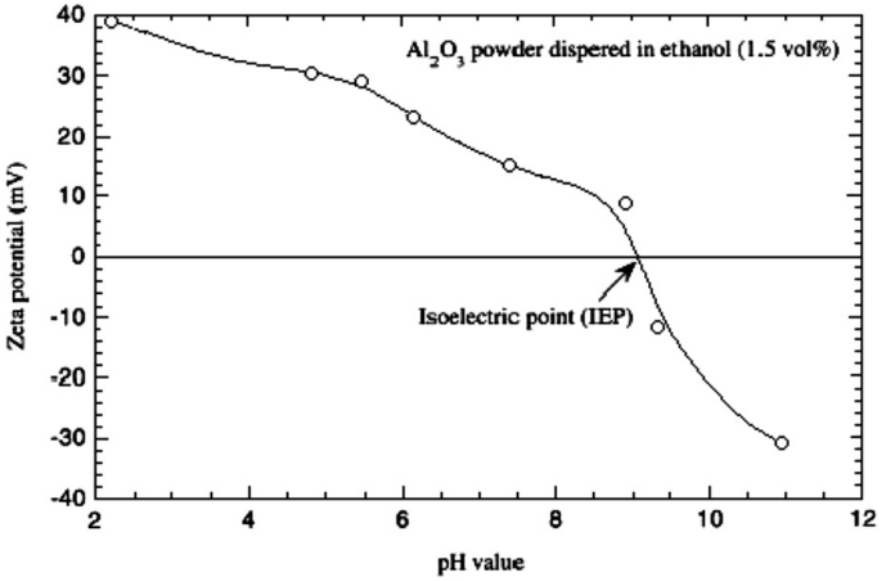

Fig. 2.8 Zeta potential of Alumina dispersed in ethanol at differing pH. Figure adapted from Reference [146]

Though zeta potential does have a direct influence on deposition rate, Zarbov et al. [143] noted that the inclusion of ionic additives to the suspension will also affect the suspension conductivity. The conductivity of a suspension determines the potential drop through the bulk of it, therefore by altering it, such additives may also have an indirect effect on deposition yield.

Stability of Suspension The stability of a suspension is directly related to the zeta potential, through mechanisms described in Section 2.2.2. The stability of a suspension, therefore, is defined by the tendency for particles to remain well dispersed, or more accurately, avoid flocculating and settling [104]. Unstable suspensions will settle rapidly and require constant agitation in order to remain dispersed, such suspensions result in uneven deposits during EPD, being thicker at the bottom than the top. For some suspensions to remain well dispersed, it is necessary to include electrolytes though this is not effective for all colloids [132].

Process Parameters

Effect of Deposition Time For prolonged deposition times, with a fixed electric field applied across a suspension, the rate at which deposition occurs will begin to decrease with time [146, 147]. A study by Wang et al. [148] corroborated these findings; they found that increasing the applied potential increased deposition rate, furthermore, for each regime the deposition rate decreased with time, as depicted in Figure 2.9. Subsequently, the initial phase of deposition is linear, but at prolonged times the deposited mass begins to plateau, as the solids in suspension become depleted.

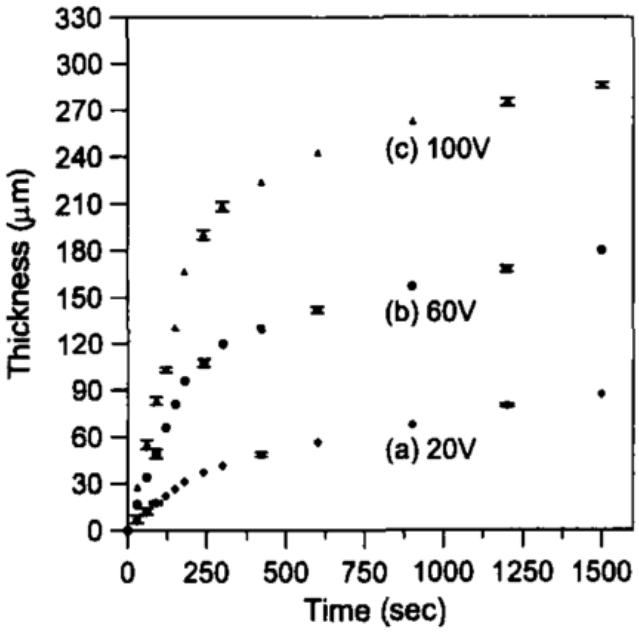

Fig. 2.9 Deposition of zinc oxide dispersed in isopropyl alcohol at different voltages with respect to time. Figure adapted from Reference [148].

Zhitomirsky et al. [149] found that as deposition time increases the current density within the EPD cell decreases, shown in Figure 2.10. It is hypothesised that two mechanisms occurring during EPD cause this phenomena: (i) as the deposit builds up, it creates an insulating layer on the electrode [149]; (ii) and as particles moving within the suspension

under an electric field are the main charge carriers, as they deposit the suspension becomes more resistant [142].

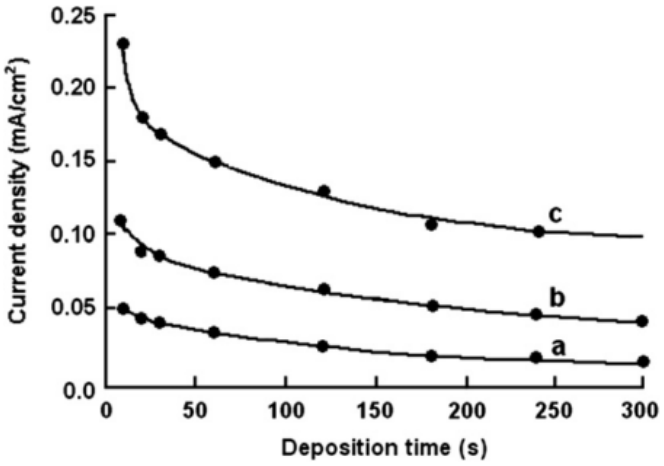

Fig. 2.10 Current density versus deposition time at different applied voltages for a suspensions of hydroxyapatite dispersed in isopropyl alcohol. Figure adapted from Reference [149].

Applied Voltage The magnitude of the applied voltage across a suspension directly affects the rate of deposition; by increasing the applied voltage the deposition yield also increases [149], this effect can be seen in Figure 2.9 and, more directly, in Figure 2.11.

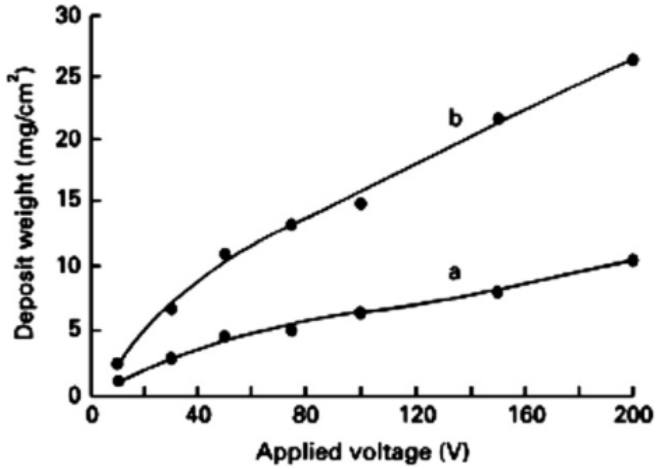

Fig. 2.11 Weight of deposited hydroxyapatite (dispersed in isopropyl alcohol) versus applied voltage, at different deposition times (a) 30s and (b) 120s. Figure adapted from Reference [149].

Greater deposit yield with higher applied voltages, however, does not mean that the deposit was of equal quality to deposits at lower applied voltages, as non-uniform deposits can form at higher voltages. Basu et al. [147] found that at moderate field, the films produced were more uniform and had an increased packing density than those produced in high applied voltage fields. This is because the film formation is a kinetic mechanism - the rate at which particles accumulate influence their packing behaviour. The higher applied fields can create turbulence within the suspension that will effect the coating during deposition. Furthermore, particles travelling at greater velocity do not have sufficient time to arrange themselves into tightly-packed, uniform deposits.

Additionally, Negishi et al. [138] found in an n-propanol solvent with no suspended particles that the current density was proportional to the applied voltage, however at higher applied voltages through the solvent the current density becomes unstable (Figure 2.12). It was hypothesised that the instability in current density generated by increased voltage could influence the deposit morphology.

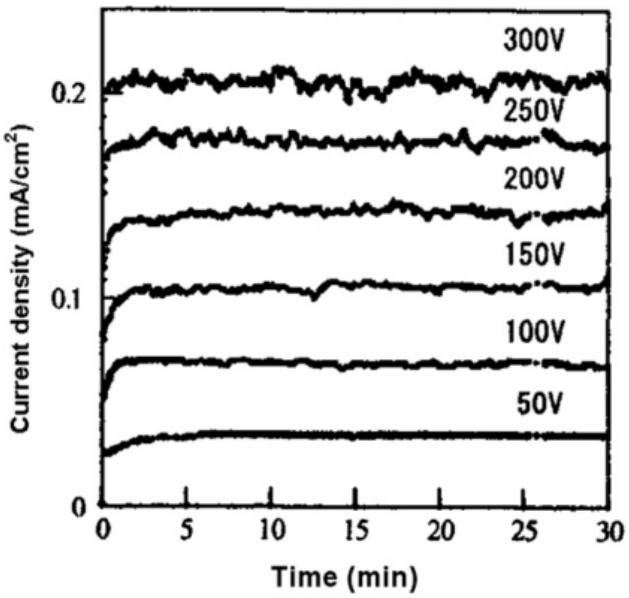

Fig. 2.12 Relationship between applied voltage and current density, from 50-300V in an n-propanol solvent with no suspended particles. After an applied voltage of 100V the current density becomes unstable. Figure adapted from Reference [138].

Concentration of Solids in Suspension As the concentration of particles in suspension increases, so too does the rate of deposition [150]. The concentration, however, also determines the suspension viscosity, and increasing concentration too much will restrict the movement of particles. In multi-component EPD (suspensions containing two or more different solid components) the influence of respective concentrations can become more interesting. Vandeperre et al. [151] found that even though different particles contain the same sign of surface charge, they can deposit at different rates depending on volume fraction of solids in suspension. At high concentrations, particles will deposit at equal rates, at low volume fractions, however, particles will deposit at rates proportional to their electrophoretic mobility.

Conductivity of Substrate The conductivity of the substrate electrode is an important factor to consider for EPD, to ensure efficient and uniform depositions. Interestingly, Peng and Liu [152] found that using a $La_{0.9}Sr_{0.1}MnO_3$ (LSM) substrates with low conductivity not only led to very low deposition rates, but also produced non-uniform deposits of poor quality. These findings were corroborated by Chen and Liu [153], where they observed slow, non-uniform YSZ deposits on substrates of low conductivity, whereas high quality deposits were obtained on highly conductive substrates.

2.2.6 Mathematical Models of EPD Systems

The factors that influence EPD systems have been described in the previous section, including the processing parameters and the suspension parameters. These measurable factors have been used to describe electrophoretic deposition systems mathematically, modelling the interaction between them and their overall effect on deposition yield. The first model to describe EPD kinetics was developed in 1940 by Hamaker [105], which incorporated suspensions properties, including the concentration of solid mass in suspension, the EPD

cell dimensions, the applied current/voltage and the electrophoretic mobility of the particles in suspension. The electrophoretic mobility is a complicated element of the system, which is a product of the interaction between the charged particles and the suspension media, and comprises elements such as the dielectric constant of the suspension media, the viscosity of the suspension media and the zeta potential of the particles in suspension. This first model was acceptable for short deposition times, but failed to account for a reduction in particle concentration over time as the solid mass deposited. Sakar and Nicholson developed a revised model which accounted for the reduction if solid concentration over time [107]. Ferrari et al. then established a further model that also considered the change in suspension resistivity as the solid concentration decreased [142]. This model by Ferrari et al. has been regarded as the most appropriate predictive model for direct current EPD systems.

These models are explored further in Chapter 4, to further understand how they are derived and their influence within EPD processing. The models that have been previously described in the literature are only suitable for direct current systems, and do not account for the issues associated with aqueous systems, which are discussed further in the next section.

2.2.7 EPD in Aqueous Suspensions

Electrophoretic deposition using aqueous media can be beneficial and is often a necessity. Although many organic solvents are popular in ceramics processing, aqueous media has the advantage of being cheaper, often having a higher dielectric constant, stimulating greater particle charge, offering better temperature control, and avoiding potential health and/or environmental risks that many organics present, such as toxicity and flammability [140, 154]. Furthermore, many colloidal particles necessitate aqueous media to form stable suspensions; many biological macromolecules, collagen included, must be suspended in aqueous media [109], discussed further in Section 2.3.2.

Depositions from aqueous suspensions, however, bring a number of problems. These problems arise as a result of the electrochemical reactions occurring at the electrodes, causing water to be electrolysed and gas bubbles to form, disrupting the quality of deposits [155]. This section explains the issues with aqueous EPD and presents the current research to troubleshoot these problems while still forming efficacious and efficient deposits.

Bubble Formation

In aqueous solutions gas bubbles of hydrogen and oxygen nucleate on the cathode and anode, respectively. This is due to the applied electric field causing the electrolysis water, in accordance with the following decomposition reactions [154]:

$$Anode: \quad 4\,OH^-(aq) \longrightarrow O_2(g) + 2\,H_2O(l) + 4\,e^- \quad (E^o = -0.40V) \tag{2.2}$$

$$2\,H_2O(l) \longrightarrow O_2(g) + 4\,H^+(aq) + 4\,e^- \quad (E^o = -1.23V) \tag{2.3}$$

$$Cathode: \quad 2\,H_2O(l) + 4\,e^- \longrightarrow 2\,H_2(g) + 4\,OH^-(aq) \quad (E^o = -0.83V) \tag{2.4}$$

$$2\,H^+(aq) + 2\,e^- \longrightarrow H_2(g) \quad (E^o = 0.00V) \tag{2.5}$$

The overall cell reaction is:

$$2\,H_2O(l) \longrightarrow 2\,H_2(g) + O_2(g) \tag{2.6}$$

The voltage potentials required for the electrochemical reactions to occur at the anode and cathode are -0.40 V and -1.23 V; and -0.83 V and 0.00 V, respectively [154]. This means

that beyond these voltage potentials, water electrolysis will occur during EPD. The dominant reaction, however, depends on weather the aqueous suspension contains sufficient H^+ or OH^- ions to occur. This therefore implies that the rate of gas evolution depends not only on applied voltage, but also suspension composition.

The bubbles generated in the above reactions during EPD can prevent particles from depositing on the substrate and can lead to bubbles being trapped within the deposit. To minimise the evolution of bubbles, and to generate high quality films from aqueous suspensions, there has been lots of research into using modulated electric fields [156]. Modifying the electric fields used to perform aqueous EPD is necessary due to the very low potential at which electrolysis occurs. An investigation by Uchikoshi et al. [157] found that using very low DC voltages, below that at which water decomposition occurs, results in negligibly low rates of deposition, and concluded such parameters are not viable.

Waveforms to Minimise Bubble Nucleation

Modulated electric fields during aqueous electrophoretic deposition allow for high throughput to be maintained, but with reduced bubble nucleation. There are two distinct regimes that oblige this: asymmetric alternating current, and pulsed current [154, 156]:

Asymmetric Alternating Current

One such method, that is showing increasing success, is the use of an asymmetric alternating current (AAC) signal for EPD. The principle here is that unbalanced AC electrical fields, as seen in Figure 2.13, have a net current of zero, as the area under the AC signal curve for one cycle is zero [156]. In this case, with the absence of a net DC component, the associated electrochemical reactions, that cause bubbles to form, are eliminated. Particle movement during electrophoresis, however, is not linear to the applied electric field exerted on them when the field strength is sufficiently high. This non-linear relationship can be described by

the equation below, where V_{eph} is the electrophoretic particle velocity, μ_1 and μ_3 are the linear and non-linear electrophoretic mobilities and E is the electric field strength [158]:

$$V_{eph} = \mu_1 E + \mu_3 E^3 \tag{2.7}$$

This means that for a suspension experiencing an asymmetric AC signal, such as the one seen in Figure 2.13, despite there being no net DC component, there is still net movement of the particles that then deposit on a substrate as normal in EPD.

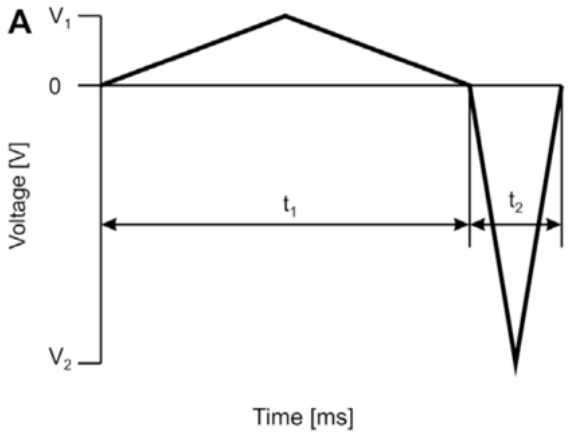

Fig. 2.13 One period of applied asymmetric AC signal, with asymmetry factor 4. Figure adapted from Reference [159].

Several studies have successfully applied asymmetric AC-EPD on materials to minimise bubble formation [156]. Table 2.4 gives a summary of successful AAC-EPD studies and the parameters they used to achieve viable deposits.

It is clear from Table 2.4 that there is great variation in the choice of parameters for AAC-EPD. Some studies, nonetheless, have attempted to underpin the optimal processing conditions. Raju et al. [167] found, after studying multiple frequencies, the 100 Hz offered the maximum deposit yield, the graphs for which can be seen in Figure 2.14. Furthermore, Neirinck et al. [159] showed that an AC asymmetry factor 4 gave the highest yield of deposit.

Table 2.4 Experimental parameters used for asymmetric AC-EPD of various materials.

Deposit material	Peak-to-peak voltage (V)	Frequency (Hz)	Deposition Time (mins)	Reference
Glucose oxidase	160	30	7	Ammam & Fransaer, 2009 [160]
Glutamate oxidase	250	30	30	Ammam & Fransaer, 2010 [161]
ß-galactosidase and glucose oxidase	120	30	30	Ammam & Fransaer, 2010 [162]
Aluminium oxide	500	1-50	20	Neirinck et al., 2009 [159]
Staphylococcus aureus and Escherichia coli	100	25	10-40	Neirinck et al., 2009 [163]
Aluminium oxide	20-80	150-450	1-7	Nold & Clasen, 2010 [164]
Polypyrrole	50-120	1.25	2-15	Pech-Rodriguez et al., 2014 [165]
Barium titanate	4-20	10-1000	4-30	Raju & Yoon, 2013 [166]
Silicon carbide	20	10-1000	5-30	Raju et al., 2014 [167]

These findings, however, may not be conclusive for all aqueous suspensions, and it is likely that the optimum conditions vary for different materials.

Pulsed Current

The other such troubleshooting method that several studies have implemented successfully is the use of a pulsed DC current [168–171]. In these studies a pulsed DC signal is used, as can be seen in Figure 2.15 below. The DC signal follows a cycle of being either on or off; the on time per cycle is termed the pulse width (T_{on}), with the total cycle time being known as the pulse period (λ), and the percentage of time the pulse is on per cycle is called the duty cycle (δ) [172]:

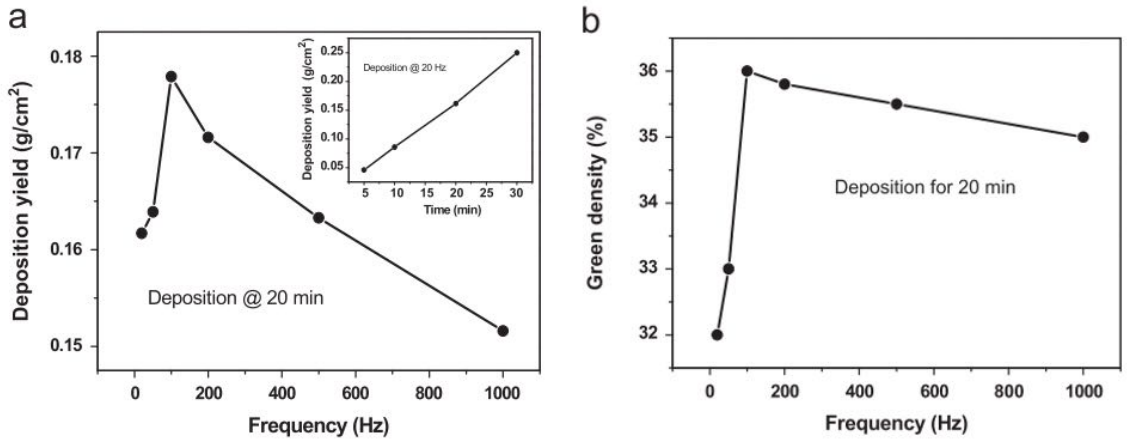

Fig. 2.14 Deposition yield of silicon carbide in an aqueous media as a function of (a) frequency and time (inset), and (b) the dependence of the green density on the AC frequency. Figure adapted from Reference [167].

$$\lambda = T_{on} + T_{off} \tag{2.8}$$

$$\delta = \frac{T_{on}}{\lambda} \tag{2.9}$$

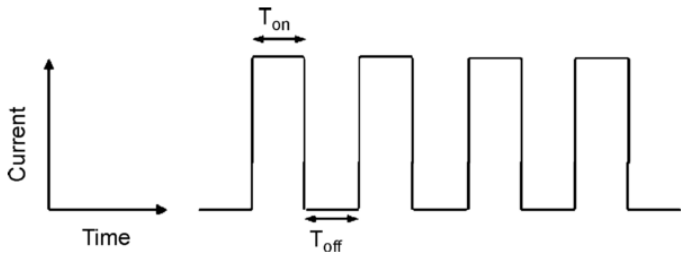

Fig. 2.15 Pulsed DC voltage with 50% duty cycle. Figure adapted from Reference [168].

Besra et al. [168] showed how maintaining the same applied voltage (20 V) and reducing the pulse width, bubbles no longer formed within a sample during EPD (Figure 2.16). The reduction in bubble formation from these waveforms may suggest that the rate of water

electrolysis is reduced. This was explored further by Besra et al. [170] who measured the pH at the anode and cathode for PC and DC electric fields. They found significantly smaller shifts in pH for PC compared with DC. It was hypothesised it is during the periods when the signal is off that allows time for oxygen and hydrogen gas molecules to diffuse away from the electrodes before gas bubbles nucleate.

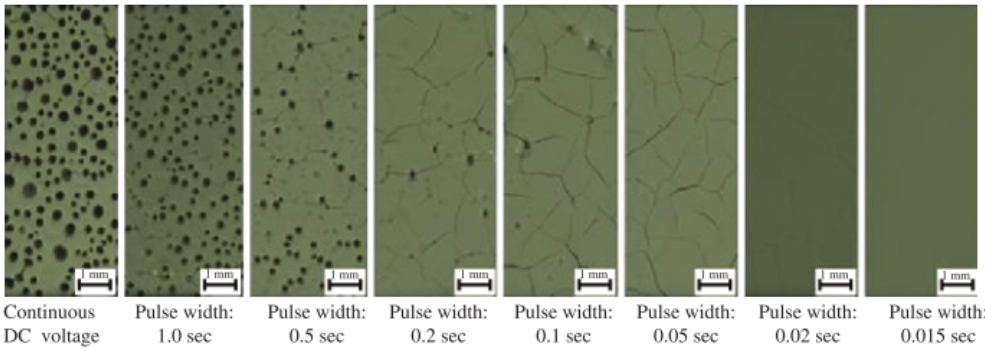

Fig. 2.16 Photographs of the top surface of deposited alumina on nickel substrate. Figure adapted from Reference [168].

It was shown by Besra et al. [168] that there exists an optimal operating window for pulse widths at certain voltages, which can be seen in Figure 2.17. Within this window smooth, bubble-free deposits form, but there is an upper-threshold of pulse width above which bubbles nucleate in the film, and a lower-threshold below which deposition does not occur. This window narrows and the thresholds converge as voltage increases.

Similar to optimal values found for AAC-EPD, this operating window is applicable to this study, but the operating window will vary for different suspension and process parameters.

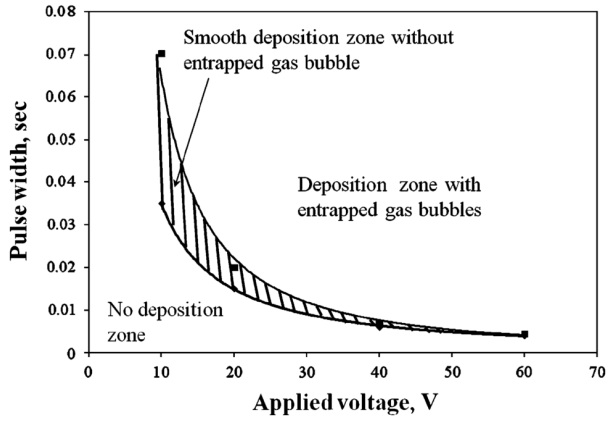

Fig. 2.17 Pulse width vs. applied voltage showing optimum region of bubble-free deposition of alumina suspended in aqueous media. Figure adapted from Reference [168].

2.3 Application of EPD to Biomaterials

2.3.1 Ceramic Biomaterials

Electrophoretic deposition has, for many years, been a well-established processing technique for ceramic-coating of substrates [173]. As such, the initial [174] and widest application of EPD for biomaterial purposes is the coating of metallic orthopaedic implants with inorganic, bioactive coatings [113]. The specific objectives of these coatings vary with the purpose, however, they all provide two basic functions: a favourable surface for host tissue to interact with and improve fixation; and a boundary layer to protect from metal breakdown and corrosion and preventing ions being released from the implant into the host [175]. EPD has been effective in applying uniform and dense oxide coatings on, often irregular-shaped, metallic substrates [148].

Of the bioactive coatings formed from EPD, the most prominent and highly researched is the deposition of synthetic hydroxyapatite (HA) [174], which has a similar composition to bone and is commonly used for orthopaedic coatings [176, 177]. Furthermore, as a ceramic, HA can form highly charged and stable suspensions ideal for EPD prcoessing, with deposits having very high purity [149]. Subsequently, advanced HA depositions include coatings

of porous structures [178], patterned coatings for implants [179] and biosensors [180], and depositions of HA nanoparticles [181, 182]. Aside from hydroxyapatite depositions, many other bioceramics have been processed using EPD for biomedical devices. There have been studies into EPD of Bioglass, a bioactive silicate glass, developed by Hench et al. [183], that has excellent orthopaedic bioactivity and biocompatability [184], similar to HA. EPD was proposed as an alternative technique to thermal spraying or enamelling, though much less research has been carried out, compared with HA studies [185]. Boccaccini et al. [186] optimised the deposition of Bioglass onto nickel-titanium wires, with a study showing aqueous suspensions yielded optimal results [185]. Further study, by Pishbin et al. [187], has sought to optimise the EPD parameters for Bioglass using the design-of-experiment technique. Results thus far, however, have been positive, with EPD showing to be a good coating process, yield uniform layers of Bioglass for biomedical materials.

Similar to previous examples, several other ceramics have been deposited onto metallic substrates for biomedical applications, though contrarily, they have more often been used as coatings to provide corrosion protection to the implant [188].

2.3.2 Biopolymers

In recent years the use of electrophoretic deposition as a processing technique for biomaterials has grown substantially [109, 113]. Notably, electrophoretic deposition has been successfully applied for processing several biological macromolecules. The ease of set-up, low cost, and, most importantly, low processing temperatures make EPD an attractive technique for use with these molecules that would otherwise be damaged or denatured with other material processing methods. Several studies have successfully applied EPD to chitosan, alginate, gelatin, heparin, and hyaluronic acid (Table 2.5).

It is apparent from Table 2.5 that EPD has been used extensively, for a range of biopolymers. This technique has mainly been implemented for surface functionalisation and coatings

Table 2.5 Experimental parameters used for EPD of various biological macromolecules. All studies used DC applied voltage.

Biological macromolecule	Electric field (Vcm^{-1})	Deposition Times (mins)	References
Chitosan	2.5-25	1-10	[189–203]
Alginate	5-25	1-5	[191, 194, 204–206]
Hyaluronic Acid	5-25	1-10	[191, 194, 206, 207]
Gelatin	3.5	3	[193]
Heparin	5-25	1-10	[202, 206]

of biomedical substrates [190, 192, 195, 198, 199, 202, 203, 208], however, free-standing films have also been reported [191, 194, 197, 207, 209]. Furthermore, many of these studies have produced co-deposit composites of two or more biopolymers [191–194, 208], and even bioploymer-ceramics [195–198, 202, 203].

2.4 Electrophoretic Deposition of Collagen

Electrophoretic deposition has proven to be a versatile tool for creating many functional biomaterial structures and coatings, without the use of toxic chemicals, with very mild processing conditions that maintain the structure and function of the materials, which does not damage or denature biopolymer materials. With these advantages in mind, further research is now exploring EPD as a processing tool for collagen. Here, electrophoretic deposition of collagen, for generating large uniform films and coatings, is discussed further.

2.4.1 Collagen in Suspension

As previously mentioned, the triple-helical tropcollagen molecule has approximately 3000 amino acid components ($\sim$1000 for each α chain), containing several acidic and basic functional groups [15]. As a result, collagen molecules act as polyelectrolytes when suspended in aqueous media, containing both negatively and positively ionisable groups [210]. The relative charge of collagen is pH dependant, with amino acid residues being protonated or deprotonated in either acidic or alkaline conditions, respectively [211]. Therefore, under certain conditions and local pH, collagen will act like every other charged colloid in suspension, and will develop an electric double layer with a measurable zeta potential [212–214]. Consequently, under an applied electric field, collagen in a suspension will migrate toward and deposit on the electrode of opposite charge.

2.4.2 Current Research into Electrochemical Processing of Collagen

There have been several studies published in recent years that use an electric field applied across a collagen solution to align and compact the collagen fibres into threads [215–218, 210] and films [219–221]. These methods use isoelectric focusing (IEF) of type-I collagen molecules, using a pH gradient and electric field. Upon application of an electric current,

collagen congregates, aligns and compacts along the isoelectric point (pI) [216]. These studies give evidence that collagen can be effectively processed with the application of an electric field, though deposition does not occur onto a substrate as in EPD. Collagen has also been successfully deposited using cathodic electrophoretic deposition to create films [213, 214, 222]. The collagen used in these studies was soluble collagen, and films were deposited using a DC voltage of 25 V for 4 mins.

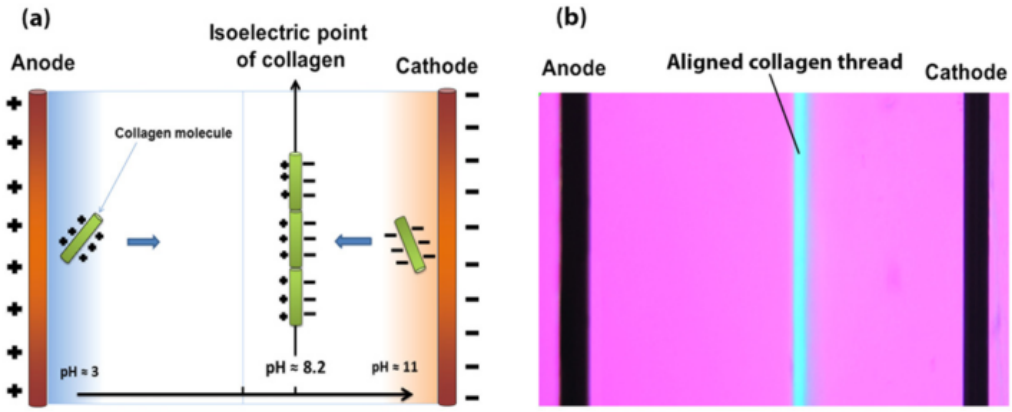

Fig. 2.18 Principle of electrocompaction process: (a) schematic of electrochemical alignment of collagen molecules. Collagen molecules between the cathode and anode assume different charges, depending on the local pH. Since collagen molecules have similar charges with electrodes, a repulsive force condenses molecules at the isoelectric point where the net charge of the collagen molecules is zero. (b) Polarized microscopy visualizes the alignment of collagen molecules in the isoelectric point of the electrochemical cell. Uniform molecular orientation is manifested in blue at the isoelectric point [210].

2.4.3 EPD of Insoluble Type I Collagen

Although there has been notable success for EPD of many biological molecules, including for soluble collagen, using direct current EPD, many studies have also noted issues with the formation of bubbles within the deposit [190, 208]. This issue is apparent when using EPD on insoluble collagen, as shown in studies by Barrett et al. [24, 25]. Collagen suspensions were formed by hydrating insoluble collagen type I in aqueous 0.05 M acetic acid solution. Barrett measured the zeta potential profile of the suspended collagen at differing pH levels

and found the collagen to be well suspended and have a high zeta potential charge in acidic conditions, around pH 3.5 [24]. However, direct current depositions were unsuitable as the aqueous suspensions always resulted in bubble formation. Investigative measures were required to find suitable deposition parameters.

EPD Parameters for Collagen Depositions

Type I collagen is hydrated in acetic acid [82] - an aqueous media. This, therefore, leads to issues with gas bubble nucleation at the electrodes due to electrolysis of the water, as previously discussed in Section 2.2.7. However, as mentioned previously, there are strategies to mitigate the formation of bubbles by altering both the suspension parameters and the processing parameters. Investigative work done by Barrett et al. sought to overcome these issues and achieved successful bubble-free collagen deposits [24, 25].

Initially EPD research with hydrated collagen suspensions in 0.05 M acetic acid aimed to systematically alter the deposition parameters in order to find an optimal window for defect-free collagen films. The deposition voltage was set to 5 V, after finding that 4 V was insufficient to deposit collagen under a pulsed current regime. While 5 V did still result in bubble formation, it was the lowest achievable voltage that could still deposit collagen onto the electrode [24]. The deposition parameters were then altered, following principles described in Section 2.2.7. A pulsed current regime was used and different combinations of duty cycle and pulse period were investigated (Figure 2.19).

The composition of the collagen suspension was also investigated. Many EPD systems, particularly in ceramic processing, use solvents as the suspension media [104]. Solvents are not susceptible to electrolysis and therefore much higher voltages can be used with no gas nucleation at the electrode [149], which is a common issue in aqueous suspensions [168]. In order to minimise the production of hydrogen and oxygen molecules, the solvent ethanol was added to the suspensions, thereby reducing the percentage of water within the system. Barrett

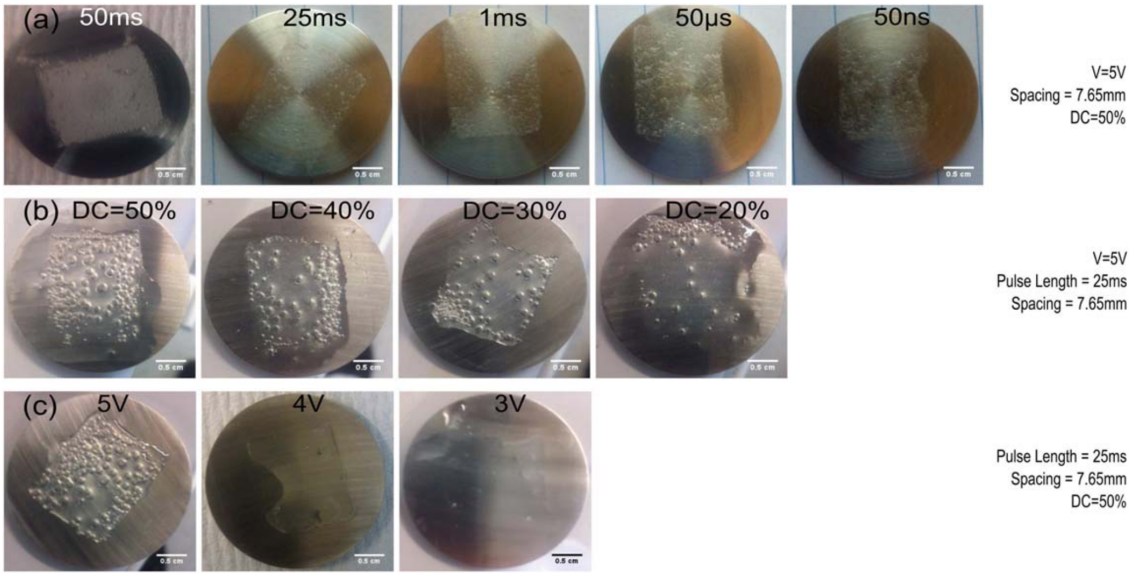

Fig. 2.19 Images of collagen deposits formed by PC-EPD, immediately after deposition: (a) with a range of pulse periods, (b) with a ranges of duty cycles, (c) with a range of voltages. Figure adapted from reference [25].

et al. found that the addition of ethanol reduced gas bubble nucleation during EPD, but that it also reduced yield [25]. It was found that 50 vol.% ethanol was an optimal compromise. Furthermore, they also discovered that the addition of ethanol increased the zeta potential of the suspension, thereby increasing the electrophoretic mobility of collagen during EPD (Figure 2.20).

The work by Barrett et al. [24, 25] found that bubbles formed within the deposit, from the aqueous suspension, unless very specific parameters were used. The aqueous suspension was diluted with ethanol (50%) and a specific pulsed current regime was used: 5 V, duty cycle of 40%, and a pulse period of 0.05 seconds. These parameters gave smooth, bubble-free films, which once dried had a thickness of approximately 40 µm, however, deposition times were extremely long, in excess of five hours.

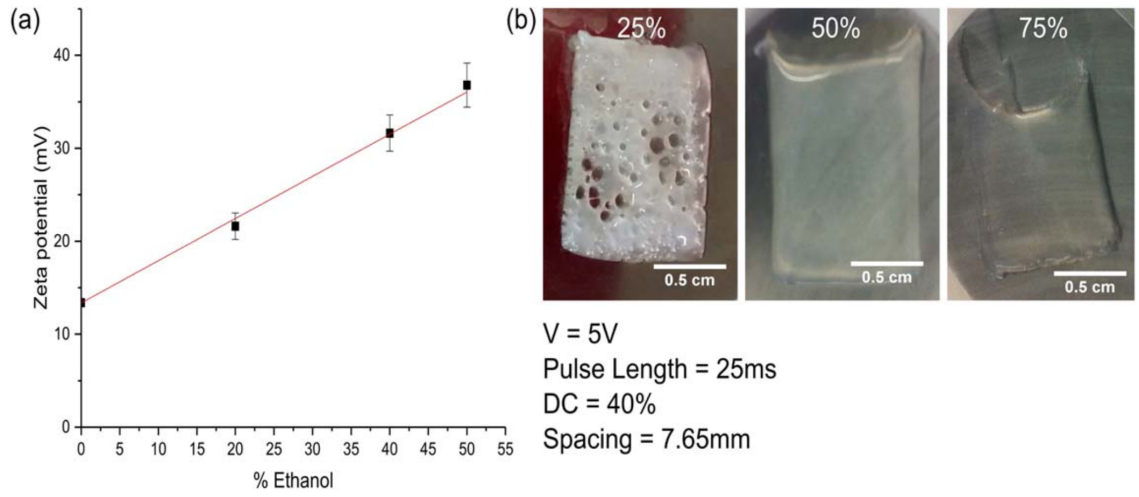

Fig. 2.20 (a) Zeta potential of collagen in suspension as a function of suspensions ethanol percentage. (b) Images of collagen deposits formed by PC-EPD with a range of ethanol suspension vol.%. Figure adapted from reference [25].

Developing Multilayer Composite Films

Upon finding a working EPD window, further study showed it was possible to deposit multiple collagen layers, on top of each other, to build very thick collagen films, and even alternating layers of collagen and hyaluronic acid [24, 25]. Following deposition of a collagen layer onto the electrode, it was left to dry before depositing another layer onto it from a collagen suspension. The study found that additional layers could be deposited onto the substrate with no loss of yield (Figure 2.21). Contrary to ceramics processing, collagen can be deposited indefinitely as charged ions can pass through the bulk of the material, maintaining the flow of electrical current - as ceramic layers build up during deposition they begin to insulate the electrode, developing resistance to current [223].

Investigating EPD Collagen Films

Collagen films produced using EPD were compared with cast collagen films. It was shown that collagen films produced by electrophoretic deposition formed a tightly packed, dense structure, when compared with collagen films produced by solvent casting [25] (Figure

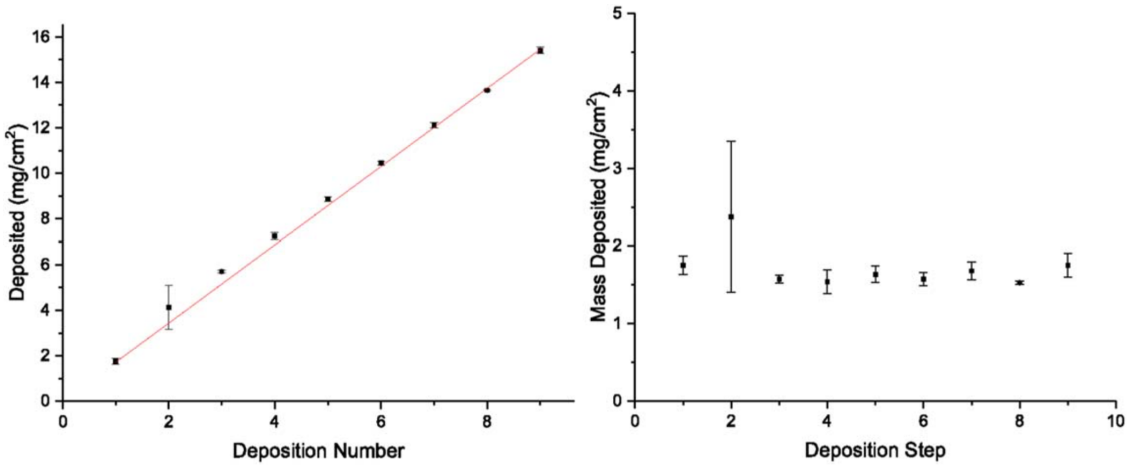

Fig. 2.21 (a) Total deposited mass of collagen with number of sequential depositions. (b) mass of collagen deposited at each step of sequential depositions. Figure adapted from reference [25].

2.22). SEM images of the cross-section of solvent cast films showed loosely packed collagen layers, which had formed as the solvent evaporated. EPD collagen films, on the other hand, showed tightly packed collagen fibres. CryoSEM images were taken of the cross-sections of freeze-fractured films, showing the packing of collagen fibres within a hydrated EPD collagen film. It is difficult to compare accurately between these two, however, as the EPD sample was hydrated at the time of imaging.

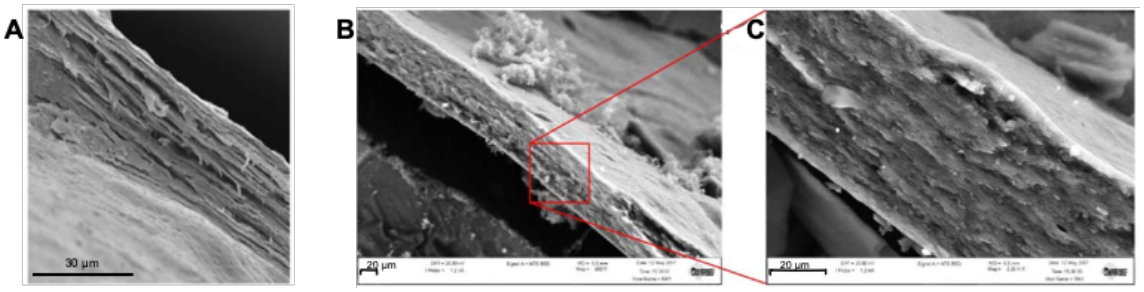

Fig. 2.22 (A) SEM image of cross-section of collagen film formed via solvent casting. (B & C) CryoSEM images of hydrated collagen film formed via pulsed-current EPD at 5 V deposition voltage. Figure adapted from reference [24].

The work in these studies showed that collagen films can be produced using EPD and seemingly had a greater packing density than cast collagen films. Furthermore, it was shown

that multilayer composite collagen hyaluronic acid films could also be produced. Despite these findings, the use of EPD has not yet been been exploited beyond what could also be achieved through solvent casting methods to produce biomaterial films. The research within this thesis builds upon the findings from Barrett et al., to further develop collagen films fabricated using electrophoretic deposition.

2.5 Conclusions and Thesis Aims

Collagen is the main structural protein and most abundant protein in mammals. Collagen presents itself as an ideal biomaterial candidate due to its structural properties, natural abundance, low toxicity, immunogenicity, and antigenicity, bioactivity, and degradation properties *in vivo*, and thus has been researched extensively in the fields of tissue engineering and regenerative medicine. Electrophoretic deposition is a materials processing technique that has been researched for decades, and is favourable due to its ease of use, low-cost, and scalability. EPD processing was applied to insoluble collagen to produce large, seamless collagen films at low cost - a process that was optimised such that reproducible, defect-free collagen films can be easily manufactured. EPD is a versatile technique, and EPD processing of insoluble collagen allows for development of collagen membranes with improved material properties.

The discussion in this Chapter has shown the versatility of EPD and its potential for collagen processing to form biomaterial films. However, while collagen films have been produced using EPD, much of the process is not well characterised, and thus far, this technique requires much longer deposition times than are typically seen in EPD systems, including other pulsed current EPD deposits of biological macromolecules. Collagen has only been deposited at 5 V, beyond which bubbles begin to form, whereas in other aqueous EPD systems higher voltages are applied without the same issues. Furthermore, while EPD is a versatile technique, the collagen films produced via EPD are not dissimilar to cast collagen films, and do not contain additional beneficial properties, thus far. There is evidence, however, that EPD collagen films have a greater density than cast collagen films, though this has not been investigated further. Therefore, this thesis will aim to investigate these themes further, specifically:

- Understand why insoluble collagen I electrophoretic deposition cannot be run at higher voltages without bubble formation and investigate how the processing efficiency can be improved.
- Develop a deeper understanding of pulsed current EPD of insoluble collagen by characterising and modelling the process.
- Utilise the potential of EPD to deposit onto substrates of any shape to create non-planar and textured collagen films, and develop a method of removing these films from the substrate.
- Investigate the density of collagen films produced using EPD and understand what effect this has on the film degradation properties.
- Develop collagen films with enhanced mechanical properties using EPD, which would otherwise be difficult to produce via casting methods.

Chapter 3

Dialysis of Collagen Suspensions

3.1 Introduction

3.1.1 Background

As reported in Section 2.2.7, aqueous suspensions necessitate pulsed-current electrophoretic deposition (PC-EPD) in order to minimise the nucleation of gas bubbles at the electrode [140, 154]. Insoluble collagen suspensions are particularly sensitive to gas bubbles forming within the collagen deposits, and such EPD systems can only function within a narrow range of parameters [25]. Even under pulsed-current parameters, it was found that a deposition voltage of greater than 5 V would always result in the nucleation of bubbles within the collagen film. However, below a deposition voltage of 5 V there was not sufficient force to deposit the insoluble collagen and form a film [24]. Thus, the only voltage where desirable films could be produced was at 5 V. Furthermore, at such low voltages the deposition time to produce a viable collagen film was extremely long (greater than five hours), compared with other EPD processes [113].

It has been shown, in other studies, that PC-EPD of aqueous suspensions can be run at much higher voltages than those performed by Barrett et al., without the formation of bubbles

[168–171]. The use of ultra-pure water in these systems keeps the current low even at higher voltages, minimising the electrolytic effect of EPD on the water. Barrett et al. also used ultra-pure type I deionised water, as well as acetic acid and ethanol, to suspend the insoluble collagen, yet bubble nucleation still frequently occurred at relatively low deposition voltages [25]. This could be due to excess charge carriers within the system causing the current to increase greatly, even at low voltages.

Extracting collagen from animal tissue often requires extensive treatments, which can involve, but are not limited to, salts, acids, alkalis, and enzymes [40, 42, 48–51]. With these treatments, although collagen powder is washed before being used, it is possible that some residual charge-carrying ions, such as salts, remain within product. Thus, when hydrated, the collagen may release these residual charge-carrying ions into the aqueous media, causing an increased current during EPD, in turn resulting in a higher likelihood of electrolysis. It is difficult, however, to know if this is true for all collagen suppliers, as they are likely to use different extraction and purification processes, and such processes are not readily known to customers.

If such charge-carriers are within the insoluble collagen suspension it would be desirable to remove them prior to electrophoretic deposition. Dialysis is a process involving a semipermeable membrane separating two solutions. The semipermeable membrane allows small molecules to pass through it freely, while larger molecules are prevented from doing so. Small molecules will diffuse through the membrane, moving from high concentration to low concentration [224]. The solution to be dialysed, in this case the collagen suspension, is dialysed against pure water such that the rate of diffusion of small molecules out of the suspension is maximised. The semipermeable membrane allows these impurities to pass through and leave the suspension, but the large, long-chained collagen molecules remain in suspension [225].

3.1.2 Aims

This study seeks to determine if there are excess charge-carriers within insoluble type I collagen suspensions and to remove such charge-carriers, via dialysis, prior to EPD. The contents within undialysed collagen suspensions may vary between collagen suppliers and tissue source, due to differing extraction protocols. Here, collagen suspensions formed from tendon and dermal sources from three different collagen suppliers will be compared to explore differences in suspension and deposition characteristics, and to give deeper understanding to the dialysis protocol in removing excess charge-carriers. All experiments were performed with collagen from Sigma and Devro suppliers, while, due to limited availability, Collagen Solutions collagen was only investigated in a limited number of experiments, primarily the EPD experiments.

3.2 Materials and Methods

3.2.1 Collagen Hydration

Collagen from three different suppliers were hydrated to test their respective behaviour and as-received composition. Collagen type I from bovine Achilles tendon (Sigma Aldrich, C9879, and Collagen Solutions) and from bovine skin (Devro Medical and Collagen Solutions) were individually hydrated in 0.05M acetic acid at 4 °C for 72 hours. Once hydrated, each type of collagen from the three suppliers was homogenised on ice for 30 minutes at 10,000 RPM using a T 18 digital Ultra-Turrax homogeniser (IKA), until almost completely homogeneous with no large particles.

Table 3.1 Insoluble collagen type I suppliers and the corresponding sources

Supplier	**Tissue Source**
Sigma Aldrich	bovine Achilles tendon
Devro Medical	bovine skin
Collagen Solutions	bovine Achilles tendon
Collagen Solutions	bovine skin

3.2.2 Dialysis of Collagen Suspensions

Cellulose dialysis membranes (Sigma Aldrich, D9527-100FT and D9402-100FT), with a molecular weight cut-off of 14 kDa, were hydrated in deionised water for 15 minutes, after which, one end of the tubing was sealed. Homogenised collagen suspensions to be dialysed were filled into the dialysis membranes, ensuring no air bubbles were present, and the membranes were sealed. The collagen-filled dialysis membranes were then placed in a large beaker of type I ultra-pure deionised water, known as dialysate, for 2 hours at room temperature. After 2 hours the deionised water (dH_2O) was drained and replenished with fresh dH_2O. Following another 2 hours, the dH_2O was replenished again, and the dialysis membranes were left in the water for 24 hours at room temperature. The dialysis membranes

were then removed from the dialysate and the collagen suspensions were emptied from them into beakers.

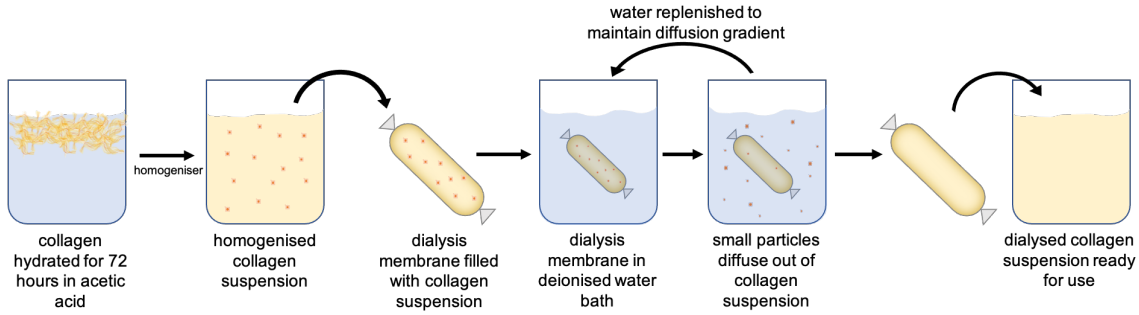

Fig. 3.1 Schematic showing the preparation of dialysed collagen suspensions. Collagen suspensions were first hydrated in 0.05 M acetic acid for 72 hours before being homogenised. Homogenised collagen suspensions were filled into dialysis membrane tubing and placed into a bath of deionised water to dialyse, where the water was replenished regularly to remove dialysed particles and maintain a strong diffusion gradient.

3.2.3 Collagen-Ethanol Suspensions

Ethanol was added to collagen suspensions to reduce the electrolytic effect associated with aqueous EPD [24]. With all collagen suspensions, unless otherwise stated, ethanol was added such that the final suspension was 50 vol.% ethanol (collagen was hydrated at double the concentration needed, such that adding the ethanol diluted collagen down to the required concentration). The suspension was then homogenised on ice again for another 30 minutes at 10,000 RPM using a T 18 digital Ultra-Turrax homogeniser (IKA) to ensure the media was well mixed and to further break down the collagen. Lastly, the suspension was blended at 21,000 RPM in a PB25EX Bar Blender (Waring Commercial) for 2 minutes to break down the last collagen particles, leaving the suspension entirely homogeneous.

3.2.4 pH Measurements

The pH of collagen suspensions and deionised water dialysates was determined using an HI 4222 pH meter (HANNA).

3.2.5 Zeta Potential

Zeta potential profiles were measured for Sigma and Devro collagen suspensions only, due to limited supply of Collagen Solutions material, to understand if these values differed for insoluble collagen I from different sources.

Initially, 0.05 wt.% collagen suspension was prepared as described in Sections 3.2.1, 3.2.2, and 3.2.3. The suspension was decanted into 10 ml beakers and the pH of each measured, with a HI 4222 pH meter (HANNA), and adjusted using 0.01 M HCl and 0.1 M NaOH to produce acid and alkali conditions, respectively, of known pH. These modified suspensions were then filtered through a Millex-SV filter with 5 µm pore size to produce a suspension containing particles of approximately 5 µm or smaller.

Zeta potential measurements were carried out using laser Doppler electrophoresis with a Zetasizer Nano-ZS (Malvern Instruments). Approximately 1 mL of suspension was added to a disposable folded capillary cell, which was then placed inside the Zetasizer. Once the Zetasizer was initialised, the sample was left to stabilise for 120 seconds before running. For each sample, 3 data sets were taken, each data set was determined from averaging measurements. By taking multiple measurements for each data set it was possible to confirm that the particles were not aggregating during measurement. For each pH value, 3 repeats were made, resulting in 9 data sets.

3.2.6 Viscosity

Viscosity profiles were observed only for Sigma and Devro collagen suspensions only, due to limited supply of Collagen Solutions material, to understand if these values differed for insoluble collagen I from different sources.

Collagen suspensions of differing concentrations, ranging from 0 wt.% to 1 wt.%, were prepared, both dialysed and undialysed, as described in Sections 3.2.1, 3.2.2 and 3.2.3. Viscosity measurements were taken using a DV3T Rheometer (Brookfield). 0.5 mL was

pipetted into the base of the rheometer, and the rheometer was sealed shut before running. For each measurement, a CPA-40Z disc was used, the temperature was 23.1 °C, the speed was 5 RPM, the shear rate was 37.5 s^{-1}, and the conditioning time was 30 seconds. For each concentration, 3 repeat measurements were made. After each measurement the base and disc of the rheometer were removed and cleaned with deionised water, before the next measurement was made.

3.2.7 Electrophoretic Deposition

EPD Rig

Electrophoretic deposition was carried out in a custom-built EPD cell, as depicted in Figure 3.2. The cell was formed of two plastic walls and bases, within which were two 316L stainless steel electrodes separated by silicone rubber spacers, as shown in Figure 3.2. The electrodes were connected to a B2901A Source Meter Unit (SMU) (Keysight Technologies) to provide a voltage/current source.

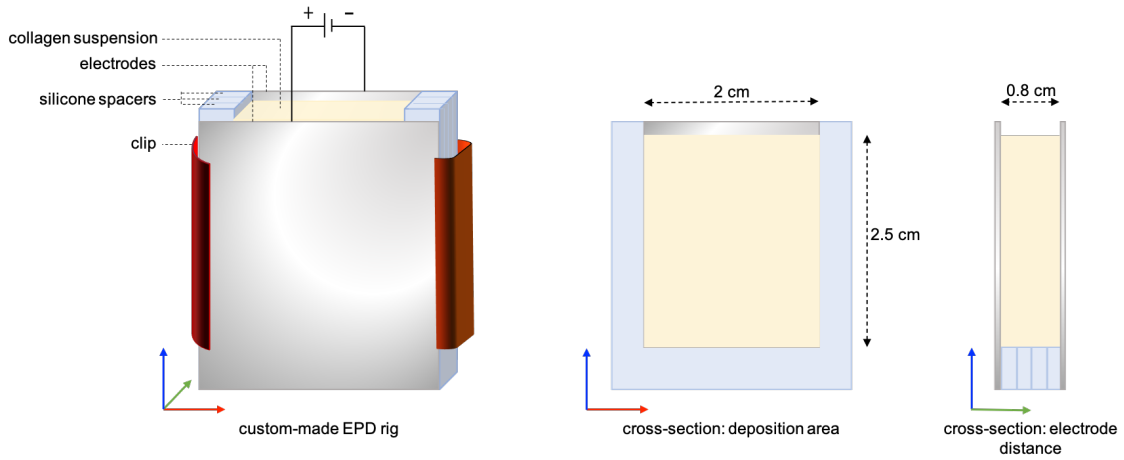

Fig. 3.2 Schematic of electrophoretic deposition rig, showing the electrodes separated by silicone spacers, held together with clips, with the collagen suspension loaded between the electrodes.

EPD Software

The SMU was connected via Universal Serial Bus (USB) to a computer, through which the processing parameters could be controlled using computer software. Quick I/V Measurement Software (Keysight) was used to generate waveforms for deposition, which were then implemented to the SMU via USB. As well as outputting an electrical source, the software was also able to measure the current and voltage of the EPD system at given time intervals. The software options allowed for choice of output (voltage/current), waveform (DC, PC, sinusoidal, custom etc.), frequency, amplitude, duration, and employed voltage/current limiters for safety.

Electrophoretic Deposition of Collagen Suspensions

Electrophoretic deposition of both undialysed and dialysed collagen suspensions from Sigma, Devro, and Collagen Solutions was carried out to understand the behaviour of collagen from different sources when subjected to EPD in aqueous media. Prior to deposition 0.25 wt.% collagen suspensions were prepared for each different collagen type (Table 3.1), as described in Sections 3.2.1, 3.2.2, and 3.2.3. For each collagen suspension, 4 mL was loaded into the EPD cell. Each deposition was run for 6 hours and the power supply was turned off before removing the depositing electrode and allowing the collagen film to air dry for 24 hours.

3.2.8 Current Measurements

Current measurements during EPD were taken for of both undialysed and dialysed collagen suspensions from Sigma, Devro, and Collagen Solutions to understand the EPD process over a greater range of collagen sources.

The current during deposition was measured using the Quick I/V Measurement Software (Keysight). Unless otherwise stated, current measurements were taken once every 60 seconds during depositions.

3.2.9 Conductivity

The conductivity was measured for dialysates of collagen suspensions from Sigma, Devro, and Collagen Solutions to understand the dialysis process for a greater range of collagen sources.

Collagen suspensions were dialysed against type I deionised water dialysates at a fixed ratio of 1:10 (collagen suspension : dialysate), where the volume of collagen suspensions was also fixed at 100 mL Furthermore, collagen suspensions were filled into equal sized dialysis membranes, such that the dialysis membrane surface area was equal for all suspensions during dialysis.

The conductivity of dialysates, after dialysis of collagen suspensions, was measured using the EPD rig and accompanying measurement software (section 3.2.7). 4 mL of each dialysate was filled into the EPD rig, which was run at 5 V for a short time. During this time the current was measured for the system. The conductivity (σ) for the dialysates was calculated using the following relationships:

$$R = \frac{V}{I} \tag{3.1}$$

$$\rho = \frac{RS}{d} \tag{3.2}$$

$$\sigma = \frac{1}{\rho} \tag{3.3}$$

where R is the resistance (Ω), V is the voltage (V), I is the current (A), ρ is the resistivity (Sm) of the collagen suspension, S is the deposition area / cross-sectional area of the collagen suspension (m^2), and d is the distance between the electrodes (m).

3.2.10 Collagen Concentration

The concentration of Sigma collagen suspensions, post-dialysis, was determined by taking a known volume of collagen suspension within a well plate and freeze-drying the suspension, using a bench-top freeze-drier (Virtis), to leave only the dry collagen. The mass of dehydrated collagen remaining was then measured using an AG204 Balance (Mettler Toledo). The concentration of the suspension, prior to freeze-drying, was calculated by dividing the measured mass by the known volume of suspension placed into the freeze-drier:

$$concentration = \frac{mass}{volume} \tag{3.4}$$

3.2.11 EDX Analysis

Energy-dispersive X-ray spectroscopy (EDX) was performed on dialysate residues from both Sigma and Devro collagen suspensions to discover what elements had been dialysed out of the suspensions. EDX analysis was not performed on dialysates from Collagen Solutions suspensions due to insufficient quantity.

To determine which elements had been removed from the collagen suspensions during dialysis, liquid dialysates were evaporated and dried in a drying oven for 72 hours, leaving dehydrated residues. The remaining residues were then investigated with energy-dispersive X-ray spectroscopy (EDX) analysis, to determine the elemental composition removed from the collagen suspensions during dialysis. The residues were coated with a thin layer of platinum prior to being placed in the electron microscope. EDX analysis was performed

using a Nova NanoSEM, and live SEM imaging was used to visualise suitable particulates, obtained from the residue, to analyse. Micrographs were taken of the analysed regions.

3.2.12 Statistical Analysis

Statistical analysis was performed and graphs generated from the collected data using Graphpad Prism 8 software.

3.3 Results

3.3.1 Collagen suspensions

Collagen type I from Sigma and Devro sources were each hydrated and homogenised to form 0.25 wt.% suspensions, as shown in Figure 3.3. Both suspensions contained type I collagen, however they were from different donor sites; tendon and dermal, respectively. The Sigma collagen suspension was not entirely homogenised after being blended and there were still some small aggregates of collagen present, whereas the collagen supplied from Devro formed a smooth and homogenous suspension.

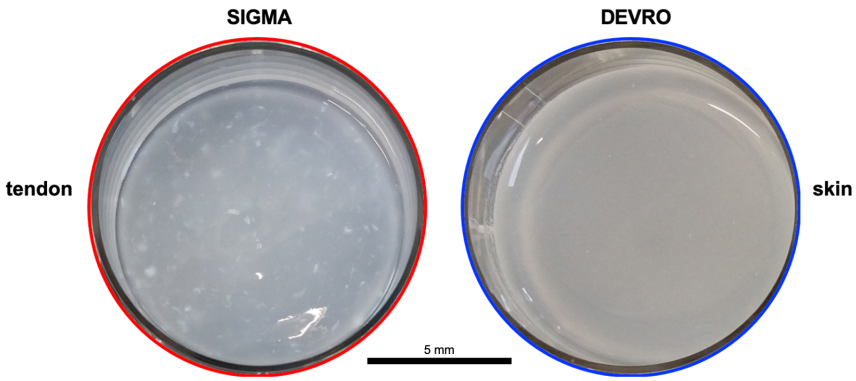

Fig. 3.3 Images of homogenised collagen suspensions in glass beakers. Sigma imaged in the left and Devro imaged on the right.

3.3.2 Zeta Potential

Zeta potential measurements were taken over a range of pH values for both dialysed and undialysed Sigma and Devro type I collagen suspensions (Figure 3.4). The greatest value for zeta potential was achieved at a pH of 3, for both dialysed and undialysed Sigma and Devro collagens. Beyond pH 5, the zeta potential curves for Sigma and Devro diverged significantly, though continued to follow a similar trend.

The zeta potential of the collagens behaved similarly both before and after dialysis. In particular, the zeta potential remained high at pH 3 for dialysed collagen, which shows that

the dialysis process did not adversely effect the collagen zeta potential and it was still suitable for EPD, even after dialysis.

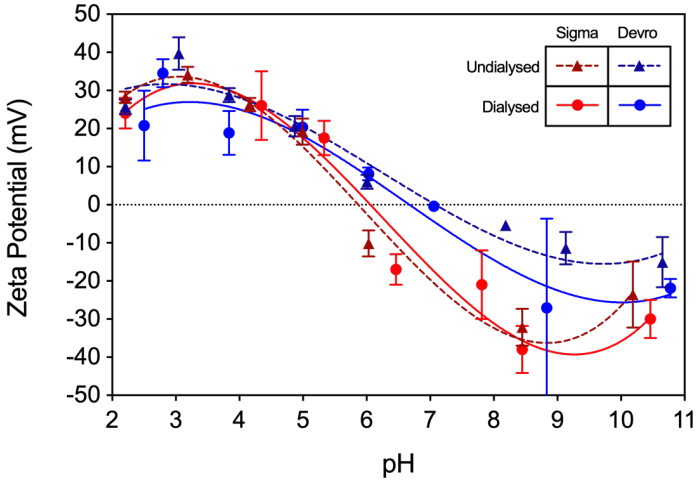

Fig. 3.4 Zeta potential measurements of 0.05 wt.% collagen in suspension as a function of pH, Sigma in red and Devro in blue, undialysed in a darker shade with dashed line and dialysed in a lighter shade with solid line.

3.3.3 Viscosity

Viscosity measurements were taken for both dialysed and undialysed, Sigma and Devro collagen suspensions, over a range of collagen concentrations in suspension (Figure 3.5). The viscosity for both dialysed and undialysed collagen suspensions increased exponentially with increasing collagen concentration. Furthermore, following dialysis, the viscosity of collagen suspensions was greater than undialysed collagen suspensions, even at the same concentrations. Additionally, it was found that Sigma collagen suspensions had a greater viscosity than Devro suspensions of the same concentration, and, while dialysis increased viscosity, dialysed Devro suspensions had a lower viscosity than undialysed Sigma suspensions.

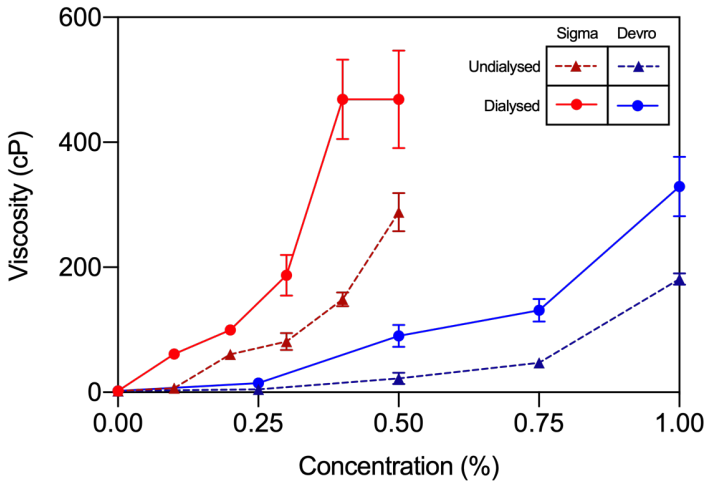

Fig. 3.5 Viscosity measurements of collagen suspensions, before and after dialysis, as a function of collagen concentration. Sigma in red and Devro in blue, undialysed in a darker shade with dashed line and dialysed in a lighter shade with solid line.

3.3.4 Collagen Concentration

The concentration of collagen in suspension was determined for both undialysed and dialysed Sigma collagen, to determine if dialysis caused a change to collagen concentration in suspension (Figure 3.6). The measured collagen concentration increased linearly with the original prepared concentration of collagen. The measured concentration of collagen in suspension remained unchanged for undialysed collagen, however the concentration of collagen in suspension decreased for dialysed collagen suspensions with respect to the original prepared concentration, though the fractional decrease remained broadly consistent for all measured concentrations.

3.3.5 Current and Voltage Measurements

Current measurements were taken during depositions of Sigma, Devro, Collagen Solutions - Dermal, and Collagen Solutions - Tendon collagen suspensions of concentration 0.25 wt.%. Collagen Solutions were included in the investigation here as it was most important to understand how dialysis affected collagen suspensions being used for electrophoretic

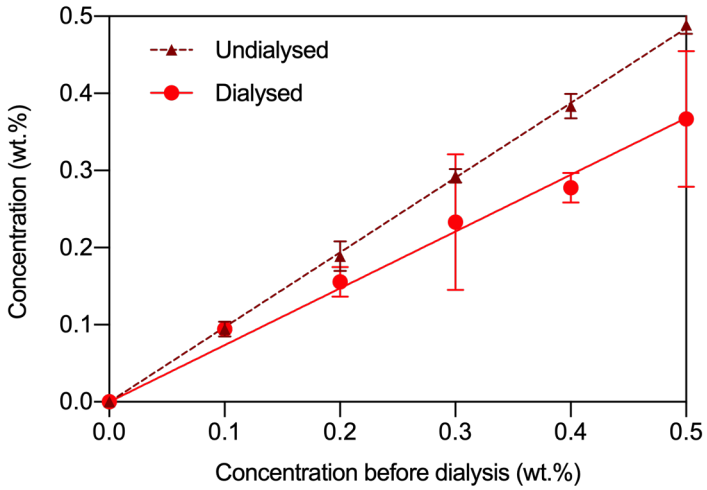

Fig. 3.6 Concentration measurements of Sigma collagen suspensions as a function of prepared collagen concentration. Dialysed collagen in light red with solid line and undialysed in dark red with dashed line.

deposition. Each of the collagen suspensions were deposited as both undialysed and dialysed suspensions. All depositions were run using exactly the same parameters of 5 V applied voltage, 40% duty cycle, 0.05 s pulse period - the parameters suggested for uniform, bubble-free depositions of collagen [25].

The measured current for each collagen source varied significantly, under the same conditions. It can be seen in Figure 3.7 that measured current within the undialysed Devro EPD system was more than double that for undialysed Sigma, at any given time, with both undialysed Collagen Solutions collagens giving current measurements about halfway between Sigma and Devro, showing a similar current measurement throughout, despite coming from different tissue sources. As well as varying in magnitude, the measured current profiles with respect to time also varied. In the initial phase, the current in the Sigma system increased slightly, before plateauing, whereas in the Devro system, after an initial rise, the current dropped slightly, then, after hitting a minimum value, increased gradually with respect to deposition time. Collagen Solutions Tendon collagen showed a current that initially dropped

before plateauing, whereas the dermal-sourced Collagen Solutions collagen had no such initial phase.

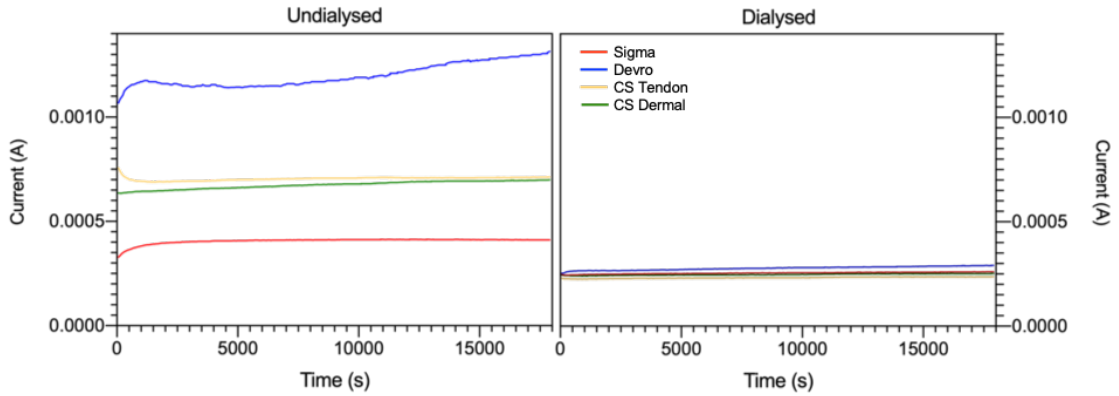

Fig. 3.7 Current measurements during depositions for Sigma (red), Devro (blue), Collagen Solutions - Tendon (yellow), and Collagen Solutions - Dermal (green) collagen. Current measurements were taken for undialysed collagen suspensions (left) and for dialysed collagen suspensions (right). All depositions were performed with equal parameters: 0.25 wt.% collagen suspensions, with 5 V applied voltage, 40% duty cycle, and 0.05 s pulse period. Plots are an average of three repeats.

Collagen suspensions that had been dialysed all showed a decreased current measurement during deposition compared with their undialysed counterpart. Furthermore, the degree of difference in current measurements, as compared with undialysed suspensions, varied throughout. There were similar values of current for each of the dialysed collagen suspensions at equal voltage, suggesting that the suspensions had been standardised by the dialysis process.

The two different collagen products from Sigma and Devro also varied in the quality of the deposited films. Barrett [25] proposed EPD parameters that gave uniform, bubble-free collagen films, for Sigma collagen suspensions. When using these parameters for Devro collagen suspensions large bubbles formed within the deposit, and the stainless steel electrode also corroded significantly (Figure 3.8). This resulted in a poor quality film, contaminated with impurities. When, however, the Devro collagen suspension had been dialysed prior to EPD the deposit formed, under the same deposition parameters, was defect-free and similar

to that of the Sigma collagen suspension. Unlike the undialysed Devro collagen deposit, the dialysed deposit did not contain bubbles or cause corrosion of the electrode.

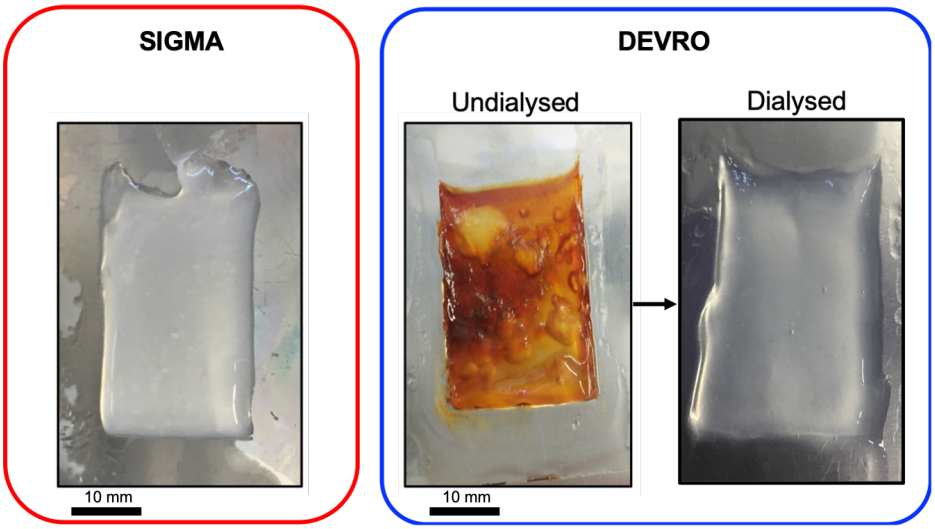

Fig. 3.8 Photographs of undialysed Sigma collagen (red box) and Devro collagen (blue box). Images of Devro collagen shows deposits of both undialysed (left) and dialysed (right) suspensions, prior to EPD. Images were taken immediately after deposition, while deposits were still wet. Both samples were formed under the same parameters: 0.25 wt.% collagen suspensions, 5 V applied voltage, 40% duty cycle, 0.05 s pulse period, 36000 s run time.

3.3.6 Conductivity of Dialysates

The conductivity of the deionised water dialysates used against each of the collagen suspensions was determined following dialysis (Figure 3.9). Furthermore, for comparison, the conductivity of deionised water was also calculated; this shows the conductivity of the dialysates prior to dialysis.

The conductivity of the deionised water was less than 0.001 S/m. Following dialysis of the collagen suspensions, the conductivity for all dialysates increased significantly. The conductivity of the dialysate from the Devro collagen suspension increased the most, with Sigma collagen suspension dialysate conductivity increasing the least. Furthermore, the conductivity of the Devro collagen dialysate increased significantly more ($p < 0.0001$) than

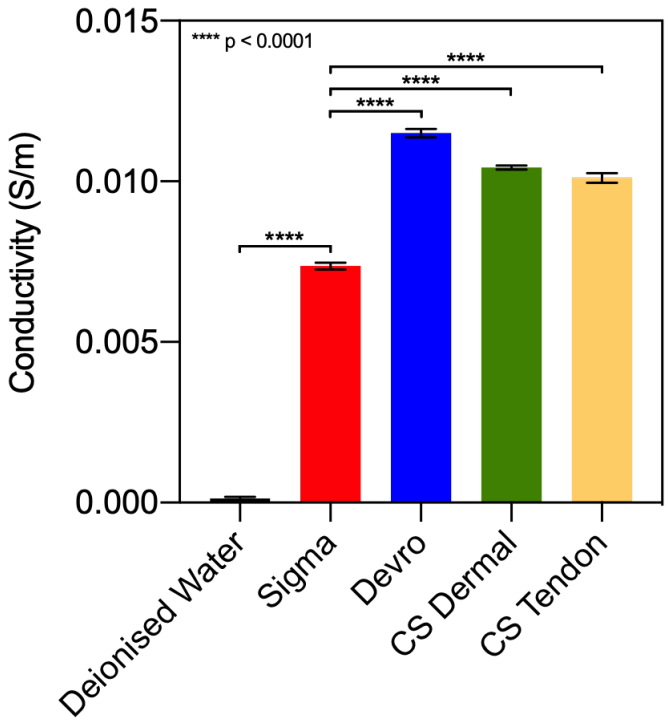

Fig. 3.9 Conductivity measurements of deionised water (grey) and the dialysates used against collagen suspensions. The conductivity measurements of the dialysates were taken after collagen suspensions had been dialysed. Respective collagen suspensions were formed from different collagen suppliers: Sigma (red), Devro (blue), Collagen Solutions - Dermal (green), and Collagen Solutions - Tendon (yellow).

that of the Sigma collagen; the same is also true for the dialysates from Collagen Solution collagens.

The relative amount by which each dialysate increased in conductivity, following dialysis, corresponded to the conductivity of the respective undialysed collagen suspension (Figure 3.10); Devro collagen had the highest measured current and the respective dialysate had the greatest conductivity (corroborated in Figures 3.7 and 3.9, respectively).

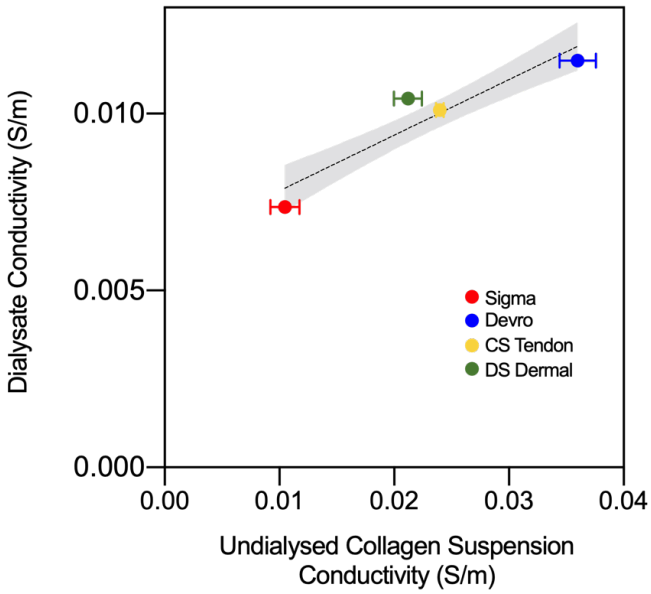

Fig. 3.10 Conductivity of dialysates as a function of the conductivity of collagen suspensions prior to dialysis. The conductivity measurements of the dialysates were taken after collagen suspensions had been dialysed. Respective collagen suspensions were formed from different collagen suppliers: Sigma (red), Devro (blue), Collagen Solutions - Dermal (green), and Collagen Solutions - Tendon (yellow).

3.3.7 pH of Dialysates

The pH of the dialysates, as well as deionised water, was also measured following dialysis of corresponding collagen suspensions (Figure 3.11). The deionised water had a measured pH of 5.5, which is slightly acidic. All the dialysates had a lower pH than that of the deionised water, between pH 3 and 4, showing that they become more acidic during the dialysis process; for all dialysates this was shown with statistical significance, where $p < 0.01$. Furthermore, there was no significant difference ($p > 0.05$) in the pH of Sigma and Devro dialysates, following dialysis.

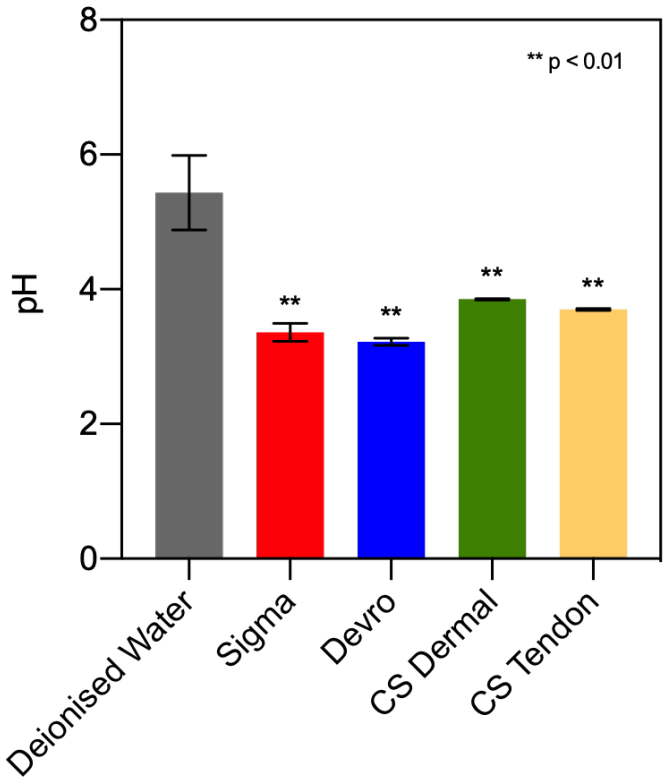

Fig. 3.11 pH measurements of deionised water (grey) and the dialysates used against collagen suspensions. The pH measurements of the dialysates were taken after collagen suspensions had been dialysed. Respective collagen suspensions were formed from different collagen suppliers: Sigma (red), Devro (blue), Collagen Solutions - Dermal (green), and Collagen Solutions - Tendon (yellow).

3.3.8 Mass of Dehydrated Dialysates

The dialysates from Sigma and Devro collagen suspensions were dehydrated to leave a residue (Figure 3.12). There was an insufficient quantity of Collagen Solutions collagen to include these samples in the investigation. More residue was observed for the Devro collagen dialysate, compared with that from the Sigma dialysate, and the mass of residue from the Devro collagen dialysate was more than double the mass recovered from Sigma (Figure 3.12).

The greater mass removed from Devro corresponded with the greater suspension conductivity before dialysis and higher dialysate conductivity following dialysis, when compared

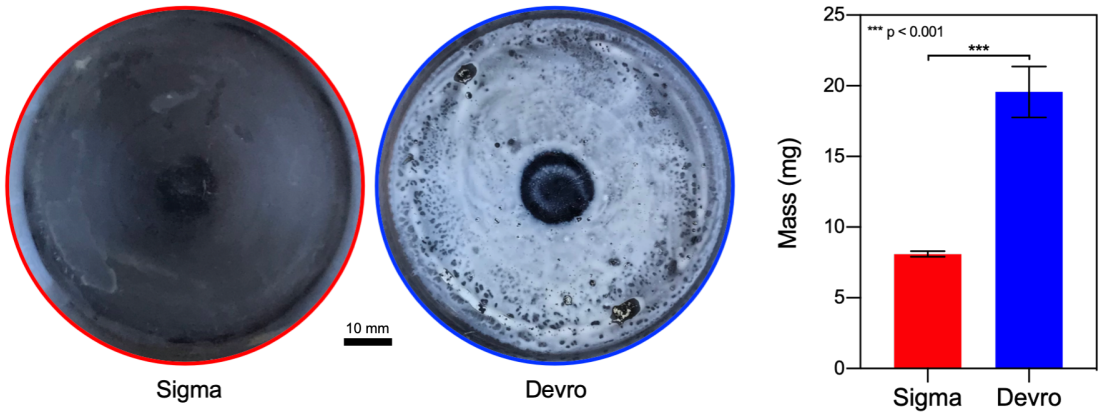

Fig. 3.12 Photographs of residual salts from dehydrated dialysates used against collagen suspensions from Sigma (left) and Devro (middle), and graph (right) showing the measured mass of salts remaining from 100 mL dialysates from Sigma (red) and Devro (blue) collagen.

with Sigma (Figure 3.13). This suggests that mass removed from the collagen suspensions was contributing to the conductivity of undialysed suspensions.

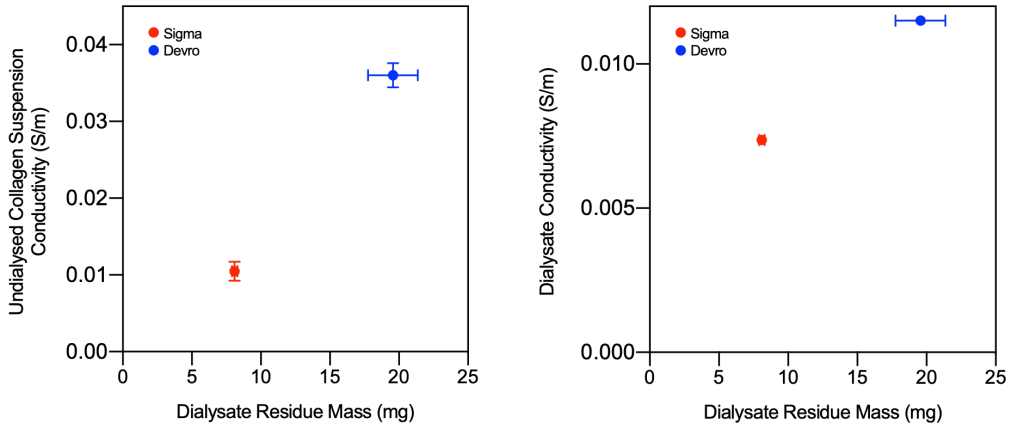

Fig. 3.13 Conductivity of undialysed collagen suspensions (left) and conductivity of dialysates following dialysis (right) as a function of the dialysate residue mass removed during dialysis. Respective collagen suspensions were formed from different collagen suppliers: Sigma (red) and Devro (blue).

3.3.9 EDX Analysis of Dehydrated Dialysates

The residues obtained from the Sigma and Devro collagen dialysates were analysed using energy-dispersive X-ray spectroscopy (EDX) analysis to determine the elemental constituents and composition. The example SEM micrographs acquired in Figure 3.14, A and C, show some of the residue structures obtained from the Sigma and Devro dialysates. The emission spectra for the dialysate residues in Figure 3.14 have unique peaks, which correspond to different elements, where the height of these peaks is broadly related the relative amount of each element. Within the graphs the peaks and corresponding elements have been highlighted and labelled. The results of this EDX analysis, along with the rest of the analyses, have been summarised in Table 3.2.

Table 3.2 EDX analysis results for dialysates from dialysis of Sigma and Devro collagen suspensions.

		Sigma		**Devro**	
Element	Atomic Number	Mean Weight %	Mean Atomic %	Mean Weight %	Mean Atomic %
C	6	25.11 ± 4.67	40.43 ± 5.39	23.06 ± 6.34	37.55 ± 7.78
O	8	30.52± 1.42	36.86 ± 1.43	25.73 ± 1.09	31.42 ± 3.05
Na	11	7.84 ± 1.79	6.59 ± 1.85	13.28 ± 1.65	11.28 ± 1.56
S	16	0.63 ± 0.91	0.38 ± 0.53	1.56 ± 0.48	0.95 ± 0.27
Cl	17	10.36 ± 0.38	5.72 ± 0.51	14.60 ± 2.43	8.15 ± 1.86
K	19	0.24 ± 0.04	0.12 ± 0.03	1.52 ± 0.67	0.76 ± 0.29
Ca	20	12.73 ± 2.35	6.15 ± 1.46	20.24 ± 4.25	9.89 ± 2.70
Cu	29	4.34 ± 0.64	1.31 ± 0.26	0.00 ± 0.00	0.00 ± 0.00
Zn	30	8.21 ± 0.81	2.44 ± 0.37	0.00 ± 0.00	0.00 ± 0.00

The atomic proportion of each element found in the Sigma and Devro dialysate residues is plotted in Figure 3.15, with those in red corresponding to what was extracted from Sigma collagen and that in blue showing the same for Devro. Here, the relative proportions for each element can be compared between Sigma and Devro, but it is important to note that this does not compare the actual amount of residue left from the two collagen sources, as seen

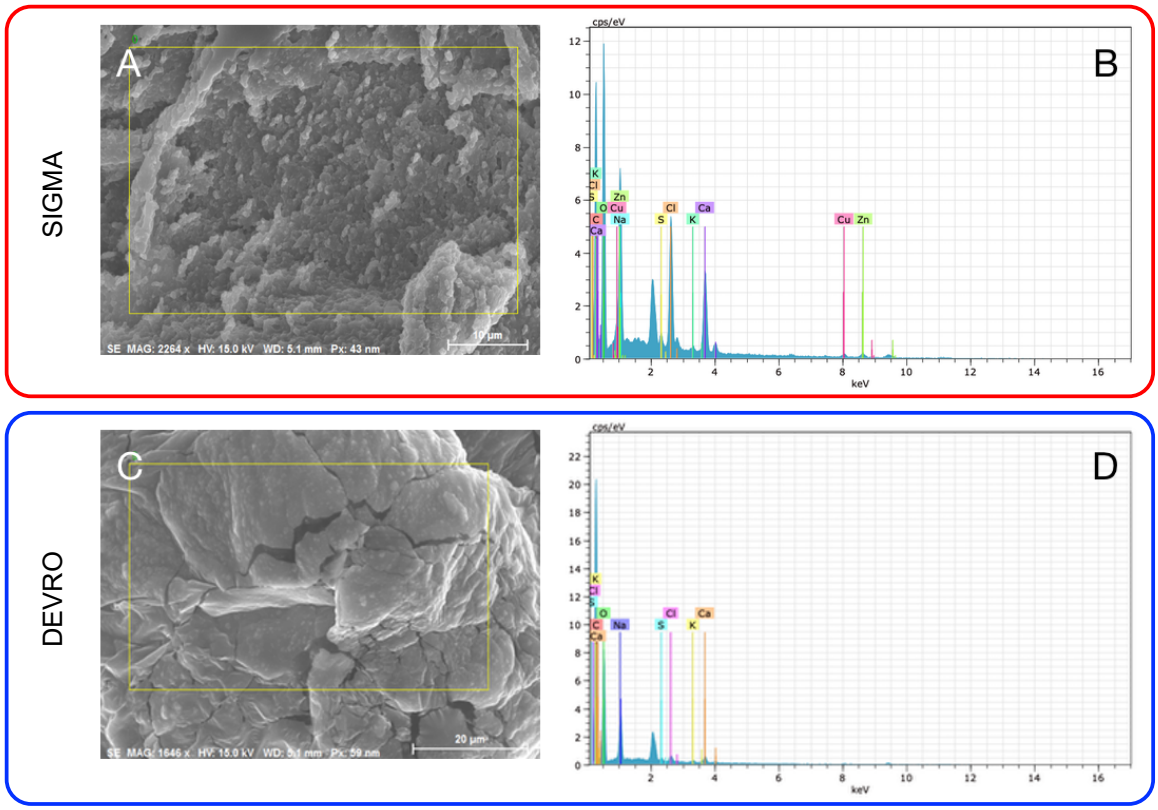

Fig. 3.14 SEM images (A and C) of salts from dialysate from dialysed Sigma and Devro collagen suspensions, where the yellow box signifies the region where EDX analysis has been performed. Graphs of EDX analysis results (B and D) for corresponding SEM images. Within the graphs peaks have been labelled with corresponding elements. The results presented in this figure are just one example from Sigma (red) and Devro (blue) dialysates from multiple analyses.

earlier in Figure 3.12. The majority of the residues for both collagen sources were made up of carbon and oxygen, and the relative proportion of carbon and oxygen was similar for both Sigma and Devro. The proportions of the remaining elements were similar in both Sigma and Devro, with larger numbers of sodium, chlorine, calcium atoms, and fewer sulphur and potassium. The residues' elemental constituents only differed where Sigma contained small amounts of copper and zinc, which were not present in Devro.

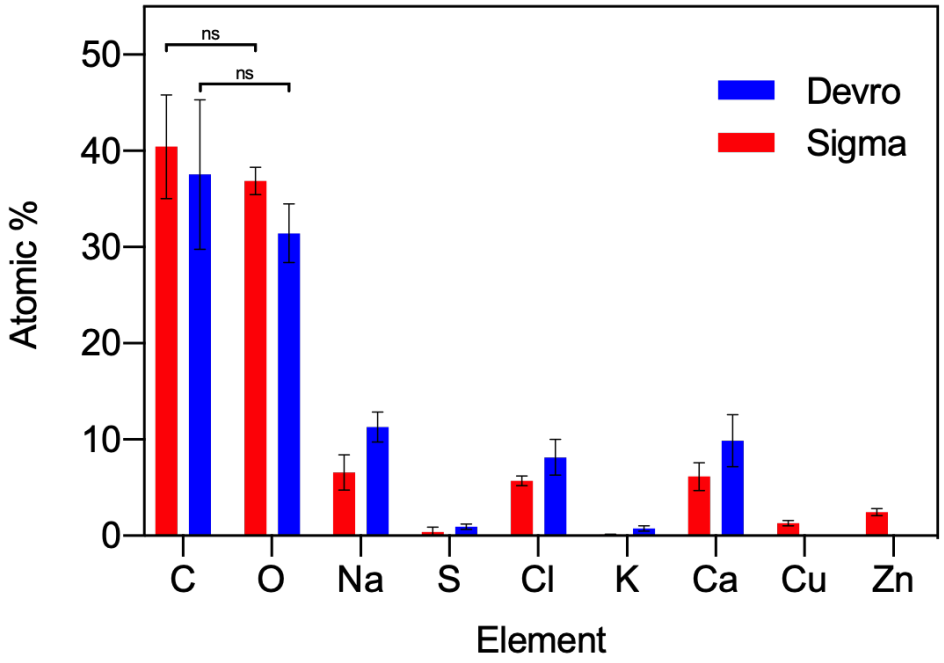

Fig. 3.15 Composition and atomic % of elements found in dialysates from dialysed Sigma (red) and Devro (blue) collagen suspensions.

3.4 Discussion

3.4.1 Effect of Dialysis on EPD of Collagen Suspensions

The nucleation of gas bubbles at the electrode during deposition of collagen suspensions results in severely defected collagen films that are unusable [25]. While it was possible to deposit insoluble collagen I from suspension using Sigma collagen, this was not possible with collagen from other suppliers, such as Devro (Figure 3.8). Due to the great difference seen between Sigma and Devro collagen suspensions, these two were compared for the majority of this study. Furthermore, EPD of Sigma collagen I could only be done at very low voltages (5 V), meaning deposition times were extremely long. It was proposed that dialysis of collagen suspensions prior to EPD could remove charge-carrying ions, which could be present as a result of the collagen extraction processes from tissue [48].

Initial comparison of homogenised Sigma and Devro collagen suspensions (Figure 3.3) showed that the Devro collagen suspension was much smoother and did not contain any lumps of collagen. The benefit of this when processing it with EPD is that the deposits that form on the electrode are much more homogeneous throughout, and devoid of lumps. This verified the difference between collagen suppliers, even when both are collagen type I, and that some may be more preferable (or cheaper). Thus, removing constraints on which collagen supplier can be used for EPD is greatly advantageous.

Collagen type I suspensions, from different suppliers — including Collagen Solutions as the effects of dialysis for EPD usage were the key aim of this study — were investigated during EPD, before and after dialysis. The current measured during EPD of collagen suspensions showed that, for undialysed suspensions, Devro had a much higher current than Sigma, with Collagen Solutions in the middle (Figure 3.7, left). This suggested that there were excess charge-carriers within these suspensions, as they were all subject to the same voltage (5 V) during EPD. Furthermore, the increased current measured during Devro

collagen EPD is corroborated by the poor condition of the deposit on the electrode, depicted in Figure 3.8. Following dialysis, however, the current measured during EPD of collagen suspensions not only decreased for all suspensions, but they were all approximately equal (Figure 3.7, right). This implies that thorough dialysis removed all excess charge-carrying ions from the suspensions, leaving only the collagen I, and that dialysis is an important step for standardising collagen suspensions prior to EPD. This is further strengthened by the resulting deposit from dialysed Devro collagen, compared with undialysed, which formed a smooth, defect-free collagen film (Figure 3.8, right).

Reducing the conductivity of suspensions not only improved the quality of the deposited collagen films, but it also allowed for more efficient depositions. EPD of dialysed collagen could be performed at higher voltages without the formation of bubbles. Previously, work by Barrett et al. [25] found that 5 V was the highest possible deposition voltage without noticeable hydrogen nucleation. Increasing the deposition voltage increases the rate of deposition significantly [149]. Furthermore, even with the same processing parameter, such as voltage, Ferrari and Moreno [139] found that the conductivity of the suspension plays a key role in deposition time, where reducing the conductivity of the suspension increased the rate of deposition.

3.4.2 Investigating the Dialysate of Dialysed Collagen Suspensions

Following dialysis, the deionised water dialysates, that the collagen suspensions were dialysed against, were also investigated. The conductivity of the dialysates all increased significantly following dialysis (Figure 3.9), where the magnitude of increased conductivity for each dialysate corresponded to the conductivity of the collagen suspension prior to dialysis (Figure 3.7). This relationship was shown in Figure 3.10, indicating that charge-carrying ions within the collagen suspensions are removed into the dialysates during dialysis. This shows clearly

the efficacy of the dialysis process of removing excess charge-carriers from the collagen suspensions.

To understand what had been removed from the collagen suspensions during dialysis, Sigma and Devro dialysates were dehydrated to leave residues. As the dialysates began as ultra-pure deionised water prior to dialysis, removal of the water via dehydration left residues that were only acquired from the collagen suspensions through dialysis. The mass of the remaining residues was compared, as they were from equal volumes of dialysate, dialysed at equal ratios to the collagen suspensions. A much greater mass was removed from the Devro collagen suspension (Figure 3.12), which could explain the disparity in suspension conductivity (Figure 3.13), but it is important to understand that dissolved mass is not indicative of solution conductivity without further investigation. EDX analysis was, therefore, used to identify which elements were present within the residues.

Carbon and oxygen were found in high proportions in both Sigma and Devro dialysates, which can be attributed, in part, to the removal of acetic acid during dialysis, as dialysate pH dropped (Figure 3.11). Note that any hydrogen atoms present are undetectable by EDX due to hydrogen only having one electron shell[1].

It can be seen from Figure 3.15 that both Sigma and Devro dialysates had similar proportions of elements, excluding the presence of copper and zinc in Sigma. This indicates that similar extraction processes could have been used for both. The literature supports that some these elements, including sodium, chlorine, and sulphur, could be present as a result of collagen extraction from tissue [227–230], including from tendon [231] and dermal [232] collagens. The presence of calcium, and zinc and copper in Sigma, however, does not appear to be attributable to extraction processes, and currently are from unknown sources.

[1]Energy-dispersive X-ray (EDX) analysis works by using an X-ray beam to excite electrons within an inner shell of an atom. An electron may jump to an outer shell, leaving an electron hole, which is filled by an electron in an outer shell jumping down into the inner shell. This jump from outer to inner shells emits characteristic X-rays, which are detected [226].

While the elemental compositions found within the dialysates from Sigma and Devro collagen suspensions were similar, the amount of residue was significantly different (Figure 3.12). The relationship between electrolyte concentration and the conductivity of a solution is linear at low concentrations [233] (Figure 3.16); at higher concentrations there is a saturation point, where the relationship becomes non-linear [234]. These collagen suspensions have a low concentration of electrolytes, so an increased amount in one will result in an equally increased conductivity. Furthermore, the elements found are monatomic ions with strong ionic strength, meaning they disassociate readily [235]. Looking at Figure 3.15 it can be determined that the majority of both residues were composed of charged ions (Na^+, K^+, Cl^-, Ca^{2+}). As Devro showed to have a much greater mass of these ions present, this correlates with the much greater conductivity of undialysed Devro suspension compared with Sigma.

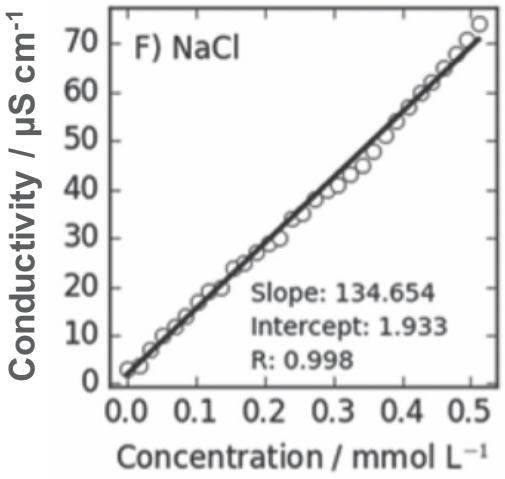

Fig. 3.16 Conductivity of a solution as a function of concentration of NaCl dissolved in the solution. Figure adapted from Reference [233].

3.4.3 Effect of Dialysis on Collagen Suspension Properties

Dialysis of the collagen suspensions and removal of these ions had a significant effect on the conductivity of suspensions (Figure 3.7), but it is important to understand how this process influenced other suspension properties, which can be vitally important for EPD [104]. The

zeta potential was analysed for Devro and Sigma collagen suspensions, both before and after dialysis. Neither zeta potential profile changed greatly for both collagen suppliers. Most importantly, the zeta potential remained unchanged and high (~30 mV) in the acidic region (between pH 3 and 4), the conditions that are used for this EPD. This is crucial as a highly positive or highly negative zeta potentials are required for effective electrophoretic deposition of particles [143, 144, 146].

Viscosity has also been reported to have an influence on EPD, though not to the same extent as zeta potential, and higher suspension viscosities can decrease the rate of deposition [139, 140]. Following dialysis of the suspensions it was seen that the viscosity increased for both Sigma and Devro collagen suspensions (Figure 3.5). While the viscosities increased for both, it is by a relatively small amount and will unlikely have a significant effect on the deposition process. The viscosities of collagen suspensions are heavily dependant on the concentration of collagen in suspension. The concentration of collagen in suspension following dialysis was investigated, but showed that there was, in fact, a slight decrease in concentration (Figure 3.6), and therefore will not have increased the suspension viscosity. Though the concentration decreased this was not due to a loss of collagen mass from the suspension — as the semi-permeable dialysis membrane, with a 14 kDa molecular cut-off weight, does not allow the 300 kDa collagen molecules to pass through — but the increase in water mass within the dialysis membrane. The osmotic pressure difference between the collagen suspension and the deionised water dialysate caused water to pass through the membrane from the dialysate into the suspension (as depicted in Figure 3.17, below), thus, lowering the overall collagen concentration.

It is still of interest to explore the mechanisms influencing viscosity, as this can be important in further studies of collagen suspensions. Polymers, and other long chain macromolecules such as collagen, in suspension can experience dramatic changes in viscosity caused by changes in the conformational or geometric structure of the polymers [236]. In

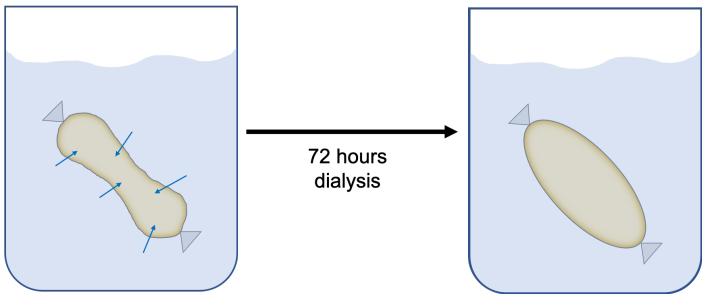

Fig. 3.17 Schematic showing the swelling of dialysis tubing with water during dialysis.

particular, collagen conformations can be affected by pH and ionic strength [237], where high ionic strength results in coiled polymers, whereas low ionic strength suspensions result in uncoiled, extended polymers [238–240]. An example of how this might occur in the presence of ions is depicted below, in Figure 3.18. A lower ionic strength suspension results in a higher viscosity because these elongated polymers are more likely to become entangled with one another, and cannot freely move past each other in suspension, thus, giving a greater viscosity [236, 241].

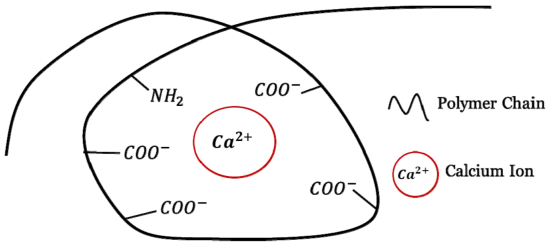

Fig. 3.18 Schematic showing, conceptually, the conformation of a polymer in suspension with negatively charged carboxylate groups coiled around a calcium cation. Figure adapted from Reference [236].

The high ionic strength of the undialysed collagen suspensions may have resulted conformations of collagen fibres that are less viscous than in the low ionic, dialysed suspensions. Collagen type I chains contain outward-facing charged side groups that have been known to have ionic interactions with water and other charged ions [242, 243]. A study by Fathima and Dhathathreyan looked at the effects of surfactants on collagen conformation [244]; surfactants are compounds that lower the interfacial tension of liquids with other liquids,

gases, or solids [245]. They found that the addition of surfactants, such as SDS, reduced the viscosity of collagen solutions significantly and concluded that the charge of surfactants plays an important role in the physico-chemical properties of collagen [244, 246]. Though there is no current research into the interactions of insoluble collagen and ionic strength of suspension, there is evidence that these interactions do occur, particularly between collagen and ionic elements, such as sodium, chlorine, and calcium [247], and removal of the ions could affect the conformation of collagen fibrils. Figure 3.19 depicts how the viscosity of collagen suspensions could be affected by dialysis, and the relationship with ionic strength.

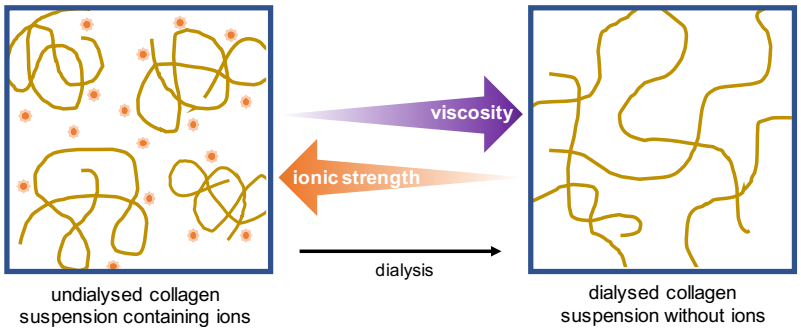

Fig. 3.19 Schematic showing the increase of viscosity of collagen suspensions with reduction in ions, following dialysis.

Lastly, it is clear that there was a significant difference in the viscosity between the Sigma and Devro collagen suspensions, both before and after dialysis (Figure 3.5). This disparity could be due the the fibril length of these two collagens; longer chained polymers are likely to have a greater viscosity owing to there being more opportunity for entanglement and intermolecular interactions [238]. Devro collagen suspensions may have had a lower viscosity due to there being shorter chains of collagen fibrils. Most insoluble collagen is not made up of individual tropocollagen units, which are 300 nm in length and < 2 nm in diameter, but much larger fibrils of collagen; fibrils can be as great as 1 cm in length and 500 nm in diameter [248]. During the extraction of collagen sonication is used to disrupt tissue and collagen, which could cause the fibrils to break down into smaller units [249]. Devro

collagen may be made up of smaller fibrils than Sigma collagen, allowing a much lower viscosity, in general.

3.5 Conclusions

Formation of defect-free collagen films formed by electrophoretic deposition from undialysed collagen suspensions was difficult or impossible, depending on the collagen supplier. Where it was possible, this only occurred within a very narrow range of pulsed-current EPD parameters. It was hypothesised that collagen suspensions contained excess charge-carriers, which had an adverse effect on the EPD process, and that these could be removed via dialysis. Insoluble collagen I suspensions, from various collagen suppliers, were dialysed and the effects of this dialysis were studied.

Dialysis of Sigma and Devro collagen suspensions did not have any effect on the zeta potentials, but found that viscosity increased greatly. This could have been due to conformational changes in the collagen fibrils from the lack of ions within the suspensions. Investigation of the dialysates, and what was removed from the collagen suspensions, showed that several ionic elements, including Na^+, K^+, Cl^-, and Ca^{2+}, were dialysed out. Highly ionic suspensions can cause polymers to coil, whereas the lower ionic strength, dialysed suspensions allowed collagen fibrils to extend, increasing intermolecular interactions, leading to a greater viscosity.

It was shown that, following dialysis, collagen suspensions from Sigma, Devro, and Collagen Solutions had reduced conductivity due to the removal of ions, and the conductivity for all suspensions converged. This allowed for defect-free depositions from these suspensions, and functional EPD parameters could be broadened, allowing for greater deposition voltage and faster deposition times. This showed that not only is dialysis a great tool for standardising collagen suspensions, but that it is also vital for increasing EPD productivity.

Chapter 4

Modelling Pulsed Current Electrophoretic Deposition

4.1 Introduction

4.1.1 Background

Electrophoretic deposition is a well-established processing technique for developing coatings and films. An important aspect of understanding the technique is to be able to predict the mass of material deposited at a given time. This can be useful in determining the operating parameters before running experiments, hence reducing material costs and time. A direct current model has been developed over many years, originally described by Hamaker in 1940 [105], which has undergone several iterations, incorporating key dynamics associated with long deposition times. The DC model, which is described in Section 4.2, is widely accepted, but is only appropriate for DC-EPD systems, and there is no such model available for pulsed current EPD.

The use of aqueous media necessitates the use of pulsed current waveforms to minimise the nucleation of gas bubbles within the deposit. Currently, there is no predictive model

for pulsed current electrophoretic deposition (PC-EPD) that incorporates all the parameters involved in this regime.

4.1.2 Aims

The aim of this chapter is to develop a model for PC-EPD, and to test this for collagen EPD. The model was developed from previously established direct current EPD models with the incorporation of further mathematical elements, taken from literature, to describe the pulsed element of the system. In order for the model to be applied to insoluble collagen EPD systems, characterisation of collagen suspension parameters was required.

4.2 Mathematical Model

4.2.1 Evolution of Direct Current EPD Models

The first attempt to describe EPD kinetics was made by Hamaker in 1940 (Equation 4.1), for planar electrophoretic cells that have parallel electrodes [105]. It is the most basic model, which relates the deposited mass, m (g), with suspension properties, electric field, E (V cm^{-1}), deposition area, S (cm^2) and time, t (s). The suspension properties in this equation include the suspension concentration, C_s (g cm^{-3}), and electrophoretic mobility, μ (cm^{2}s^{-1}V^{-1}).

$$m = C_s \mu S E t \tag{4.1}$$

The electrophoretic mobility, μ, can be expressed in measurable terms as [154]:

$$\mu = \frac{\varepsilon_m \varepsilon_0 \zeta}{\eta} \tag{4.2}$$

where ε_m is the dielectric permittivity of the suspension media, ε_0 is the dielectric permittivity of a vacuum, ζ is the zeta potential of the suspension, and η is the viscosity of the suspension media. The value for dielectric permittivity of a liquid is often available in standard tables, however this becomes more complicated for mixtures. Jouyban et al. [250] determined that the dielectric permittivity of a mixture can be found by inputting values into the following equation:

$$\ln \varepsilon_m = \phi_1 \ln \varepsilon_1 + \phi_2 \ln \varepsilon_2 + \phi_3 \ln \varepsilon_3 + \phi_1\phi_2 \sum_{j=0}^{2} \left[\frac{(\phi_1 - \phi_2)^2}{T} \right] + \phi_1\phi_3 \sum_{j=0}^{2} \left[\frac{(\phi_1 - \phi_3)^2}{T} \right] + \phi_2\phi_3 \sum_{j=0}^{2} \left[\frac{(\phi_2 - \phi_3)^2}{T} \right] + \phi_1\phi_2\phi_3 \sum_{j=0}^{2} \left[\frac{(\phi_1 - \phi_2 - \phi_3)^2}{T} \right] \tag{4.3}$$

where ε_1, ε_2, and ε_3 are the dielectric permittivities of solvents 1, 2, and 3, respectively, within the mixture, ϕ_1, ϕ_2, and ϕ_3 are the volume fractions of each component within the mixture, and T is the temperature (K). The dielectric permitivities of the suspension's media components (water, acetic acid, and ethanol) are shown in Table 4.1.

Table 4.1 Table of dielectric permittivity of suspension media components

Liquid	Dielectric permittivity
Water	80.1
Acetic acid	6.15
Ethanol	24.5

Using the output for ε_m from Equation 4.3 into Equation 4.2, and putting Equation 4.2 back into the Hamaker equation (4.1), we now have an expression in measurable values.

The Hamaker equation, however, assumes a linear relationship between the deposited mass and time, which assumes that the other parameters remain constant with deposition time. For very short deposition times this holds true, as the amount of particles deposited from the media in such a short period are negligibly small and do not affect the suspension concentration, C_s.

The limitations of Equation 4.1 were apparent for Sarkar and Nicholson, who developed a model more suitable for long deposition times [107]. They firstly proposed that not all the particles at the electrode form part of the deposit, so introduced an efficiency parameter, f, to the Hamaker equation, where $0 < f \leqslant 1$, such that if all particles at the electrode form the deposit $f = 1$. This parameter into Equation 4.1 gives:

$$\frac{dm}{dt} = fC_s\mu SE \tag{4.4}$$

For longer deposition times, the suspension concentration will decrease as particles deposit onto the electrode, and, as such, C_s decreases with time. As a result, Sarkar and Nicholson [107] stated that the deposited mass can be related to the solids in suspension with the following equation:

$$m = v(C_0 - C_s) \tag{4.5}$$

where v is the volume of suspension (cm^3) and C_0 is the initial suspension concentration ($g\ cm^{-1}$). Given that:

$$C_0 = \frac{M_0}{v} \tag{4.6}$$

where M_0 is the initial solid mass in suspension (g), Equation 4.5 can be rewritten as:

$$m = \frac{M_0}{C_0}(C_0 - C_s) \tag{4.7}$$

Rearranging Equation 4.7 for C_s we get:

$$C_s = C_0\left(1 - \frac{m}{M_0}\right) \tag{4.8}$$

Combining Hamaker's initial EPD model (Equation 4.4) with this expression for change in concentration (Equation 4.8) we have Sarkar and Nicholson's model for long deposition times [107]:

$$\frac{d}{dt}\left(\frac{m}{M_0}\right) = \frac{1}{\tau}\left(1 - \frac{m}{M_0}\right) \tag{4.9}$$

where τ defines the characteristic time scale:

$$\tau = \frac{M_0}{f\mu SEC_0} \tag{4.10}$$

The characteristic time scale is an inverse of the "kinetics parameter", k, defined by Sarkar and Nicholson [107].

Assuming that the only change in concentration is due to the mass of solids deposited by EPD, for initial time, $t = 0$, the deposited mass is $m(0) = 0$, which leads to the solution of Equation 4.10:

$$m(t) = M_0(1 - e^{-t/\tau}) \tag{4.11}$$

This model by Sarkar and Nicholson [107] has been widely accepted in the literature since its conception [134], which shows that the mass deposited at time t is a function of the initial solid, increasing at an exponential rate defined by the kinetics parameter. For short times, it reduces down to the original model by Hamaker [105] and it is also able to predict deviations from linearity of deposited mass during electrophoretic deposition, with respect to time, for constant-voltage regimes [251, 252].

A theory was described by Biesheuvel et al. [141], based on the equations for planar and cylindrical depositions by Hamaker [105] and Avgustinik [253], respectively. The theory showed that a factor was missing due to a non-linear relationship between suspension concentration and deposition yield, and was in agreement with the Sarkar model [107], but further pointed out the need to incorporate charge balance (Poisson equation) into models. It has been shown that the resistivity of colloidal suspensions depends directly on the solid concentration [140, 254–256].

Despite this being accepted, none of the previous models accounted for the change in resistivity during the deposition process. A new model was therefore developed by Ferrari et al. [142] in 2006, which modelled the relationship between concentration and resistivity during aqueous EPD. In this study, with experimental results, they determined a linear relationship between solids concentration and suspension resistivity, in an aqueous zirconia suspension.

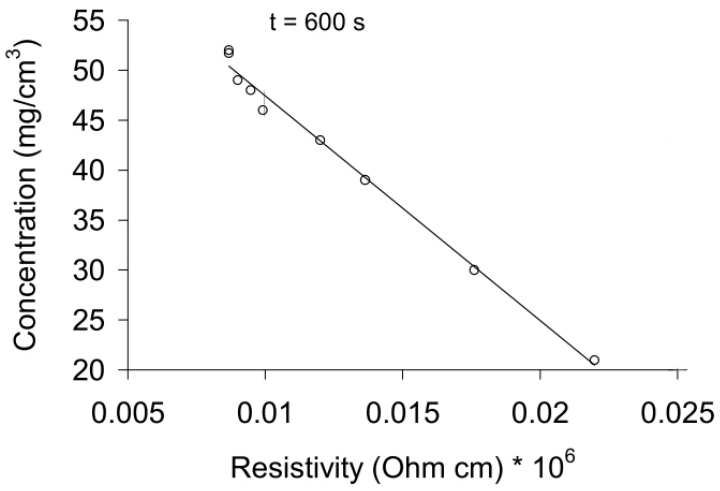

Fig. 4.1 The relationship of solids concentration as a function of resistivity. Figure adapted from Reference [142].

From this, Ferrari et al. [142] determined that the dependence of resistivity of solids concentration can be expressed as:

$$\rho = \rho_\infty - (\rho_\infty - \rho_0)\frac{C_s}{C_0} \tag{4.12}$$

where ρ_∞ is the resistivity of the suspension at infinite time (Ω) (i.e. when $C_s = 0$) and ρ_0 is the initial resistivity of the suspension (Ω). Now substituting Equations 4.8 and 4.12 into 4.4 a differential equation is obtained:

$$\frac{d}{dt}\left(\frac{m}{M_0}\right) = \frac{1}{\tau_0}\left(1 - \frac{m}{M_0}\right)\left(1 + \left(\frac{\rho_\infty}{\rho_0} - 1\right)\frac{m}{M_0}\right) \tag{4.13}$$

where τ_0 is the characteristic time scale at initial time, defined by Equation 4.10, where $\rho = \rho_0$. Assuming the same conditions used to solve Equation 4.11 ($m(0) = 0$) the solution to Equation 4.13 is:

$$m(t) = M_0\left(1 - \frac{1}{1 + \dfrac{\rho_0}{\rho_\infty}(e^{t/\tau_\infty} - 1)}\right) \tag{4.14}$$

where τ_∞ is the characteristic time scale at infinite time, defined by Equation 4.10, where $\rho = \rho_\infty$. This equation reduces down to the Sarkar and Nicholson model [107] when $\rho_\infty = \rho_0$, and at extremely small times (i.e. $t << \tau_\infty$) it reduces down to the linear Hamaker Equation [105].

In the study by Ferrari et al. [142] they validated their resistivity model by plotting the deposited mass of zirconia and comparing it to the predictive model, as seen in Figure 4.2. They also compared its efficacy to the Sarkar and Nicholson model [107], which for shorter times still holds true but becomes less valid at longer deposition times.

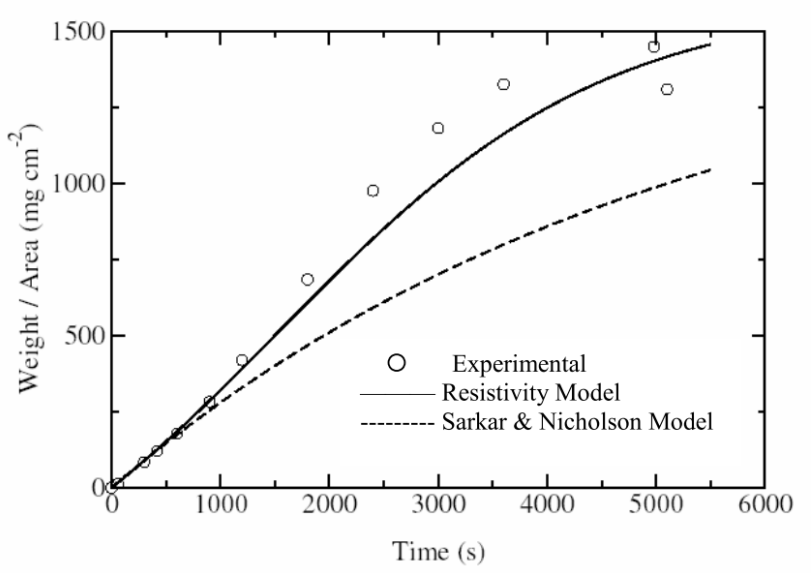

Fig. 4.2 Comparison of the resistivity model and the Sarkar and Nicholson model to experimental results. Figure adapted from Reference [142].

The curves and experimental data shown in Figure 4.2 are corroborated by results given in other studies for long deposition times, in both aqueous [257, 258] and non-aqueous suspensions [148, 259, 260].

4.2.2 Developing a Pulsed EPD Model

The previous model has proven sufficient for predicting deposit yield for direct current (DC) electrophoretic deposition, but does not account for the kinetics involved in pulsed current (PC) EPD. Due to the nature of PC-EPD the kinetics become much more complicated, with an increased number of parameters required to describe the process, such as duty cycle and pulse period. The pulse period is the duration of time of one full pulsed cycle during PC-EPD, $(T_{ON} + T_{OFF})$. The duty cycle is the proportion of time the current is applied for one pulse period $(T_{ON}/[T_{ON} + T_{OFF}])$, given as a percentage. These can affect several factors such as local pH at the substrate and variations in particle movement (i.e. diffusion), that are a symptom of the applied current being turned off for periods of time. The following section aims to describe a predictive model for pulse current EPD.

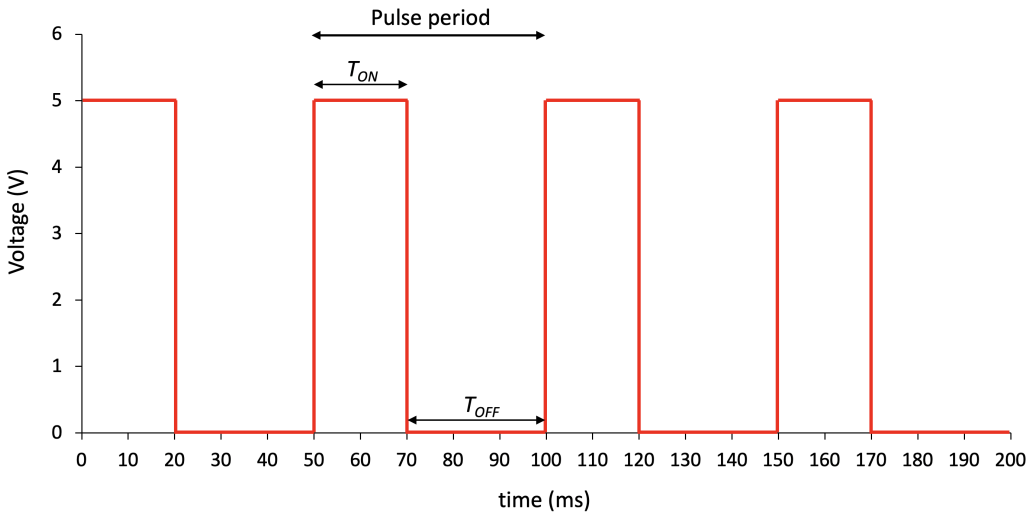

Fig. 4.3 Pulsed current waveform schematic with 40% duty cycle and 50 ms pulse period, showing T_{ON} and T_{OFF} regions.

There are two separate kinetic effects acting on particles in suspension during PC-EPD: electrophoretic motion in a finite electric field, and diffusion, when the applied electric field is on and off, respectively [261]. Assuming the particles are well dispersed in suspension prior to EPD, there will be no diffusion. Applying an electric field across the charged particles will cause them to accumulate at the oppositely charged electrode, resulting in a concentration gradient. This gradient will grow until the electric field is removed, at which point the particles begin to diffuse away from the electrode, along the concentration gradient. It is therefore suggested that the movement of particles towards the depositing electrode can be described with the following dimensionless parameter, κ [261]:

$$\kappa = \frac{L_e - L_D}{V_{eph}\lambda} \tag{4.15}$$

where L_e is the electrophoretic movement length and L_D is the diffusion length, as vectors in the direction of the deposition electrode, when the electric field is on and off, respectively.

As previously shown, λ is the pulse period (s) and V_{eph} is the steady-state velocity of a particle under an electric field, which can be expressed as [262]:

$$V_{eph} = \mu E \tag{4.16}$$

The pulsed current parameter, κ (equation 4.15), determines the movement of particles in a PC system compared with the same particles in a DC system, such that $0 \leqslant \kappa \leqslant 1$. Where the fraction denominator, $V_{eph}\lambda$, would be the particle displacement under a DC field for one pulse period, and the numerator, $L_e - L_D$, is the displacement of particles with the PC system for the same time. Furthermore, if $L_e = L_D$ deposition would be zero, as diffusion counteracts any electrophoretic movement, and if $L_e - L_D \ll V_{eph}\lambda$, then $\kappa \to 0$, and electrophoretic movement is so small that deposit yield would be negligible.

It is necessary, therefore, that κ accounts for the parameters of the pulsed waveform: applied voltage/current, frequency, and duty cycle. For this, the electrophoretic movement length, L_e, and the diffusion length, L_D, can be expressed as [155, 261]:

$$L_e = V_{eph}\delta\lambda \tag{4.17}$$

$$L_D = \sqrt{2Dt} = \sqrt{2D(1-\delta)\lambda} \tag{4.18}$$

where δ is the duty cycle, and D is the diffusivity of the particles in suspension, which is defined by the Einstein-Smoluchowski equation for the diffusion of charged particles [263]:

$$D = \mu k_B T \tag{4.19}$$

where k_B is Boltzmann's constant. By putting Equation 4.17 and Equation 4.18 into Equation 4.15, κ can now be expressed as:

$$\kappa = \frac{V_{eph}\delta\lambda - \sqrt{2D(1-\delta)\lambda}}{V_{eph}\lambda} \tag{4.20}$$

This revised equation for κ has been developed, in this chapter, from several sources and is proposed as the factor that is necessary for a pulsed current EPD model. Because the pulsed current parameter, κ, affects the deposition kinetics it is suitable for it to be merged into the kinetic determining parameter of the EPD model, τ (Equation 4.10). The pulsed current characteristic time scale now becomes:

$$\tau = \frac{M_0}{f\mu SEC_0\kappa} \tag{4.21}$$

Notice that for a duty cycle of 100% ($\delta = 1$), i.e. a DC system, $\kappa = 1$ and Equation 4.21 becomes equal to Equation 4.10, and the model acts exactly as a DC system.

Characterizing the Collagen Suspension

For the model to be implemented effectively, it is necessary to gather information about the collagen suspension that is needed for the model. This chapter describes the characterisation of variables of the collagen suspension, such as zeta potential, viscosity, and resistivity, so that the model could be easily and effectively implemented.

4.3 Materials and Methods

4.3.1 Collagen Preparation

Collagen from two different sources was characterised in this study. Collagen type I from bovine achilles tendon (Sigma Aldrich, C9879) and from bovine skin (Devro Medical) were each hydrated to form collagen suspensions. They were each hydrated in 0.05 M acetic acid at 4 °C for 72 hours. Once hydrated, the suspensions were homogenised on ice for 30 minutes at 10,000 RPM using a T 18 digital Ultra-Turrax homogeniser (IKA), until almost completely homogeneous with no visibly large particles. The hydrated collagen suspensions were then dialysed against deionised water, following the protocol in Section 3.2.2. Ethanol was added to the dialysed collagen suspensions such that the final suspension was 50 vol.% ethanol (collagen was hydrated at double the concentration needed, such that adding the ethanol diluted collagen to the required concentration). The suspensions were then homogenised on ice for a further 30 minutes at 10,000 RPM to ensure the media was well mixed and to further break down the collagen. Lastly, the suspensions were blended at 21,000 RPM in a PB25EX Bar Blender (Waring Commercial) for 2 minutes to break down the remaining collagen particles, leaving the suspension entirely homogeneous. Suspension pHs were measured, with a HI 4222 pH meter (HANNA), and adjusted to 3.5 using 0.01M HCl if needed.

4.3.2 Zeta Potential

Initially, 0.05 wt.% collagen suspensions were prepared as described in Section 4.3.1. The suspensions, of pH 3.5, were then filtered through a Millex-SV filter with 5 μm pore size to produce a suspension containing particles of approximately 5 μm or smaller.

Zeta potential measurements were carried out using laser Doppler electrophoresis with a Zetasizer Nano-ZS (Malvern Instruments). Approximately 1 mL of suspension was added to a disposable folded capillary cell, which was then placed inside the Zetasizer. Once the

Zetasizer was initialised, the sample was left to stabilise for 120 seconds before running. For each sample, 3 data sets were taken, each data set was determined from averaging measurements. By taking multiple measurements for each data set it was possible to confirm that the particles were not aggregating during measurement. For each pH value, 3 repeats were made, resulting in 9 data sets.

4.3.3 Viscosity

Suspensions comprising 0.25 wt.% collagen were prepared as described in Section 4.3.1. Viscosity measurements were taken using a DV3T Rheometer (Brookfield). 0.5 mL was pipetted into the base of the rheometer, and the rheometer was sealed shut before running. For each measurement a CPA-40Z disc was used, the temperature was 23.1 °C, the speed was 5 RPM, the shear rate was 37.5 s^{-1}, and the conditioning time was 30 seconds. After each measurement the base and disc of the rheometer were removed and cleaned with deionised water, before the next measurement was made.

4.3.4 Electrophoretic Deposition

Electrophoretic deposition was carried out in a custom built EPD cell, as depicted in Figure 4.4. The cell was formed of two 316L stainless steel electrodes separated by silicon rubber spacers. The EPD cell was designed with specific dimensions, labelled in Figure 4.4, for accurate comparisons to the model. The electrodes were connected to a B2901A Source Meter Unit (SMU) (Keysight Technologies) to provide a voltage/current source. The SMU was connected via Universal Serial Bus (USB) to a computer, through which the processing parameters could be controlled using computer software, explained further in Section 4.3.5. Prior to deposition, collagen suspensions were prepared, as described in Section 4.3.1. A volume of 4 mL of suspension was pipetted into the EPD cell. After each deposition, the

power supply was turned off and the depositing electrode was removed. The collagen film was air dried for 24 hours.

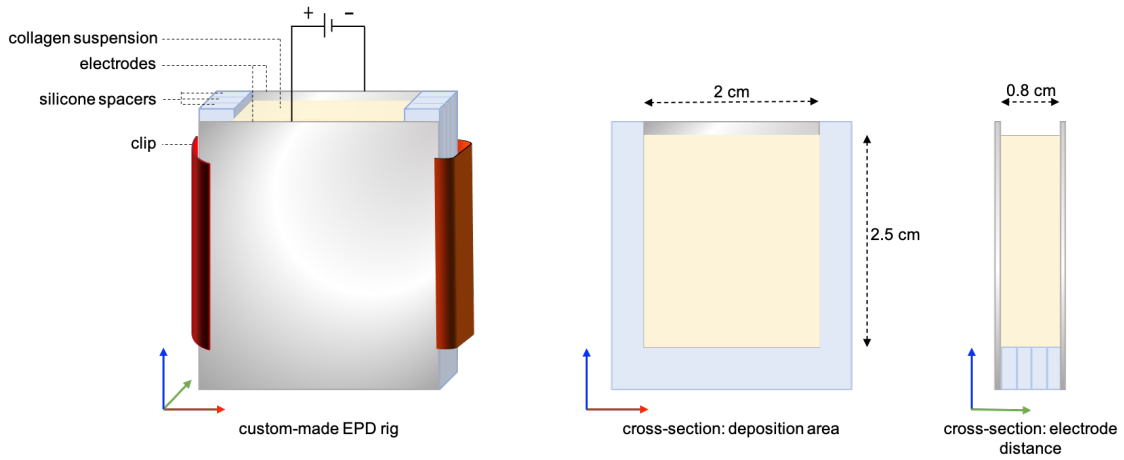

Fig. 4.4 Schematic of electrophoretic deposition rig, showing the electrodes separated by silicone spacers, held together with clips, with the collagen suspension loaded between the electrodes. The cell dimensions are shown in the cross-sectional views, required to model the system.

4.3.5 Current Measurements

Quick I/V Measurement Software (Keysight) was used to generate waveforms for deposition, which were then implemented to the SMU via USB. The software outputted an electrical source, and also measured the current and voltage of the EPD system at given time intervals. The software options allowed for choice of output (voltage/current), waveform (DC, PC, sinusoidal, custom etc.), frequency, amplitude, duration, and employed voltage/current limiters, for safety. EPD was run with a pulsed current at different voltages, with a pulse period of 50 ms and duty cycle of 40%, unless otherwise stated. The SMU, and accompanying Quick I/V Measurement Software, was used to measure the currents during collagen depositions.

4.3.6 Resistivity

The resistivity of collagen suspensions, at the beginning and end of depositions, was calculated from the measured currents and known applied voltages and EPD cell dimensions through the following relationships of Ohm's Law:

$$R = \frac{V}{I} \tag{4.22}$$

$$\rho = \frac{RS}{d} \tag{4.23}$$

where R is the resistance (Ω), V is the voltage (V), I is the current (A), ρ is the resistivity (Sm) of the collagen suspension, S is the deposition area / cross-sectional area of the collagen suspension (cm^2), and d is the distance between the electrodes (cm).

4.3.7 Deposited Collagen Mass

The mass of collagen deposited during EPD was measured using a AG204 Balance (Mettler Toledo). The mass of the depositing electrode was determined prior to deposition. After deposition, the electrode, with deposited collagen, was removed from the EPD cell and left to dry, leaving a collagen film adhered to electrode. The mass of the electrode and film was then measured. The mass of collagen deposited was determined by finding the difference in these two measurements.

4.3.8 Deposition Model

The pulsed current deposition model was built using the programming language Python 3.0, using the equations from Section 4.2, in particular the resistivity model described by Equation 4.14, with the proposed pulsed current characteristic time scale, τ, in Equation 4.21, which features the pulsed current parameter, κ, Equation 4.20.

The predictive model, which was coded for in Python 3.0 (the script can be found in Appendix A), provided deposited mass as a function of time. Results of the model were saved as an array of the values generated as a .csv file, so that the data could be used and plotted further in other software packages.

4.3.9 Statistical Analysis

Statistical analysis was performed and graphs generated from the collected data using Graphpad Prism 8 software.

4.4 Results

4.4.1 Zeta Potential

Zeta potential measurements were taken for both Sigma and Devro collagen suspensions at pH 3.5 (Figure 4.5), to assess there were a differences between the collagen sources and to find an appropriate value for the PC-EPD model. It was found that collagen supplied by both Sigma and Devro had similar zeta potentials at pH 3.5 of around 35 - 40 mV, and that, statistically, there was no difference between the two ($p > 0.05$). Thus, an average zeta potential value for collagen I was determined to be 38 mV, shown in purple in Figure 4.5.

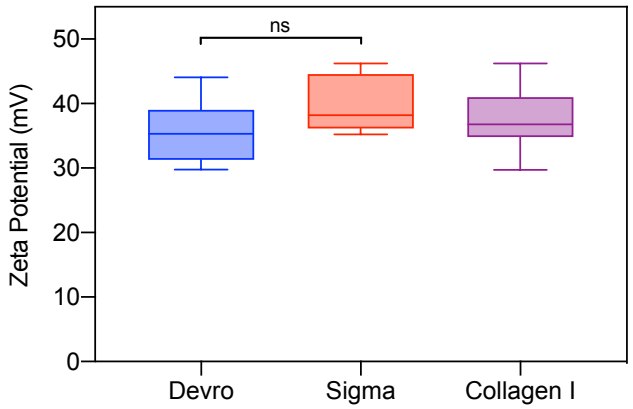

Fig. 4.5 Zeta potential measurements of 0.05 wt.% collagen in suspension at pH 3.5, Devro in blue, Sigma in red, and data combined from for Sigma and Devro collagen in purple.

4.4.2 Viscosity

The viscosities of suspensions of collagen supplied by both Sigma and Devro were measured at 0.25 wt.% collagen concentration; the concentration adopted as the standard for insoluble collagen EPD [24, 25]. It was found that the viscosity for Sigma collagen suspensions was significantly greater than Devro ($p < 0.0001$) at the same concentration.

These collagen suspensions, of equal concentration but significantly different viscosities, were deposited under the same pulsed-current parameters, both for two hours, and the dry

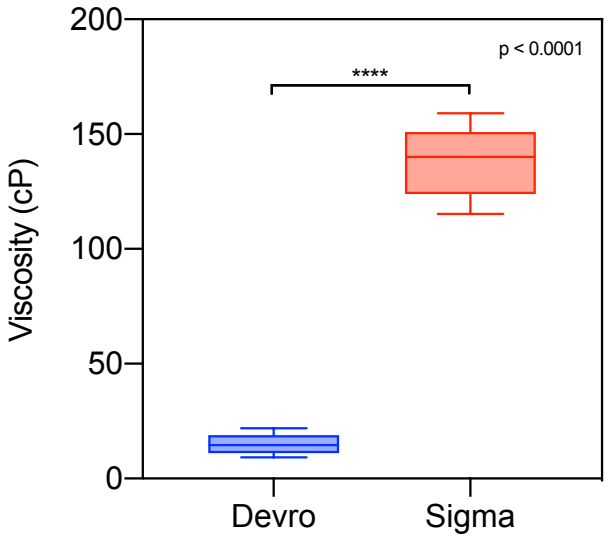

Fig. 4.6 Viscosity measurements of collagen suspensions at collagen concentration 0.25 wt.%, Devro in blue and Sigma in red.

deposited mass was measured (Figure 4.7). It was found that, after equal deposition times, the deposited mass for both Sigma and Devro were not significantly different ($p > 0.05$). This indicated that overall suspension viscosity did not have an effect on EPD deposition, and confirmed that the viscosity of the suspension media, which remained constant for both (0.89 cP), was the important factor for the model.

4.4.3 Resistivity

The current was measured during deposition of collagen suspensions at a range of deposition voltages (Figure 4.8), in order to determine the resistivity of the suspensions. It can be seen that initially the current increased with time before plateauing and becoming constant. The rate at which the current increased correlates positively with voltage, and with current levelling out sooner at higher voltages.

These results were then used to determine the suspension resistivity values for use within the EPD model. Resistivity was calculated using the equations of Ohm's Law. The calculated resistivity results of suspensions at the initial phase of deposition and at the end of deposition

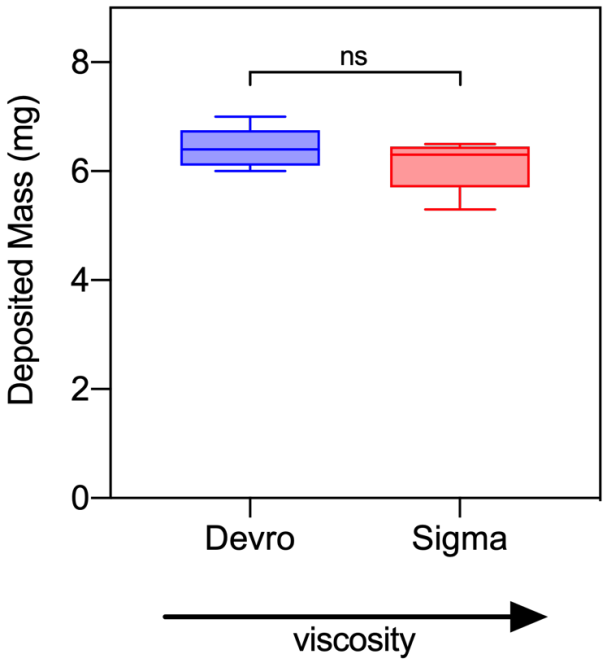

Fig. 4.7 Deposited mass of collagen via EPD of 0.25 wt.% collagen suspensions, Devro in blue and Sigma in red. EPD parameters: 6V applied voltage, 2 hour deposition time, 0.05 s pulse period, 40% duty cycle.

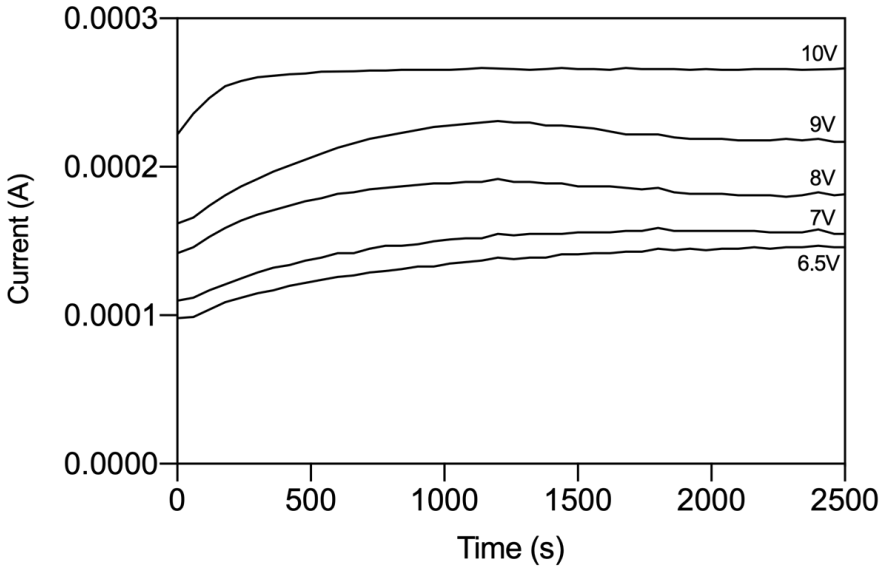

Fig. 4.8 Measured current over time of 0.25 wt.% collagen suspensions at varying applied voltages.

are shown below, in Figure 4.9. It can be seen that the resistivity of collagen suspensions dropped slightly throughout deposition, which is corroborated by the increase of current during EPD.

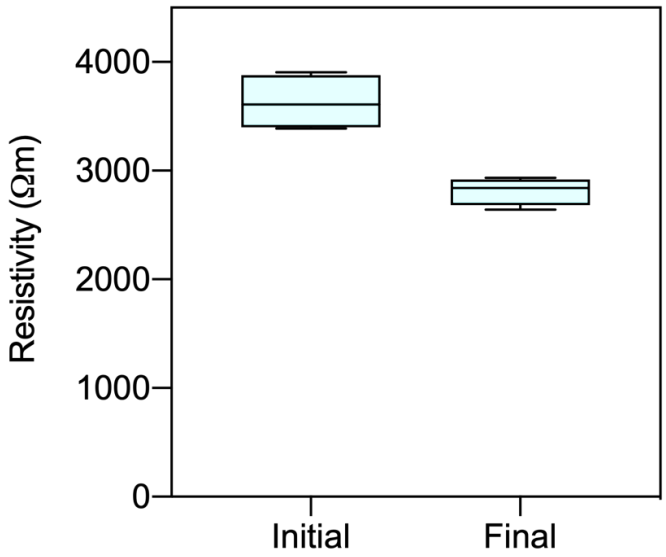

Fig. 4.9 Measured resistivity of collagen suspensions initially during EPD and at the end of EPD.

4.4.4 Pulse Period and Duty Cycle

To determine, experimentally, how pulse period and duty cycle affect deposition in pulse current EPD, deposited collagen mass measurements were taken, varying each parameter individually. In both instances, the total on time, T_{ON}, and voltage were kept constant, at 30 minutes and 10 V, respectively. The deposited mass was measured at varying pulse periods, λ, (Figure 4.10) and varying duty cycles, δ, (Figure 4.11). For each, a line of best fit was imposed. Neither pulse period nor duty cycle had any significant effect on deposited mass under an equal T_{ON} time. It must be noted, however, that decreasing the duty cycle but maintaining T_{ON} time results in longer total deposition times.

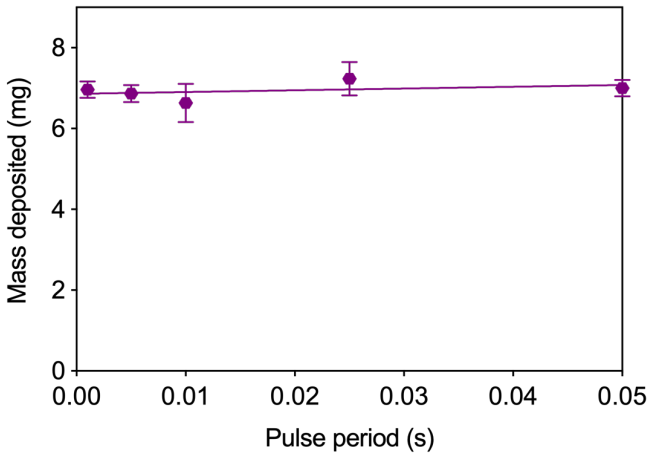

Fig. 4.10 The effect of pulse width on the mass of collagen deposited, at 10 V. For varying pulse period, deposition was run for 60 minutes with a fixed duty cycle of 50%, giving total T_{ON} time of 30 minutes.

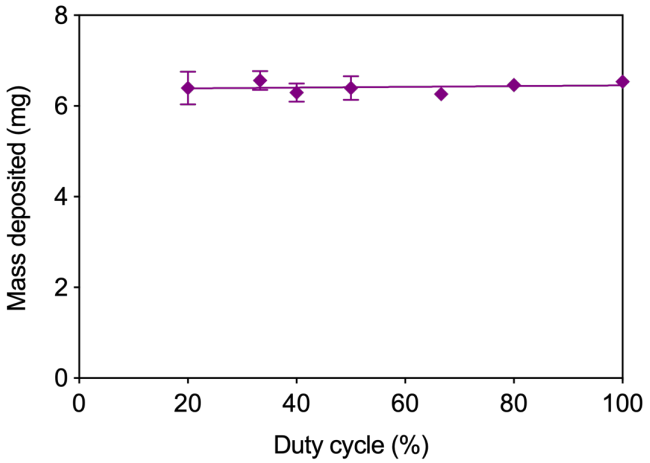

Fig. 4.11 The effect of duty cycle on the mass of collagen deposited, at 10 V. For varying duty cycle, deposition was run with a fixed total T_{ON} time of 30 minutes and fixed pulsed period of 0.01 seconds. Note, with varying duty cycle, total deposition time also varied.

4.4.5 Deposition Model

The variables for modelling pulsed-current EPD of collagen suspensions were determined by characterising the suspensions in this chapter. The values used for each variable are displayed below in Table 4.2, with explanations as to the determination of each variable. The deposition voltage was varied as this is the parameter most often changed during EPD processing.

Table 4.2 Table of variables within the model, the corresponding symbols used in equations, and the measured values used to run the model. The reasoning indicates why the measured values were selected.

Variable	**Symbol**	**Value**	**Reasoning**
Deposition voltage	V	variable (V)	Deposition voltage will vary and model results tested against experimental data
Initial suspension concentration	C_0	0.25 wt.%	The standard used by Barrett [24, 25]
Suspension volume	N/A	4 mL	The size of the EPD cell created in Figure 4.4
Deposition area	S	5 cm^2	The deposition area of the EPD rig created in Figure 4.4
Distance between electrodes	N/A	0.8 cm	The cell width of the EPD rig created in Figure 4.4
Electric field	E	dependant on voltage (Vcm^{-1})	Electric field = voltage / distance between electrode
Zeta potential	ζ	38 mV	Average ζ of collagen I at pH 3.5 shown in Figure 4.5
Suspension media viscosity	η	0.89 cP	Viscosity of suspension media: dH_2O, ethanol, and acetic acid
Acetic acid strength	N/A	0.05 M	Standard used for hydrating collagen I
Ethanol content	N/A	50 v.%	Standard used by Barrett et al. to mitigate bubbles [25]
Initial suspension resistivity	ρ_0	3628 Ωm	Measured average initial resistivity of suspension, shown in Figure 4.9
Final suspension resistivity	ρ_∞	2813 Ωm	Measured average final resistivity of suspension, shown in Figure 4.9
Pulse period	λ	0.05 s	Standard used by Barrett et al. to mitigate bubbles [25]
Duty cycle	δ	40%	Standard used by Barrett et al. to mitigate bubbles [25]

Deposited mass of 0.25% Sigma collagen was plotted as a function of time with 10 V and 5 V applied current, 40% duty cycle, and 0.05 s pulse period. The deposition model was also run with the same experimental parameters. The results for both are shown in Figure 4.12. It can be seen that there is a good agreement between the model and experimental data for the 10 V applied current regime. The model, however, overestimates the deposited mass with time for 5 V applied current, and is not representative of the experimental data. For the model to be viable, it must be valid for all values of parameters.

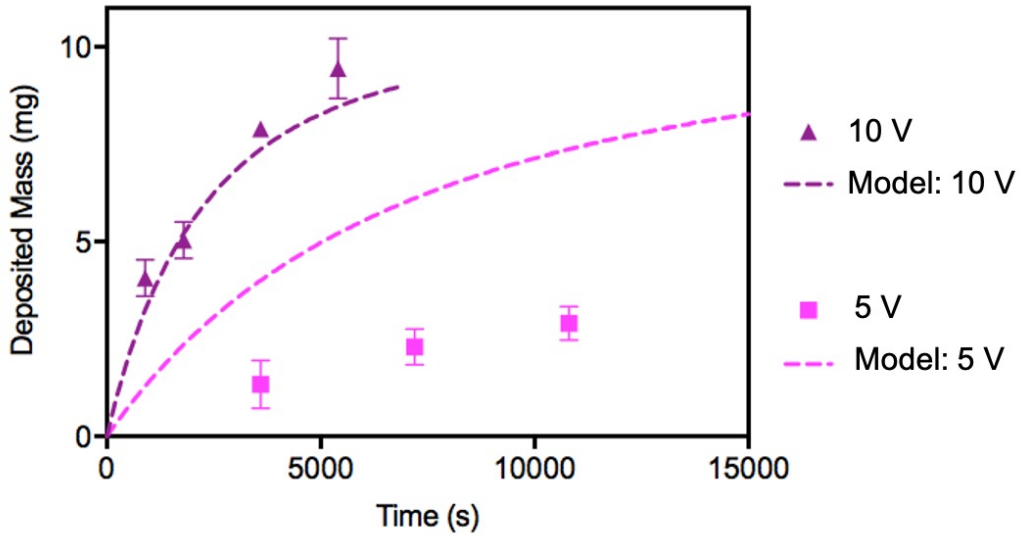

Fig. 4.12 Electrophoretic deposition model (dashed lines) plotted against experimental data (symbols) with same parameters. Depositions were for 10 V (purple) and 5 V (pink) applied current. All other parameters were equal: 0.25% Sigma collagen suspensions, 40% duty cycle, 0.05 s pulse period.

4.5 Discussion

The model proposed here, based on the Sakar and Nicholson model [107] and the resistivity model [142], showed initial promise. The results generated were shaped as expected, from previous literature. The previous models, however, were only suitable for direct current EPD regimes, and were not viable for pulsed current depositions. The model proposed here introduced a new parameter, the pulsed current parameter (κ), which incorporated duty cycle and pulse period parameters into the model. The influence of these factors was measured experimentally (Figures 4.10 and 4.11), which, at the measured voltage (10 V) seem to validate the mathematically derived pulsed current parameter. The dominant factor for the proposed pulsed current parameter, κ, is duty cycle. Therefore, to maximise deposition yield, duty cycle should be maximised, however in doing so bubbles tend to form in the deposit.

The model was then scrutinised against experimental results (Figure 4.12), which, for higher voltage regimes (10 V) fitted well. This, in part, validated the underlying framework of the model. At lower voltage (5 V), however, the model significantly overestimated the deposited mass.

The lack of deposition at lower applied voltage could be attributed to more complex factors than the model accounts for. Koelmans and Overbeek [131] first proposed that an increase in electrolyte concentration at the electrode alters the zeta potential of depositing particles, for a range of inorganic materials suspended in a non-aqueous media. They found that a finite amount of time was necessary before particles began to deposit; the time needed to generate enough electrolyte to alter the zeta potential of particles, before which no deposition would occur. This critical time was found to be inversely proportional to the applied current/voltage of the system. This mechanism is also valid for aqueous suspensions using pulsed current EPD, and is corroborated with results found by Besra et al. [170]. They found that at reduced current and pulse widths, there was also a significant reduction in pH change at the electrode. They also noted, for pulsed current depositions, that smaller

pulse widths resulted in lower deposition yield of alumina. Those results disagree with the findings of this study, with lower pulse width not having a significant affect on deposit yield (Figure 4.10), however, the applied voltage may have been so great that it negated these effects. Another accompanying, and simpler, factor is that particles are not given sufficient driving force for a long enough time to overcome repulsive forces and flocculate [107, 116] and deposition is neutralised. Again, these mechanisms were negligible, and thus masked, at the higher current/voltage regimes.

Other mechanisms may also have been neglected by the model developed in this chapter. The pulsed current parameter assumed two separate phases of movement within each pulse period: electrophoretic mobility of particles toward the depositing electrode during applied voltage (T_{ON} time); and diffusion away from the electrode when there is no applied voltage(T_{OFF} time). However, it may be a four phase process. This model does not account for the acceleration of the particles when the voltage is initially applied, up to a constant velocity. This is then followed by deceleration of the particles, which will continue to move toward the electrode slightly once the applied voltage is removed, before reaching a velocity of 0, and then diffusing away from the electrode. This, therefore, results in a four phase process: acceleration of the particles under applied voltage, constant velocity of the particles with applied voltage, deceleration of the particles once applied voltage has been switched off, and very small levels of diffusion away from the electrode. This theory was similarly described, and corroborated, by Asano et al., who described the acceleration and deceleration of conductive particles in viscous fluid under an electric field [264].

Under this regime, it is possible that a deposition voltage of 5 V offers too low a driving force for the collagen fibres to accelerate, and it is possible that they do not achieve a constant velocity within that time. This reduced velocity will mean the deceleration time is also much smaller. This means that the distance travelled by the collagen fibres is much less than predicted in the proposed two-phase model, which assumed constant velocity of particles

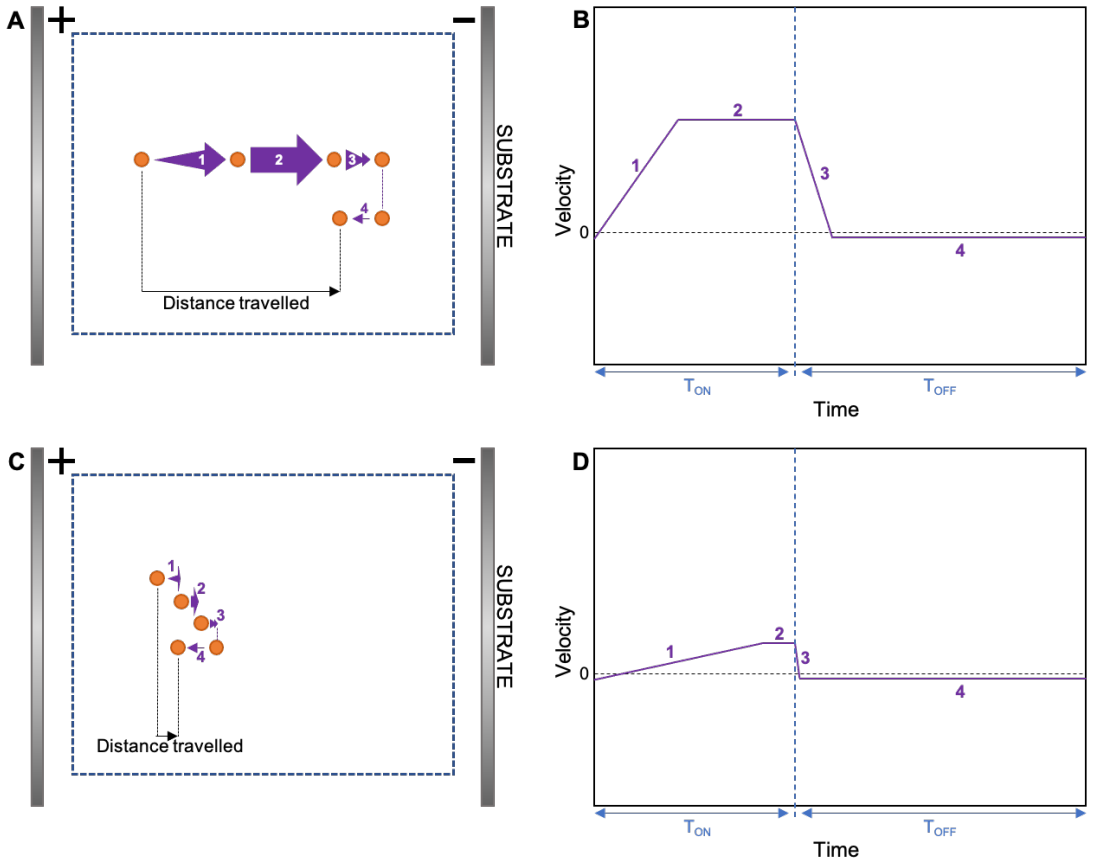

Fig. 4.13 Proposed four phases of particle movement during one pulsed period of pulsed current EPD. (1) acceleration (2) constant velocity (3) deceleration (4) diffusion from substrate. A and B show higher applied voltage, C and D show lower applied voltage. A and C show the movement of a particle between electrodes at each phase, and B and D show the velocity profile of a particle during one pulse period, with positive velocity towards the deposition substrate.

is achieved immediately once the applied voltage is switch on. This would also explain why no deposition is achieved under pulsed current EPD at 4 V and lower [25], where the acceleration during T_{ON} is negligible, before the T_{OFF} time, where diffusion back to steady state occurs.

Furthermore, it is possible these mechanisms — namely, acceleration and deceleration — are exacerbated by the use of biological macromolecules such as collagen, which are much larger than the ceramic particles typically used in EPD processing. All previous EPD models have been based on deposition of small inorganic particles [105, 107, 142]. The relatively

large collagen fibres used in this study would have been much more heavily influenced by viscous drag and with each molecule having a greater mass, the acceleration will be reduced at an equal force, compared with small particle systems. This further highlights the need to incorporate these mechanisms into this model.

In order to incorporate these four phases into the model more features must be accounted for. To determine the acceleration of the particles, the driving force, caused by the voltage on the charged particle, needs to be established, as well as the mass of each particle. Furthermore, the particle radius and viscous drag experienced by each particle should also be defined [264]. These data require the known mass and size of the collagen fibres - something that is unknown within this system, and would be too difficult to ascertain. It is also possible that fibres cannot be modelled in a similar manner to spherical particles, which previous models have assumed. More complicated dynamics may also need to be considered when modelling a system of fibrous material, particularly at lower deposition voltages - in this study these issues were apparent for collagen EPD at 5 V, but these mechanisms were masked at 10 V where they were negligible. This also emphasises the need to validate and test EPD models over a range of parameters.

4.6 Conclusions

Models have previously been developed to describe deposited mass during electrophoretic deposition for direct current systems, but no such models existed for pulsed current EPD. Here, a model was developed that incorporated the additional parameters associated with PC-EPD, namely pulsed period and duty cycle. This model, while accurate for higher applied voltage systems, was not appropriate at lower voltages, where it did not account for mechanisms which are likely to be present in reality. At higher voltages these effects become negligible and the model appeared to be accurate, but at lower voltages these mechanisms may have much greater influence on the system. It seems, therefore, that this model is only valid beyond a threshold of applied current/voltage, duty cycle, and pulse period. Below this threshold, more complicated mechanisms must be accounted for. Further investigation will, therefore, be necessary, scrutinising a wider range of test parameters, to explore their effect to allow the development of a revised model.

Chapter 5

Developing Complex Shaped Films

5.1 Introduction

5.1.1 Background

Collagen films produced using EPD offer the potential for a variety of applications, including barrier membranes and wound dressings. In previously reported literature, collagen films generated by EPD are planar and not intended to contain any topographical features [25]. However, surface texture could be beneficial for different applications, for example, grooves or surface roughness could help to promote or direct cell growth — it has been shown that orientated scaffolds improve cell alignment [265]. Additionally, curved, non-planar, and tubular collagen films can be appropriate for blood vessels or nerve guidance applications.

Textured films can be produced by depositing onto a shaped substrate, where the features of the substrate are translated onto the deposited collagen. Electrophoretic deposition is beneficial for this because particles can be deposited on extremely complex substrates, while maintaining a uniform deposit throughout [266]. However, casting thick, uniform collagen films is limited to substantially planar surfaces as it relies on gravity.

Electrophoretic deposition of collagen results in a thick collagen gel deposit on the substrate. This must first be left to dry into a collagen film before it can be removed from the substrate [25]. During this drying process the collagen adheres strongly to the substrate, making it difficult to remove into a free standing film. Collagen will naturally strongly adhere to surfaces as it dries — the name collagen derives from the Greek *kolla*, meaning "glue" [267].

Much of the EPD work in the field of ceramics has focused on the production of coatings, hence there is no need for the removal of the deposit from the substrate. However, removal from the substrate is sometimes desired, and in the case of collagen, this requires intervention to assist the process. Several methods have been described for removing deposits from their substrate following EPD. These will now be considered, particularly focussing on their suitability for non-planar collagen films with topographical features.

Mechanical cleavage is the most basic method of removing a deposit from the substrate. It involves prying the deposit off, often with a sharp tool such as a razor blade [268]. While this can remove a well-adhered deposit, it can often result in damage to the deposit [24, 268]. Previous attempts to remove collagen films with a razor blade have often resulted in tearing the film and damaging the substrate [24]. Furthermore, the use of a razor blade to scrape the collagen film off the substrate is only appropriate if the substrate is a flat surface. If the substrate were of a complex shape (curved or grooved, for example) the use of a razor blade would be impractical.

The use of conductive, non-stick polyethylenimine electrodes [269] and graphene coated electrodes [172, 270, 271] have been investigated to assist film detachment, however these can be expensive, and require complex protocols and toxic chemicals [272–274]. There are reports in the literature of an alternative technique known as post-EPD electrochemical separation (PEPDECS), which was used to detach films of carbon nanotubes (CNT), whereby the substrate and dried CNT deposit are returned to the EPD cell with deionised water and a

reverse voltage is applied until the CNT film separates [275]. However, this method can cause bubble formation at the substrate electrode, damaging the film [276], and would also result in unwanted hydration of collagen, which would then need to be dried again. Another strategy to develop free-standing films is to deposit onto a non-stick semi-permeable membrane from which it is easier to remove the deposit [155]. The semi-permeable membrane, placed in front of the electrode, allows ions to pass through it, maintaining the electric field, but acts as a barrier to the depositing particles. This technique also acts as an effective measure for preventing bubbles forming in the deposit during aqueous deposition [277]. This method, however, can be expensive and necessitates a complex experimental set up, and is only appropriate in this context if the semi-permeable membrane also contained the complex features desired, such as grooves.

Another method for deposit removal from the substrate is the use of a sacrificial layer. A sacrificial layer is a very thin boundary layer, or coating, around the substrate that, after deposition is complete, is dissolved (sacrificed), relieving the deposit from the substrate [278, 279]. It is important to select the correct sacrificial layer for purpose; it must be dissolved in a solvent, but not a solvent that will dissolve or damage the deposit, and it must also remain intact (i.e. not dissolve) within the suspension media [280]. Cellulose acetate presents itself as a suitable sacrificial layer for collagen EPD. Cellulose acetate dissolves readily in acetone [281, 282], a solvent that does not affect the properties of collagen. Furthermore, cellulose acetate is unaffected in the suspension media, of acetic acid and ethanol [283]. This method has been successful in removing graphene layers from a substrate [282], but had not previously been applied to collagen deposits.

5.1.2 Aims

This study aimed to evaluate the effectiveness of using a cellulose sacrificial layer for removing EPD collagen deposits from the substrate. Furthermore, the efficacy of EPD was

also assessed under these conditions to see if the sacrificial layer affects the process. The aim of this study was not only to generate good quality free-standing collagen films, but also evaluate the potential of this method in fabricating complex-shaped and patterned films, by depositing onto differently shaped substrates, remove collagen via a cellulose sacrificial layer, and determine what features, if any, were translated from the substrates to the collagen films.

To assess which features that can be translated to collagen films, a 3D printed stainless steel grooved substrate was produced. 3D printed stainless steel resolution pieces were also fabricated to assess the features produced via 3D printing, and these were compared with the features observed in the collagen films.

5.2 Materials and Methods

5.2.1 3D Printing Stainless Steel Substrates

A stainless steel substrate and a resolution piece were designed and drawn using 3-dimensional computer aided design (CAD) software (Fusion 360, Autodesk) and were produced using 3D printing. The resolution piece was designed with angular feature sizes ranging from 400 µm to 1400 µm. The CAD drawings of the resolution piece can be seen below, in Figure 5.1.

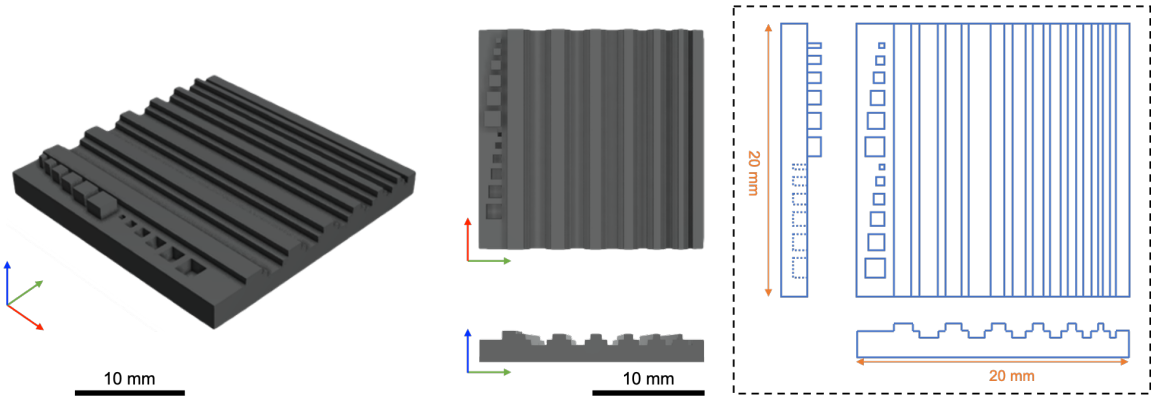

Fig. 5.1 Left: CAD design of squared resolution piece with features of varying sizes. Images show the same piece at different angles, with the colour arrows showing the relative orientation. Right: Schematic of square resolution piece from top and side views.

A grooved substrate was also designed using CAD software, with grooves of varying sizes, ranging from 100 µm to 1000 µm (Figure 5.2).

The 3D CAD designs were saved as '.stl' files, which were then uploaded to Shapeways (Netherlands), a 3D printing company. The stainless steel resolution piece and grooved substrate were 3D printed by Shapeways, using a selective laser sintering technique.

5.2.2 Coating Substrates in Cellulose Acetate

1 wt.% cellulose acetate solution was prepared by dissolving cellulose acetate (Sigma Aldrich, 180955) in acetone. Stainless steel substrates were submerged in the cellulose acetate solution

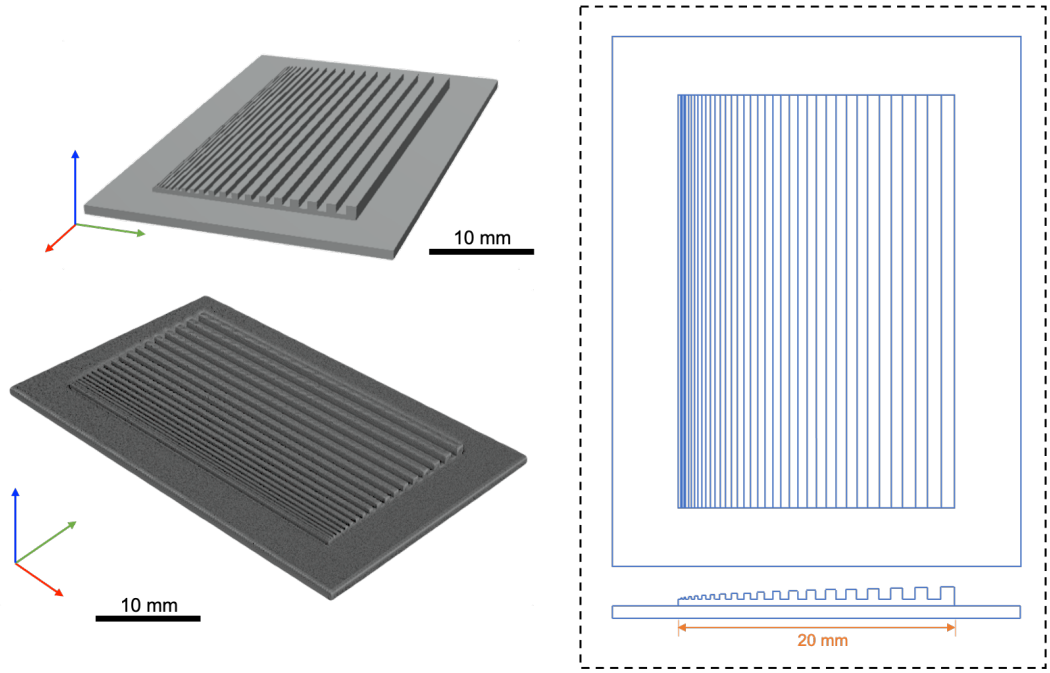

Fig. 5.2 Left: CAD design of grooved substrate with features of varying sizes. Images show the same substrate at different angles, with the colour arrows showing the relative orientation. Right: Schematic of the grooved substrate from top and side views.

for 60 seconds, after which they were slowly removed and left to air dry for 2 hours, leaving a thin coating on the substrates [284].

5.2.3 Collagen Preparation

Insoluble collagen type I, from bovine achilles tendon (Sigma Aldrich, C9879), was hydrated, following the protocol in Section 3.2.1, at an initial concentration of 0.5 wt.% in 0.05 M acetic acid at 4 °C for 72 hours. Once hydrated, the collagen was homogenised for 30 minutes at 10,000 RPM using a T 18 digital Ultra-Turrax homogeniser (IKA), until a smooth milky appearance was achieved. Following the protocol in Section 3.2.2, the collagen suspension was then dialysed using cellulose dialysis membranes (Sigma Aldrich, D9527-100FT) against ultra-pure type 1 deionised water dialysate. The collagen suspension was dialysed for 30 hours, replenishing the dH_2O dialysate regularly. Ethanol was added to the dialysed collagen suspension, following the protocol in Section 3.2.3, such that the suspension was 50 vol.%

ethanol, and the final concentration of collagen was 0.25 wt.%. The suspension was then homogenised for a further 30 minutes, ensuring the ethanol was well mixed and the collagen was visually homogeneous.

5.2.4 Electrophoretic Deposition

Electrophoretic deposition of collagen films was performed following the protocol in Section 3.2.7. Prior to deposition, the electrode (substrate) was coated in cellulose acetate (Section 5.2.2). The collagen suspension, as prepared in Section 5.2.3, was loaded into the EPD rig. Pulsed current EPD was run at a deposition voltage of 7 V, pulse period of 50 ms, and duty cycle of 40 %. EPD was preformed with both normal planar substrates and the grooved substrate described in Section 5.2.1.

5.2.5 EPD of Tubular Collagen Scaffold

A tubular electrophoretic deposition rig was custom-built by placing a cylindrical deposition electrode (with a diameter of 10 mm) inside a larger cylindrical counter electrode (with a diameter of 35 mm), both housed within a glass beaker (Figure 5.3). The electrode on to which collagen was deposited was coated in cellulose acetate prior to deposition. Pulsed current EPD was run at a deposition voltage of 7 V, pulse period of 50 ms, and duty cycle of 40 %, following the protocol described in Section 3.2.7.

Following deposition, collagen films were air-dried onto the substrate. Flat and grooved electrodes were laid flat with the collagen coating facing upwards as it dried, and the cylindrical electrode was stood upright, with the base at the bottom (Figure 5.3, right).

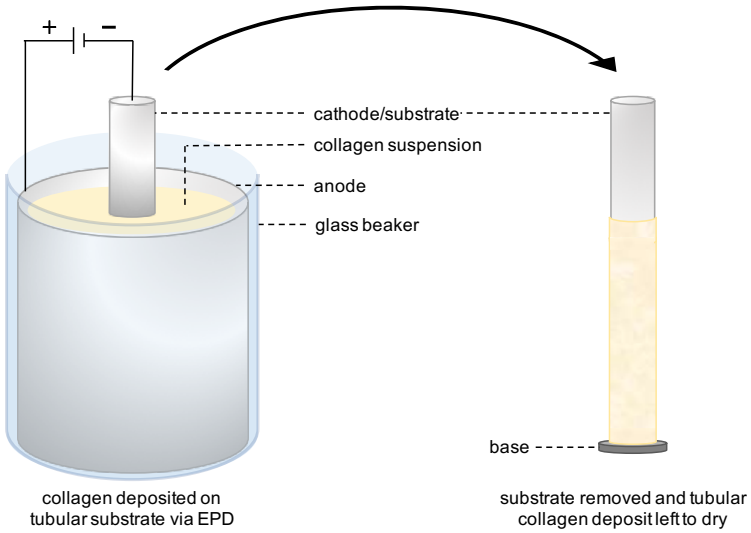

Fig. 5.3 Schematic showing the set-up of the tubular EPD rig, for depositing tubular collagen deposits. Formed of one cylindrical electrode (the cathode and substrate) situated inside a larger cylindrical electrode (the anode), both inside a glass beaker. The collagen suspension is the loaded into the rig, between the electrodes.

5.2.6 Current Measurements

Current measurements were taken during collagen depositions at 60 s time intervals using Quick I/V Measurement Software (Keysight) for cellulose coated and uncoated substrates. More details of the current measurement software can be found in Section 3.2.7.

5.2.7 Removing Collagen from the Substrate

Once deposited collagen was dry, the cellulose acetate-coated substrate, together with its adhering collagen, was submerged in acetone for 2 hours [282]. The acetone dissolved the cellulose acetate layer, relieving the collagen from the substrate (Figure 5.4). For tubular collagen deposits, the collagen scaffold was gently pulled off the substrate, after being submerged in acetone.

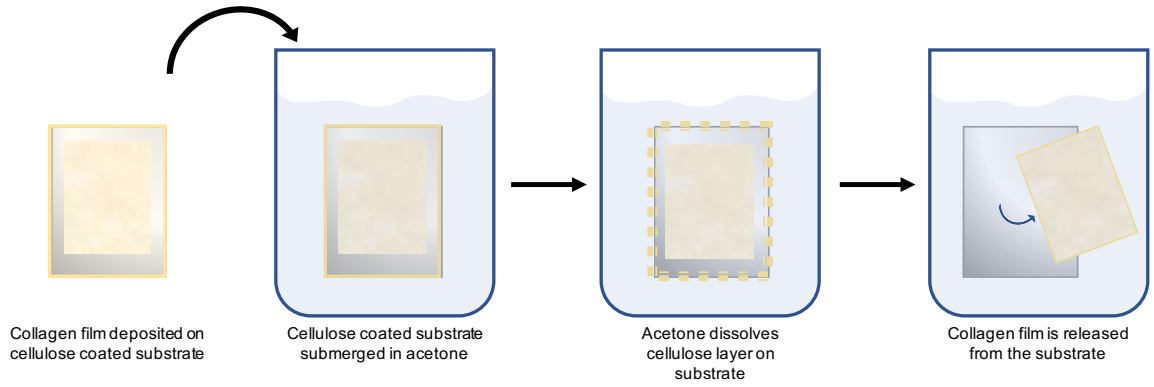

Fig. 5.4 Schematic showing the method for removing dry collagen deposits from the cellulose acetate-coated substrate.

5.2.8 Fourier Transform Infrared Spectroscopy

Fourier Transform Infrared (FTIR) spectroscopy analysis was performed on dry collagen films that had been removed from the substrate via cellulose acetate and on collagen films that had mechanically cleaved off using a razor blade. FTIR analysis was performed using a Bruker Tensor 27 FTIR machine.

5.2.9 Scanning Electron Microscopy

SEM was used to assess the features produced on 3D printed stainless steel pieces and grooved collagen films. The stainless steel resolution piece was produced to analyse these features, as the 3D printed grooved substrate was too large to image within the electron microscope.

Collagen samples were prepared for scanning electron microscopy by first coating them in a thin layer of gold, before placing them on a stub and into the electron microscope. The 3D printed stainless steel resolution piece did not need coating prior to SEM. SEM micrographs were taken using a Nova NanoSEM, with a beam voltage of 5 kV using secondary electron mode. Micrographs were taken over various regions of the collagen films and resolution

piece, at a range of magnifications, from 40 – 390×, and working distances from 5.4 – 10.8 mm.

5.2.10 Image Analysis

Images were analysed using ImageJ Software (NIH). Features present on the 3D printed stainless steel resolution pieces and the collagen films were measured from the SEM micrographs in ImageJ using the measure tool.

5.2.11 Statistical Analysis

Statistical analysis was performed and graphs generated from the collected data using Graphpad Prism 8 software.

5.3 Results

5.3.1 Cellulose Acetate Sacrificial Layer for Removal of Collagen from Substrate

Planar Collagen Films

Collagen was deposited on cellulose-coated substrates via electrophoretic deposition. Once the deposits had been allowed to dry down into films, measuring approximately 50 µm in thickness, the substrates were submerged in acetone for 2 hours to dissolve the cellulose acetate coating and remove the collagen films. It was found, after 2 hours, that the collagen was completely free from the substrate and floating in the acetone. No further action was needed to remove the collagen from the substrate. Furthermore, the collagen did not absorb the acetone.

The films removed using this technique remained completely intact, suffering none of the damage often seen in films removed using a razor blade. Images of films removed by the two techniques are compared in Figure 5.5. The films were also consistently removed without issue, inconsistency being a major problem in razor blade removal.

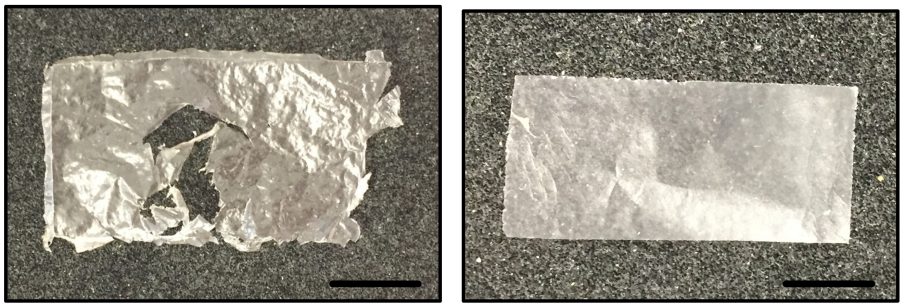

Fig. 5.5 Dry collagen films of thickness approximately 50 µm formed by electrophoretic deposition, removed from the substrate via a razor blade (left) and a cellulose sacrificial layer (right). Black scale bars are 10 mm.

Tubular Collagen Films

Following the successful removal of planar collagen films from their substrates it was proposed that seamless collagen tubes could be fabricated and then removed from the tubular substrate using a sacrificial layer. The tubular collagen EPD rig was able to form seamless collagen tubes with a film thickness of approximately 80 µm, which were easily removed from the substrate due to the cellulose acetate sacrificial layer. Previous attempts at such a tube would previously been impossible to remove from the substrate with mechanical cleavage. The tubular collagen scaffold, which can be seen in Figure 5.6, held its shape after drying and removal from the substrate support.

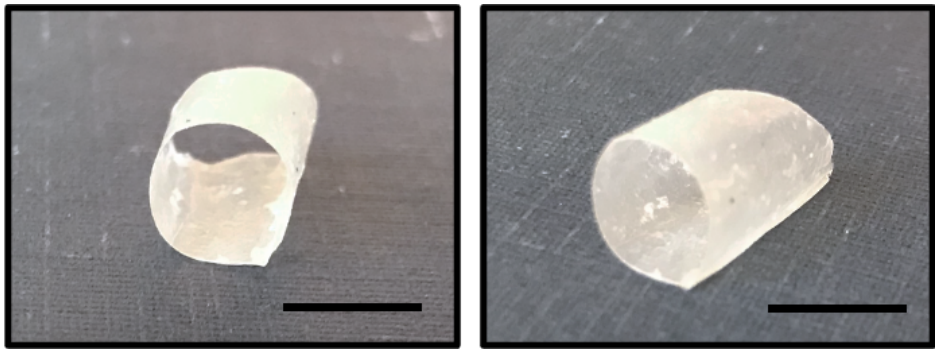

Fig. 5.6 Free-standing tubular collagen film of thickness approximately 80 µm formed from electrophoretic deposition and removed from the substrate using a cellulose sacrificial layer. Scale bars are 10 mm.

5.3.2 Current Measurements with Cellulose Acetate Coatings

The current was measured during deposition of collagen suspensions onto a stainless steel substrate with a cellulose acetate coating and onto the same substrate but without any coating; the voltage was equal for both processes, at 5 V. The current profile was unchanged by the presence of cellulose acetate (Figure 5.7). Coating of the electrode did not appear to influence the current during deposition, compared with deposition using uncoated electrodes. Furthermore, the deposition yield appeared unchanged, as did the visual film quality, for

films deposited under the same parameters; there was no decrease in deposition or apparent bubble formation.

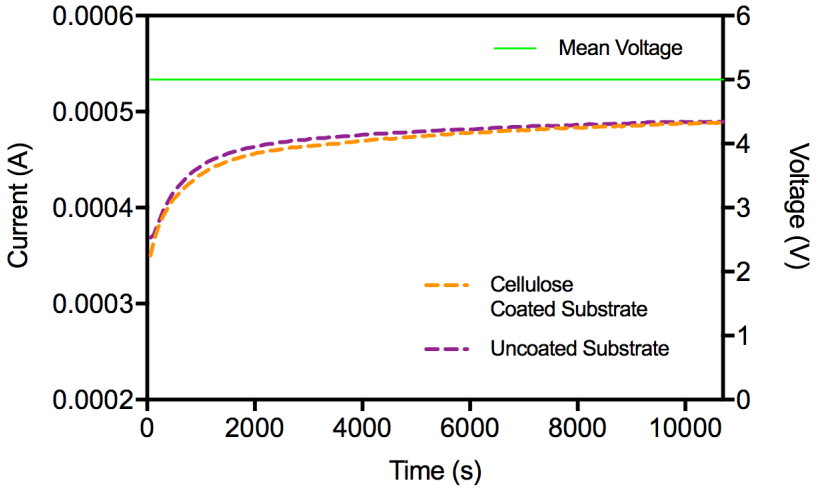

Fig. 5.7 Current measurements during depositions for cellulose coated (orange) and uncoated (purple) substrates. The voltage was also measured and is shown (green, right Y axis) to ensure it remained unchanged. Deposition parameters: 5 V, 40% duty cycle, 50 ms pulse period.

5.3.3 FTIR analysis of Collagen Films

Infrared spectroscopy was performed on samples to determine whether any residual cellulose acetate remained on collagen films removed via a sacrificial layer, and to highlight any other changes to the collagen films. There were no changes to the peaks present in the output signal compared with collagen without a cellulose layer (Figure 5.8). All major peaks for collagen were present and matched in the critical region between 1900-700 cm^{-1}, indicating that the collagen had not been damaged or altered in the process. FTIR analysis, therefore, suggests that no cellulose acetate remained on collagen films after they had been relieved from the substrate. The peak at approximately 2400 cm^{-1} is likely an artefact from gas in the FTIR.

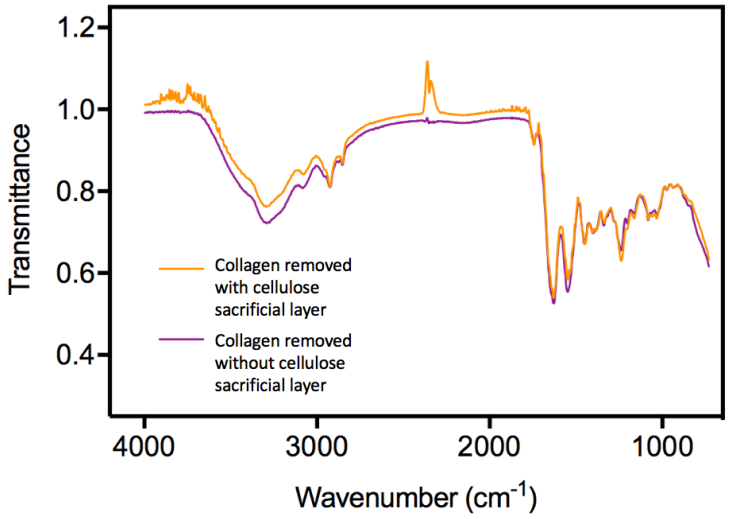

Fig. 5.8 FTIR plots of a collagen film removed from the substrate using mechanical cleavage (purple), and a collagen film removed via a cellulose acetate sacrificial layer (orange).

5.3.4 Grooved Collagen Films using Cellulose Sacrificial Layer

Grooved Substrate

The 3D printed stainless steel grooved substrate (for depositing collagen on) was photographed, and can be seen Figure 5.9 (A1) alongside the original schematic design (A2). The surface of the substrate was rough, unlike the original CAD design. The 3D printed substrate was designed with grooves sizes ranging from 1 mm to 0.1 mm, with each groove being 0.05 mm smaller than the previous (Figure 5.9, A1 from left to right). The larger grooves were distinct and clear, however, resolution appeared to reach a limit at 0.3 mm.

Grooved Collagen Films

Collagen suspensions were deposited onto the 3D printed grooved stainless steel substrate (Figure 5.9, A) via electrophoretic deposition. Deposited collagen films, which had a thickness of approximately 50 µm, were removed from the grooved substrate using a sacrificial layer. The grooved films produced are shown in Figure 5.9, B. The two photographs in the grey box (B3) show the dry collagen films, and the photograph on the right (B4), in the blue

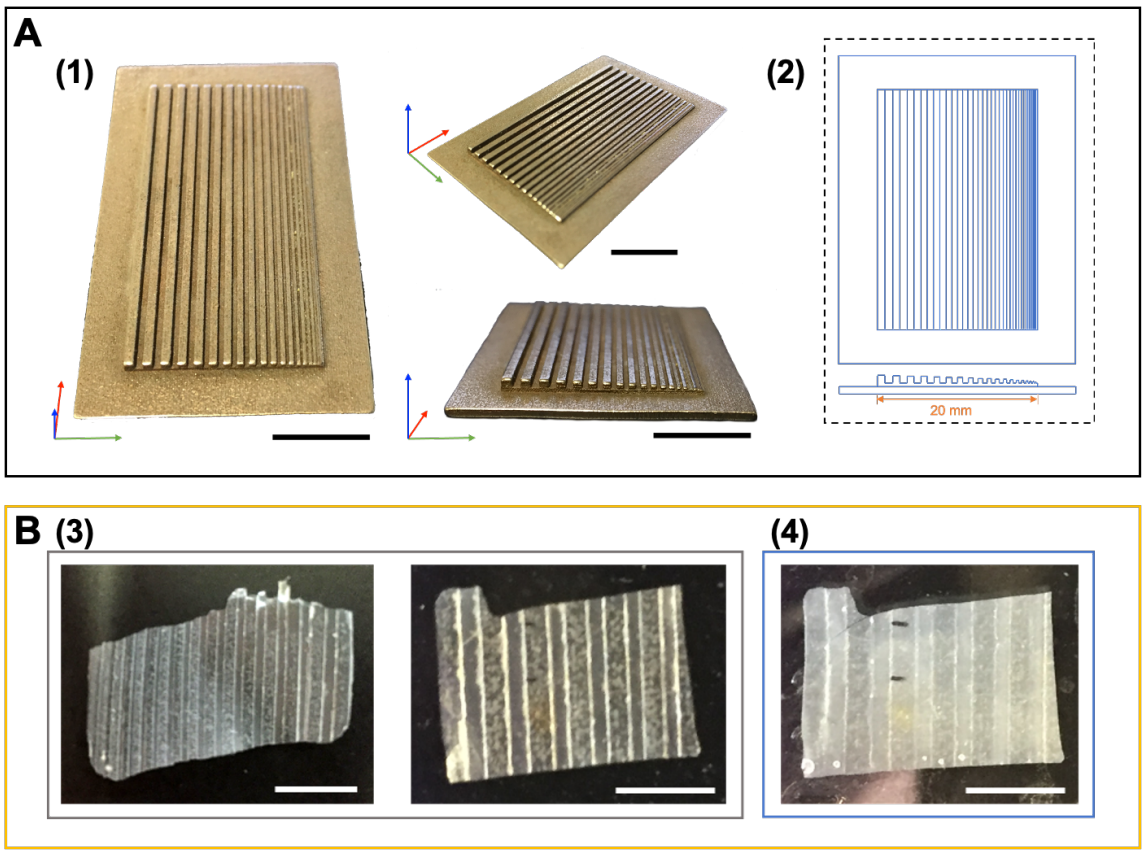

Fig. 5.9 A1: Photographs of 3D printed stainless steel grooved substrate. Photographs show the same substrate at different angles, with the colour arrows showing the relative orientation. Black scale bars are 10 mm. A2: Schematic of the grooved substrate from top and side views. B: Photographs of free-standing grooved collagen films formed from electrophoretic deposition and removed from the substrate using a cellulose sacrificial layer. B3: dry grooved films with approximate of thickness 50 µm; and B4: a hydrated grooved collagen film in water. White scale bars are 5 mm.

box, shows a hydrated grooved collagen film following immersion in water. The photographs show that the grooves from the substrate are replicated by the free-standing collagen films. Furthermore, once the films were hydrated the grooved features were maintained and not lost due to swelling.

5.3.5 Feature Analysis of Grooved Collagen Films

3D Printed Substrate Material

3D printed stainless steel resolution pieces were analysed to understand what resolution was achieved for features using this technique. The photograph in Figure 5.10 (A) shows the 3D printed stainless steel resolution piece, with the schematic of the piece depicted underneath. The resolution piece was imaged using a scanning electron microscope to observe the features and surface characteristics in more detail, the micrographs of which can be seen below, in Figure 5.10 (C - E), alongside schematic drawings of the imaged area for comparison with the original design. The grooved substrate was too large to analyse using an SEM.

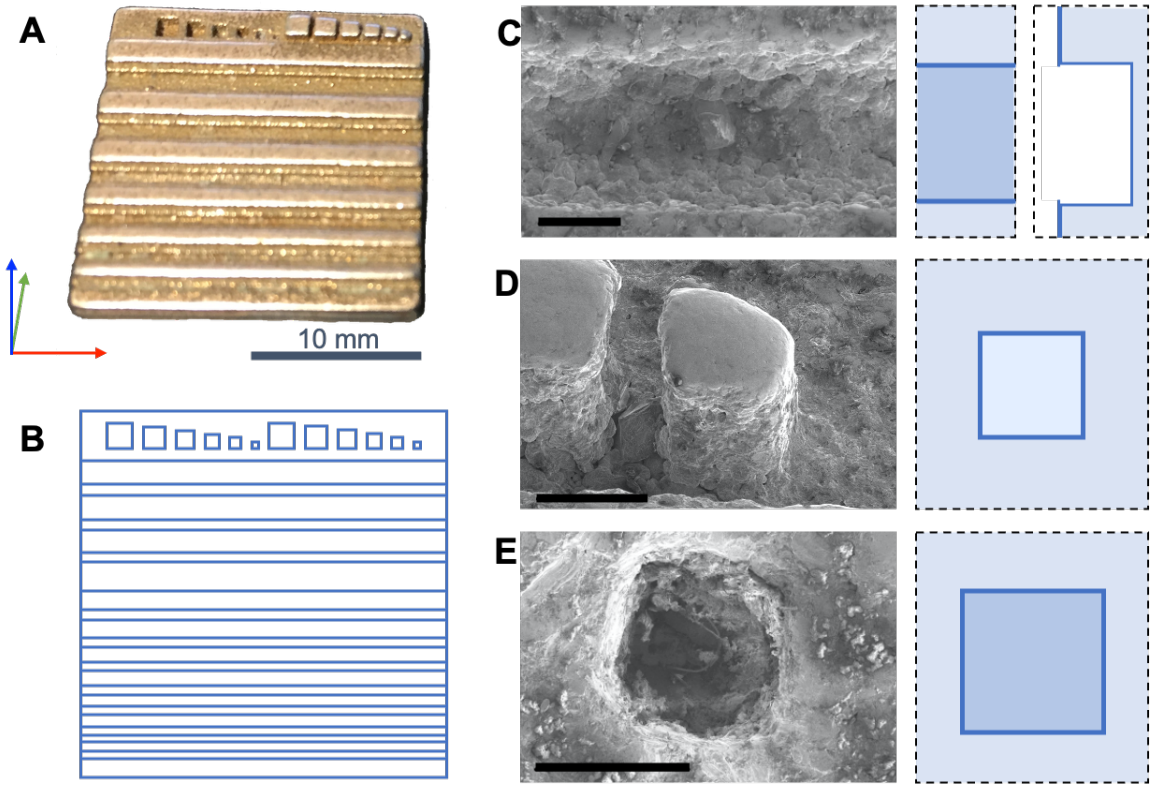

Fig. 5.10 Stainless steel resolution piece: (A) photograph (scale bar is 10 mm), (B) schematic drawing, and (C - E) SEM micrographs with corresponding schematic design of area (right). Black scale bars are 500 µm.

In all the micrographs the surface roughness of the resolution piece was apparent. The square groove and column (Figure 5.10, C & D) did not contain the right-angles typical of a square; this was also true of the square hole (E). The protruding surface of the column appeared smooth, which may have occurred due to abrasion. Conversely, other surfaces appeared very rough; the rough features were in the range of 10 – 100 µm in size. Further feature size analysis was performed and is shown in the section below.

Grooved Collagen Films

SEM micrographs of grooved collagen films are presented above schematic drawings of the substrate in the corresponding region in which they were deposited (Figure 5.11). The grooves were apparent within the collagen films and were translated from the substrate. However, the depth of the deeper grooves was not maintained upon drying of the films, where the tension in the film pulled the collagen out of the grooves. This can be seen in the images in the smoother regions of the films. Quantitative feature size analysis was performed on grooved films and compared with the stainless steel resolution pieces, the results of which are presented in the following section.

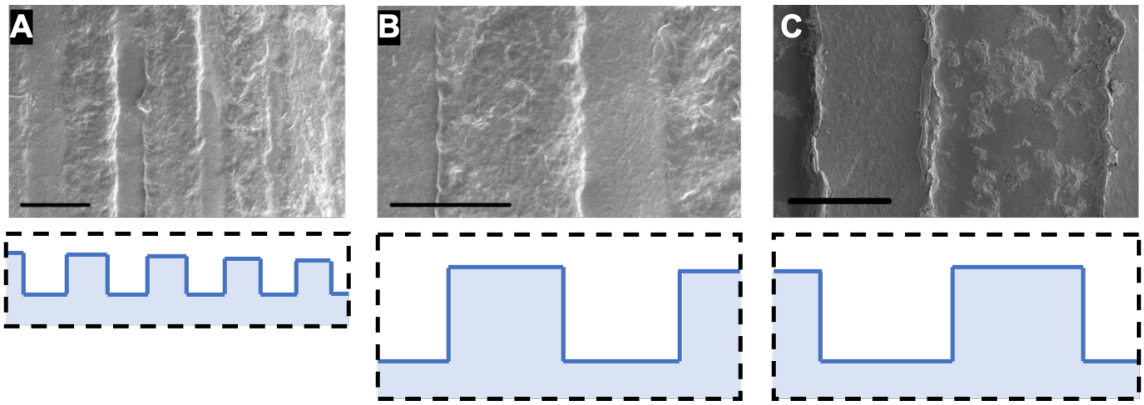

Fig. 5.11 SEM micrographs of grooved collagen films and, below, corresponding schematic designs of grooved substrate onto which they were deposited. Black scale bars are 500 µm.

The collagen that dried on the protruding grooves appeared to maintain the surface roughness of the 3D printed stainless steel substrate. The small features, caused by the

inherent roughness, were also translated onto the collagen (Figure 5.12), with rough features measuring approximately 10 – 100 µm in size.

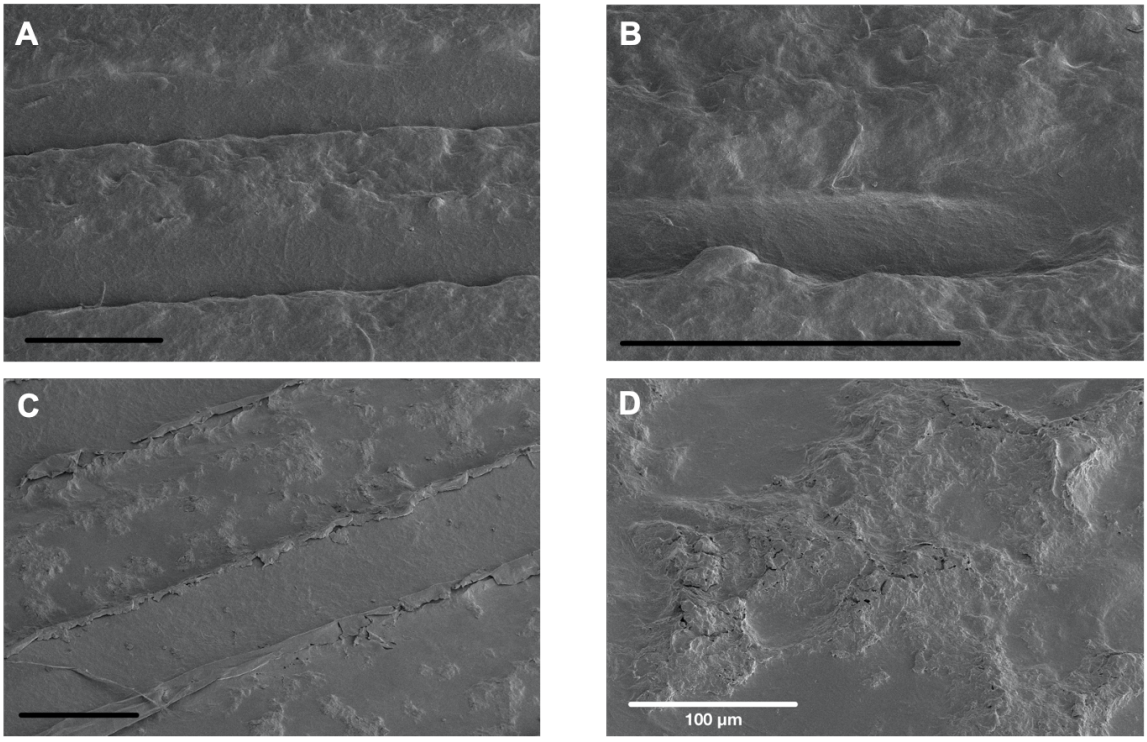

Fig. 5.12 SEM micrographs of deposited grooved collagen films. Black scale bars are 500 µm.

Feature Size Analysis

Feature sizes of the 3D printed stainless steel were measured and compared with their original design (Figure 5.13, D1). At 400 µm features deviated in size much more than for features greater than this size (> 400 µm), which all deviated a similar amount. The range of measured features for each feature design size was approximately 100 µm, with the deviation from the schematic being ±50 µm.

Analysis of the features imaged in the grooved collagen films showed that the produced features were consistently larger than the original CAD design of the substrate (Figure 5.13, D2). Furthermore, the features measured on the outward facing side of the collagen

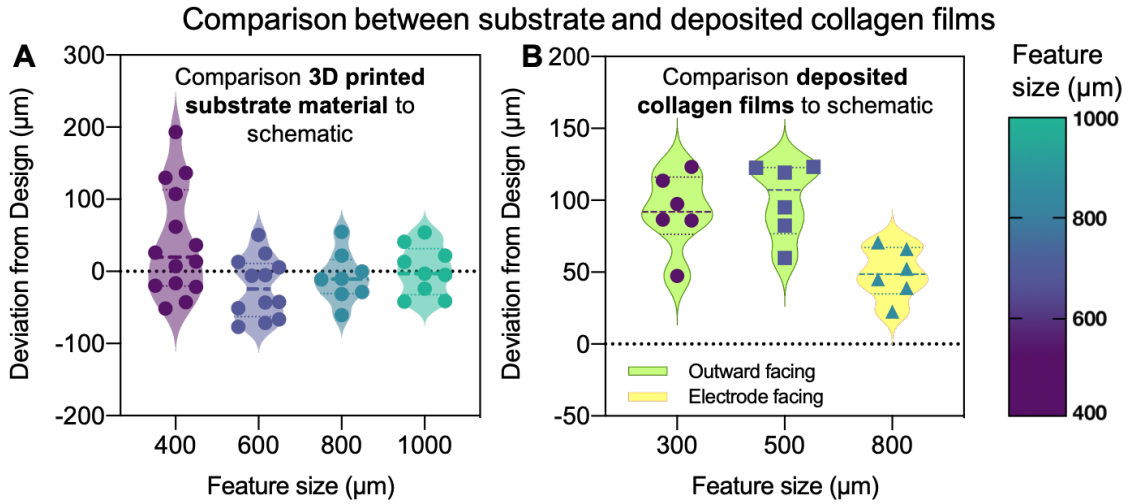

Fig. 5.13 Scatter and violin plot of measured deviations from (A) original design of 3D printed resolution pieces for different feature sizes and (B) grooved collagen film from original grooved substrate design for different feature sizes.

film (away from the deposition substrate) consistently deviated to a greater degree than the features measured on the substrate-facing side on the film. The range of deviation measured for each feature size remained broadly similar across measured feature sizes, and were equal to that of the substrate material with a range of approximately 100 µm. These results show accurate translation of the substrate features to the collagen films.

5.4 Discussion

5.4.1 Efficacy of Cellulose Sacrificial Layer for Collagen Films

Removing dried collagen deposits from metal substrates, without damaging the collagen, proved to be a challenge [24]. The use of a sacrificial layer during deposition [280] presented itself as a solution to this problem. One aim of this chapter was to determine if using cellulose acetate as a sacrificial layer was a viable option for removing collagen deposits from substrates. Furthermore, it also sought to highlight any potential detrimental side-affects, if any, of using a cellulose acetate sacrificial layer.

It was found that the use of a cellulose acetate sacrificial layer was extremely effective and consistent in removing collagen from the substrate. No physical damage was seen in collagen removed using this technique, unlike films removed using mechanical cleavage (Figure 5.5). Further investigation also showed that the deposition process and film compositions were unaffected, with no contamination of the collagen (Figures 5.7 and 5.8). Additionally, cellulose acetate is cheap and non-toxic, minimising any potential risks for use in medical materials, and the protocol for application is easy and scalable [282]. Furthermore, this technique is quick, only requiring an additional 2 hours to remove films. Following these findings, it is concluded that a cellulose acetate sacrificial layer is not only viable, but also advisable for removing collagen films effectively.

5.4.2 Producing Tubular Collagen Films using a Cellulose Sacrificial Layer

A tubular EPD rig was developed (Figure 5.3) to make free-standing seamless collagen tubes using electrophoretic deposition (Figure 5.6). Currently, there is no research to suggest that a thick, uniform, tubular collagen film could be achievable with casting methods. The use of the sacrificial layer was crucial for removing the tube from the substrate, as the collagen

strongly adhered and could not be removed via mechanical cleavage with a razor blade. This shows the advantages of using EPD processing with a sacrificial layer, over casting of collagen films. While only tubes have been formed, this is evidence that substantially curved shapes can be achieved with the technology. This is one potential use for shaped EPD collagen films, and shows the versatility of the technique, which could be adapted to a whole host of biomedical uses such as in nerve guidance conduits.

5.4.3 Producing Grooved Collagen Films using a Cellulose Sacrificial Layer

A grooved stainless steel substrate was produced to assess the ability to create complex shaped collagen films and the efficacy of using a cellulose acetate sacrificial layer in this process. The grooved stainless steel substrate was produced using the 3D printing technique of selective laser sintering of powdered stainless steel.

Collagen was successfully deposited onto cellulose-coated grooved substrates, and was subsequently removed after drying using a sacrificial layer. The collagen films that were removed maintained the grooved features provided by the substrate, including when hydrated (Figure 5.9). Analysis of the grooved collagen films using SEM showed that the features present were larger than originally designed (approximately 50 – 100 µm), particularly of the non-electrode-facing side of films (Figure 5.13). This artefact could be attributed to the thickness of the film adding the feature size at each edge (Figure 5.14). The thickness of a collagen film produced using equal parameters was approximately 40 – 60 µm [24].

It was also found that the rough features on the surface of the stainless steel were replicated onto the collagen films. SEM micrographs of the 3D printed stainless steel and the collagen films surface showed features of roughness that measured approximately 10 – 100 µm in size for both (Figures 5.10, 5.11, and 5.12). This indicated that there was an accurate translation of features to the collagen films, and that the cellulose sacrificial layer did

not inhibit this translation. The translation of roughness from substrate to collagen suggests that many other small topographical characteristics could be achieved in collagen films. This could be beneficial for a range of applications, particularly in regulating cellular activity. It has been shown that certain cell type prefer to spread on rougher surfaces (Ra = 0.2435 µm) [285], or will align along grooves (3 - 60 µm deep and wide) [286]. Furthermore, it has been found that specific grooved architectures of 400 µm in width can promote the formation of blood vessels in co-culture [287]. These characteristics could be tuned to enhance specific responses *in situ*.

From the findings presented in this chapter, it is apparent that there is a disparity in accuracy of replicated features between the large-scale grooves and the small-scale roughness. It is possible that the thickness of the deposited collagen is causing the measured sizes to be greater for the larger grooved features, as the thickness of the collagen film overhangs at each edge of protruding groove from the substrate, as depicted in Figure 5.14. While the roughness features were translated more accurately as they did not suffer from this artefact, caused by the film thickness.

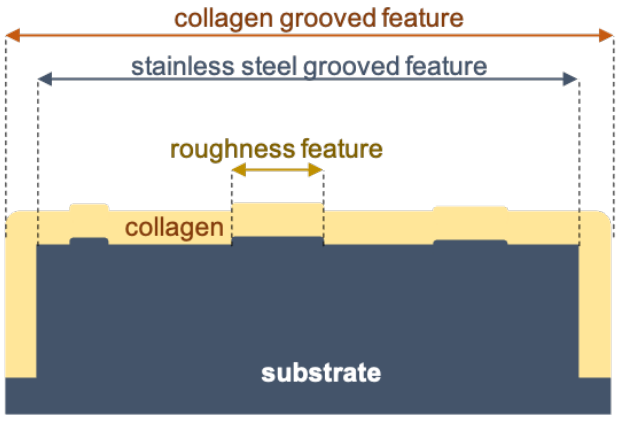

Fig. 5.14 Schematic showing cross-section of collagen deposited onto protruding ridge of grooved substrate. The thickness of the collagen film at the vertical edges of the ridge causes the measured collagen feature to be greater than the substrate feature size. Features caused by the surface roughness of the substrate are translated accurately, as film thickness not not attribute to the measured feature.

5.5 Conclusions

Removing well-adhered collagen films from the substrate post-EPD proved challenging, requiring the use of a razor blade and often damaging the film in the process. A cellulose acetate sacrificial layer was implemented as an effective method for easily removing collagen films from their substrate, without damage. Not only did this work with great effectiveness, it was found that the use of a cellulose acetate layer on the substrate did not detriment the EPD process or the collagen films produced.

Lastly, as well as an effective solution to the problem, a sacrificial layer also shows further potential for collagen deposits. The ability to make free-standing seamless collagen tubes and grooved films indicates the potential to form much more complicated shapes. Previously, deposits were flat in order to remove them using a razor blade. However, using a sacrificial layer, deposits can be a great range of shapes or topographies. One of the notable benefits of EPD, particularly in the ceramics industry, is its capacity for uniform depositions on almost any shaped substrate [21]. This means collagen scaffolds can be formed in a range of shapes and sizes for different applications, for example a tube for blood vessel replacement. Collagen deposit shapes could also be site- or patient-specific. Additionally, different topographies can be explored by depositing onto patterned substrates. Collagen films with patterned topographies may be beneficial in promoting and controlling cell growth. The future potential for collagen deposits is, therefore, great and varied.

Chapter 6

Degradation of EPD Collagen Films

6.1 Introduction

6.1.1 Background

Bioresorbable materials are biomaterials that degrade *in vivo* into non-toxic by-products [288]. Collagen is a natural structural protein, which can be broken down into small peptides and amino acids by the body [14], obviating the need for second surgery and making it an ideal material for developing implantable devices. However, in order for bioresorbable implantable medical materials to be fit for purpose it is important that they degrade within the body at the correct rate for their intended use [288]. For example, bioresorbable sutures, for internal stitching, should not break down before the tissue has healed otherwise the wound would reopen [289]. Furthermore, the controlled degradation of an implantable device may be utilised for the controlled release of a drug *in situ* from the bulk of the material [14, 290]. Therefore, it is extremely beneficial to have influence on the rate of degradation of a biodegradable implantable device.

Native collagen structures contain multiple inter- and intramolecular bonds that naturally stabilise and provide mechanical strength for the collagen. However, the extraction of

collagen often causes these cross-links to be broken down [51]. The stability of collagen in physiological conditions can be controlled by cross-linking the collagen, forming bonds between the collagen molecules and reinforcing it. Carbodiimide is a commonly used and effective cross-linking technique for collagen, increasing mechanical strength and degradation resistance [291]. Carbodiimide cross-linking, however, leads to reduction in available binding sites for site specific cell adhesion, thus reducing bioactivity [68]. It would, therefore, be beneficial to influence the degradation properties of collagen films without interfering with key binding sites and bioactivity, where possible.

It is theorised that the packing density of a material can influence its degradation properties. Closely packed molecules are likely to have stronger intermolecular bonds and less intermolecular space within the bulk of the material for infiltration of degradation-inducing molecules, such as collagenase for collagen materials [292]. Electrophoretic deposition (EPD) has been noted for its ability to form tightly packed, dense layers of materials [157]. Additionally, EPD processing allows for great deposition parameter control, which could be utilised to tailor the density of collagen films deposited in this manner.

It was suggested by Barrett et al. that collagen films produced using EPD had a greater density than solvent cast collagen films [25]. It is possible that the force arising from the electric field, driving the collagen during electrophoretic deposition, causes the collagen to pack together tightly during deposition. There is evidence to support this, with multilayer collagen-hyaluronic acid films [24]. As more layers were deposited, the previous layers, which were deposited with the same masses and under equal parameters, were compressed and became thinner (Figure 6.1). This suggests that driving force causing the deposition of addition layers caused the already-deposited layers to compress further. The driving force here, in EPD systems, is caused by the voltage; increasing the voltage of the system increases the deposition force and may result in denser films. This has previously been reported as a potential mechanism within EPD systems [293, 294]. However, the packing density of

materials processed with EPD is not so straightforward. Other EPD mechanisms have been described in the literature that suggest the packing density is also strongly affected by packing arrangement of individual particles as they approach the deposition substrate [295]. Particles that approach at a lower velocity, under a reduced electric field, have more time to arrange themselves into a more tightly packed structure upon deposition. However, this effect appears to be associated with ceramic materials at much higher voltages [23], while these deposition mechanics are much less characterised in biological macromolecular systems, such as with collagen.

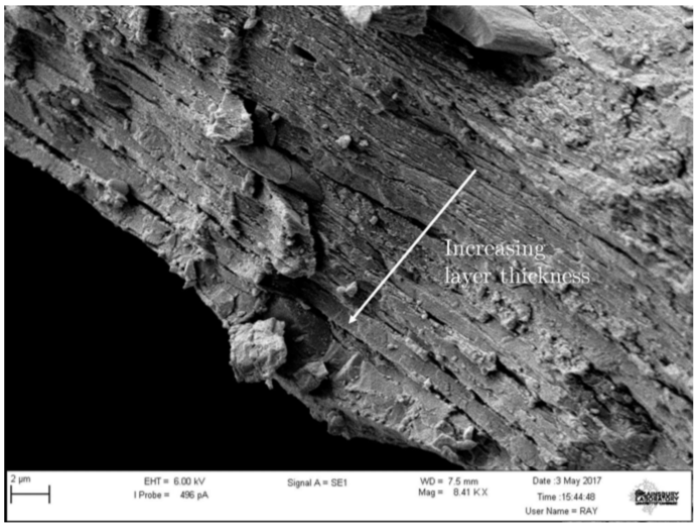

Fig. 6.1 CryoSEM image of hydrated collage-hyaluronic acid multilayer film showing compression of layers within the film. Figure adapted from reference [24].

6.1.2 Aims

There were two aims to this study. The first aim was to determine whether the densities of collagen films can be controlled by changing the force arising from the electric field by altering the deposition voltage during electrophoretic deposition of collagen, and to also compare these with the densities of solvent cast collagen films. The second aim of this study was to determine if the degradation properties of collagen films formed using electrophoretic

deposition can be controlled by manipulating the densities of these films. Films of differing densities were produced and measured, before being subjected to enzymatic degradation to understand what role density has in film degradation properties.

6.1.3 Chapter Structure

This chapter comprises three experimental sections. The first two experimental sections investigated the density of collagen films produced using EPD. Following initial results (described in Section 6.3) it was found that the EPD setup up required development in order to successfully achieve the aims of this chapter. Controllable collagen film density using EPD was achieved in a novel EPD rig, as described in Section 6.4. The effect of density on collagen film degradation properties was then explored in Section 6.5.

6.2 General Methods

6.2.1 Collagen Preparation

Collagen type I (Sigma Aldrich, C9879) was hydrated in 0.05 M acetic acid to a concentration of 0.5 wt.% and homogenised on ice for 30 minutes at 10,000 RPM using a T 18 digital Ultra-Turrax homogeniser (IKA), following the protocol in Section 3.2.1. The collagen suspension was then dialysed against deionised water for approximately 30 hours, using the protocol in Section 3.2.2. The dialysed collagen suspension was mixed with ethanol and homogenised for 30 minutes, following the protocol in Section 3.2.3, such that the final concentration was 50 vol.% ethanol, 0.25 wt.% collagen I.

6.2.2 Solvent Cast Collagen Films

Collagen suspension, as prepared in Section 6.2.1, was pipetted into a silicone mould and left to air dry for three days, or until completely dry. The volume of collagen suspension was 4 mL, equal to the volume of suspension used within the EPD rig, and the mould shaped, also equal to the deposition area of the EPD rig, was 2×2.5 cm. Once dry the collagen film were carefully removed from the silicone moulds.

6.2.3 Substrate Preparation

Deposition substrates were coated with a cellulose acetate (Sigma Aldrich, 180955) sacrificial layer, following the protocol in Section 5.2.2, prior to EPD.

6.2.4 Electrophoretic Deposition

Electrophoretic deposition of collagen films was performed following the protocol in Section 3.2.7. The EPD rig setups for each experiment are described in Sections 6.3.1 and 6.4.1. In

each EPD rig collagen suspensions were deposited under pulsed current parameters, with pulse period of 50 ms, duty cycle of 40%, and a range of deposition voltages between 5–10 V.

6.2.5 Removing Collagen Deposits from the Substrate

Following deposition, once the collagen films had dried on the substrates, collagen films were removed by dissolving the cellulose acetate sacrificial layer in acetone, following the protocol in Section 5.2.7.

6.2.6 Measuring Collagen Film Density

The density of dry collagen films was determined by measuring their flat area with digital calipers and thickness with a digital micrometer; thicknesses were measured across five points on the films to ensure accuracy. From these measurements the volume was determined. The masses of the films was measured using a AG204 Balance (Mettler Toledo). The density of films was calculated by dividing the mass by the volume.

6.2.7 Scanning Electron Microscopy

Dry collagen samples were prepared for scanning electron microscopy by coating them in a thin layer of gold, before placing them onto a stub and into the electron microscope. SEM micrographs of the top surface of collagen films were taken using a Nova NanoSEM, beam voltage 5 kV.

6.2.8 Statistical Analysis

Statistical analysis was performed and graphs generated from the collected data using Graphpad Prism 8 software.

6.3 Density of Collagen Deposited onto the Electrode

In this section the density of collagen films deposited onto the electrode via EPD was investigated. Electrophoretic deposition of collagen suspensions was run at varying voltages to understand what effect deposition voltage had on film density. These were also compared with the density of collagen films formed via solvent casting.

6.3.1 Materials and Methods

Electrophoretic Deposition onto Electrode

The stainless steel deposition electrode (substrate) was coated in cellulose acetate (Section 6.2.3), prior to EPD. The collagen suspension, as prepared in Section 6.2.1, was loaded into the EPD rig, which comprised two electrodes separated by silicone spacers (Figure 6.2). Pulsed-current EPD was run at various voltages between 5–10 V with pulse period of 50 ms, and duty cycle of 40%.

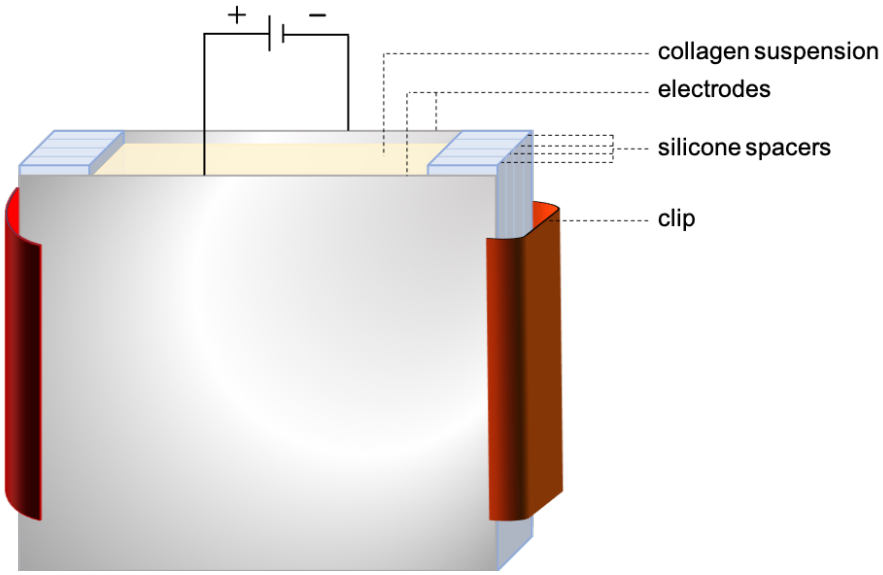

Fig. 6.2 Schematic showing the EPD rig. The EPD cell was formed of two stainless steel electrodes separated by silicone spacers. collagen suspension was loaded into the EPD cell and the stainless steel electrodes were connected to a waveform generating power supply.

Visual Observations

Following deposition, electrodes with collagen deposits were removed and immediately photographed using a hand-held camera, before the deposit had dried into a film.

6.3.2 Results

Density of Collagen Films Deposited onto the Electrode

Collagen was deposited onto electrodes. Photographs were taken of collagen deposits formed at 5 V and 10 V immediately after deposition, but before drying (Figure 6.3). The 5 V wet collagen deposit formed a thick gel-like structure before drying down into a film. The wet 10 V deposit, on the other hand, formed a visibly more compacted layer of collagen, prior to drying.

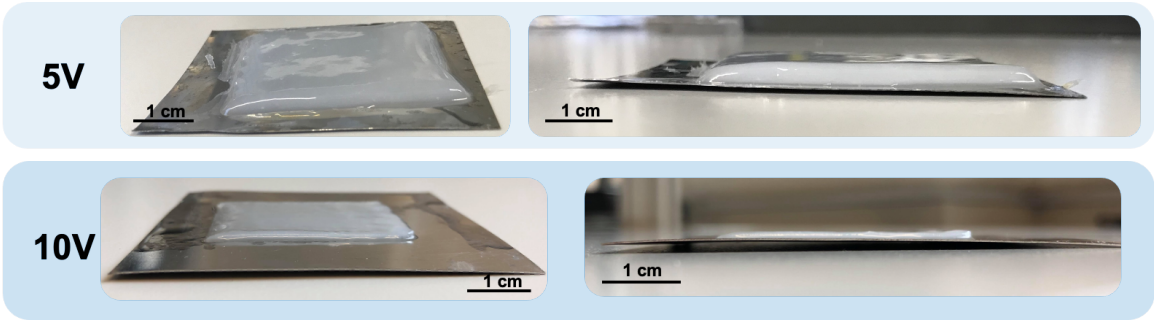

Fig. 6.3 Photographs of collagen deposits on the deposition substrate immediately after EPD, before the collagen had been allowed to dry. Top: collagen deposited at 5 V onto an electrode. Bottom: collagen deposited at 10 V onto an electrode.

The density of the EPD films produced, as well as of cast films, was measured (Figure 6.4). Films deposited onto the electrode initially increased in density with voltage until a deposition voltage of 7 V giving a density of 590 $\mathrm{kg\,m^{-3}}$, after which density of films dropped at 8 V. The density of films increased between deposition voltages 8 V and 10 V, however this did not exceed the density of film produced at 7 V. With a density of 320 $\mathrm{kg\,m^{-3}}$, solvent cast film density was lower than EPD films, including those produced at low voltages.

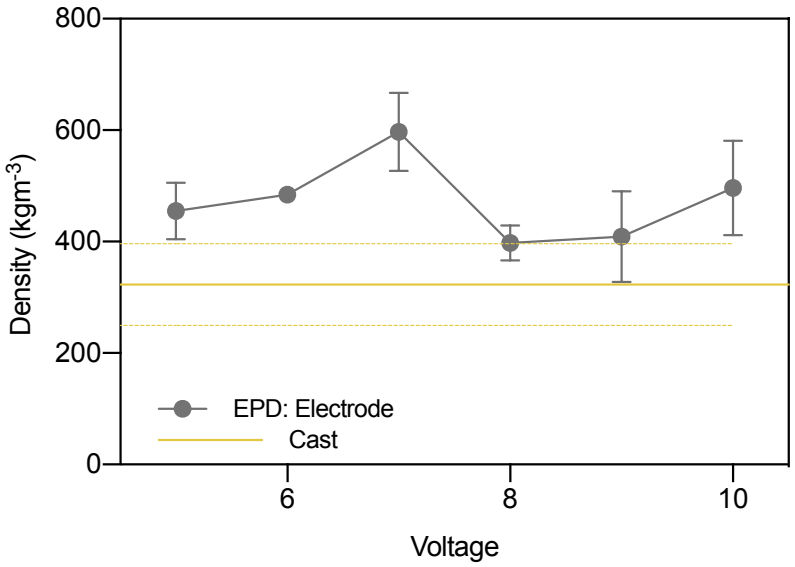

Fig. 6.4 Density of dry collagen films form via EPD and solvent casting. Density of EPD deposited collagen films are plotted as a function of the deposition voltage, for films deposited onto the electrode (grey). The density of solvent cast collagen films are shown as a yellow line, which bares no relation to voltage.

Scanning Electron Microscopy of Collagen Films

SEM micrographs were taken of dried collagen films produced via EPD on the electrode. The SEM image of a collagen film deposited onto the electrode at 5 V showed a flat surface with no notable features (Figure 6.5).

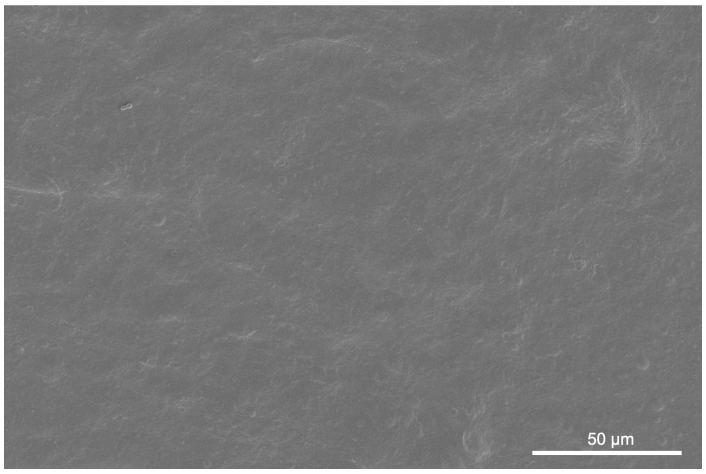

Fig. 6.5 SEM micrograph of the surface of a collagen film formed via EPD onto the electrode with a deposition voltage of 5 V.

On the other hand, the SEM image of a film deposited at 10 V onto the electrode showed the presence of many microscopic bubbles formed within the collagen film (Figure 6.6). These pockets of gas were unnoticeable to the naked eye and were encapsulated beneath the top surface of the film.

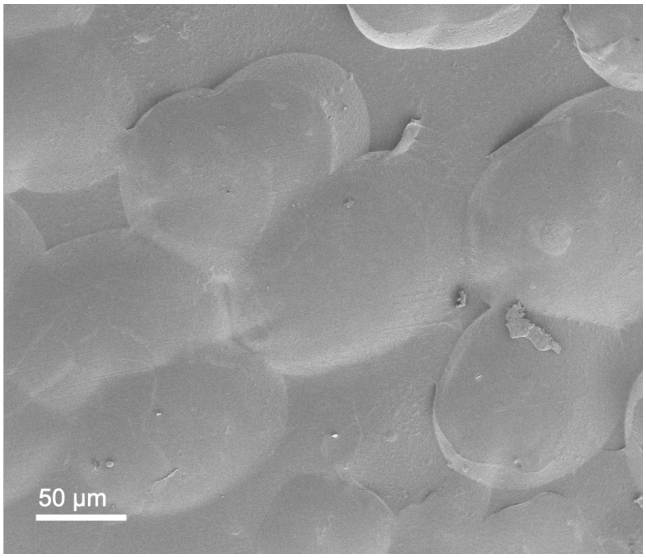

Fig. 6.6 SEM micrograph of the surface of a collagen film formed via EPD onto the electrode with a deposition voltage of 10 V.

6.3.3 Discussion

Collagen films produced using EPD were consistently found to have a greater density than solvent cast collagen films, which confirms the initial findings by Barrett et al. [25]. Furthermore, the density of collagen films produced using EPD appeared to initially increase with increasing deposition voltage, however, at a deposition voltage of 8 V the density of the produced films dropped, increasing slightly at 10 V. Investigation of collagen films produced at 5 V and 10 V using SEM showed that films deposited onto the electrode at 10 V contained many microscopic encapsulated bubbles.

While altering the deposition parameters could be an effective strategy for controlling film density, collagen suspensions require an aqueous medium and electrophoretic deposition

of aqueous suspensions is associated with issues relating to gas bubble nucleation. These problems are caused by an electrochemical reaction at the electrodes, where the applied electric field results in electrolysis of water. This electrochemical breakdown of water causes the formation of hydrogen and oxygen molecules at the cathode and anode, respectively, which can nucleate into bubbles under certain EPD conditions [154, 155]. To minimise this effect, pulsed-current EPD has been developed, allowing these molecules to diffuse away before being allowed to nucleate [168–171]. Previous work into EPD of collagen films optimised the pulsed current parameters to allow for defect-free collagen films. Upon further investigation, however, it was found that the formation of gas bubbles within the collagen films was not entirely avoided. Figure 6.7 shows AFM and SEM images of the surface of collagen films produced via EPD within the specific window of parameters for defect-free films (with PC-EPD parameters of 5 V, 50 ms pulse period, and 40% duty cycle) [24]. It can be seen that microscopic bubbles are still present within the collagen films, under the surface. Examination of the cross-section of these films revealed that bubbles were present within the bulk of the films, encapsulated by collagen (Figure 6.7). The SEM image showed a void within the collagen film, where the collagen lamellar of the film can be seen packed tightly together. Surrounding the void, the collagen appeared to be further compressed, forming a "skin" around it [24]. Similar voids can also seen in the cross-sectioned collagen films imaged in Figure 2.22 [25].

There may be several issues in controlling the density of collagen films by changing deposition parameters while using suspensions of this type. The parameters used in the study by Barrett et al. [24] were found to be the only region in which these collagen suspensions can be deposited defect-free. The investigations in this chapter used dialysed collagen suspensions, as described in Chapter 3. Dialysis of collagen suspensions has been found to remove excess charge carriers from the suspensions, resulting in reduced current during depositions, thereby reducing the electrolytic effect on water. This means that collagen

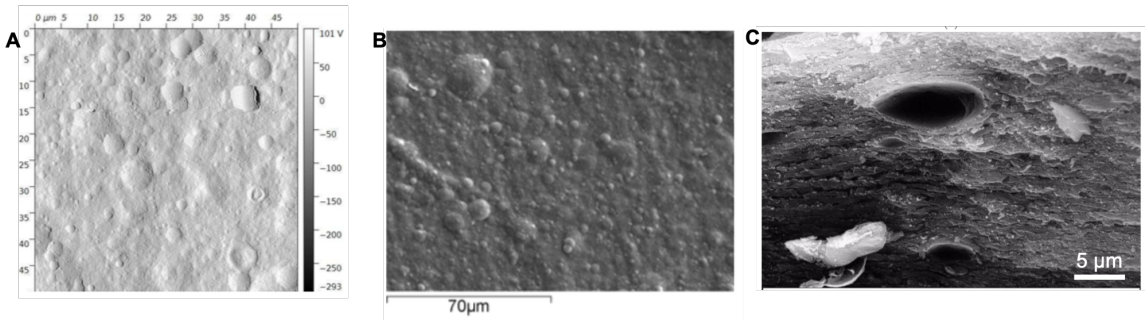

Fig. 6.7 (A) AFM image of the surface of a collagen film deposited onto the electrode at 5V, pulsed-current. (B) SEM image of surface of a collagen film deposited onto the electrode at 5 V, pulsed-current. (C) CryoSEM image of the cross-section of a collagen film, showing an enclosed pore within the film formed from the nucleation of a bubble during deposition. The collagen film was formed via PC-EPD at 5 V. Figure adapted from Reference [24].

can be deposited at much greater voltages than previously reported without the risk of gas nucleation and damaged films. This can explain why the collagen films produced at 5 V did not show evidence of microscopic bubbles, which were seen in previous studies of non-dialysed collagen deposits [24]. However, at greater deposition voltages it was found that bubbles were present within the films – SEM micrographs highlighted this in films produced at 10 V. The presence of air pockets within films will result in reduced bulk density. This issue would explain why the measured density of collagen films dropped at deposition voltages greater than 7 V. A schematic depicting how the bulk density of EPD collagen films varies is shown in Figure 6.8.

An issue for controlling film density is that, while films may appear defect-free, it has been shown that microscopic gas bubbles may still form within the bulk of collagen films deposited on the electrode, leading to open pores within films and reduced density. Depositing onto ion-permeable barrier membranes has been found to be another effective technique in mitigating gas bubble nucleation within deposits [277]. The ion-permeable barrier membrane is positioned within the EPD cell, away from the electrode. It permits the passing of ions through it, maintaining the electric field, but larger molecules cannot pass through, and therefore deposit onto the membrane, while any gas bubble nucleation occurs at

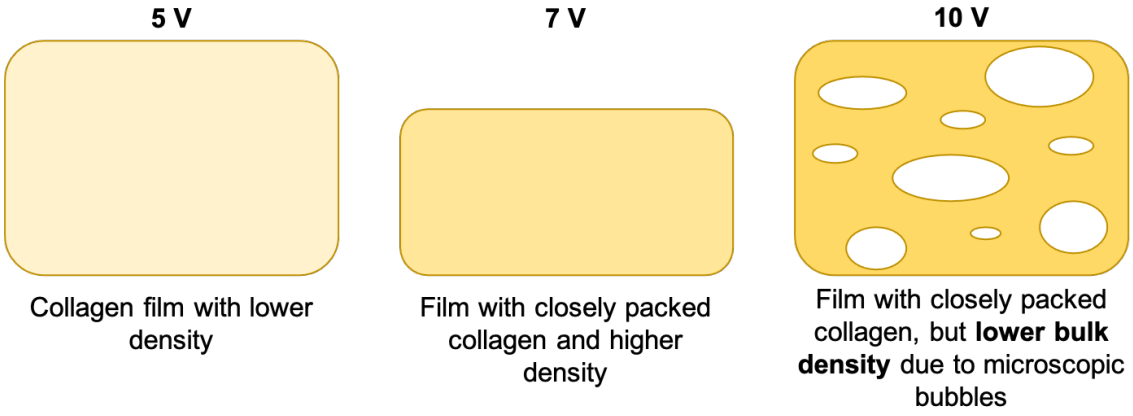

Fig. 6.8 Schematic diagram showing how the bulk density varies between collagen films produced at varying deposition voltages. In this depiction, all the collagen films have equal mass. The collagen film formed at 5 V has lower density than the film produced at 7 V, which has closely packed collagen. The film produced at 10 V has closely packed collagen, however, the bulk density of the film is reduced due to the presence of microscopic voids formed from gas bubble nucleation during EPD.

the electrodes, away from the deposit. This requires a more complicated set up, but relieves any chance of bubbles forming within the deposit.

6.4 Density of Collagen Deposited onto an Ion-permeable Membrane

It has been found that, even using suitable deposition parameters, collagen films deposited onto the electrode may encapsulate microscopic gas bubbles, which, in turn, leaves pores within films affecting their densities. Collagen suspensions were dialysed prior to deposition, allowing for defect-free collagen films at a greater range of voltages than has previously been reported in the literature [24, 25]. While this study used dialysed collagen suspensions to minimise the nucleation of gas bubbles within films during EPD, deposition onto the electrode may still result in encapsulated gas bubbles within collagen films, albeit defect-free. Therefore, to judge the effectiveness of controlling density of collagen films deposited onto the electrode, and to avoid complications associated with gas bubble nucleation at the electrode, collagen films were also deposited onto ion-permeable barrier membranes away from the electrode.

6.4.1 Materials and Methods

Electrophoretic Deposition onto Ion-permeable Barrier Membrane

Electrophoretic deposition was carried out with collagen depositing onto an ion-permeable barrier membrane (Sigma Aldrich, D9527-100FT), located between two electrodes. Figure 6.9 shows a schematic of the custom-built EPD rig with the barrier membrane situated within the EPD cell, creating two chambers. The collagen suspension (prepared in Section 6.2.1) was loaded into one chamber of the EPD cell, and water was loaded into the other chamber. The electrodes were connected to the power supply as normal, with the positive electrode on the collagen side and the negative electrode on the water side such that, during EPD, the collagen would deposit onto the barrier membrane. EPD was run at various voltages between 5–10 V and at 40 V with pulse period of 50 ms, and duty cycle of 40%.

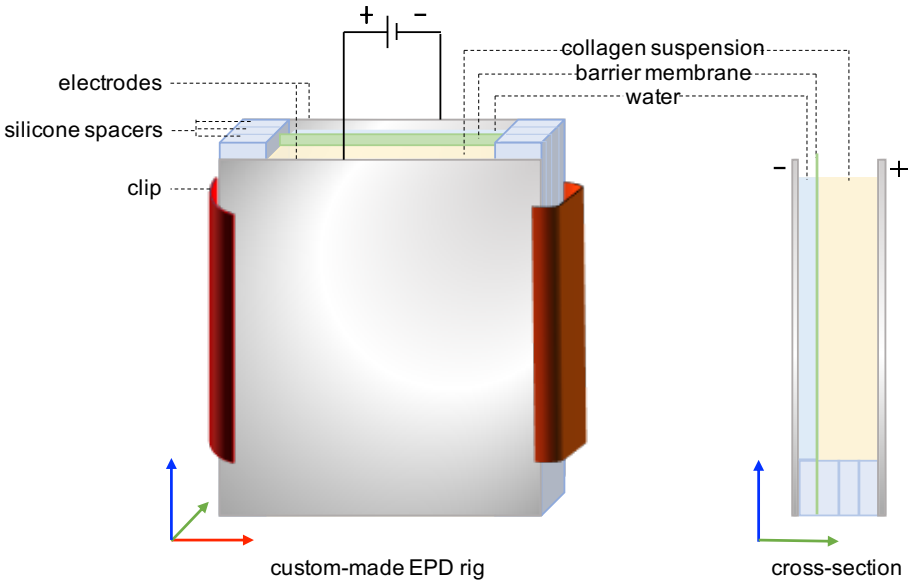

Fig. 6.9 Schematic showing the EPD rig containing a ion-permeable barrier membrane. On one side, with the positive electrode, collagen suspension is filled, the other side contains water, to maintain the flow of current during EPD. During deposition collagen migrates to the negative electrode and deposits onto the barrier membrane.

6.4.2 Results

The density of the EPD films produced on the barrier membrane was measured, along with EPD films deposited on the electrode and solvent cast films (Figure 6.10). The density of films produced onto a barrier membrane increased with increasing voltage, but appeared to reach a maximum density as the density of films produced at 40 V was not much more than at 10 V. Here, the densities of collagen films deposited onto the barrier membrane were compared with collagen deposited onto the electrode, produced in Section 6.3. The measured densities of collagen films were equal at deposition voltages of up to 7 V, after which the density of films deposited onto the barrier membrane continued to increase up to a deposition voltage of 10 V, whereas, as previously shown, the density of collagen deposited onto the electrode dropped at greater voltages.

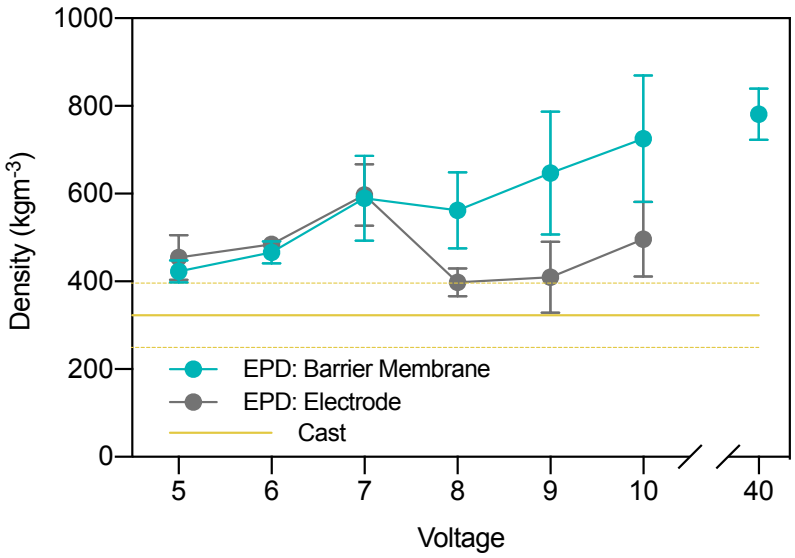

Fig. 6.10 Density of dry collagen films form via EPD and solvent casting. Density of EPD deposited collagen films are plotted as a function of the deposition voltage, for films deposited onto the electrode (grey) and onto a semipermeable barrier membrane (turquoise). The density of solvent cast collagen films are shown as a yellow line, which bares no relation to voltage.

6.4.3 Discussion

Microscopic bubble formation within collagen depositions — a by-product of aqueous EPD — caused issues in controlling collagen film density. An EPD rig containing a barrier membrane within the EPD cell was developed such that collagen from suspension could deposit onto the membrane away from the electrode, where bubbles nucleate due to the electrolysis of water. The revised rig allowed collagen to be deposited onto the barrier membrane without issue, as suggested by previous studies [277]. Furthermore, the issues associated with enclosed pores within the collagen film appeared to no longer be present, when comparing the densities of collagen films produced on the electrode and on the barrier membrane. It was shown that the density of films produced on the barrier membrane at 10 V were greater than their counterpart produced on the electrode.

This study showed that the density of collagen films could be controlled by changing the voltage at which collagen was deposited at. These results support the findings of Farrokhi-

Rad et al., who also showed that titania nanoparticle deposits increased in density when electrophoretically deposited at greater voltages [294].

6.5 Degradation of Collagen Films

The investigations in the previous sections showed that collagen film density can be manipulated by controlling the deposition voltage during EPD. However, it is of interest to understand what effect material density has on the degradation properties of collagen films. Degradation is an important property to consider for biomaterial implant designs, such that the implanted device breaks down at an appropriate rate for its purpose [288, 292]. This Section explores what effect density had on the rate of enzymatic degradation of non-cross-linked collagen films.

6.5.1 Materials and Methods

Collagen Film Degradation

A solution containing bacterial collagenase (from *Clostridium histolyticum*, Sigma Aldrich) in PBS was prepared to a concentration of 0.025 mg/mL, pH 7.4. Collagen films were producing using solvent casting (Section 6.2.2) and electrophoretic deposition onto a barrier membrane (Section 6.4.1). Collagen films, of varying density, but equal size and shape (maintaining similar surface area to volume ratios), were weighed, using a AG204 Balance (Mettler Toledo), before each being incubated in 20 mL collagenase solution at 37 °C for 4 hours. After this time the films were gently removed from the collagenase solution and washed three times with deionised water and left to air dry for 24 hours. Once films were completely dry, they were weighed again and the percentage mass loss was calculated.

6.5.2 Results

Collagen films were degraded using the enzyme collagenase, and their percentage mass loss was determined as a function of their density (Figure 6.11). The films used were produced by solvent casting and electrophoretic deposition at 5 and 10 V onto a barrier membrane, and

their density was recorded. It was found that the denser films retained more of their mass when subjected to collagenase and, thus, degradation decreased with increasing density of collagen films.

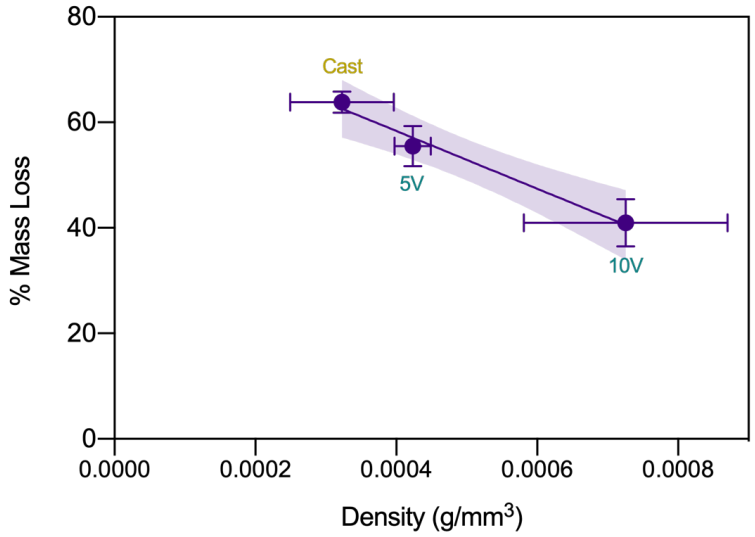

Fig. 6.11 Degradation of collagen films incubated in 0.025mg/mL collagenase in PBS solution at 37°C for 4 hours plotted as a function of film density. The films were formed via solvent casting and EPD at 5 and 10 V, labelled on the plot.

6.5.3 Discussion

Collagen films were produced with a range of densities using EPD and also solvent casting. These collagen films of differing densities were investigated to understand their resistance to enzymatic degradation. It was suggested that collagen materials could have a greater enzymatic degradation resistance at greater densities [292], amongst other properties, such as cross-linking. Here, it was shown that collagen films with greater density degraded at a slower rate. Therefore, the degradation properties of collagen films can be controlled, to a degree, by altering the electrophoretic deposition parameters at which they are produced. However, it is important to note the enzymatic conditions used here are not representative of physiological conditions and that these results do not directly relate to degradation *in*

vivo. The enzymatic conditions used in this study were chosen to provide a comparison of degradation resistance between films of different densities.

6.6 Chapter Discussion

6.6.1 Density of Collagen Films

Electrophoretic deposition has proven effective at forming dense materials, due to the electric force and packing mechanisms associated with the processing technique [157, 293]. It was found that collagen films produced with EPD contained tightly packed collagen fibres compared with the loose layering of solvent cast collagen films, though bubble encapsulation within the films was also reported [24, 25]. This study used dialysed collagen suspensions to form collagen films via EPD, as dialysis of collagen suspensions reduces the nucleation of gas bubbles at the electrode and allows for a greater range of deposition voltages able to form defect-free films.

Before collagen deposits were dried down into films, it was shown from the wet deposits that the films formed at the greater voltage (10 V) were much more tightly packed than at the lower voltage of 5 V (Figure 6.3). This corresponded to results shown in Figure 6.10, where, for collagen deposited onto the barrier membrane, the density of collagen films increased with increasing deposition voltage. This has been corroborated in the literature where it was found that increasing the electric field increased the density of titania nanoparticles [294] and alumina [140]. However, in the same study, beyond a certain electric field strength the density of alumina decreased [140]. This characteristic is apparent in several studies, and it appears there are two mechanisms governing the density of EPD deposits: initially, as the deposition voltage is increased, so is the density of the deposit, however, at much higher voltages the velocity at which particles are deposited does not allow sufficient time to arrange themselves into tightly packed layers, resulting in inhomogeneous, porous layers [296]. The point at which this occurs, however, is at extremely high voltages, often greater than 100 V, which are frequently used in ceramics processing but are not used in this study, and these forces likely do not affect collagen deposition.

A further mechanism for increasing deposit density is also described, where increased deposition times, even after all the material has deposited, caused greater densities. In this instance the force arising from deposition voltage continues to be applied onto the deposit, causing it to continue packing and increase in density [294, 297]. Evidence of this mechanism was already observed in collagen deposits, where Barrett formed multilayer collagen deposits, the initial layers where thinner than the more-recently deposited layers (Figure 6.1) [24]; these layers, for each deposition, would have felt cumulatively a much longer duration of applied force.

While the density of collagen films increased with increasing voltage when deposited onto the barrier membrane, the trend was not true for EPD onto the electrode. Initially, the density of collagen films deposited onto the electrode increased with voltage, however, after 7 V the density of films dropped significantly (Figure 6.4). SEM images were taken of films produced on the electrode at 5 V and 10 V to understand this decrease in density. While there were no notable features on the film produced at 5 V, it was found that the film produced at 10 V contained many microscopic bubbles beneath the surface (Figures 6.5 and 6.6). This finding is similar to those found in previous collagen films produced by EPD of non-dialysed collagen suspensions, and suggests that the film produced at 10 V contains enclosed pores [24]. These enclosed pores were likely caused by the same mechanism of gas bubble nucleation at higher voltages. Thus, while the lower voltage films contain no evidence of bubbles, due to the suspensions being dialysed prior to EPD, microscopic bubble nucleation does still occur at the electrode at greater voltages. The presence of these enclosed pores formed from microscopic gas bubble nucleation within the film will ultimately lower the density of the collagen films, explaining the reduced density measurement of Figure 6.4.

6.6.2 Degradation of Collagen Films

Controlling the degradation properties of collagen biomaterials has previously involved chemical cross-linking. The most common technique, carbodiimide cross-linking, forms covalent bonds between collagens, which use up amine groups that are key for integrin binding of cell specific adhesion [68]. Therefore, carbodiimide cross-linking of collagen reduces collagen bioactivity. While other forms of collagen cross-linking exist, such as genipin cross-linking [298], carbodiimide remains popular due to its ability to improve the degradation and mechanical strength, without using harmful chemicals.

The degradation properties of collagen films can be manipulated by controlling the film density. As previously discussed, the density of electrophoretically deposited collagen films can controlled by changing the deposition voltage. It was found that increasing the film density reduces the rate of enzymatic degradation. Densely packed collagen molecules form stronger intermolecular, non-covalent bonds, which make the films more resistant to attack by collagenase. Degradation properties can, therefore, be controlled by controlling the EPD parameters, without the need for chemical cross-linking, maintaining the collagen's inherent bioactivity.

6.7 Conclusions

Increasing deposition voltage increased the density of collagen films, however, the increase in voltage also resulted in gas bubble nucleation at the electrode due to the electrolysis of water. These bubbles formed within collagen films deposited onto the electrode, causing the formation of enclosed pores, reducing film density This complication was overcome by depositing collagen onto an ion-permeable barrier membrane, away from the electrode and bubbles. By depositing onto the membrane, density of collagen films can be controlled by varying the deposition voltage.

Increasing the density of collagen films resulted in reduced enzymatic degradation of collagen. The degradation properties of collagen films formed from EPD can, therefore, be controlled by manipulating film density. This reduces the need to stabilise collagen films with chemical cross-linkers that reduce their bioactivity.

Chapter 7

Aligning Collagen Fibres within Films

7.1 Introduction

7.1.1 Background

In order for collagen films to be used clinically, in applications such as maxillofacial bone ridge augmentation surgery, it is necessary that they can be secured using sutures. The collagen films currently produced tear easily [24] and, if sutured, may not remain fixed in place. It is hypothesised that the mechanical properties of the films can be controlled by aligning the collagen fibrils in one direction. Following previous studies that have aligned collagen threads to increase mechanical strength [216, 217], it is proposed that tensile strength of films will increase, for loading parallel to the alignment of fibrils. Furthermore, creating multilayer, multi-orientated collagen films would, in turn, improve suture tear resistance of films by increasing the tensile strength in many directions.

There have been several attempts at aligning collagen fibrils *in vitro*, most often during fibrillogenesis. Some techniques used to align collagen fibres include extrusion of collagen slurries [99, 299] and mechanical stretching of collagen materials [221, 300]. Other work has introduced a high magnetic field (> 1T) during gelation [301–305] — this is possible

to align collagen fibres in very high magnetic fields as collagen has a small diamagnetic susceptibility [306]. However, these methods are not suitable to be combined with EPD, since they require either extrusion, stretching, or extremely powerful and expensive magnets. A protocol, proposed by Guo et al. [307], described a method to align collagen without expensive or complicated equipment. Following the same principles for aligning collagen with strong magnets, they generated a magnetic field with very weak magnets and induced collagen alignment with conjugated carboxylate modified magnetic iron oxide beads. This addition would be unsuitable within the electric field of EPD and, although non-toxic, the addition of iron oxide into an implantable material is undesirable [308].

Another technique for artificially aligning collagen fibrils is the use of induced flow; a study by Goffin et al. described a method to align collagen fibres through interfacial flow processing of collagen while inducing fibre formation [309]. Similarly to extrusion to align collagen, this technique relies on shear force to cause long collagen fibrils to align in the direction of flow. Furthermore, a study into elongational flow of polymer solutions showed that such flow conditions resulted in greater alignment of polymer chains in solution, determined by measuring the birefringence [310]. Inducing relative flow during EPD between the collagen suspension and the deposition electrode creates a shear force that could induce alignment of the collagen fibrils during deposition.

7.1.2 Aims

The aim of this study was to develop a method for aligning collagen fibrils in collagen depositions and determine the effect this had on the mechanical properties. In previous studies methods have been described to align collagen fibres through generating flow and shear forces to act on collagen during structure formation, such as during gelation. The aim of this study was to develop a method of generating shear force on collagen suspensions during electrophoretic deposition in order to align collagen fibres within deposited collagen films.

Here, several attempts were made to consistently produce uniform alignment of collagen within films produced using EPD. Furthermore, this study aimed to optimise the processing parameters to produce high levels of collagen alignment, and then understand what effect this had on the mechanical properties of collagen films. Finally, this study sought to develop a method of producing multilayer, cross-ply collagen films, with each layer aligned in a different orientation, thus potentially increasing the tear resistance of collagen films.

7.1.3 Chapter Structure

The work in this chapter was developed through many iterations in order to achieve the study aims. Each section outlines an attempt to achieve the aims of this study of aligning collagen within deposited films, and the techniques are described along with the reasoning behind each methodology, followed by the results of the experiments. Where the aims were not achieved, the shortcomings are discussed, and the potential to further develop the process is considered. These reflections then lead onto the next section and the next attempt to achieve the chapter aims, incorporating knowledge gained from the previous sections.

7.2 General methods

7.2.1 Collagen Preparation

Type I collagen (Sigma, C9879) was hydrated in 0.05 M acetic acid for 72 hours at 4 °C, similarly to the protocol in Section 3.2.1. The hydrated collagen was then homogenised on ice for 30 minutes at 10,000 RPM with a T 18 digital Ultra-Turrax homogeniser (IKA). The homogenised collagen was then dialysed in cellulose dialysis membranes (Sigma Aldrich, D9527-100FT) against ultra-pure type I deionised water, following the protocol in Section 3.2.2, for 30 hours, changing the dialysate regularly. Ethanol was then added to the dialysed collagen suspension, such that the final concentration was 50 vol.% ethanol, which was then homogenised for a further 30 minutes.

7.2.2 Viscosity

Collagen suspensions of concentrations from 0.1 – 0.5 wt.% were prepared as described in Section 7.2.1, in order to produce suspensions of differing viscosities, from 50-500 cP. Viscosity measurements were taken using a DV3T Rheometer (Brookfield). 0.5 mL was pipetted into the base of the rheometer, and the rheometer was sealed shut before running. For each measurement, a CPA-40Z disc was used, the temperature was 23.1 °C, the speed was 5 RPM, the shear rate was 37.5 s^{-1}, and the conditioning time was 30 seconds.

7.2.3 Substrate Preparation

Stainless steel electrodes and barrier membrane (Sigma Aldrich, D9527-100FT) substrates were coated with a cellulose acetate (Sigma Aldrich, 180955) sacrificial layer, following the protocol in Section 5.2.2, prior to EPD.

7.2.4 Electrophoretic Deposition of Collagen

Electrophoretic deposition was carried out using collagen suspensions (as prepared in Section 7.2.1) based on the methods in section 3.2.7. In each of the following sections, the experimental setup, EPD rig design and EPD parameters are explained.

7.2.5 Removing Collagen Deposits from the Substrate

Following deposition, once the collagen films had air dried on the substrates, collagen films were removed from the substrate by dissolving the cellulose acetate sacrificial layer in acetone, following the protocol in Section 5.2.7.

7.2.6 Deposited Collagen Mass

The dry mass of collagen deposited during EPD was measured using a AG204 Balance (Mettler Toledo).

7.2.7 Birefringence

Birefringence was used to determine the alignment of collagen fibres within the films. Birefringence is a measure of the optical anisotropy of a material, which in this case is brought about by the anisotropic alignment of collagen within films [311]. The greater the birefringence measurement of a collagen film the greater the alignment.

Firstly, collagen films were hydrated in water, and the thickness of the films was measured with a digital micrometer (Mitutoyo). Collagen films were then placed in a polarised light microscope, between the analyser and the polariser lenses that were oriented 90° to each other (schematic in Figure 7.1). The collagen sample was rotated so that the alignment of the collagen was oriented 45° to the analyser and polariser, this was seen when the maximum intensity of light was able to pass through the analyser. A quartz compensator

(Carl Zeiss) was inserted into the microscope between the sample and the analyser. The quartz compensator was rotated until no light passed through the microscope eye-piece, and the angle of the quartz compensator was recorded.

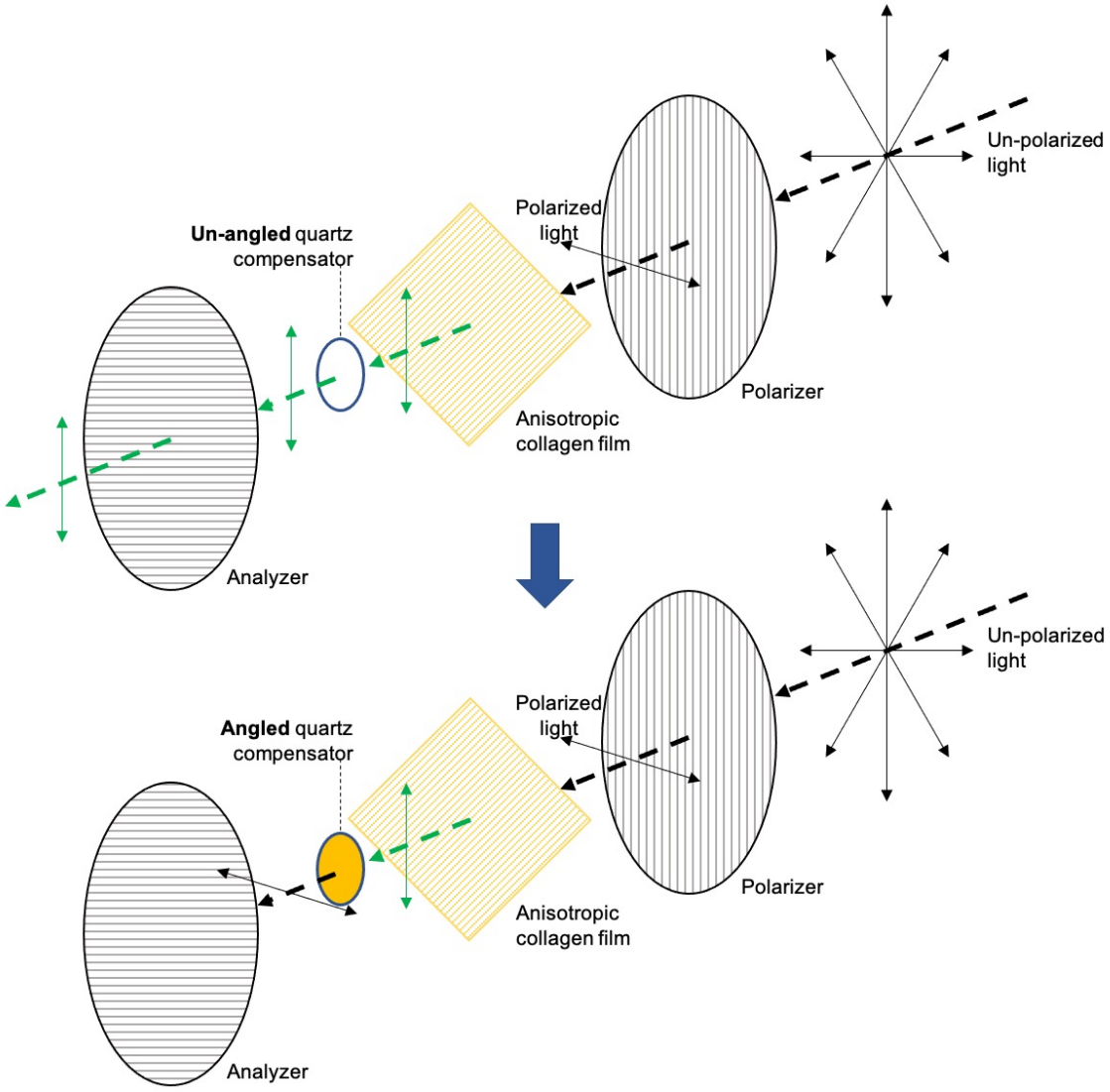

Fig. 7.1 Schematic showing the set up for measuring the birefringence of collagen films. Top: schematic shows the quartz compensator at an angle of 0° having no influence on the light. Bottom: schematic with the quartz compensator angled such that no light can pass through the analyser.

Using the angle recorded on the quartz compensator, the retardation (in nm) of light from the birefringent sample was calculated, using the following equation [312]:

$$retardation(nm) = -0.004(a)^3 + 1.2539(a)^2 - 0.54(a) - 5.3114 \tag{7.1}$$

where a is the angle recorded on the quartz compensator. The birefringence of the collagen films was then calculated using the retardation and sample thickness in the following equation:

$$birefringence = \frac{retardation(nm)}{thickness(nm)} \tag{7.2}$$

7.2.8 Statistical Analysis

Statistical analysis was performed and graphs generated from the collected data using Graphpad Prism 8 software.

7.3 Generating Flow during EPD to Align Collagen

As previously discussed, alignment of fibres can be induced in collagen materials by generating interfacial flow during material formation, causing a shear force [309]. During EPD, collagen deposits are formed on the surface of the electrode and, therefore, generating a flow of collagen across the electrode could cause a shear force that aligns collagen at the electrode surface while it deposits.

Here, an electrophoretic deposition rig was designed such that the collagen suspension could flow over the surface of the electrode during deposition. As shown in previous chapters, the EPD cell was formed of two parallel electrodes with silicone spacers between them acting as walls to the cell. Within the silicone spacers holes were made and inlet and outlet tubes were inserted, attached to a pump, which was used to flow a collagen suspension through the EPD cell and across the deposition electrode.

7.3.1 Materials and Methods

Electrophoretic Deposition in Flow Rig

The flow rig was custom-built such that the EPD cell had inlet and outlet tubes connected to a peristaltic pump (Watson-Marlow, 323S/D, 3-400 RPM). The EPD cell and tubing throughout the system was filled with collagen suspension. The peristaltic pump generated a flow of collagen through the EPD rig (Figure 7.2). Collagen was deposited onto the electrode using pulsed current electrophoretic deposition, while flowing through the EPD cell via the peristaltic pump, which ran at 1 – 10 RPM — the relative velocity was calculated in the next section. The deposition parameters used were as follows: pulsed current with deposition voltage of 10 V, duty cycle of 40% and pulse period of 50 ms.

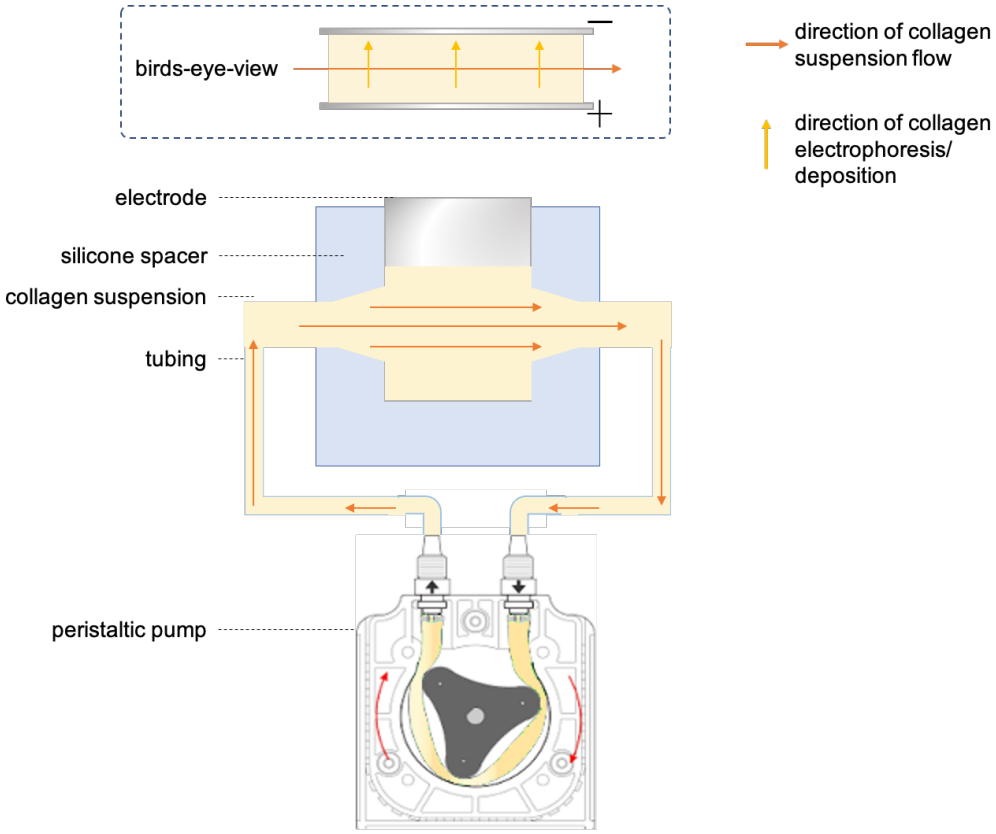

Fig. 7.2 Schematic showing a cross-sectional the EPD flow rig containing inlet and outlet tubes to a peristaltic pump. The top schematic shows a birds-eye-view of the EPD cell. The peristaltic pump generated flow of collagen through the rig and across the electrode surface during EPD: orange arrows depict the direction of flow of collagen suspension. When an electric field was applied across the cell collagen migrated to, and deposited on the negative electrode: the yellow arrows depict the direction of collagen fibre electrophoresis.

Volumetric Flow Rate

The volumetric flow rate of collagen suspension through the EPD cell was determined from the RPM of the peristaltic pump, where 1 RPM was equivalent to a volumetric flow 1 mL/min, as given in the peristaltic pump user manual (Watson-Marlow, 323S/D). The cross-sectional area in the EPD cell, perpendicular to the electrodes, was 100 mm^2. The volumetric flow rate was then given in $mL\,s^{-1}$, such that:

$$1RPM = 0.0167mL/s$$

7.3.2 Results

Collagen films deposited both with and without relative flow in the flowing EPD rig (Figure 7.2) were removed from the substrate and imaged in a polarising microscope to visualise any birefringent properties (Figure 7.3). Under brightfield conditions, where the light had not been polarised, both films could be seen clearly in the microscope. When the polariser was rotated the collagen film produced without relative flow could not be seen, in contrast to the film produced with relative flow, which could be seen but in a different colour and shade to the original brightfield image, due to its birefringent properties.

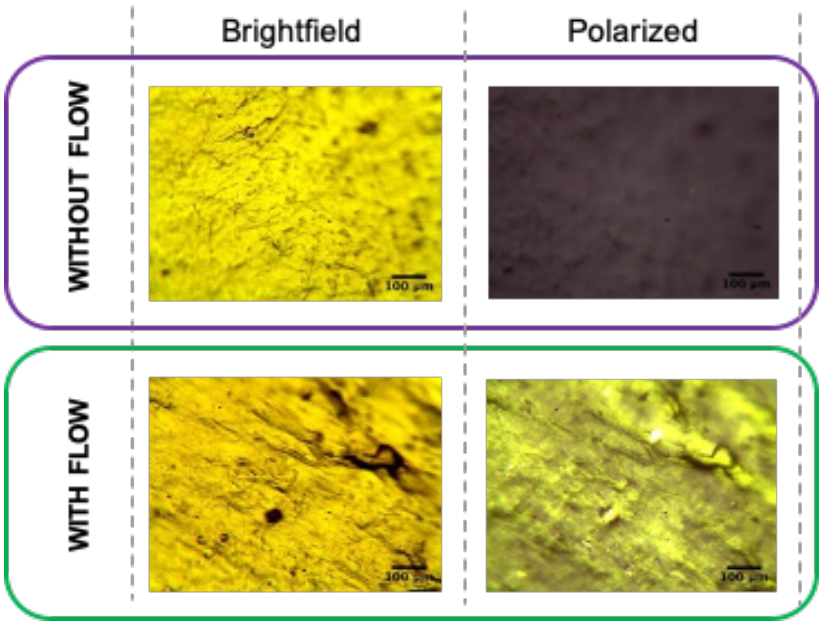

Fig. 7.3 Images of collagen films produced without (above) and with (below) relative flow during electrophoretic deposition within the rotating tubular rig. Collagen films were imaged under brightfield light (left) and polarised light (right).

The film produced here showing birefringent properties was produced with a volumetric flow rate of $0.083\,\mathrm{mL\,s^{-1}}$ (RPM of 5), however birefringence was only apparent in limited regions of the collagen film and was not consistent throughout the material. Furthermore, the peristaltic pump was not able to maintain a constant flow at such low RPM ranges, with the rotary rollers causing a pulsed flow of collagen, resulting in additional turbulence of the suspension within the EPD cell. At relative flow velocities below that represented in Figure 7.3 birefringence was less frequent and difficult to ascertain, where at flow rates greater than $0.083\,\mathrm{mL\,s^{-1}}$ no collagen was deposited onto the electrode. Table 7.1 below summarises the findings of the collagen films produced in the EPD flow rig at different relative flow velocities.

Table 7.1 Deposition and birefringence outcomes of collagen films deposited at 10 V PC-EPD with differing flow rates

RPM	Volumetric flow rate	Deposition Outcome	Birefringence
1	$0.017\,\mathrm{mL\,s^{-1}}$	Collagen deposited as normal	No birefringence was observed
2	$0.033\,\mathrm{mL\,s^{-1}}$	Collagen deposited as normal	No birefringence was observed
3	$0.050\,\mathrm{mL\,s^{-1}}$	Collagen deposited as normal	Few regions of limited birefringence were observed
4	$0.067\,\mathrm{mL\,s^{-1}}$	Collagen deposited as normal	Few regions of birefringence were observed
5	$0.083\,\mathrm{mL\,s^{-1}}$	Collagen deposited, with non-uniform thickness	Some regions of birefringence were observed
6	$0.100\,\mathrm{mL\,s^{-1}}$	Collagen deposited, with non-uniform thickness	Some regions of birefringence were observed
7	$0.117\,\mathrm{mL\,s^{-1}}$	Collagen only deposited at the edges of the EPD cell	Few regions of birefringence were observed
8	$0.133\,\mathrm{mL\,s^{-1}}$	Little collagen deposited, only at the edges of the electrode	Limited birefringence was observed
9	$0.150\,\mathrm{mL\,s^{-1}}$	Very small amount of collagen deposit, too thin to form a film	No birefringence was observed
10	$0.167\,\mathrm{mL\,s^{-1}}$	No collagen appeared to deposit	No birefringence was observed

7.3.3 Discussion

An EPD rig was developed such that the collagen suspension being deposited also flowed through the EPD cell during deposition. Based on previous studies [309], it was theorised that flowing collagen across the surface of the deposition electrode could induce alignment of the fibres during deposition. Collagen was deposited at 10 V with PC-EPD, while varying the flow rate to determine which parameters produced the greatest birefringence in collagen

films. At greater flow rates the collagen was not deposited onto the electrode to produce a film, therefore reduced velocities were necessary for collagen deposits to form. However, at very low flows, while collagen films were deposited as expected, they did not show evidence of birefringence, suggesting that the flow rate was not great enough to induce alignment. It was found that there was a window of parameters that provided sufficient flow to align collagen, but was not too fast to inhibit deposition. Within this region it was shown that collagen can be aligned during deposition.

While collagen films that were deposited with sufficient flow did have birefringent properties, this was only seen in some regions throughout the films, and was not consistent. It was noted that at these low RPMs the peristaltic pump produced a pulsed flow, instead of a constant flow rate. Peristaltic pumps, and other positive replacement pump systems, generate flow by increasing pressure at regular intervals [313], which, at the low flow rate required, will result in a noticeable pulsed flow. The pulsation in flow and pressure outputs of peristaltic pumps can be visualised in Figure 7.4. At higher flow rates these intervals become so frequent that the pulsed effect is lost. Furthermore, pumps that can maintain a constant flow at low flow rates often exert high shear stress on the liquid media being pumped, such as in axial or centrifugal pumps [314]. This would result in damaged collagen that could clump and drop out of suspension. The pulsed flow caused by the peristaltic pump resulted in turbulence of the collagen suspension, which was not conducive to smooth laminar flow across the surface of the electrode. Therefore, this made consistent alignment throughout the film difficult to achieve. Furthermore, irregular flow appeared to affect the uniformity of deposited mass onto the substrate, where films were deposited with unequal thickness throughout.

The results here showed that alignment can be produced in collagen films by generating flow of the suspension during deposition, however the alignment was inconsistent and the

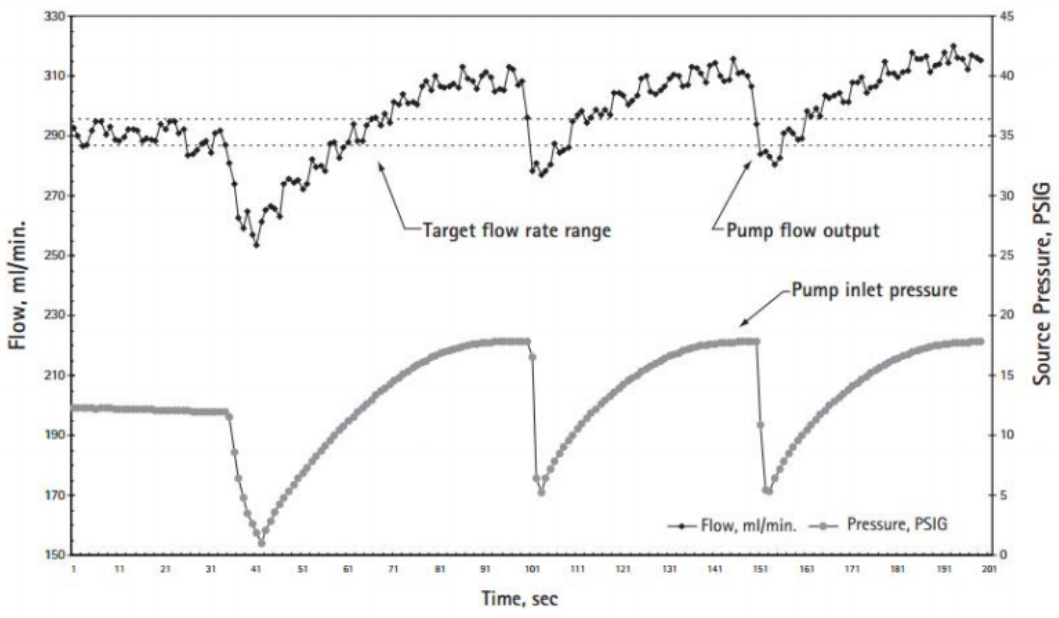

Fig. 7.4 Pulsation in flow and pressure output of a peristaltic pump. Figure adapted from Reference [313].

films were non-uniform. Therefore, it was necessary to develop an EPD rig that could generate a uniform, consistent flow of collagen suspension over the substrate during EPD.

7.4 Depositing onto a Rotating Substrate to Align Collagen

The EPD flow rig developed in the previous section showed that alignment of collagen was possible during deposition by generating an interfacial flow between the substrate surface and the collagen suspension. However, the peristaltic pump used caused irregular pulsed flow at such low flow rates. Finally, the EPD flow rig in the previous section only generated flow across the electrode in-line with the inlet and outlet tubes, and other regions of the substrate were not subjected to such flow.

In this section an EPD rig was developed that address the shortcomings associated with the previous design. Instead of generating interfacial flow between the substrate and the collagen by flowing the suspension across the electrode with an inadequate pump and non-uniform flow, here the substrate was mobilised relative to static collagen suspension, thus resulting in a relative interfacial flow between the two. The substrate needed to remain in contact with the collagen suspension throughout the EPD process, which can last several hours, such that the deposit has time to build up. A rotating tubular substrate was, therefore, decided as a suitable approach, and a rotating EPD rig was developed based on the design of the tubular rig used in Chapter 5, Section 5.2.5. It is possible that this tubular rotating substrate could allow for a uniform relative flow velocity throughout the deposition surface, and there would not be pulsed flow affect issues that were associated with the peristaltic pump.

7.4.1 Materials and Methods

Electrophoretic Deposition in Rotating Tubular Rig

The custom-built rotating tubular rig was an evolution of the tubular rig design used in Section 5.2.5. A small cylindrical electrode was placed inside a larger cylindrical electrode, both housed within a glass beaker. The small cylindrical deposition electrode was attached

via an axel to a DC motor, which, when connected to a power supply, caused the axel to rotate. The RPM produced by the DC motor was controlled by changing the input voltage, between 0-24 V. The rotating electrode, on the end of the axel, was connected to a cable brush, which maintained the electric circuit within the EPD system while the electrode rotated; a brush was necessary to avoid the cable wrapping around the electrode during rotation. The counter electrode was connected to the power supply using a crocodile clip (Figure 7.5).

Collagen suspension was loaded into the rig and the rotating electrode was spun at varying speeds by controlling the input voltage to the DC motor. The rotating electrode generated a relative velocity between the static collagen suspension and the electrode surface, resulting in a shear force. The electrodes were connected to a power supply and the collagen was deposited onto the rotating electrode via pulsed-current electrophoretic deposition, with deposition parameters: applied voltage of 10 V, pulse period of 0.05 s, and a duty cycle of 40%.

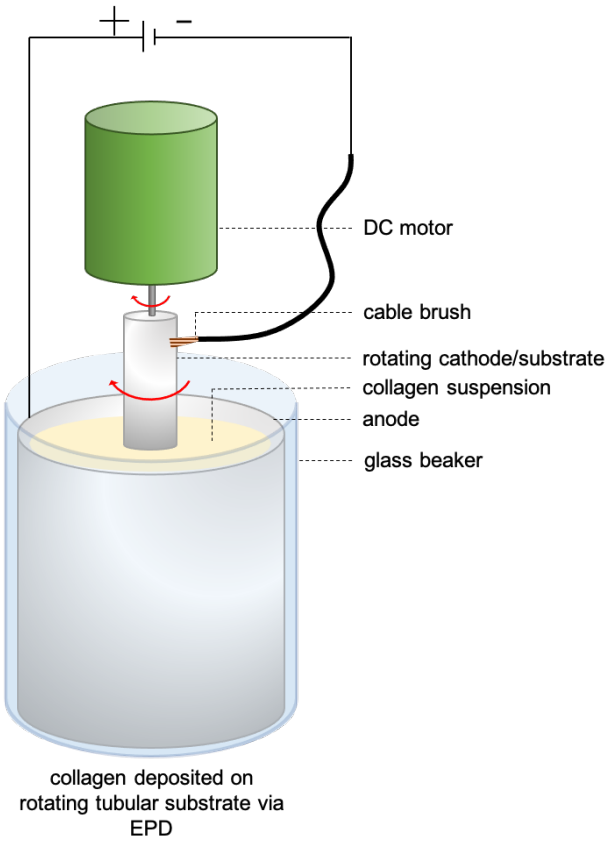

Fig. 7.5 Schematic showing the set-up of the rotating tubular EPD rig for depositing radially aligned tubular collagen deposits. Formed of one cylindrical electrode (the cathode/substrate) situated inside a larger cylindrical electrode (the anode), both inside a glass beaker. The deposition electrode, at the centre, was connected to a DC motor via an axel that, when switched on, caused the substrate to rotate. This electrode was connected to a power supply with a cable brush, to avoid the cable wrapping around the substrate as it rotated. The collagen suspension was the loaded into the rig, between the electrodes.

7.4.2 Results

The DC motor used to rotate the substrate in the EPD cell was run at differing input voltages to control the RPM and, therefore, control the relative velocity between the substrate surface and the collagen suspension. The DC motor runs on a range of input voltages from 2 – 24 V, according the the manufacturers guidelines. However, it was found that the DC motor rotated too quickly to deposit collagen on above an input voltage of 1 V, even when the deposition voltage was increased to 15 V. Table 7.2 shows the outcomes from pulsed current depositions

at varying input voltages to the DC motor. Below 0.5 V input voltage the DC motor was unable to rotate, though the static substrate did allow collagen deposition, however alignment was not achieved in these films. Between 0.5 – 1 V the DC motor did rotate at times, but would also stop intermittently. Here, when collagen deposited, no evidence of birefringence was observed within the films.

Table 7.2 DC motor performance and deposition outcomes of collagen films deposited at 10 V PC-EPD with differing voltage input to the DC motor

DC Motor Voltage	DC Motor Performance	Deposition Outcome	Birefringence
0 – 0.5 V	No rotation through lack of torque	Collagen deposited as normal	No birefringence was observed
0.5 – 1 V	Intermittent rotation through lack of torque	Collagen deposited as normal	No birefringence was observed
> 1 V	Rotated smoothly and quickly	No collagen deposited	N/A

7.4.3 Discussion

The concept of a rotating substrate within the EPD cell was to overcome the issues associated with the EPD flow rig caused by the pump at low flow rates and the non-linear velocity over the substrate surface. Here, the DC motor used to rotate the substrate functioned within a range of input voltages that caused it to rotate at a speed that was too great for collagen to deposit at the same time. Reducing the input voltage of the DC motor caused it to lose torque and not rotate consistently, or not at all. Brushed DC motors suffer from low torque, particularly at low voltages, and cannot run smoothly at low speeds [315]. In order for this design to work it needed to run at low RPMs, allowing collagen deposition, but also maintain high torque so that the rotation speed remains constant.

7.5 Optimising Collagen Alignment on a Rotating Substrate

Gears can be used to alter the output rotation of a motor while also maintaining, and increasing, the output torque [316]. Here, with sufficient gears and gear ratios, the DC motor could be run at the higher operational voltages for which it was designed, while also reducing the outputted rotation speed by multiple orders of magnitude. Furthermore, in doing so the torque of the system remains very high. The addition of the gears to the rotating rig also allowed for greater control of the rotation speed, meaning that the relative velocity could be controlled and the optimal parameters could be determined for aligning collagen during EPD.

7.5.1 Materials and Methods

7.5.2 Electrophoretic Deposition in Rotating Tubular Rig with Gears

The custom-built rotating tubular rig with gears was a development of the rig design used in Section 7.4.1. Here, the cylindrical substrate was attached to an axel, which was connected to the DC motor. Between the axel and the DC motor were a series of gears that reduced the axel RPM relative to the DC motor output RPM. The RPM produced by the DC motor was controlled by changing the input voltage, between 4-24 V. The electrodes were connected to the power supply as previously described, with the rotating electrode connected to a cable brush (Figure 7.6).

Collagen suspension was loaded into the rig and the rotating electrode was spun at varying speeds by controlling the input voltage to the DC motor. The electrodes were connected to a power supply and the collagen was deposited onto the rotating electrode via pulsed-current electrophoretic deposition, with deposition parameters: applied voltage of 10 V, pulse period of 0.05 s, and a duty cycle of 40%.

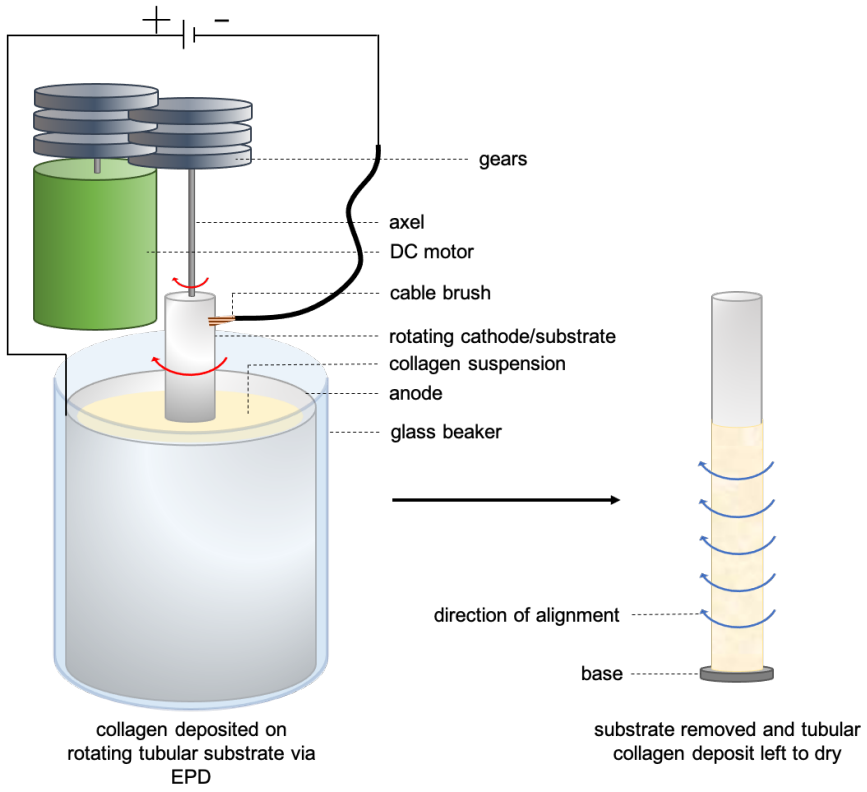

Fig. 7.6 Schematic showing the set-up of the rotating tubular EPD rig for depositing radially aligned tubular collagen deposits. Formed of one cylindrical electrode (the cathode/substrate) situated inside a larger cylindrical electrode (the anode), both inside a glass beaker. The deposition electrode, at the centre, was connected to a DC motor via an axel and set of gears that, when switched on, caused the substrate to rotate. This electrode was connected to a power supply with a cable brush, to avoid the cable wrapping around the substrate as it rotated. The collagen suspension was the loaded into the rig, between the electrodes.

Electrode Surface Tangential Velocity

The electrode surface tangential velocity, moving through the collagen suspension, was calculated from the RPM produced at different input voltages to the DC motor. The circumference of the rotating electrode was calculated to establish the tangential velocity of the electrode surface at corresponding RPM rates. With the gears in place, the cylindrical substrate rotated at 0.12 RPM with an input voltage of 1 V to the DC motor. This, with cylindrical diameter (d), was used to calculated the circumference (c) and then the tangential velocity (v) of the substrate surface:

$$d = 0.01m$$

$$\begin{aligned} c &= \pi d \\ &= 0.0314m \end{aligned}$$

$$1RPM = 0.0314m/min = 0.000524m/s$$

$$\begin{aligned} v &= 0.000524 \times 0.12 \\ &= 0.00006288m/s \end{aligned}$$

Therefore, the tangential velocity at the substrate surface was $0.000\,062\,88\,\mathrm{m\,s^{-1}}$ at 1 V input voltage to the DC motor.

EPD parameters

The DC motor was run at varying input voltages during EPD, to determine which relative interfacial flow velocity was best to optimise both alignment of collagen and deposition yield. Collagen suspensions of varying viscosities, ranging from 50 - 500 cP — dependant on their concentrations — was deposited to determine if there was an optimal viscosity to increase alignment in collagen films.

7.5.3 Results

Collagen films were deposited in the tubular rotating rig at varying tangential velocities (with the substrate rotating at different speeds). It was found that collagen films produced in this

manner contained aligned fibres and the birefringence of these films was determined using a quartz compensator. The birefringence of the collagen films was plotted as a function of the relative flow velocity, and it was found that increasing the velocity during deposition increased the birefringence of collagen films (Figure 7.7). As birefringence is an indication of alignment within a material, it was found that increasing the relative flow velocity during deposition increased the alignment of collagen within films.

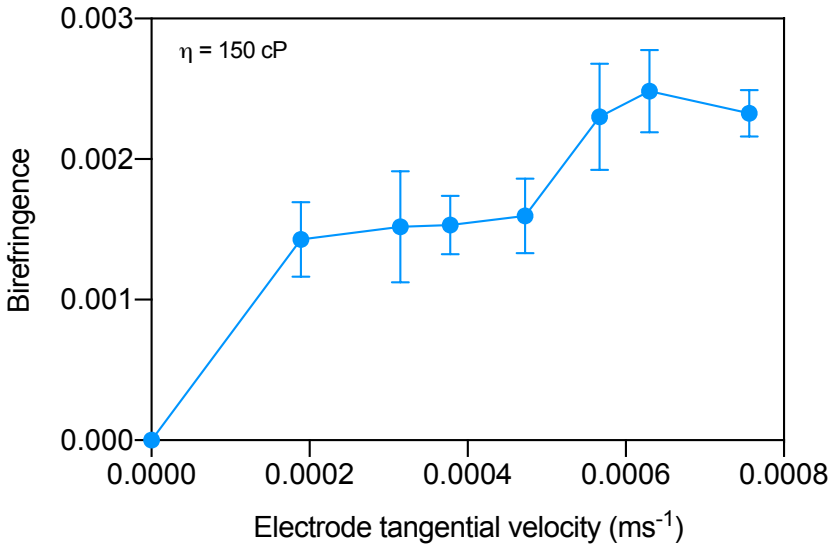

Fig. 7.7 Birefringence of EPD deposited collagen films plotted as a function of electrode surface tangential velocity during deposition. The collagen suspension had a viscosity of 150 cP and the deposition parameters were pulsed current, 10 V deposition voltage, 50 ms pulse period, and 40% duty cycle.

Suspension viscosity was also found to be an important factor in alignment of deposited collagen films. Collagen suspensions of differing viscosities were prepared and deposited onto the rotating electrode and the birefringence of the films produced was measured (Figure 7.8). Birefringence of collagen films peaked with a suspension viscosity of 170 cP, after which the alignment of collagen films dropped. It was observed that at increased suspension viscosities, that during deposition and while the substrate rotated, the viscous suspension also rotated with the substrate within the EPD rig, and thus the relative velocity between the substrate and the collagen suspension would have dropped.

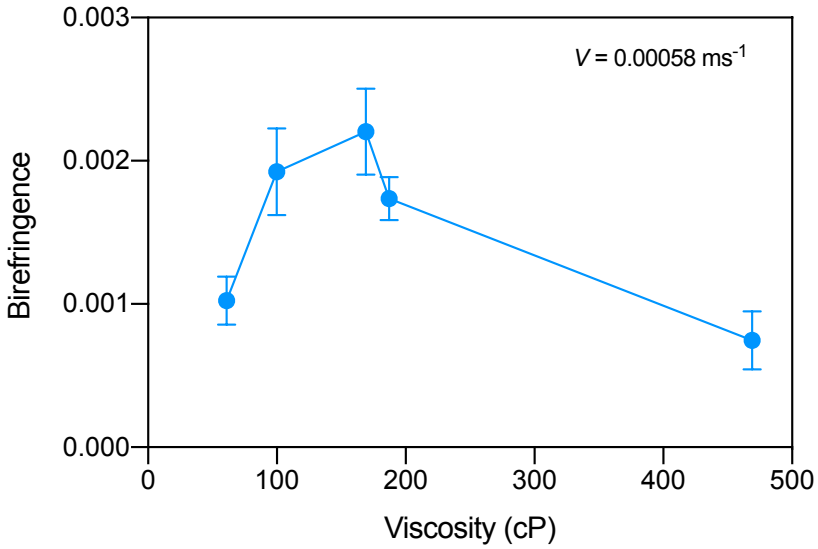

Fig. 7.8 Birefringence of collagen films deposited with relative flow during EPD plotted as a function of suspension viscosity. Deposition parameters were 0.000 58 m s^{-1} electrode tangential velocity in the rotating tubular rig, pulsed current, 10 V deposition voltage, 50 ms pulse period, and 40% duty cycle.

The deposited mass of collagen after 2 hours of deposition at varying electrode tangential velocities was determined (Figure 7.9). It was found that at higher velocities a smaller mass of collagen was deposited in the same amount of time, thus at greater velocities the collagen deposited at a slower rate. At a tangential velocity of approximately 0.000 95 m s^{-1} very little collagen was deposited in a period of 2 hours, but at 0.0003 m s^{-1} there was almost no difference in deposited mass compared with no velocity.

7.5.4 Discussion

Introduction of gears to the rotating rig design allowed the DC motor to operate with high torque, while reducing the rotational speed of the deposition substrate. This meant that sufficiently low velocities were achieved such that collagen could be deposited onto the rotating substrate. Previous literature has shown that shear forces can cause the alignment of polymers in solution [317]. Here, the interfacial flow generated at the substrate surface resulted in alignment of collagen within the films. This confirmed the findings of Section

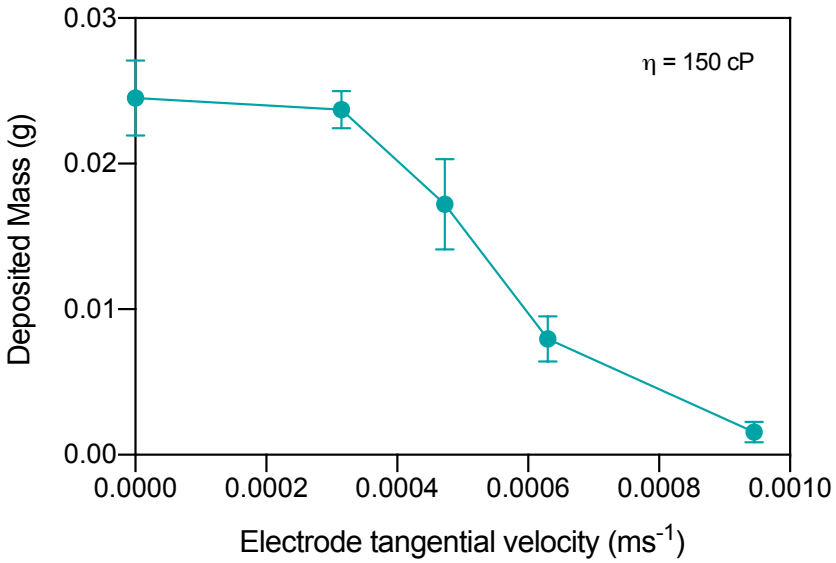

Fig. 7.9 Deposited mass of collagen after 2 hours PC-EPD with plotted as a function of electrode surface tangential velocity. The collagen suspension had a viscosity of 150 cP and the deposition parameters were pulsed current, 10 V deposition voltage, 50 ms pulse period, and 40% duty cycle, deposition time of 2 hours.

7.3.1, and corroborated the results seen by Goffin et al., who described that a relative interfacial flow between collagen solution and a boundary resulted in the alignment of collagen [309], and did not necessitate the flow of collagen suspension. Furthermore, it was found that increasing the rotation of the substrate resulted in increased alignment — this is a similar find to Pope and Keller, who found that the birefringence of polymer solutions increased at greater elongational flows of the solution [310], therefore suggesting the degree of alignment within films can be tuned by controlling the interfacial flow velocity. Investigation of the suspension viscosity also found that this was an important factor for optimising alignment of collagen within films, with a study by Huang et al. confirming that both viscosity and polymer concentration can influence alignment under shear flow [318]. Here, it was found that at increased viscosity, alignment also increased, however, at high viscosities the relative velocity was disrupted as the collagen suspension no longer remained static, and rotated with the substrate.

The introduction of gears to the rotating rig allowed for great control over the electrode tangential velocities, without a loss of torque. Optimal velocities were established, such that alignment was optimised, but deposition yield was not compromised too greatly.

7.6 Mechanical Testing of Aligned Collagen Films

Following successful development of aligned collagen films, it was important to understand what effect this alignment had on the mechanical properties of these films. In nature highly aligned collagen structures are often found in tissues and structures that must support tensile loading [100]. It was theorised that aligning collagen fibres within films would increase the tensile strength of these materials, as has previously been reported in highly aligned collagen fibres biomaterials [100]. In order to assess this, aligned and non-aligned collagen films were cross-linked and mechanical tensile testing was performed.

7.6.1 Materials and Methods

Collagen Visible Light Cross Linking with Riboflavin

Collagen films were cross-linked prior to mechanical testing using visible light and riboflavin, using the protocol used by Barrett [24] to cross-link collagen films. The cross-linking solution was prepared by dissolving 0.01 wt.% riboflavin and 0.1 M triethanolamine (TEOHA) in deionised water under agitation. The cross-linking solution was kept in the dark until use. 2 mL of riboflavin cross-linking solution was dropped onto each film and was left for 10 minutes to fully hydrate. The films were then subject to a blue light source (Coltolux LED, Coletene Ltd.) for 300 seconds from a distance of 10 mm. Excess cross-linking solution was then removed and the films were left to air-dry for at least 24 hours.

Mechanical Testing

Tensile testing of films was performed with a Tinius Olsen machine with a 5 N load cell in physiological conditions using a heated water chamber (MTS) at 37 °C. Collagen films were gripped in place. For each measurement the crosshead speed was 0.1 mm/s.

7.6.2 Results

Tensile testing was performed on collagen films produced both with alignment and without alignment. Aligned collagen films were produced in the rotating tubular rig from Section 7.5. Tensile tests were performed with load applied parallel to the direction of alignment and orthogonal to the direction of alignment. Collagen films loaded orthogonally to their alignment had similar ultimate tensile strength (UTS) to non-aligned collagen films. Aligned collagen films loaded parallel to the direction of alignment had nearly double the UTS of non-aligned collagen films.

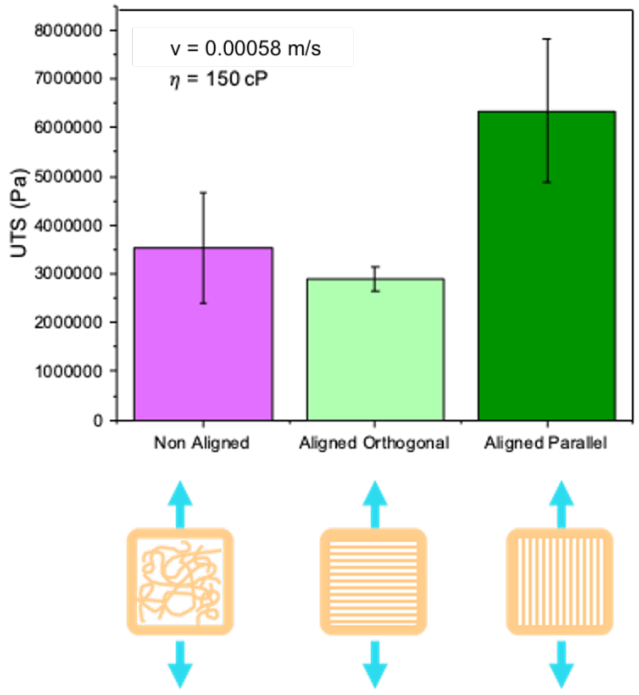

Fig. 7.10 The ultimate tensile strength (UTS) of non-aligned and aligned collagen films produced with relative flow during deposition. Aligned collagen films were loaded orthogonally and in parallel with the direction of alignment.

7.6.3 Discussion

Alignment of collagen within films was achieved by generating an interfacial flow between the deposition substrate and the collagen suspension, and the effect of this alignment on the mechanical properties was investigated. It was shown that aligned collagen films have an increased UTS in the direction of alignment compared with non-aligned films. These findings are in agreement with previous studies that aligned collagen to increase the biomaterial tensile strength in aligned collagen fibres [99, 100] and electrochemically aligned collagen threads [216]. Furthermore, the UTS of aligned films loaded orthogonally to the direction of alignment showed no difference to the UTS of non-aligned films. This further supports the effect of alignment in determining mechanical properties and that mechanical properties are dependant on orientation.

7.7 Optimising Flow Rig to Develop Cross-Ply Collagen Films

The results from the previous section showed that mechanical properties can be manipulated by aligning collagen within films. These properties could also be highly utilised in multilayer cross-ply collagen films, increasing the tensile strength in multiple directions, and potentially increasing the tear resistance of the collagen films. This would be beneficial when suturing these films in place *in situ*.

While it was shown in previous work here that alignment can be achieved using the modified geared EPD rig, this rig design was not conducive to producing multi-orientated collagen films. In order to develop multi-orientated films it is necessary to realign the substrate between deposition layers, which was not possible with the cylindrical substrate. A more preferable setup would be to deposit onto a planar substrate which can then be re-orientated in between deposition steps. Work by Barrett et al. found that multiple collagen layers could be deposited onto the same substrate, drying each layer between deposition steps, with no loss of yield [24]. This would be possible in the EPD flow rig design, however, it needed to be modified such that aligned collagen films could be produced reliably at each deposition step.

It was determined, in the rotating rig, that sufficiently low velocities allowed for collagen deposition at 10 V, and increasing velocity reduced deposition yield, whereas increasing deposition voltage maximised yield; it was proposed that high velocities could be possible when implemented in conjunction with high deposition voltages. High flow rates mitigate the problems associated with the peristaltic pump at low RPMs [313], where the flow became pulsed. However, beyond 10 V deposition voltages, bubbles begin to nucleate at the electrode. Here, in order to deposit at high voltages, collagen was deposited onto an ion-permeable barrier membrane, similarly to the EPD rig in Chapter 6, Section 6.4. As bubbles nucleate at

the electrode at high voltages the collagen deposits onto the barrier membrane away from the bubbles [277], and defect-free collagen films are formed.

7.7.1 Materials and Methods

Electrophoretic Deposition in Flow Rig

The barrier membrane flow rig was custom-built and was a development of the flow EPD rig produced in Section 7.3.1. Electrophoretic deposition was carried out with collagen depositing onto an ion-permeable barrier membrane (Sigma Aldrich, D9527-100FT), located between two electrodes. Either side of the barrier membrane was a chamber. On one side of the barrier membrane approximately 1.5 mL water was loaded until it was full, alongside the negative cathode. The other chamber had inlet and outlet tubes connected to a peristaltic pump (Watson-Marlow, 323S/D, 3-400 RPM), and was filled with collagen suspension. The peristaltic pump generated a flow of collagen through the EPD rig (Figure 7.11).

Collagen was deposited onto the barrier membrane using direct current electrophoretic deposition while flowing through the chamber via the peristaltic pump, which ran at varying RPM. The barrier membrane was used to avoid gas bubbles nucleating within the collagen film, and instead nucleated at the cathode. The deposition parameters used were as follows: direct current, applied voltage of 30 V and 40 V, collagen viscosity of 150 cP.

Volumetric Flow Rate

The volumetric flow rate of collagen suspension through the EPD cell was calculated from the RPM of the peristaltic pump following the calculations in Section 7.3.1.

Electrophoretic Deposition of Multilayer Cross-ply Collagen Films

Multilayer, multi-orientated, cross-ply collagen films were developed using the flow rig, shown in Section 7.7.1. The process for developing these films is depicted in Figure 7.12. A

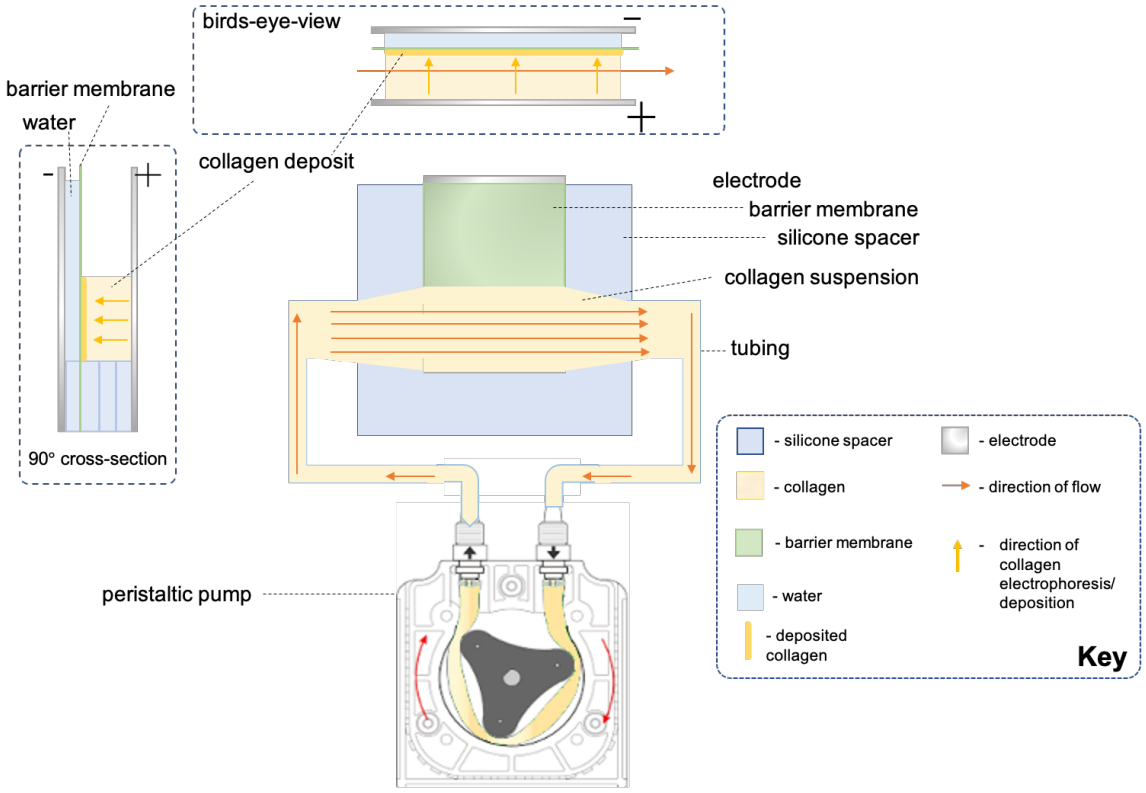

Fig. 7.11 Schematic showing the EPD flow rig containing a ion-permeable barrier membrane substrate and inlet and outlet tubes to a peristaltic pump. On one side, with the positive electrode, collagen suspension was filled, the other side contained water, to maintain the flow of current during EPD. The tubes only ran into and from the chamber containing collagen. The peristaltic pump generated flow of collagen through the rig and across the barrier membrane surface during EPD: orange arrows depict the direction of flow of collagen suspension. When an electric field was applied across the cell collagen migrated to the negative electrode and deposited onto the barrier membrane.

first layer of collagen was deposited following the protocol in Section 7.7.1, with a volumetric flow rate of 1.67 mL s^{-1} and direct current applied voltage of 40 V. Once deposited the aligned collagen was left to air dry onto the barrier membrane for 24 hours. The barrier membrane with collagen film was placed back into the EPD flow rig with the alignment of the collagen film orientated perpendicular to the direction of flow. EPD with flowing collagen suspension was then carried out again, with the same parameters as before, depositing a new layer of collagen onto the existing collagen film, where the new layer was aligned perpendicular to the original. The multilayer, cross-ply film was then left to air dry for 24 hours. The process

could then be continued indefinitely, if required. The multilayer film was then removed from the barrier membrane substrate via a sacrificial layer, as explained in Section 7.2.5.

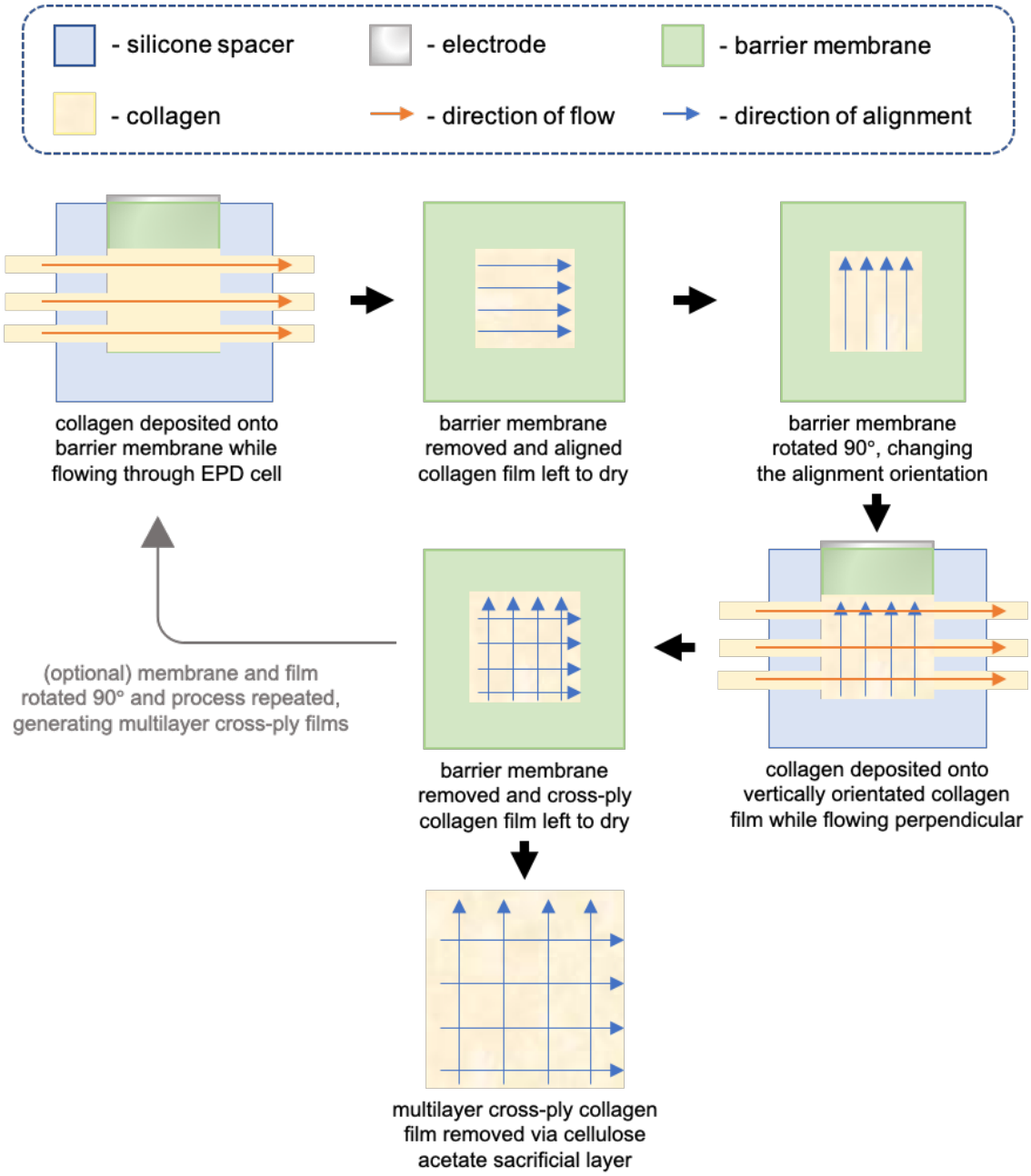

Fig. 7.12 Schematic showing the process of developing multilayer, cross-ply collagen films via EPD in the flow rig, which is depicted in Figure 7.11.

7.7.2 Results

Alignment in Collagen Films

Collagen was deposited in the flow rig (Figure 7.11) onto a barrier membrane, at greater flow velocities and higher voltages than the rotating rig. The birefringence of collagen films produced at these voltages was measured for varying volumetric flow rates (Figure 7.13). Increased flows during deposition induced greater alignment within collagen films, and collagen films produced at 40 V had reduced birefringence compared with films deposited at 30 V when deposited at the same flow rate.

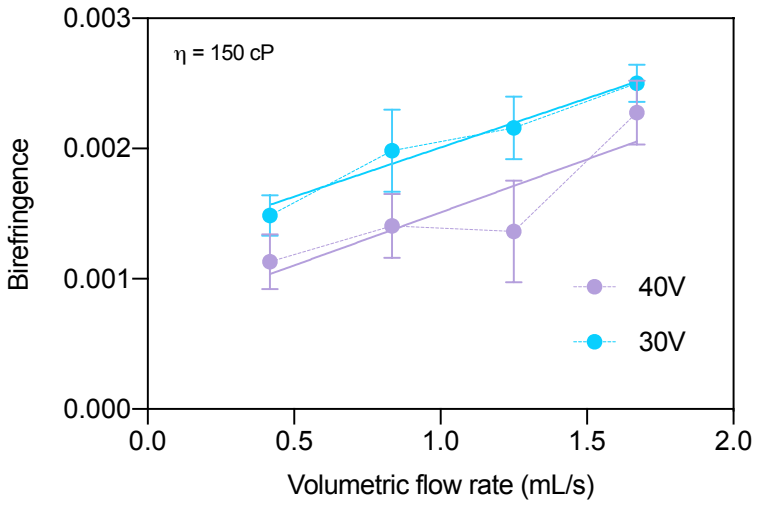

Fig. 7.13 Birefringence of deposited collagen films plotted as a function of volumetric flow rate during deposition. The collagen suspension had a viscosity of 150 cP and the deposition parameters were direct current with applied voltages of 30 V (blue) and 40 V (purple).

The deposited mass of collagen during deposition at varying flow rates was also determined in the flow rig (Figure 7.14). The mass of collagen deposited declined with increasing flow rate. Furthermore, at the higher deposition voltage of 40 V a greater mass of collagen was deposited in the same duration when compared with the mass deposited at 30 V for the same flow rates, but both had the same profiles.

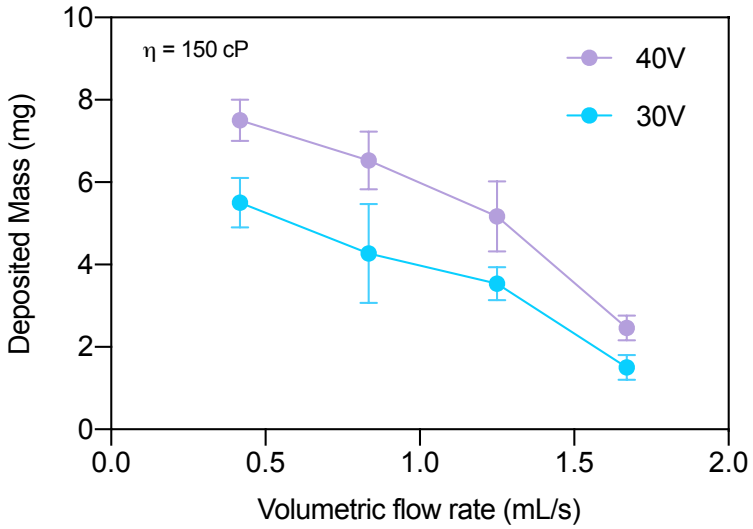

Fig. 7.14 Deposited mass of collagen after 2 hours DC-EPD as a function of volumetric flow rate during deposition. The collagen suspension had a viscosity of 150 cP and the deposition parameters were direct current with applied voltages of 30 V (blue) and 40 V (purple), deposition time of 2 hours.

Cross-ply Collagen films

Cross-ply collagen films were produced in the flow rig, following the protocol in Section 7.7.1. A photograph of a cross-ply collagen film (Figure 7.15, left) shows the lengths of the two collagen layers, with the cross-ply region within the middle. In the image there were no features to note and no indications of alignment within the film could be seen. A brightfield microscope image of the cross-ply film at the boundary between one layer of collagen and two layers of collagen showed no notable features, other than the boundary (Figure 7.15, middle). The same region was imaged with polarised light (Figure 7.15, right) and showed light passing through in the single layer region, due to birefringence, but no light was able to pass through in the cross-ply region of the film, which was found to be darker. The cross-ply nature of the film did not elicit visible birefringence as the differently-orientated second collagen layer blocked the light from passing through.

Fig. 7.15 Images of a multi-layer cross-ply aligned collagen film produced using flow during deposition, with each layer having an approximate thickness of 60 µm. Left: photograph of cross-ply collagen film, with superimposed red arrows indicating the direction of alignment in each collagen layer, with the red circle indicating the region which is imaged in the middle and right images. Middle: brightfield image of cross-ply collagen film at the boundary between single-layer and multi-layer. Right: same region as middle image, under polarised light.

7.7.3 Discussion

Previous attempts to deposit planar aligned collagen films by flowing collagen through the EPD cell were unsuccessful because at high flow rates collagen did not deposit onto the electrode. Increasing the voltage resulted in bubble formation and decreasing the flow speed led to pulsed flow through the EPD cell from the peristaltic pump, causing non-uniform alignment throughout the film (Section 7.3.1). Here, depositions at high flow rates were achieved using high deposition voltages and direct current. Collagen was deposited onto an ion-permeable barrier membrane away from the electrode to avoid damage caused by bubble-nucleation at the electrode. These deposition parameters allowed for alignment of collagen within films and were consistent throughout. Furthermore, these parameters were optimised to find the maximum achievable alignment in collagen films. As found in the previous section, achieving collagen materials with high birefringence resulted in increased UTS of the collagen films.

This EPD rig allowed for alignment of collagen films on a planar substrate, which was utilised to re-orientate the collagen film between deposition steps and develop multi-

orientated cross-ply collagen films. Investigation of these films showed that cross-ply collagen films were achieved. From the results in Section 7.6, each layer, therefore, had increased UTS compared with non-aligned films. Xie et al. developed double-layer nerve guidance conduit scaffolds from electrospun PCL nanofibres and found that aligning each layer in a different orientation increased the tear-resistance of the material [319]. The cross-ply films produced here, therefore, could have increased tear-resistance, due to their internal structure and multi-directional increased UTS.

7.8 Chapter Discussion

7.8.1 Developing EPD Processing to Align Collagen Fibres

In this chapter, alignment in collagen films was produced by generating an interfacial flow between the collagen suspension and the deposition substrate, however, several iterations were required to optimise the technique. Initial attempts involved flowing the collagen suspension across the deposition substrate, however at the low flow rates required for deposition the peristaltic pump did not produce consistent flow — though regions of alignment were achieved, validating the method and corroborating previous studies that have produced alignment of collagen with flow [309]. Similar issues were apparent when depositing onto a rotating substrate, operated by a DC motor. At such low input voltages to the DC motor it lost torque and would not rotate consistently, which is a known issue in DC motors running at low power [315]. This was corrected by introducing gears, allowing for much slower speeds, greater control and with no loss of torque [316]. While the rotating rig had succeeded in producing optimised aligned collagen films, it was not possible to create cross-ply collagen films using this rig, so the flow rig was then redeveloped to deposit at high voltages and high flow rates, by depositing onto a barrier membrane away from the electrode and nucleating bubbles. This rig allowed for consistent aligned collagen films that could be re-orientated between deposition steps.

7.8.2 Alignment of Collagen in Films

Collagen was deposited in an EPD rig with a rotating cylindrical deposition electrode to generate a shear force between collagen suspension and the substrate, which has been shown to align polymers in solution [317]. Polarised microscopy showed that the collagen deposited with interfacial shear displayed birefringent properties, while collagen deposited with no relative movement between the suspension and substrate did not (Figure 7.3). The suspension

parameters were investigated to understand if the viscosity of the collagen had an effect on the achievable alignment. It was found that as the viscosity increased so did the alignment, when all other parameters were constant, until a maximum alignment was achieved, after which increasing the viscosity further reduced alignment. These findings are in agreement with the literature, which suggests that polymer solutions with increased viscosity will have greater alignment under shear stress [318]. A factor that influences viscosity in collagen suspensions is the conformation of the collagen fibrils (as discussed in Chapter 3). Long, uncoiled collagen fibrils have a greater viscosity, but can also form greater aligned structured when subjected to a shear force, as seen by Smith et al. who showed that uncoiled polymers showed greater elongation and alignment under shear flow [320], which was also found to increase with polymer concentration [321]. After achieving a maximum amount of alignment, the measured birefringence then dropped with increasing viscosity as at such great concentrations the suspension was no longer static, and began to rotate with the rotating electrode. This could have been due to the increased amount of collagen fibres entangled and interacted with each other [236, 241]. Therefore, at these viscosities, the rotating suspension resulted in a reduced interfacial flow and reduced shear force. The optimal viscosity, therefore, was found to be at 150 cP.

The rotational speed of the deposition electrode was altered and the effect on the alignment of the deposited collagen films was determined. It was found that increasing the electrode surface tangential velocity resulted in increased alignment of the deposited collagen, similarly to Pope et al. who showed increased polymer alignment at increased flow [310]. However, while increasing the speed resulted in greater alignment, it also caused a reduced rate of deposition, and at high RPM the velocities were too great and no collagen deposited, thus a compromise was necessary. Aligned collagen films were also produced within an EPD rig that deposited onto an ion-permeable membrane substrate. Flow of the collagen suspension was generated using a peristaltic pump. By depositing onto the ion-permeable membrane,

aqueous EPD-associated problems with gas nucleation at the electrode were avoided and therefore much higher voltages were used. It was found that depositing at higher voltages also allowed for much greater flow rates, when compared with the lower pulsed current voltages within the rotating rig. Similarly, however, increasing the flow rate also resulted in reduced deposition of collagen. This was found to agree, in part, with a study by Koenen et al. [322] which found that metal nanoparticles deposited under continuous flow had a reduced yield at lower voltages, and below an electric field of 4 V/cm no deposit was formed. However, they found at sufficiently high voltages that yield also increased with flow, as the concentration of nanoparticles remained high due to constant replenishment.

While greater flow rates were achievable at greater voltages, this did not result in greater alignment of collagen compared with collagen produced in the rotating rig. Furthermore, collagen deposited at 30 V had a greater alignment than collagen deposited at 40 V when deposited with the same flow rate. These suggest that there is a relationship between the incoming deposition velocity of the collagen (perpendicular to the substrate), determined by the voltage, and the flow velocity of the collagen (parallel to the substrate), which will have been further influenced by the parabolic flow profile through the EPD cell, as shown in a study that deposited colloidal nanocrystals under continuous flow [323]. If the flow velocity is much greater than the deposition velocity no collagen will be deposited, whereas if the flow velocity is not great enough, compared with the deposition velocity, there will be insufficient alignment of the collagen (Figure 7.16).

This chapter has shown that alignment of collagen films can be produced using interfacial shear, and one method for generating shear was within the tubular rotating rig. While these films were dried flat in order to assess their birefringence, the nature of the rotating rig demonstrated that these films could remain as tubes (as reported in Chapter 5). This development, therefore, showed that radially aligned collagen tubes could be produced,

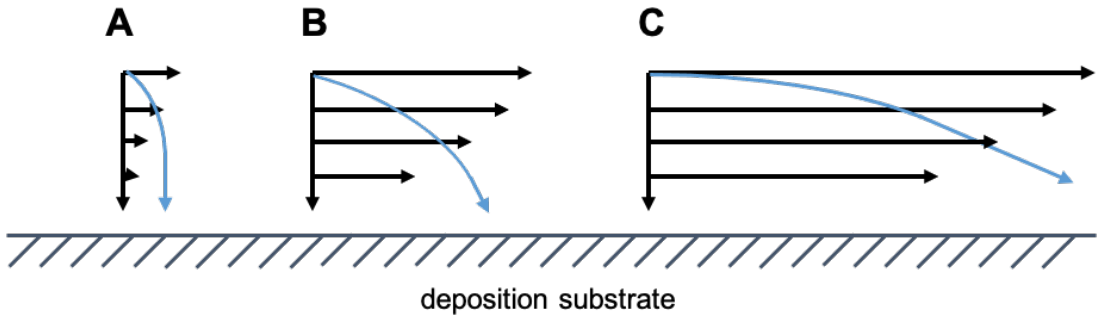

Fig. 7.16 Arbitrary vector fields of collagen depositing under flow, with horizontal black arrows showing the flow velocity, vertical black arrows showing the deposition velocity, blue arrows show the collagen velocity, and the grey lined edge showing the deposition substrate. (A) No alignment of deposited collagen - insufficient flow velocity relative to the deposition velocity. (B) Alignment in deposited collagen - correct ratio between deposition velocity and flow velocity. (C) No deposited collagen - flow velocity too great compared to deposition velocity to allow collagen to deposit.

which could be used as potential blood vessel replacements - structures that are subjected to great radial loads [324], as opposed to tensile loads.

7.8.3 Developing Cross-ply Collagen Films

Alignment in single-layer collagen films was achieved and established with polarised microscopy to confirm birefringence. Multilayer EPD collagen films have been produced before, where once one collagen layer had been deposited and left to dry, more collagen layers were electrophoretically deposited on top, with no reduction in yield [24]. Here, cross-ply aligned collagen films were produced by first depositing one aligned collagen layer, leaving it to dry, and then changing the orientation of the substrate before depositing another layer.

Polarised microscopy was used to determine that the cross-ply collagen film had been produced, by imaging first images both layers individually (where each layer was overhanging from the centre multilayer region) confirming their birefringence, then at the intersect between single-layer and double-layer. At the intersect it was clear that the differently-orientated layers were blocking the birefringent properties of each individual layer, when stacked on

top of each other. Multilayer, multi-orientated films could therefore be produced to create alignment and increased strength in many directions, by reorientating the substrate between depositions. The process could be repeated several times, as Barrett found that multiple layers of collagen could be deposited on top of each other without any reduction in yield, in a study that went as great as 10 layers [25].

7.8.4 Mechanical Properties of Aligned Films

Aligned collagen films produced within the rotating rig were tensile tested to investigate the influence of alignment on mechanical properties. Alignment of collagen within films increased the ultimate tensile strength (UTS) in the direction of alignment compared with both non-aligned collagen films and the UTS of aligned films loaded orthogonally to the alignment. Aligning collagen films could therefore be beneficial if they are required to be loaded with tensile force when implanted. Furthermore, based of these data, creating multilayer cross-ply films would have greater resistance to tearing, particularly at suture sites when sutured — multilayered, cross-ply electrospun nerve guidance conduits were found to have increased tear-resistance [319].

The tested films were flat, but as already discussed, these films could also be produced as radially aligned tubes. The mechanical data showed, therefore, that these tubes would have greater tensile strength in the radial orientation. Arterial blood vessel are loaded radially when blood is pumped through them at high pressure [324]. These seamless, radially aligned collagen tubes therefore present themselves as extremely suitable candidates for blood vessel implants.

7.9 Conclusions

Generating a interfacial flow between the collagen suspension and the deposition substrate during EPD caused collagen to align during deposition, however the correct window of parameters was necessary to achieve this. With a flow velocity too great, compared with the deposition velocity, the collagen did not deposit onto the substrate, while insufficient flow velocity, relative to the deposition velocity, resulted in non-aligned collagen films. Multilayer cross-ply collagen films were produced by aligning collagen during deposition and changing the orientation of the substrate between depositions.

Aligning collagen within films increased their tensile strength parallel to the direction of alignment, while orthogonal loading was no different non aligned films. The rotating tubular rig was able to produce, therefore, seamless collagen tubes that had radial alignment, which could be beneficial as blood vessel replacements. Cross-ply collagen films would also have improved mechanical properties in many directions, potentially providing them with increased tear resistance when sutured.

Chapter 8

Conclusions and Future Perspectives

8.1 Key Findings

8.1.1 Dialysis of Collagen Suspensions

It has been noted that electrophoretic deposition of aqueous media suspensions can result in the nucleation of gas bubbles at the electrodes due to electrolysis of the water to form hydrogen and oxygen molecules. The formation of gas bubbles at the depositing substrate electrode results in damaged and defective films, which was apparent when depositing insoluble type I collagen under direct current EPD. Insoluble type I collagen was hydrated and suspended in an aqueous media, with 0.05 M acetic acid. Pulsed current electrophoretic deposition was found to be an effective solution for minimising gas bubble nucleation in aqueous deposits, including in collagen depositions. However, only a very small operating window of processing parameters was found to be effective for collagen EPD, and that the deposition voltage could not be greater than 5 V. The current in collagen EPD was found to be much higher than other systems and was also variable between collagen suppliers. Furthermore, collagen suspensions prepared from material supplied by Devro Medical resulted in corrosion of the electrode. This indicated that there were other charge-carrying

ions within the system that had not been accounted for, and were increasing the current during EPD, thus resulting in a higher likelihood of gas bubble nucleation. It was proposed that removal of these extra charge-carriers could improve the processing parameters for collagen EPD, as well as standardising collagen suspensions prior to EPD.

Effect of dialysis on EPD collagen suspensions

In order to remove undesirable charge-carrying ions, collagen suspensions were dialysed against deionised water. Following dialysis, collagen suspension conductivities were measured and were found to be reduced in all suspensions, compared with undialysed collagen. Furthermore, it was seen that undialysed collagen suspensions with the greatest conductivities had the largest reduction in conductivity following dialysis, and that all dialysed suspensions were not significantly different in conductivity. This highlighted that dialysis could be an effective process for standardising collagen suspensions.

Collagen suspensions from different suppliers were deposited onto substrates using electrophoretic deposition processing to form collagen films. Prior to dialysis, collagen suspensions formed from insoluble collagen supplied by Devro were unable to form defect-free collagen films via EPD, and during the processing the stainless steel electrode corroded. Following dialysis it was found that suspensions from all collagen suppliers formed smooth, defect-free films on a consistent basis. Work done by Barrett et al., which deposited undialysed collagen via EPD, found the optimal deposition parameters to be a pulsed current regime, with a deposition voltage of 5 V [25]. They found that increasing the voltage beyond 5 V resulted in the formation of gas bubbles within collagen film. However, in this study it was found that deposition voltages could be increased up to 15 V in collagen suspensions that had been dialysed, without the nucleation of gas bubbles at the electrodes, due to the reduction in current through the system. Increasing the deposition voltage increases the rate of deposition yield, thus resulting in much shorter deposition times at higher voltages to

achieve the same mass of deposit as at lower voltages. This further highlights the benefit of dialysing collagen suspensions prior to electrophoretic deposition, as it allows for consistent collagen films to be produced more quickly.

Investigation of the dialysate

Following dialysis, the dialysates — the liquid media used to dialyse the suspensions against — were analysed to understand the contents that had been removed from the collagen suspensions and better understand the effect of dialysis on the suspensions. Dialysates were dehydrated to determine what remained from the deionised water and further understand what had been removed from the collagen suspensions, leaving a residue of salts. As the dialysates began as deionised water, any residue left after dehydration was a result of products that had been dialysed out of the collagen suspensions. Dialysate residues were compared from the dialysis of collagen suspensions from two different collagen suppliers, which had greatly different conductivities prior to dialysis. It was found that the collagen suspensions with much higher initial conductivity left a much greater mass of residue from the dialysate, signifying that a larger amount of salts were dialysed from this suspension compared with the collagen suspension with lower conductivity. This finding corroborated the previous data, suggesting that additional charge-carrying ions were comprised within the collagen suspensions and that dialysis was effective at removing them. EDX analysis was then carried out on the the dialysate residues in order to understand their atomic constituents. The elements that were discovered suggested that these residues could have been an artefact from the collagen extraction processes, which supported the disparity seen between different collagen suppliers.

Effect of dialysis on collagen suspension viscosity

Dialysis was found to reduce the conductivity of collagen suspensions by removing charge-carrying ions, however, it also had another effect on the suspension properties. Following

dialysis, the viscosity of collagen suspensions was found to increase. This suggested that the removal of ions was causing the viscosity to increase. Collagen molecules are long chain polymers that can experience conformational changes depending on pH and ionic forces acting on them, due to charged functional groups on the collagen chain. In high ionic strength suspensions, the ionic forces caused the long collagen chains to coil, however, removal of these ions via dialysis allowed the collagen molecule to elongate. Elongated long chain molecules in suspension are more likely to entangle and interact with each other, and cannot move freely, resulting in a higher viscosity suspension.

Summary

Chapter 3 demonstrated the effectiveness of dialysis in removing excess charge-carrying products from collagen suspensions prior to electrophoretic deposition. Furthermore, it showed the impact of removing excess charge-carriers in reducing suspension conductivity and improving EPD efficiency, allowing for defect-free collagen films to be formed at higher voltages, resulting in greater yield rates. Lastly, Chapter 3 highlighted great variability in collagen type I products obtained from different suppliers, and the importance of standardising them prior to processing them, and the efficacy of dialysis in achieving this.

8.1.2 Modelling PC-EPD for Collagen Deposition

Developing a model of a system can provide a better understanding of the components and inputs to the system, and their influence on each other and the output. Predicting the deposited mass at a given time is an important understanding of the system and develops an in depth knowledge of parameters and the system mechanics. Furthermore, modelling EPD to predict deposition yield allows for processing parameters to be assessed much more quickly and without the cost of materials. EPD is a process that has been optimised for many materials over many years, and during this time has been developed into reliable models.

However, these models were only suitable for direct current electrophoretic deposition, and did not account for the additional mechanisms and parameters of pulsed current EPD.

Developing a pulsed current EPD model

Here, a predictive model for pulsed current electrophoretic deposition was described, incorporating the additional factors that were not previously associated with direct current EPD. The model was developed as an extension to previously described and well-established DC-EPD models, derived from the Hamaker Equation [105]. The additional parameters included were duty cycle and pulse period. These parameters meant that additional kinetics had to be considered. During time in which the deposition voltage was applied, charged particles would move in the direction of the oppositely-charged electrode, then during the time where there is no applied voltage it is possible that the charged particle would diffuse in the opposite direction along the concentration gradient that was developed during the initial phase of migration. This process is repeated with each pulse period. These kinetics were described as a dimensionless factor, the pulsed current parameter, which was then incorporated into the DC-EPD model, thus producing the pulsed current EPD model.

Validating the PC-EPD model with experimental data

Collagen suspension properties and insoluble collagen EPD were characterised. The measured properties of the collagen suspension and results of deposited mass with time were used to validate the mathematical PC-EPD model. The suspension properties were implemented into the model and it was run at 5 V and 10 V, while collagen suspensions were deposited using PC-EPD at the same voltages, and the results compared. It was found that at 10 V the model matched the experimental results, and was able to predict the deposited mass with time accurately. However, at 5 V the model overestimated the deposited mass and it was shown that the collagen deposited was much less than expected.

It is possible that the model oversimplified the kinetics in action, and that the proposed two phases within a pulse period did not account for all mechanisms, thus, the electrophoretic velocity of particles during applied voltage and the diffusion away from the electrode while there was no voltage was an insufficient description. It was proposed that there are four phases during the pulse period, the two aforementioned phases of electrophoretic velocity and diffusion, and also the acceleration and deceleration phases before and after velocity. Therefore, at low voltages, such as 5 V, the rate of acceleration may be so low that particles in suspension never reach constant velocity before the voltage is switched off again. This would have large impacts within the model. It is possible that these effects were not seen at higher voltages, such as 10 V, as the acceleration phase is so short with a higher driving force.

Summary

Here, a model was developed to describe pulsed current EPD systems, which could generate further incites into the underlying mechanisms of the process. The model was developed using well-established models for DC-EPD, with the incorporation of a pulse current parameter. This PC-EPD model was found to be effective at predicting deposited mass for higher voltages, but it was not accurate at lower voltages. The model developed in Chapter 4 presents a potential first-step in developing an effective PC-EPD, showing a degree of accuracy at some voltages. Possible mechanisms that were not accounted for within the model were discussed within the chapter, and these represent the next steps in achieving this model.

8.1.3 Shaped and Textured Collagen Films

Previous studies using electrophoretic deposition to create collagen films found that, once dry, collagen films adhered strongly to the substrate they had deposited onto. Removal of

deposited collagen films from the substrate required intervention. Mechanical cleavage is a basic method of removing deposits from substrate and involves prying off the deposited material with a sharp tool. Collagen films were removed from the substrate via mechanical cleavage, using a razor blade, which often resulted in damage of the films as they were removed. Furthermore, the use of a razor blade to remove deposits is only effective on substantially planar substrates, and does not facilitate non-planar or topographical substrates, which could be beneficial in developing complex-shaped films.

Removing collagen films from the substrate using a sacrificial layer

It was proposed that a sacrificial layer on the substrate could be used as an effective method for removing collagen films following deposition. Sacrificial layers coat the substrate prior to deposition, and can then be easily dissolved in a solvent after EPD, resulting in detachment of the deposit. It is important to have a sacrificial layer that can be dissolved in a solvent that does not effect the deposition material, and the layer must not be effected by the suspension media. Cellulose acetate was chosen as the sacrificial layer, as it is not soluble in the aqueous suspension media, but does readily dissolve in acetone, which does not effect collagen.

Substrates were coated in cellulose acetate prior to EPD and collagen was deposited under normal conditions. It was found that the use of a cellulose sacrificial layer did not effect the deposition process, and the current during EPD was unaffected. Following deposition the cellulose coated substrate with adhering collagen film were submerged in acetone to dissolve the sacrificial layer. The layer was dissolved and the deposit was detached from the substrate without further intervention, and the collagen film was not affected by the acetone.

Developing Tubular Collagen Films

After it was found that a cellulose sacrificial layer was effective for removing collagen films from a planar substrate, the use of a sacrificial layer on a non-planar substrate was

investigated, where mechanical cleavage would be ineffective. Tubular collagen films were created using a cylindrical EPD rig. A cylindrical substrate was coated in cellulose acetate and collagen was deposited onto it using electrophoretic deposition. Following deposition, and once the collagen deposit had dried, the sacrificial layer was dissolved and the collagen tube was able to slide off from the substrate. This resulted in a seamless, free-standing collagen tube. Furthermore, a tubular collagen film would not have been achievable using casting methods, highlighting the benefit of utilising EPD processing with a sacrificial layer.

Translation of Topographies from Substrate to Film

A substrate containing grooves was developed in order to understand if these features would be translated onto a collagen films. Collagen was deposited onto the cellulose-coated substrate using EPD and was successfully removed using the sacrificial layer, which would not have been possible using mechanical cleavage. It was found that the grooves from the substrate were replicated by the collagen, resulting in a grooved film. Further investigation also highlighted that the microscopic surface roughness of the substrate was also translated onto the collagen film, suggestion that very small feature size (approximately 10 µm) could be designed into collagen films, which may be beneficial for influencing cellular activity.

Summary

The work in Chapter 5 showed that using a cellulose sacrificial layer is an effective method for removing deposited collagen films from the substrate without damaging them. Furthermore, it increased the versatility for developing collagen films using electrophoretic deposition, by allowing deposits that are formed on textured or non-planar substrates to be easily removed, with the collagen films inheriting the features of the substrate.

8.1.4 Degradation of Collagen Films

Collagen Film Density

It was suggested in previous research that EPD collagen films had a greater density than solvent cast films. Here, the density of EPD films was measured and compared with cast films and it was found that the deposited collagen had a greater density. It was theorised that the driving force arising from the deposition voltage gave rise to increasing material density, and that at higher voltages films would have a greater density. This was was found to be true, up until a voltage of 7 V, where at 8 V the density of films decreased. Analysis of the films suggested that they contained microscopic bubbles as a result of gas bubble nucleation at the electrode during EPD, which was corroborated by previous studies. An EPD rig was developed such that collagen was deposited onto a barrier membrane away from the electrode, preventing bubble formation within the films. Within the revised EPD rig, it was found that collagen deposited at higher voltages and increased densities.

The Effect of Density on Degradation

Collagen films produced with deposition voltages of 5 V and 10 V and solvent cast films all had different densities. The enzymatic degradation of these collagen films with different densities were compared. The films were incubated in collagenase solution at 37 °C. The rate of degradation was found to be greatest in the cast collagen film, which had the lowest density. It was found that at increased density collagen films had a greater enzymatic degradation resistance.

Summary

The work in Chapter 6 found that, by changing the deposition parameters, the density of deposited collagen films can be altered and controlled. Furthermore, by changing the density of collagen films, the degradation properties of films can be controlled. Previously, collagen

film degradation rates would have to be controlled by altering the degree of cross-linking. These results potentially remove the need for chemical cross-linkers, which reduce collagen bioactivity, and allow for biomaterial membranes with tunable degradation properties while maintaining cellular activity.

8.1.5 Alignment of Collagen within EPD Films

Implantable biomaterial membranes often require sutures to be fixed in place, and as such, these materials must be resistant to tearing. Previous research, and natural collagen structures, have shown that aligning collagen fibres increases the tensile strength of the material. It was, therefore, proposed that aligning the fibres within collagen films would increase the ultimate tensile strength, and that cross-ply collagen films would have increased tear resistance.

Aligning Collagen Fibres During EPD

Based on previous studies, it was thought that collagen could be aligned during EPD by flowing the suspension across the electrode, generating interfacial shear. Initially, an EPD rig was developed where the collagen suspension was pumped through the EPD cell using a peristaltic pump. While evidence of alignment was discovered in the films, by measuring birefringence, depositions were only achievable at low flow rates, which resulted in uneven pulsed flow cause by the peristaltic pump.

In order to achieve uniform alignment across the collagen films, a new EPD rig was developed. Based on the tubular collagen rig from Chapter 5, a rotating cylindrical electrode allowed for an interfacial flow between the revolving substrate and the static collagen suspension. The initial design, which used a DC motor to rotate the electrode, was found to spin too quickly for deposition to occur, and at low RPM the DC motor lost torque and would not rotate. A system of gears was introduced to the EPD rig to reduce the RPM but maintain high torque from the DC motor. Here, it was found that collagen could be aligned

uniformly within during EPD. Alignment increased at higher velocities, however increasing the velocity resulted in reduced deposition yield.

The Effect of Alignment of Mechanical Properties

The mechanical properties of aligned collagen films were compared with non-aligned films. The ultimate tensile strength (UTS) was measured for aligned films loaded parallel to the direction of alignment, as well as orthogonally. The UTS of aligned films, in the direction of alignment, was greater than non-aligned films and orthogonally loaded films.

Developing Cross-ply Collagen Films

Alignment of collagen had been achieved using the rotating cylindrical EPD rig. However, to develop cross-ply collagen films it was necessary to deposit onto a planar substrate that could be re-orientated between depositions, building a multilayer films, with each layer aligned in a different orientation. The initial flowing EPD rig was redesigned to allow for the peristaltic pump to run at higher flow rates, removing the pulsed flow issues. In order to deposit at increased flow rates, it was necessary to use DC-EPD at higher voltages of 30 – 40 V. To allow for defect-free deposits from high-voltage DC-EPD, collagen was deposited onto a barrier membrane away from the electrode and nucleating gas bubbles. With this redeveloped EPD flow rig, consistent flows resulted in planar aligned collagen films. The barrier membrane substrate was then re-orientated between deposition steps, resulting in the production of cross-ply collagen films. Based on the mechanical results that showed increased tensile strength in aligned collagen films, it was suggested that these cross-ply collagen film could have increased tear resistance to non-aligned films.

Summary

In Chapter 7, it was found that alignment of collagen within films could be achieved by generating an interfacial flow between the collagen suspension and the deposition substrate, in both a flowing and a rotating EPD rig. The tensile strength of the aligned collagen films was found to be greater than non-aligned films. Furthermore, by re-orientating the collagen deposit and substrate between deposition steps, multilayer cross-ply collagen films were produced, potentially with increased tear resistance.

8.2 Future Perspectives

Following the investigations that have been carried out within this thesis, the subsequent section outlines areas of potential development and future directions. As well as prospective ideas, this section also includes some preliminary experimental work on nerve guidance conduits, that would merit further development; here, initial experimental methods are described and results presented.

8.2.1 Improving Collagen EPD Processing

Improving Pulsed Current EPD Modelling for Collagen Suspensions

A model for pulsed current EPD was developed in Chapter 4, with the introduction of a novel factor, the pulse current factor, to previously-described DC-EPD models. The model was accurate at higher voltages, but deviated from experimental results at low voltages. A theory was developed accounting for additional mechanisms that should be included within the model. The model should be developed further to incorporate acceleration and deceleration times of particles during each pulse during PC-EPD. In order to calculate this, it is necessary to know the particle size within the system, which is difficult for collagen fibres of unknown size and mass. It would therefore be beneficial to develop the PC-EPD model with a more standard EPD system first using well-characterised particles in suspension, to establish a working model before introducing it to more complex biological macromolecule systems.

8.2.2 Investigating the Mechanical Properties of EPD Collagen Films

The effect of film density

In Chapter 6, the density of EPD collagen films was investigated, with films produced at higher voltages having increased densities. While these were found to have increased degradation resistance, the mechanical properties of these films was not investigated. With the

collagen molecules packed together more tightly, it may be that the mechanical properties of films are altered, which would further reduce the need for additional cross-linkers. However, the full affect of density on mechanical properties must be investigated in order to better understand its influence.

Aligned Collagen Films

It was found, in Chapter 7, that aligned collagen films had increased ultimate tensile strength. It would be of interest to also understand the effect alignment on film stiffness and Young's modulus, by also measuring the strain during tensile testing. Furthermore, the effect alignment on mechanical properties should be further explored, to understand if controllable alignment allows for tunable mechanical properties within films.

Cross-ply Collagen Films

Cross-ply collagen films were also developed in Chapter 7, with each layer aligned in a different orientation, with the aim of achieving membranes with increased tear resistance. It was found that alignment of collagen increased the UTS of the films, but it is important to understand what effect this has in cross-ply collagen films. To evaluate this, tear tests should be performed on cross-ply films and compared with non-aligned films. Further to this, suture pull-out tests could also be performed, to understand the effectiveness of these films at remaining intact once sutured in place.

8.2.3 Investigating the Bioactivity of EPD Collagen Films

In Vitro Testing

These collagen membranes were developed to be implanted within the body to aid in tissue regeneration. Therefore, it is important that they are shown to be non-toxic and viable for cells, and to show that the EPD processing technique does not cause the material to

develop unknown but detrimental properties. *In vitro* studies would, therefore, be necessary to understand the viability and bioactivity of the collagen films. Further to understanding how different cells may interact with the films, there are more specific studies that would also be beneficial for the development of EPD collagen films:

Grooved Films It was shown in Chapter 5 that collagen films could be developed with specific shapes and topographies that replicated the deposition substrate. Grooved collagen films, with a feature resolution of 100 µm, were produced and removed from the substrate using a cellulose acetate sacrificial layer. It was proposed that these grooves, or other features, could be used to influence or direct cell growth. Previous studies have shown that cells will grow in a preferential direction or orientation along the alignment of fibres, for example [325]. Furthermore, other studies have shown that specific architectures have been beneficial for cell proliferation and blood vessel formation [287], and stem cell differentiation [326]. Further work here could make use of this EPD technique, to develop a variety of topographies and architectures to grow cells on.

Films density Films density was altered in order to understand the effect on degradation properties without the use of chemical cross-linkers, which often use up cell attachment sites. While it was shown that films with greater density had increased degradation resistance, it is important to validate that these films remain as bioactive as other non-cross-linked collagen materials. Furthermore, it is possible that changing the films density may affect cell growth, for cells that are more sensitive to material properties, such as nerve cells, which have been shown to proliferate more on materials with lower stiffness [327].

8.2.4 Future Biomaterial Applications for EPD Collagen

As well as consistent defect-free films, the use of a sacrificial layer to remove collagen from the substrate also allowed for a greater variety of shapes and topographies to be produced,

as there was no longer the requirement to remove films with a razor blade via mechanical cleavage. Substrates with varying topographies, features, and non-planar surfaces could be deposited on, and the collagen effectively removed by dissolving the cellulose sacrificial layer. In Chapter 5 it was shown that both grooved and tubular films could be produced and that features with a resolution of less than 100 µm could be translated onto the collagen films. Here, only these substrates were used, but this provided proof-of-concept for further substrates, designed with specific medical applications.

Blood Vessels

As shown in Chapter 5, the development of seamless collagen tubes using EPD was found to be effective, by deposited collagen onto a cylindrical electrode. This method was then developed further, in Chapter 7, by rotating the electrode to generate alignment within the collagen tube. The alignment of collagen fibres was in the radial plane of the tube, which is the same plane that is mechanically loaded within blood vessels in the systolic phase as blood is pumped around the body. The radially aligned collagen could provide additional strength in the loaded plane. Furthermore, EPD has been used to fabricate composite films [24]. Future work could also incorporate elastin within the suspension to be deposited with collagen, adding elasticity to the tubular devices.

Nerve Guidance Conduits

Nerve guidance conduits (NGC) are used to direct growth of damaged or severed nerves in order to restore functionality to peripheral nerves. One issue with nerve tissue repair is the infiltration of fibroblasts into the NGC, which produce scar tissue and inhibit the growth of healthy nerves. One solution to this problem is to prevent in the ingrowth of fibroblasts using a barrier or sheath around the NGC. In Chapter 5, seamless collagen tubes were developed using a cylindrical EPD rig, which were removed via a cellulose sacrificial layer. These

tubes could be used as sheaths around NGC. Furthermore, aligned NGCs made from porous collagen sponges could be fabricated within the collagen tubes.

Initial research was undertaken into the development of sheathed nerve guidance conduits, in collaboration with Robert Murphy (PhD student, Cambridge Centre for Medical Materials). Here, the initial experimental work and findings so far are presented:

Materials and Methods A free-standing, seamless tubular collagen film was produced, as described in Section 5.2.5. An internal aligned, porous collagen scaffold was produced within the collagen tube, in collaboration with Robert Murphy (PhD student, Cambridge Centre for Medical Materials). 1 wt.% collagen suspension, prepared following the protocol in Section 3.2.1, was poured into the tubular collagen film, which was situated within a cylindrical mould designed by Robert Murphy. The mould used to produce scaffolds was made of insulating Perspex with cylindrical holes of depth 30 mm and diameter 10 mm drilled into it. The base of the moulds was a flat copper sheet to aid heat conduction. These dimensions give a suitable ratio between the size of the insulating wall and conductive base to induce temperature gradients suitable to produce scaffolds with aligned pore architecture [82]. The mould containing the collagen tube and collagen slurry was placed into a bench-top freeze drier and Robert Murphy programmed the freeze-drying protocol: a relatively fast cooling rate (to induce nucleation at only a small region at the bottom of the mould and thus give aligned structures) of $-2\,^{\circ}\mathrm{C\,min^{-1}}$ was used, and the shelf freezing temperature was set at $-30\,^{\circ}\mathrm{C}$. A thermal hold for 200 minutes at $-30\,^{\circ}\mathrm{C}$ was used to ensure the samples had fully frozen prior to the drying step. The drying step consisted of a 20 minute ramp to 80 mTorr, followed by a $1\,^{\circ}\mathrm{C\,min^{-1}}$ ramp to $0\,^{\circ}\mathrm{C}$, the scaffolds were then held for 1000 minutes at 80 mTorr in order to remove all ice from the structure, this was followed by a $1\,^{\circ}\mathrm{C\,min^{-1}}$ ramp to $20\,^{\circ}\mathrm{C}$ and then a 10 minute hold at $20\,^{\circ}\mathrm{C}$.

In collaboration with Robert Murphy, the aligned porous collagen scaffold within collagen sheath was imaged using micro-computed tomography (μ-CT). For 3 dimensional imaging

by μ-CT a Skyscan 1072 system (Bruker, BE) was used to image the scaffold. Robert Murphy imaged the scaffold as follows: images were taken at 25 kV and 136 µA (3 W power) with a 0.2° rotation step and pixel size of 5.46 µm. Images were averaged over two frames with a 0.95 second acquisition time. The projections were reconstructed into 3D data sets using NRecon software, produced by Skyscan which allowed images to be viewed in CTVox software (Bruker) for production of images that represent the pore structure.

Robert Murphy reconstructed the images: The reconstructed data sets are loaded into CTAn software (Bruker) and a volume of interest (VOI) was selected which enclosed the entire scaffold. The slices of this VOI were then thresholded using the Otsu method by the CTAn software. Next the sweep function was used to despeckle the individual slices of the image, removing noise. Then the '3D analysis' function was used to analyse the scaffold characteristics, the relevant portions to this work being the structure separation and thickness which are required for visualisation. The scaffold was then visualised using CTVox software, which allows a cross section to be seen through the scaffold at different angles and depths throughout the structure.

Results As a proof-of-concept for sheathed nerve guidance conduits (NGCs), collagen tubes (fabricated and shown in Section 5.3.1) were filled with collagen slurry and freeze-dried to form an internal aligned collagen structure. These sheathed NGC scaffolds were imaged using μ-CT to see the internal structure within the collagen tube; a section of the 3D μ-CT reconstruction can be seen in Figure 8.1.

The internal structure formed an aligned porous collagen scaffold. There was a good connection between the film and the internal scaffold, with little delamination. The collagen film sheath, however, had a reduced density compared with a collagen film produced with the same EPD parameters (Figure 8.1, C), where the collagen sheath, post slurry and freeze-drying, was much thicker than a regular EPD collagen film (D). This indicates that the collagen film was hydrated by the collagen slurry that was poured into into it, before freeze-

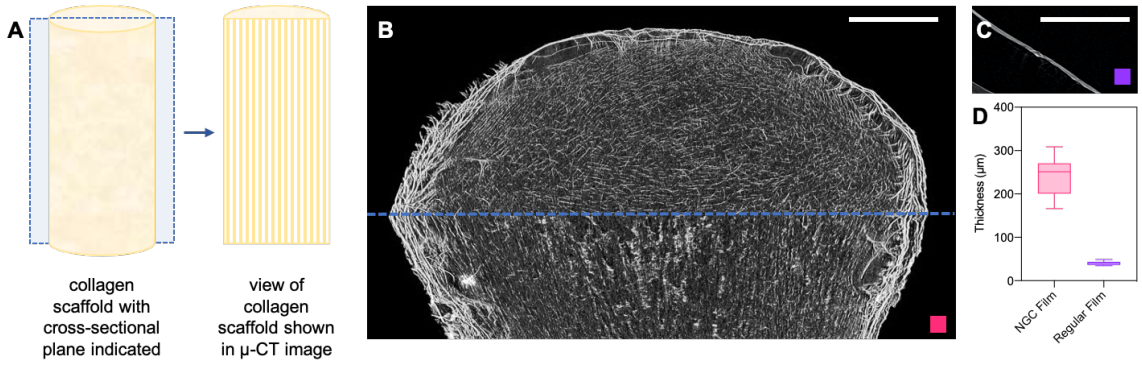

Fig. 8.1 (A) Schematic showing the orientation and cross-section of the μ-CT image in B (B) μ-CT image of tubular collagen film with internal freeze-dried aligned collagen scaffold, to act as a sheathed collagen nerve guidance conduit (C) μ-CT image of collagen film only, formed via EPD under the same parameters as the film used as a sheath in B (D) Plot showing the measured thickness of the collagen films formed via EPD in the μ-CT images of B and C. White scale bars are 1000 µm

drying. The freeze-drying process caused the tube to dry with a less dense layer — though much more dense than internal collagen scaffold, and with no external pores.

Not only were seamless collagen tubes formed, but their potential use as nerve guidance conduits was explored. NGCs are used to bridge the gap in acute peripheral nerve damage, guiding the axon from the proximal damaged region distally [328]. This requires a tubular shaped scaffold with highly aligned pore architecture. Aligned collagen scaffold have been created, but nerves require idyllic conditions to fully repair and are slow to do so. One of the greatest failures in restoring nerve functionality is the infiltration of invasive fibroblast cells, which can cause scar tissue [329]. Creating a collagen sheath (tubular film) around the aligned scaffold could act as a barrier membrane, preventing fibroblast migration and protecting the repairing nerve tissue. This is one potential use for shaped EPD collagen films, and shows the versatility of the technique, which could be adapted to a whole host biomedical uses.

The work in this thesis has described the optimisation of collagen films using electrophoretic deposition, for developing membranes with tunable material properties. Together, the future perspectives set out here present further developments of EPD collagen films, allowing for the design of membranes for a range of medical applications.

References

[1] J. P. Fiorellini and M. L. Nevins, "Localized Ridge Augmentation/Preservation.A Systematic Review," *Annals of Periodontology*, vol. 8, pp. 321–327, Dec. 2003.

[2] D. Buser, K. Schenk, and H. P. Hirt, "Lateral Ridge Augmentation Using Autografts and Barrier Membranes: A Clinical Study With 40 Partially Edentulous Patients," *Jounral of Oral Maxillofacial Surgery*, vol. 54, pp. 420–432, 1996.

[3] J. D. Kassolis, P. S. Rosen, and M. A. Reynolds, "Alveolar Ridge and Sinus Augmentation Utilizing Platelet-Rich Plasma in Combination With Freeze-Dried Bone Allograft: Case Series," *Journal of Periodontology*, vol. 71, pp. 1654–1661, Oct. 2000.

[4] C. H. F. Hämmerle, R. E. Jung, D. Yaman, and N. P. Lang, "Ridge augmentation by applying bioresorbable membranes and deproteinized bovine bone mineral: A report of twelve consecutive cases," *Clinical Oral Implants Research*, vol. 1, pp. 201–211, Oct. 2007.

[5] N. Mardas, V. Chadha, and N. Donos, "Alveolar ridge preservation with guided bone regeneration and a synthetic bone substitute or a bovine-derived xenograft: A randomized, controlled clinical trial: Alveolar ridge preservation," *Clinical Oral Implants Research*, vol. 21, pp. 688–698, Apr. 2010.

[6] J. Liu and D. G. Kerns, "Mechanisms of Guided Bone Regeneration: A Review," *The Open Dentistry Journal*, vol. 8, pp. 56–65, May 2014.

[7] D. Hutmacher, M. B. Hürzeler, and H. Schliephake, "A Review of Material Properties of Biodegradable and Bioresorbable Polymers and Devices for GTR and GBR Applications," *International Jounral of Oral Maxillofacial Implants*, vol. 11, pp. 667–678, 1996.

[8] W. Becker, S. E. Lynch, U. Lekholm, B. E. Becker, R. Caffesse, K. Donath, and R. Sanchez, "A Comparison of ePTFE Membranes Alone or in Combination with Platelet-Derived Growth Factors and Insulin-Like Growth Factor-I or Demineralized Freeze-Dried Bone in Promoting Bone Formation Around Immediate Extraction Socket Implants," *Journal of Periodontology*, vol. 63, pp. 929–940, Nov. 1992.

[9] W. Becker, C. Dahlin, B. E. Becker, D. van Steenberghe, K. Higuchi, and C. Kultje, "The Use of e-PTFE Barrier Membranes for Bone Promotion Around Titanium Implants Placed Into Extraction Sockets: A Prospective Multicenter Study," *Journal of Oral and Maxillofacial Implants*, vol. 9, pp. 31–40, 1994.

[10] W. Becker, C. Dahlin, U. Lekholm, C. Bergstrom, D. Steenberghe, K. Higuchi, and B. E. Becker, "Five-Year Evaluation of Implants Placed at Extraction and with Dehiscences and Fenestration Defects Augmented with ePTFE Membranes: Results from a Prospective Multicenter Study," *Clinical Implant Dentistry and Related Research*, vol. 1, pp. 27–32, July 1999.

[11] R. Faria-Almeida, I. Astramskaite-Januseviciene, A. Puisys, and F. Correia, "Extraction Socket Preservation with or without Membranes, Soft Tissue Influence on Post Extraction Alveolar Ridge Preservation: A Systematic Review," *Journal of Oral and Maxillofacial Research*, vol. 10, Sept. 2019.

[12] V. Lekovic, P. M. Camargo, P. R. Klokkevold, M. Weinlaender, E. B. Kenney, B. Dimitrijevic, and M. Nedic, "Preservation of Alveolar Bone in Extraction Sockets Using Bioabsorbable Membranes," *Journal of Periodontology*, vol. 69, pp. 1044–1049, Sept. 1998.

[13] O. M. Böstman, "OSTEOLYTIC CHANGES OF ABSORBABLE ACCOMPANYING DEGRADATION FRACTURE FIXATION IMPLANTS Osteolytic Changes Accompanying Degradation of Absorbable Fraccture Fixation Implants," *The Journal of Bone and Joint Surgery*, vol. 73, no. 4, pp. 679–682, 1991.

[14] W. Friess, "Collagen – biomaterial for drug delivery," *European Journal of Pharmaceutics and Biopharmaceutics*, vol. 2, pp. 113–136, 1998.

[15] K. Gelse, "Collagens—structure, function, and biosynthesis," *Advanced Drug Delivery Reviews*, vol. 55, pp. 1531–1546, Nov. 2003.

[16] L. Cen, W. Liu, L. Cui, W. Zhang, and Y. Cao, "Collagen Tissue Engineering: Development of Novel Biomaterials and Applications," *Pediatric Research*, vol. 63, pp. 492–496, May 2008.

[17] D. L. Butler, S. Goldstein, and F. Guilak, "Functional Tissue Engineering: The Role of Biomechanics," *Journal of Biomechanical Engineering*, vol. 122, no. 6, pp. 570–575, 2000.

[18] G. A. Di Lullo, S. M. Sweeney, J. Körkkö, L. Ala-Kokko, and J. D. San Antonio, "Mapping the Ligand-binding Sites and Disease-associated Mutations on the Most Abundant Protein in the Human, Type I Collagen," *Journal of Biological Chemistry*, vol. 277, pp. 4223–4231, Feb. 2002.

[19] L. Sbricoli, R. Guazzo, M. Annunziata, L. Gobbato, E. Bressan, and L. Nastri, "Selection of Collagen Membranes for Bone Regeneration: A Literature Review," *Materials*, vol. 13, p. 786, Feb. 2020.

[20] R. B. Vernon, M. D. Gooden, S. L. Lara, and T. N. Wight, "Microgrooved fibrillar collagen membranes as scaffolds for cell support and alignment," *Biomaterials*, vol. 26, pp. 3131–3140, June 2005.

[21] G. E. F. Brewer, "Electrophoretic painting," *Journal of Applied Electrochemistry*, vol. 13, pp. 269–275, 1983.

[22] P. E. Pierce, "The physical chemistry of the cathodic electrodeposition process," *Journal of Coatings Technology and Research*, vol. 53, p. 52, 1981.

[23] I. Corni, M. P. Ryan, and A. R. Boccaccini, "Electrophoretic deposition: From traditional ceramics to nanotechnology," *Journal of the European Ceramic Society*, vol. 28, pp. 1353–1367, Jan. 2008.

[24] D. J. Barrett, *Electrophoretic Deposition of Command-Set Collagen/Hyaluronic Acid Multilayer Films for Ridge Augmentation Applications*. PhD thesis, University of Cambridge, Cambridge, 2017.

[25] D. J. Barrett, M. D. Linley, S. M. Best, and R. E. Cameron, "Fabrication of free standing collagen membranes by pulsed-electrophoretic deposition," *Biofabrication*, vol. 11, p. 045017, Aug. 2019.

[26] S. Chattopadhyay and R. T. Raines, "Collagen-based biomaterials for wound healing," *Biopolymers*, vol. 101, pp. 821–833, Aug. 2014.

[27] V. R. Sherman, W. Yang, and M. A. Meyers, "The materials science of collagen," *Journal of the Mechanical Behavior of Biomedical Materials*, vol. 52, pp. 22–50, Dec. 2015.

[28] G. Cameron, I. Alberts, J. Laing, and T. Wess, "Structure of Type I and Type III Heterotypic Collagen Fibrils: An X-Ray Diffraction Study," *Journal of Structural Biology*, vol. 137, pp. 15–22, Jan. 2002.

[29] S. Ricard-Blum, "The Collagen Family," *Cold Spring Harbor Perspectives in Biology*, vol. 3, pp. 497–499, Jan. 2011.

[30] E. J. Kucharz, "Structure, Heterogeneity, and Distribution," *The Collagens: Biochemistry and Pathophysiology*, pp. 5–29, 1992.

[31] J. P. R. O. Orgel, T. C. Irving, A. Miller, and T. J. Wess, "Microfibrillar structure of type I collagen in situ," *Proceedings of the National Academy of Sciences*, vol. 103, pp. 9001–9005, June 2006.

[32] J. P. R. O. Orgel, J. D. San Antonio, and O. Antipova, "Molecular and structural mapping of collagen fibril interactions," *Connective Tissue Research*, vol. 52, pp. 2–17, Feb. 2011.

[33] J.-J. Wu, P. Woods, and D. Eyre, "Identification of Cross-linking Sites in Bovine Cartilage TypeIX Collagen Reveals an Antiparallel Type 11-Type IX Molecular Relationship and Type IX to TypeIX Bonding," *The Journal of Biological Chemistry*, vol. 207, no. 35, pp. 23007–23014, 1992.

[34] H. P. Bächinger, K. Mizuno, J. Vranka, and S. P. Boudko, "Collagen formation and structure," *Comprehensive Natural Products II: Chemistry and Biology*, pp. 469–530, Mar. 2010.

[35] D. Hulmes, "Collagen Diversity, Synthesis and Assembly," in *Collagen* (P. Fratzl, ed.), pp. 15–47, Boston, MA: Springer US, 2008.

[36] C.-W. Franzke, P. Bruckner, and L. Bruckner-Tuderman, "Collagenous Transmembrane Proteins: Recent Insights into Biology and Pathology," *Journal of Biological Chemistry*, vol. 280, no. 6, pp. 4005–4008, 2004.

[37] H. G. Welgus, J. J. Jeffrey, A. Z. Eisen, W. T. Roswit, and G. P. Stricklin, "Human Skin Fibroblast Collagenase: Interaction with Substrate and Inhibitor," *Collagen and Related Research*, vol. 5, pp. 167–179, Jan. 1985.

[38] M. Van Der Rest and R. Mayne, "Type IX collagen proteoglycan from cartilage is covalently cross-linked to type II collagen," *Journal of Biological Chemistry*, vol. 263, no. 4, pp. 1615–1618, 1988.

[39] K. E. Kadler, C. Baldock, J. Bella, and R. P. Boot-Handford, "Collagens at a glance," *Journal of Cell Science*, vol. 120, pp. 1955–1958, May 2007.

[40] K. Piez, "Collagen," in *Encyclopedia of Polymer Science and Engineering* (J. Kroschwitz, ed.), pp. 699–727, New York: Wiley-Interscience, second ed., 1985.

[41] R. Timpl, "Immunological Studies on Collagen," in *Biochemistry of Collagen* (G. N. Ramachandran and A. H. Reddi, eds.), pp. 319–375, Boston, MA: Springer US, first ed., 1976.

[42] K. A. Piez, "Molecular and aggregate structures of the collagens," in *Extracellular Martrix Biochemistry* (K. A. Piez and A. H. Reddi, eds.), pp. 1–39, New York: Elsevier, first ed., 1984.

[43] J. W. Smith, "Molecular Pattern in Native Collagen," *Nature*, vol. 219, pp. 157–158, 1968.

[44] W. Yang, V. R. Sherman, B. Gludovatz, M. Mackey, E. A. Zimmermann, E. H. Chang, E. Schaible, Z. Qin, M. J. Buehler, R. O. Ritchie, and M. A. Meyers, "Protective role of Arapaima gigas fish scales: Structure and mechanical behavior," *Acta Biomaterialia*, vol. 10, pp. 3599–3614, Aug. 2014.

[45] S. Kimura, Y. Takema, and M. Kubota, "Octopus Skin Collagen. Isolation and characterization of collagen comprising two distinct alpha chains," *The Journal of Biological Chemistry*, vol. 256, no. 24, pp. 13230–13234, 1981.

[46] M. Spira, B. Liu, Z. Xu, R. Harrell, and H. Chahadeh, "Human amnion collagen for soft tissue augmentation—biochemical characterizations and animal observations," *Journal of Biomedical Materials Research*, vol. 28, pp. 91–96, Jan. 1994.

[47] P. D. Toman, F. Pieper, N. Sakai, C. Karatzas, E. Platenburg, de Wit, C. Samuel, A. Dekker, G. A. Daniels, and R. A. Berg, "Production of recombinant human type I procollagen homotrimer in the mammary gland of transgenic mice," *Transgenic Research*, vol. 8, pp. 415–427, 1999.

[48] G. Chandrakasan, K. A. Piez, and A. Torchia, "Preparation of Intact Monomeric Collagen from Rat Tail Tendon and Skin and the Structure of the Nonhelical Ends in Solution," *The Journal of Biological Chemistry*, vol. 251, no. 19, pp. 6062–6067, 1976.

[49] J. Bowes, R. G. Elliot, and J. A. Moss, "The Composition of Collagen and Acid-Soluble Collagen of Bovine Skin," *The Biochemical Journal*, vol. 61, no. 1, pp. 143–150, 1955.

[50] G. Cioca, "Process for Preparing Macromolecular Biologically Active Collagen," 1981.

[51] M. Roreger, "Collagen Prepartation for the Controlled Release of Active Substances," 2004.

[52] F. Steven and H. Thomas, "Preparation of insoluble collagen from human cartilage," *The Biochemical Journal*, vol. 135, pp. 245–247, 1973.

[53] K. R. Meade and F. H. Silver, "Immunogenicity of collagenous implants," *Biomaterials*, vol. 11, pp. 176–180, Apr. 1990.

[54] L. Cooperman and D. Michaeli, "The immunogenicity of injectable collagen. I. A 1-year prospective study," *Journal of the American Academy of Dermatology*, vol. 10, pp. 638–646, Jan. 1984.

[55] K. Wangerin and H.-U. Wottge, "Immunological reactions against collagen," *European Journal of Plastic Surgery*, vol. 17, Nov. 1994.

[56] U. Takeda, M. Odaki, M. Yokota, H. Sasaki, T. Niizato, H. Kawaota, H. Watanabe, T. Ito, N. Ishiwatari, H. Hayasaka, M. Seki, and T. Koeda, "Acute and subacute toxicity studies on collagen wound dressing (CAS) in mice and rats," *The Journal of Toxicological Sciences*, vol. 7, no. 2, pp. 63–91, 1982.

[57] S. Gorham, T. Hyland, D. French, and M. Willins, "Cellular invasion and breakdown of three different collagen films in the lumbar muscle of the rat," *Biomaterials*, vol. 11, pp. 113–118, Mar. 1990.

[58] W. Friess, W. Zhou, and M. J. Groves, "In-vivo Activity of Collagen Matrices Containing PS1, an Antineoplastic Glycan, Against Murine Sarcoma Cells," *Pharmaceutical Sciences*, vol. 2, pp. 121–124, 1996.

[59] M. Boon, "Collagen implants remain supple not allowing fibroblast ingrowth," *Biomaterials*, vol. 16, pp. 1089–1093, Sept. 1995.

[60] R. J. Ruderman, C. W. R. Wade, W. D. Shepard, and F. Leonard, "Prolonged resorption of collagen sponges: Vapor-phase treatment with formaldehyde," *Journal of Biomedical Materials Research*, vol. 7, pp. 263–265, Mar. 1973.

[61] M. D. Harriger, A. P. Supp, G. D. Warden, and S. T. Boyce, "Glutaraldehyde crosslinking of collagen substrates inhibits degradation in skin substitutes grafted to athymic mice," *Journal of Biomedical Materials Research*, vol. 35, pp. 137–145, 1997.

[62] X. Wu, L. Black, G. Santacana-Laffitte, and C. W. Patrick, "Preparation and assessment of glutaraldehyde-crosslinked collagen–chitosan hydrogels for adipose tissue engineering," *Journal of Biomedical Materials Research Part A*, vol. 81A, pp. 59–65, Apr. 2007.

[63] R. Tu, R. Quijano, and C. Lu, "A Preliminary Study of the Fixation Mechanism of Collagen Reaction with a Polyepoxy Fixative," *The International Journal of Artificial Organs*, vol. 16, no. 7, pp. 537–544, 1993.

[64] H. Petite, I. Rault, A. Huc, P. Menasche, and D. Herbage, "Use of the acyl azide method for cross-linking collagen-rich tissues such as pericardium," *Journal of Biomedical Materials Research*, vol. 24, pp. 179–187, Feb. 1990.

[65] D. I. Zeugolis, G. R. Paul, and G. Attenburrow, "Cross-linking of extruded collagen fibers-A biomimetic three-dimensional scaffold for tissue engineering applications," *Journal of Biomedical Materials Research Part A*, vol. 89A, pp. 895–908, June 2009.

[66] H. M. Powell and S. T. Boyce, "EDC cross-linking improves skin substitute strength and stability," *Biomaterials*, vol. 27, pp. 5821–5827, Dec. 2006.

[67] H. M. Powell and S. T. Boyce, "Wound closure with EDC cross-linked cultured skin substitutes grafted to athymic mice," *Biomaterials*, vol. 28, pp. 1084–1092, Feb. 2007.

[68] D. V. Bax, N. Davidenko, D. Gullberg, S. W. Hamaia, R. W. Farndale, S. M. Best, and R. E. Cameron, "Fundamental insight into the effect of carbodiimide crosslinking on cellular recognition of collagen-based scaffolds," *Acta Biomaterialia*, vol. 49, pp. 218–234, Feb. 2017.

[69] K. Weadock, "Effect of physical crosslinking methods on collagen-fiber durability in proteolytic solutions," *Journal of Biomedical Materials Research*, vol. 32, no. 221-226, p. 6, 1996.

[70] K. S. Weadock, E. J. Miller, L. D. Bellincampi, J. P. Zawadsky, and M. G. Dunn, "Physical crosslinking of collagen fibers: Comparison of ultraviolet irradiation and dehydrothermal treatment," *Journal of Biomedical Materials Research*, vol. 29, pp. 1373–1379, Nov. 1995.

[71] S. T. Khew, Q. J. Yang, and Y. W. Tong, "Enzymatically crosslinked collagen-mimetic dendrimers that promote integrin-targeted cell adhesion," *Biomaterials*, vol. 29, pp. 3034–3045, July 2008.

[72] A. K. Nguyen, S. D. Gittard, A. Koroleva, S. Schlie, A. Gaidukeviciute, B. N. Chichkov, and R. J. Narayan, "Two-photon polymerization of polyethylene glycol diacrylate scaffolds with riboflavin and triethanolamine used as a water-soluble photoinitiator," *Regenerative Medicine*, vol. 8, pp. 725–738, Nov. 2013.

[73] G. Wollensak, E. Spoerl, and T. Seiler, "Riboflavin/ultraviolet-a–induced collagen crosslinking for the treatment of keratoconus," *American Journal of Ophthalmology*, vol. 135, pp. 620–627, May 2003.

[74] D. F. Thompson and H. S. Saluja, "Prophylaxis of migraine headaches with riboflavin: A systematic review," *Journal of Clinical Pharmacy and Therapeutics*, vol. 42, pp. 394–403, Aug. 2017.

[75] E. P. Brennan-Pierce, I. MacAskill, R. B. Price, and J. M. Lee, "Riboflavin-sensitized photo-crosslinking of collagen using a dental curing light," *Bio-Medical Materials and Engineering*, vol. 24, no. 4, pp. 1659–1671, 2014.

[76] S. Ibusuki, G. J. Halbesma, M. A. Randolph, R. W. Redmond, I. E. Kochevar, and T. J. Gill, "Photochemically Cross-Linked Collagen Gels as Three-Dimensional Scaffolds for Tissue Engineering," *Tissue Engineering*, vol. 13, pp. 1995–2001, Aug. 2007.

[77] J. Heo, R. H. Koh, W. Shim, H. D. Kim, H.-G. Yim, and N. S. Hwang, "Riboflavin-induced photo-crosslinking of collagen hydrogel and its application in meniscus tissue engineering," *Drug Delivery and Translational Research*, vol. 6, pp. 148–158, Apr. 2016.

[78] C. H. Lee, A. Singla, and Y. Lee, "Biomedical applications of collagen," *International Journal of Pharmaceutics*, vol. 221, pp. 1–22, June 2001.

[79] J. Glowacki and S. Mizuno, "Collagen scaffolds for tissue engineering," *Biopolymers*, vol. 89, pp. 338–344, May 2008.

[80] K. M. Pawelec, A. Husmann, S. M. Best, and R. E. Cameron, "A design protocol for tailoring ice-templated scaffold structure," *Journal of The Royal Society Interface*, vol. 11, p. 20130958, Mar. 2014.

[81] J. C. Ashworth, M. Mehr, P. G. Buxton, S. M. Best, and R. E. Cameron, "Cell Invasion in Collagen Scaffold Architectures Characterized by Percolation Theory," *Advanced Healthcare Materials*, vol. 4, pp. 1317–1321, June 2015.

[82] N. Davidenko, T. Gibb, C. Schuster, S. Best, J. Campbell, C. Watson, and R. Cameron, "Biomimetic collagen scaffolds with anisotropic pore architecture," *Acta Biomaterialia*, vol. 8, pp. 667–676, Feb. 2012.

[83] C. N. Grover, R. E. Cameron, and S. M. Best, "Investigating the morphological, mechanical and degradation properties of scaffolds comprising collagen, gelatin and elastin for use in soft tissue engineering," *Journal of the Mechanical Behavior of Biomedical Materials*, vol. 10, pp. 62–74, June 2012.

[84] C. N. Grover, J. H. Gwynne, N. Pugh, S. Hamaia, R. W. Farndale, S. M. Best, and R. E. Cameron, "Crosslinking and composition influence the surface properties, mechanical stiffness and cell reactivity of collagen-based films," *Acta Biomaterialia*, vol. 8, pp. 3080–3090, Aug. 2012.

[85] S. MacNeil, "Biomaterials for tissue engineering of skin," *Materials Today*, vol. 11, pp. 26–35, May 2008.

[86] G. Monaco, R. Cholas, L. Salvatore, M. Madaghiele, and A. Sannino, "Sterilization of collagen scaffolds designed for peripheral nerve regeneration: Effect on microstructure, degradation and cellular colonization," *Materials Science and Engineering: C*, vol. 71, pp. 335–344, Feb. 2017.

[87] X. Duan and H. Sheardown, "Dendrimer crosslinked collagen as a corneal tissue engineering scaffold: Mechanical properties and corneal epithelial cell interactions," *Biomaterials*, vol. 27, pp. 4608–4617, Sept. 2006.

[88] P. Buijtenhuijs, L. Buttafoco, A. A. Poot, W. F. Daamen, T. H. van Kuppevelt, P. J. Dijkstra, R. A. I. de Vos, L. M. T. Sterk, B. R. H. Geelkerken, J. Feijen, and I. Vermes, "Tissue engineering of blood vessels: Characterization of smooth-muscle cells for culturing on collagen-and-elastin-based scaffolds," *Biotechnology and Applied Biochemistry*, vol. 39, p. 141, Apr. 2004.

[89] Y. Miyagi, L. L. Chiu, M. Cimini, R. D. Weisel, M. Radisic, and R.-K. Li, "Biodegradable collagen patch with covalently immobilized VEGF for myocardial repair," *Biomaterials*, vol. 32, pp. 1280–1290, Feb. 2011.

[90] J. M. McPherson, P. W. Ledger, S. Sawamura, A. Conti, S. Wade, H. Reihanian, and D. G. Wallace, "The preparation and physicochemical characterization of an injectable form of reconstituted, glutaraldehyde cross-linked, bovine corium collagen," *Journal of Biomedical Materials Research*, vol. 20, pp. 79–92, Jan. 1986.

[91] D. G. Wallace, W. Rhee, H. Reihanian, G. Ksander, R. Lee, W. B. Braun, B. A. Weiss, and B. B. Pharriss, "Injectable cross-linked collagen with improved flow properties," *Journal of Biomedical Materials Research*, vol. 23, pp. 931–945, Aug. 1989.

[92] J. Slavin, J. R. Nash, and A. N. Kingsnorth, "Effect of transforming growth factor beta and basic fibroblast growth factor on steroid-impaired healing intestinal wounds," *British Journal of Surgery*, vol. 79, pp. 69–72, Jan. 1992.

[93] S. Cusack, M. Kuss, M. Jaros, L. Hemsen, and H. Minkowitz, "A randomized, multicenter, pilot study comparing the efficacy and safety of a bupivacaine-collagen implant (XaraColl®) with the ON-Q PainBuster® Post-op Pain Relief System following open gynecological surgery," *Journal of Pain Research*, p. 453, Nov. 2012.

[94] G. J. Shaker, S. Ueda, J. A. LoCascio, and J. V. Aquavella, "Effect of a collagen shield on cat corneal epithelial wound healing.," *Investigative Ophthamology & Visual Science*, vol. 30, no. 7, pp. 1565–1569, 1989.

[95] D. Smith, J, "Indications for use of Biobrane in wound management," *Jounral of Burn Care & Rehabilitation*, pp. 317–321, 1994.

[96] S. Lal, "Biomembrane improved wound healing in burned children without increased risk of infection," *Shock*, vol. 14, no. 3, pp. 314–319, 2000.

[97] J. Zitelli, "Wound healing for the clinician," *Advanced Dermatology*, vol. 2, pp. 243–267, 1987.

[98] D. Enea, J. Gwynne, S. Kew, M. Arumugam, J. Shepherd, R. Brooks, S. Ghose, S. Best, R. Cameron, and N. Rushton, "Collagen fibre implant for tendon and ligament biological augmentation. In vivo study in an ovine model," *Knee Surgery, Sports Traumatology, Arthroscopy*, vol. 21, pp. 1783–1793, Aug. 2013.

[99] S. Kew, J. Gwynne, D. Enea, R. Brookes, N. Rushton, S. Best, and R. Cameron, "Synthetic collagen fascicles for the regeneration of tendon tissue," *Acta Biomaterialia*, vol. 8, pp. 3723–3731, Oct. 2012.

[100] S. Kew, J. Gwynne, D. Enea, M. Abu-Rub, A. Pandit, D. Zeugolis, R. Brooks, N. Rushton, S. Best, and R. Cameron, "Regeneration and repair of tendon and ligament tissue using collagen fibre biomaterials," *Acta Biomaterialia*, vol. 7, pp. 3237–3247, Sept. 2011.

[101] S. E. Bloomfield, T. Miyata, M. W. Dunn, N. Bueser, K. H. Stenzel, and A. L. Rubin, "Soluble Gentamicin Ophthalmic Inserts as a Drug Delivery System," *Archives of Ophthalmology*, vol. 96, pp. 885–887, May 1978.

[102] Z. Ruszczak, "Collagen as a carrier for on-site delivery of antibacterial drugs," *Advanced Drug Delivery Reviews*, vol. 55, pp. 1679–1698, Nov. 2003.

[103] R. Parenteau-Bareil, R. Gauvin, and F. Berthod, "Collagen-Based Biomaterials for Tissue Engineering Applications," *Materials*, vol. 3, pp. 1863–1887, Mar. 2010.

[104] L. Besra and M. Liu, "A review on fundamentals and applications of electrophoretic deposition (EPD)," *Progress in Materials Science*, vol. 52, pp. 1–61, Jan. 2007.

[105] H. C. Hamaker, "Formation of a Deposit by Electrophoresis," *Transactions of the Faraday Society*, vol. 36, pp. 279–283, 1940.

[106] H. C. Hamaker and E. J. W. Verwey, "The Role of the Forces Between the Particles in Electrodeposition and Other Phenomena," *Transactions of the Faraday Society*, vol. 36, pp. 180–185, 1940.

[107] P. Sarkar and P. S. Nicholson, "Electrophoretic Deposition (EPD): Mechanisms, Kinetics, and Application to Ceramics," *Journal of the American Ceramic Society*, vol. 79, no. 8, pp. 1987–2002, 1996.

[108] Y. Fukada, N. Nagarajan, W. Mekky, Y. Bao, H.-S. Kim, and P. S. Nicholson, "Electrophoretic deposition—mechanisms, myths and materials," *Journal of Materials Science*, vol. 39, pp. 787–801, Feb. 2004.

[109] S. Seuss and A. R. Boccaccini, "Electrophoretic Deposition of Biological Macromolecules, Drugs, And Cells," *Biomacromolecules*, vol. 14, pp. 3355–3369, Oct. 2013.

[110] O. O. Van der Biest and L. J. Vandeperre, "Eelctrophoretic Deposition of Materials," *Annual Review of Materials Science*, vol. 29, pp. 327–352, Aug. 1999.

[111] F. Bouyer and A. Foissy, "Electrophoretic Deposition of Silicon Carbide," *Journal of the American Ceramic Society*, vol. 82, no. 8, pp. 2001–2010, 1999.

[112] W. F. Pickard, "Remarks on the Theory of Electrophoretic Deposition," *Journal of The Electrochemical Society*, vol. 115, no. 4, p. 105C, 1968.

[113] A. R. Boccaccini, S. Keim, R. Ma, Y. Li, and I. Zhitomirsky, "Electrophoretic deposition of biomaterials," *Journal of The Royal Society Interface*, vol. 7, Oct. 2010.

[114] P. Kordomenos and J. Nordstrom, "Polymer Compositions for Cationic Electrodepositable Coatings," *Journal of Coatings Technology*, vol. 54, no. 686, pp. 33–41, 1982.

[115] Raju and P. Kumar, "Cathodic electrodeposition of self-curable polyepoxide resins based on cardanol," *Journal of Coatings Technology and Research*, vol. 8, pp. 563–575, Oct. 2011.

[116] S. N. Heavens, "Electrophoretic deposition as a processing route for ceramics," *Advanced Ceramic Processing and Technology*, vol. 1, pp. 255–283, 1990.

[117] M. S. J. Gani, "Electrophoretic deposition. A review," *Industrial Ceramics*, vol. 14, pp. 163–174, 1994.

[118] D. Hanaor, M. Michelazzi, C. Leonelli, and C. C. Sorrell, "The effects of carboxylic acids on the aqueous dispersion and electrophoretic deposition of ZrO2," *Journal of the European Ceramic Society*, vol. 32, pp. 235–244, Jan. 2012.

[119] H. Mueller, "Theory of Electrophoretic Migration," *Annals New York Academy of Sciences*, vol. 1, pp. 111–121, 1928.

[120] R. Hunter, *Zeta Potential in Collaid Science*, vol. 1. San Diego, CA: Academic Press, third ed., 1988.

[121] J. Lyklema, "Water at Interfaces: A Colloid-Chemical Approach," *Journal of Colloid and Interface Science*, vol. 58, no. 2, pp. 242–250, 1977.

[122] Z. Adamczyk, "Particle adsorption and deposition: Role of electrostatic interactions," *Advances in Colloid and Interface Science*, vol. 100-102, pp. 267–347, Feb. 2003.

[123] M. Boström, V. Deniz, G. Franks, and B. Ninham, "Extended DLVO theory: Electrostatic and non-electrostatic forces in oxide suspensions," *Advances in Colloid and Interface Science*, vol. 123-126, pp. 5–15, Nov. 2006.

[124] B. Derjaguin and L. Landau, "Theory of the stability of strongly charged lyophobic solutions and of the adhesion of strongly charged particles in solution of electrolytes," *Acta Physicochim*, vol. 14, pp. 633–662, 1941.

[125] E. J. W. Verwey and J. T. G. Overbeek, "J150453a001.pdf," *The Journal of Physical and Colloid Chemistry*, vol. 51, no. 3, pp. 631–636, 1947.

[126] J. Mahanty and B. W. Ninham, *Dispersion Forces (Colloid Science)*. London: Academic Press, 1976.

[127] J. Lyklema, *Fundamentals of Interface and Colloid Science*. Liquid-Fluid Interfaces, London: Academic Press, second ed., 1995.

[128] P. Hiemenz and R. Rajagopalan, *Principles of Colloid and Surface Chemistry*. New York: Marcel Dekker, third ed., 1997.

[129] A. R. Boccaccini and J. H. Dickerson, "Electrophoretic Deposition: Fundamentals and Applications," *The Journal of Physical Chemistry B*, vol. 117, pp. 1501–1501, Feb. 2013.

[130] F. Grillon, D. Fayeulle, and M. Jeandin, "Quantitative image analysis of electrophoretic coatings," *Journal of Materials Science Letters*, vol. 11, no. 5, pp. 272–275, 1992.

[131] H. Koelmans and J. T. G. Overbeek, "Stability and electrophoretic deposition of suspensions in non-aqueous media," *Discussions of the Faraday Society*, vol. 18, p. 52, 1954.

[132] D. R. Brown and F. W. Salt, "The mechanism of electrophoretic deposition," *Journal of Applied Chemistry*, vol. 15, no. 1, pp. 40–48, 1965.

[133] I. Zhitomirsky, "Cathodic electrodeposition of ceramic and organoceramic materials. Fundamental aspects," *Advances in Colloid and Interface Science*, vol. 97, pp. 279–317, Mar. 2002.

[134] B. Ferrari and R. Moreno, "EPD kinetics: A review," *Journal of the European Ceramic Society*, vol. 30, pp. 1069–1078, Mar. 2010.

[135] N. Sato, M. Kawachi, K. Noto, N. Yoshimoto, and M. Yoshizawa, "Effect of particle size reduction on crack formation in electrophoretically deposited YBCO ®lms," *Physica C*, p. 4, 2001.

[136] S. E. Braslavsky, "Glossary of terms used in photochemistry, 3rd edition (IUPAC Recommendations 2006)," *Pure and Applied Chemistry*, vol. 79, pp. 293–465, Jan. 2007.

[137] R. W. Powers, "The Electrophoretic Forming of Beta-Alumina Ceramic," *Journal of The Electrochemical Society*, vol. 122, no. 4, p. 490, 1975.

[138] H. Negishi, K. Yamaji, N. Sakai, T. Horita, H. Yanagishita, and H. Yokokawa, "Electrophoretic deposition of YSZ powders for solid oxide fuel cells," *Journal of Materials Science*, vol. 39, pp. 833–838, Feb. 2004.

[139] B. Ferrari and R. Moreno, "The conductivity of aqueous Al2O3 slips for electrophoretic deposition," *Materials Letters*, vol. 28, pp. 353–355, Oct. 1996.

[140] B. Ferrari and R. Moreno, "Electrophoretic deposition of aqueous alumina slips," *Journal of the European Ceramic Society*, vol. 17, pp. 549–556, Feb. 1997.

[141] P. M. Biesheuvel and H. Verweij, "Theory of Cast Formation in Electrophoretic Deposition," *Journal of the American Ceramic Society*, vol. 82, no. 6, pp. 1451–1455, 1999.

[142] B. Ferrari, R. Moreno, and J. Cuesta, "A Resesitivity Model for Electrophoretic Deposition," *Key Engineering Materials*, vol. 314, pp. 175–180, July 2006.

[143] M. Zarbov, I. Schuster, and L. Gal-Or, "Methodology for selection of charging agents for electrophoretic deposition of ceramic particles," *Journal of Materials Science*, vol. 39, pp. 813–817, Feb. 2004.

[144] H. G. Krüger, A. Knote, U. Schindler, H. Kern, and A. R. Boccaccini, "Composite ceramic-metal coatings by means of combined electrophoretic deposition and galvanic methods," *Journal of Materials Science*, vol. 39, pp. 839–844, Feb. 2004.

[145] G. Wang, P. Sarkar, and P. S. Nicholson, "Influence of Acidity on the Electrostatic Stability of Alumina Suspensions in Ethanol," *Journal of the American Ceramic Society*, vol. 80, no. 4, pp. 965–972, 1997.

[146] C.-Y. Chen, S.-Y. Chen, and D.-M. Liu, "Electrophoretic deposition forming of porous alumina membranes," *Acta Materialia*, vol. 47, pp. 2717–2726, July 1999.

[147] R. N. Basu, C. A. Randall, and M. J. Mayo, "Fabrication of Dense Zirconia Electrolyte Films for Tubular Solid Oxide Fuel Cells by Electrophoretic Deposition," *Journal of the American Ceramic Society*, vol. 84, pp. 33–40, Jan. 2001.

[148] Y.-C. Wang, I.-C. Leu, and M.-H. Hon, "Kinetics of Electrophoretic Deposition for Nanocrystalline Zinc Oxide Coatings," *Journal of the American Ceramic Society*, vol. 87, pp. 84–88, Jan. 2004.

[149] I. Zhitomirsky and L. Gal-Or, "Electrophoretic deposition of hydroxyapatite," *Journal of Materials Science in Medicine*, vol. 8, pp. 213–219, 1997.

[150] D. M. Kalaskar, C. Poleunis, C. Dupont-Gillain, and S. Demoustier-Champagne, "Elaboration of Nanostructured Biointerfaces with Tunable Degree of Coverage by Protein Nanotubes Using Electrophoretic Deposition," *Biomacromolecules*, vol. 12, pp. 4104–4111, Nov. 2011.

[151] L. Vandeperre, O. Van Der Biest, F. Bouyer, J. Persello, and A. Foissy, "Electrophoretic forming of silicon carbide ceramics," *Journal of the European Ceramic Society*, vol. 17, pp. 373–376, Jan. 1997.

[152] Z. Peng and M. Liu, "Preparation of Dense Platinum-Yttria Stabilized Zirconia and Yttria Stabilized Zirconia Films on Porous La0.9Sr0.1MnO3 (LSM) Substrates," *Journal of the American Ceramic Society*, vol. 84, no. 2, pp. 283–88, 2001.

[153] F. Chen and M. Liu, "Preparation of yttria-stabilized zirconia (YSZ) ®lms on La0.85Sr0.15MnO3 (LSM) and LSM±YSZ substrates using an electrophoretic deposition (EPD) process," *Journal of the European Ceramic Society*, p. 8, 2001.

[154] M. Ammam, "Electrophoretic deposition under modulated electric fields: A review," *RSC Advances*, vol. 2, no. 20, p. 7633, 2012.

[155] A. J. Bard and L. R. Faulkner, *Electrochemical Methods: Fundamentals and Applications*. New York: Wiley, 2nd ed ed., 2001.

[156] B. Neirinck, O. Van der Biest, and J. Vleugels, "A Current Opinion on Electrophoretic Deposition in Pulsed and Alternating Fields," *The Journal of Physical Chemistry B*, vol. 117, pp. 1516–1526, Feb. 2013.

[157] T. Uchikoshi, K. Ozawa, B. D. Hatton, and Y. Sakka, "Dense, bubble-free ceramic deposits from aqueous suspensions by electrophoretic deposition," *Journal of Materials Research*, vol. 16, pp. 321–324, Feb. 2001.

[158] A. S. Dukhin and S. S. Dukhin, "Aperiodic capillary electrophoresis method using an alternating current electric field for separation of macromolecules," *Electrophoresis*, vol. 26, pp. 2149–2153, June 2005.

[159] B. Neirinck, L. Van Mellaert, J. Fransaer, O. Van der Biest, J. Anné, and J. Vleugels, "Electrophoretic deposition of bacterial cells," *Electrochemistry Communications*, vol. 11, pp. 1842–1845, Sept. 2009.

[160] M. Ammam and J. Fransaer, "AC-electrophoretic deposition of glucose oxidase," *Biosensors and Bioelectronics*, vol. 25, pp. 191–197, Sept. 2009.

[161] M. Ammam and J. Fransaer, "Alternating current electrophoretic deposition of Saccharomyces cerevisiae cells and the viability of the deposited biofilm in ethanol production," *Electrochimica Acta*, vol. 55, pp. 3206–3212, Mar. 2010.

[162] M. Ammam and J. Fransaer, "Highly sensitive and selective glutamate microbiosensor based on cast polyurethane/AC-electrophoresis deposited multiwalled carbon nanotubes and then glutamate oxidase/electrosynthesized polypyrrole/Pt electrode," *Biosensors and Bioelectronics*, vol. 25, pp. 1597–1602, Mar. 2010.

[163] B. Neirinck, J. Fransaer, O. V. der Biest, and J. Vleugels, "Aqueous electrophoretic deposition in asymmetric AC electric fields (AC–EPD)," *Electrochemistry Communications*, vol. 11, pp. 57–60, Jan. 2009.

[164] A. Nold and R. Clasen, "Bubble-free electrophoretic shaping from aqueous suspension with micro point-electrode," *Journal of the European Ceramic Society*, vol. 30, pp. 2971–2975, Oct. 2010.

[165] W. Pech-Rodríguez, D. González-Quijano, G. Vargas-Gutiérrez, and F. Rodríguez-Varela, "Electrophoretic deposition of polypyrrole/Vulcan XC-72 corrosion protection coatings on SS-304 bipolar plates by asymmetric alternating current for PEM fuel cells," *International Journal of Hydrogen Energy*, vol. 39, pp. 16740–16749, Oct. 2014.

[166] K. Raju and D. Yoon, "Electrophoretic deposition of BaTiO3 in an aqueous suspension using asymmetric alternating current," *Materials Letters*, vol. 110, pp. 188–190, Nov. 2013.

[167] K. Raju, H.-W. Yu, and D.-H. Yoon, "Aqueous electrophoretic deposition of SiC using asymmetric AC electric fields," *Ceramics International*, vol. 40, pp. 12609–12612, Sept. 2014.

[168] L. Besra, T. Uchikoshi, T. S. Suzuki, and Y. Sakka, "Bubble-Free Aqueous Electrophoretic Deposition (EPD) by Pulse-Potential Application," *Journal of the American Ceramic Society*, vol. 91, pp. 3154–3159, Oct. 2008.

[169] L. Besra, T. Uchikoshi, T. Suzuki, and Y. Sakka, "Application of constant current pulse to suppress bubble incorporation and control deposit morphology during aqueous electrophoretic deposition (EPD)," *Journal of the European Ceramic Society*, vol. 29, pp. 1837–1845, July 2009.

[170] L. Besra, T. Uchikoshi, T. S. Suzuki, and Y. Sakka, "Experimental verification of pH localization mechanism of particle consolidation at the electrode/solution interface and its application to pulsed DC electrophoretic deposition (EPD)," *Journal of the European Ceramic Society*, vol. 30, pp. 1187–1193, Mar. 2010.

[171] M. N. Naim, M. Iijima, H. Kamiya, and I. W. Lenggoro, "Electrophoretic packing structure from aqueous nanoparticle suspension in pulse DC charging," *Colloids and Surfaces A: Physicochemical and Engineering Aspects*, vol. 360, pp. 13–19, May 2010.

[172] A. Chávez-Valdez and A. R. Boccaccini, "Innovations in electrophoretic deposition: Alternating current and pulsed direct current methods," *Electrochimica Acta*, vol. 65, pp. 70–89, Mar. 2012.

[173] T. Engelhardt, P. Reijnen, and L. Hellkuhl, "Physical and chemical processes in electrophoretic enameling," *Mitt. Ver. Dtsch. Emailfachleute*, vol. 38, no. 4, pp. 37–45, 1990.

[174] P. Ducheyne, W. Van Raemdonck, J. Heughebaert, and M. Heughebaert, "Structural analysis of hydroxyapatite coatings on titanium," *Biomaterials*, vol. 7, pp. 97–103, Mar. 1986.

[175] Y. Ramaswamy, C. Wu, and H. Zreiqat, "Orthopedic coating materials: Considerations and applications," *Expert Review of Medical Devices*, vol. 6, no. 4, pp. 423–430, 2009.

[176] W. Suchanek and M. Yoshimura, "Processing and properties of hydroxyapatite-based biomaterials for use as hard tissue replacement implants," *Journal of Materials Research*, vol. 13, pp. 94–117, Jan. 1998.

[177] T. Sridhar, N. Eliaz, U. K. Mudali, and B. Raj, "Electrophoretic Deposition of Hydroxyapatite Coatings and Corrosion Aspects of Metallic Implants," *Corrosion Reviews*, vol. 20, Jan. 2002.

[178] P. Ducheyne, S. Radin, M. Heughebaert, and J. Heughebaert, "Calcium phosphate ceramic coatings on porous titanium: Effect of structure and composition on electrophoretic deposition, vacuum sintering and in vitro dissolution," *Biomaterials*, vol. 11, pp. 244–254, May 1990.

[179] S. Yamaguchi, T. Yabutsuka, M. Hibino, and T. Yao, "Generation of hydroxyapatite patterns by electrophoretic deposition," *Journal of Materials Science: Materials in Medicine*, vol. 19, pp. 1419–1424, Mar. 2008.

[180] C. Wang, J. Ma, W. Cheng, and R. Zhang, "Thick hydroxyapatite coatings by electrophoretic deposition," *Materials Letters*, vol. 57, pp. 99–105, Nov. 2002.

[181] M. Wei, A. J. Ruys, B. K. Milthorpe, C. C. Sorrell, and J. H. Evans, "Electrophoretic Deposition of Hydroxyapatite Coatings on Metal Substrates: A Nanoparticulate Dual-Coating Approach," *Journal of Sol-Gel Science and Technology*, vol. 21, pp. 39–48, 2001.

[182] M. Wei, A. J. Ruys, B. K. Milthorpe, and C. C. Sorrell, "Precipitation of hydroxyapatite nanoparticles: Effects of precipitation method on electrophoretic deposition," *Journal of Materials Science: Materials in Medicine*, vol. 16, pp. 319–324, Apr. 2005.

[183] L. L. Hench, R. J. Splinter, W. C. Allen, and T. K. Greenlee, "Bonding mechanisms at the interface of ceramic prosthetic materials," *Journal of Biomedical Materials Research*, vol. 5, pp. 117–141, Nov. 1971.

[184] L. L. Hench, "Genetic design of bioactive glass," *Journal of the European Ceramic Society*, vol. 29, pp. 1257–1265, Apr. 2009.

[185] D. Krause, B. Thomas, C. Leinenbach, D. Eifler, E. J. Minay, and A. R. Boccaccini, "The electrophoretic deposition of Bioglass® particles on stainless steel and Nitinol substrates," *Surface and Coatings Technology*, vol. 200, pp. 4835–4845, Apr. 2006.

[186] A. R. Boccaccini, E. J. Minay, and D. Krause, "Bioglass Coatings on Superelastic NiTi Wires by Electrophoretic Deposition (EPD)," *Key Engineering Materials*, vol. 314, pp. 216–224, 2006.

[187] F. Pishbin, A. Simchi, M. Ryan, and A. Boccaccini, "A study of the electrophoretic deposition of Bioglass® suspensions using the Taguchi experimental design approach," *Journal of the European Ceramic Society*, vol. 30, pp. 2963–2970, Oct. 2010.

[188] M. I. Espitia-Cabrera, H. D. Orozco-Hernández, M. A. Espinosa-Medina, L. Martínez, and M. E. Contreras-García, "Comparative Study of Corrosion in Physiological Serum of Ceramic Coatings Applied on 316L Stainless Steel Substrate," *Advanced Materials Research*, vol. 68, pp. 152–158, 2009.

[189] T. Casagrande, G. Lawson, H. Li, J. Wei, A. Adronov, and I. Zhitomirsky, "Electrodeposition of composite materials containing functionalized carbon nanotubes," *Materials Chemistry and Physics*, vol. 111, pp. 42–49, Sept. 2008.

[190] F. Gebhardt, S. Seuss, M. Turhan, H. Hornberger, S. Virtanen, and A. Boccaccini, "Characterization of electrophoretic chitosan coatings on stainless steel," *Materials Letters*, vol. 66, pp. 302–304, Jan. 2012.

[191] K. Grandfield, F. Sun, M. FitzPatrick, M. Cheong, and I. Zhitomirsky, "Electrophoretic deposition of polymer-carbon nanotube–hydroxyapatite composites," *Surface and Coatings Technology*, vol. 203, pp. 1481–1487, Feb. 2009.

[192] K. Grandfield and I. Zhitomirsky, "Electrophoretic deposition of composite hydroxyapatite–silica–chitosan coatings," *Materials Characterization*, vol. 59, pp. 61–67, Jan. 2008.

[193] T. Jiang, Z. Zhang, Y. Zhou, Y. Liu, Z. Wang, H. Tong, X. Shen, and Y. Wang, "Surface Functionalization of Titanium with Chitosan/Gelatin via Electrophoretic Deposition: Characterization and Cell Behavior," *Biomacromolecules*, vol. 11, pp. 1254–1260, May 2010.

[194] R. Ma and I. Zhitomirsky, "Electrophoretic deposition of chitosan–albumin and alginate–albumin films," *Surface Engineering*, vol. 27, pp. 51–56, Feb. 2011.

[195] X. Pang and I. Zhitomirsky, "Electrodeposition of hydroxyapatite–silver–chitosan nanocomposite coatings," *Surface and Coatings Technology*, vol. 202, pp. 3815–3821, May 2008.

[196] X. Pang, T. Casagrande, and I. Zhitomirsky, "Electrophoretic deposition of hydroxyapatite–CaSiO3–chitosan composite coatings," *Journal of Colloid and Interface Science*, vol. 330, pp. 323–329, Feb. 2009.

[197] X. Pang and I. Zhitomirsky, "Electrodeposition of composite hydroxyapatite–chitosan films," *Materials Chemistry and Physics*, vol. 94, pp. 245–251, Dec. 2005.

[198] X. Pang and I. Zhitomirsky, "Electrophoretic deposition of composite hydroxyapatite-chitosan coatings," *Materials Characterization*, vol. 58, pp. 339–348, Apr. 2007.

[199] S. Sharma, V. P. Soni, and J. R. Bellare, "Chitosan reinforced apatite–wollastonite coating by electrophoretic deposition on titanium implants," *Journal of Materials Science: Materials in Medicine*, vol. 20, pp. 1427–1436, July 2009.

[200] S. Sharma, V. P. Soni, and J. R. Bellare, "Electrophoretic deposition of nanobiocomposites for orthopedic applications: Influence of current density and coating duration," *Journal of Materials Science: Materials in Medicine*, vol. 20, pp. 93–100, Dec. 2009.

[201] A. Simchi, F. Pishbin, and A. Boccaccini, "Electrophoretic deposition of chitosan," *Materials Letters*, vol. 63, pp. 2253–2256, Oct. 2009.

[202] F. Sun and I. Zhitomirsky, "Electrodeposition of hyaluronic acid and composite films," *Surface Engineering*, vol. 25, pp. 621–627, Nov. 2009.

[203] F. Pishbin, A. Simchi, M. Ryan, and A. Boccaccini, "Electrophoretic deposition of chitosan/45S5 Bioglass® composite coatings for orthopaedic applications," *Surface and Coatings Technology*, vol. 205, pp. 5260–5268, Sept. 2011.

[204] M. Cheong and I. Zhitomirsky, "Electrodeposition of alginic acid and composite films," *Colloids and Surfaces A: Physicochemical and Engineering Aspects*, vol. 328, pp. 73–78, Oct. 2008.

[205] X.-W. Shi, C.-Y. Tsao, X. Yang, Y. Liu, P. Dykstra, G. W. Rubloff, R. Ghodssi, W. E. Bentley, and G. F. Payne, "Electroaddressing of Cell Populations by Co-Deposition with Calcium Alginate Hydrogels," *Advanced Functional Materials*, vol. 19, pp. 2074–2080, July 2009.

[206] F. Sun and I. Zhitomirsky, "Electrochemical deposition of composite biopolymer films," *Surface Engineering*, vol. 26, pp. 546–551, Oct. 2010.

[207] R. Ma, R. Epand, and I. Zhitomirsky, "Electrodeposition of hyaluronic acid and hyaluronic acid–bovine serum albumin films from aqueous solutions," *Colloids and Surfaces B: Biointerfaces*, vol. 77, pp. 279–285, June 2010.

[208] T. Jiang, Z. Zhang, Y. Zhou, Y. Liu, Z. Wang, H. Tong, X. Shen, and Y. Wang, "Surface Functionalization of Titanium with Chitosan/Gelatin via Electrophoretic Deposition: Characterization and Cell Behavior," *Biomacromolecules*, vol. 11, pp. 1254–1260, May 2010.

[209] A. T. Poortinga, R. Bos, and H. J. Busscher, "Controlled electrophoretic deposition of bacteria to surfaces for the design of biofilms," *Biotechnology and Bioengineering*, vol. 67, no. 1, pp. 117–120, 2000.

[210] M. Younesi, A. Islam, V. Kishore, S. Panit, and O. Akkus, "Fabrication of compositionally and topographically complex robust tissue forms by 3D-electrochemical compaction of collagen," *Biofabrication*, vol. 7, p. 035001, June 2015.

[211] S. Tanaka, R.-I. Hata, and Y. Nagai, "Two-dimensional Electrophoresis Patterns of the CNBr Peptides of Collagen Types I, II, III and V," *Collagen and Related Research*, vol. 1, pp. 445–452, Sept. 1981.

[212] A. A. Marino and R. O. Becker, "The effect of electric current on rat tail tendon collagen in solution," *Calcified Tissue Research*, vol. 4, pp. 330–338, Dec. 1969.

[213] V. A. Webster, E. L. Hawley, O. Akkus, H. J. Chiel, and R. D. Quinn, "Fabrication of Electrocompacted Aligned Collagen Morphs for Cardiomyocyte Powered Living Machines," in *Biomimetic and Biohybrid Systems* (S. P. Wilson, P. F. Verschure, A. Mura, and T. J. Prescott, eds.), vol. 9222, pp. 429–440, Cham: Springer International Publishing, 2015.

[214] V. A. Webster, E. L. Hawley, O. Akkus, H. J. Chiel, and R. D. Quinn, "Effect of actuating cell source on locomotion of organic living machines with electrocompacted collagen skeleton," *Bioinspiration & Biomimetics*, vol. 11, p. 036012, May 2016.

[215] X. Cheng, U. A. Gurkan, C. J. Dehen, M. P. Tate, H. W. Hillhouse, G. J. Simpson, and O. Akkus, "An electrochemical fabrication process for the assembly of anisotropically oriented collagen bundles," *Biomaterials*, vol. 29, pp. 3278–3288, Aug. 2008.

[216] J. A. Uquillas, V. Kishore, and O. Akkus, "Genipin crosslinking elevates the strength of electrochemically aligned collagen to the level of tendons," *Journal of the Mechanical Behavior of Biomedical Materials*, vol. 15, pp. 176–189, Nov. 2012.

[217] J. A. Uquillas and O. Akkus, "Modeling the Electromobility of Type-I Collagen Molecules in the Electrochemical Fabrication of Dense and Aligned Tissue Constructs," *Annals of Biomedical Engineering*, vol. 40, pp. 1641–1653, Aug. 2012.

[218] M. Younesi, A. Islam, V. Kishore, J. M. Anderson, and O. Akkus, "Tenogenic Induction of Human MSCs by Anisotropically Aligned Collagen Biotextiles," *Advanced Functional Materials*, vol. 24, pp. 5762–5770, Sept. 2014.

[219] H. R. Baker, E. F. Merschrod S, and K. M. Poduska, "Electrochemically Controlled Growth and Positioning of Suspended Collagen Membranes," *Langmuir*, vol. 24, pp. 2970–2972, Apr. 2008.

[220] S. D. Huelin, H. R. Baker, K. M. Poduska, and E. F. Merschrod S, "Aggregation and Adsorption of Type I Collagen near an Electrified Interface," *Macromolecules*, vol. 40, pp. 8440–8444, Nov. 2007.

[221] A. Islam, S. Cotey, M. Younesi, and O. Akkus, "Tuning of Stiffness Anisotropy in Collagen Sheets by Planar Stretch," *Society for Biomaterials*, no. 87, p. 1, 2014.

[222] P. Benzoni, P. Ginestra, L. Altomare, A. Fiorentino, L. De Nardo, E. Ceretti, and P. Dell'Era, "Biomanufacturing of a Chitosan/Collagen Scaffold to Drive Adhesion and Alignment of Human Cardiomyocyte Derived from Stem Cells," *Procedia CIRP*, vol. 49, pp. 113–120, 2016.

[223] S. Put, J. Vleugels, and O. Van Der Biest, "Gradient profile prediction in functionally graded materials processed by electrophoretic deposition," *Acta Materialia*, vol. 51, pp. 6303–6317, Dec. 2003.

[224] D. Klemm, B. Heublein, H.-P. Fink, and A. Bohn, "Cellulose: Fascinating Biopolymer and Sustainable Raw Material," *Angewandte Chemie International Edition*, vol. 44, pp. 3358–3393, May 2005.

[225] S. Song, A. K. Singh, T. J. Shepodd, and B. J. Kirby, "Microchip Dialysis of Proteins Using in Situ Photopatterned Nanoporous Polymer Membranes," *Analytical Chemistry*, vol. 76, pp. 2367–2373, Apr. 2004.

[226] J. Goldstein, D. E. Newbury, D. C. Joy, P. Echlin, C. E. Lyman, E. Lifshin, L. Sawyer, and J. R. Michael, *Scanning Electron Microscopy and X-Ray Microanalysis: Third Edition*, vol. 1. Springer US, 2003.

[227] P. Kittiphattanabawon, S. Benjakul, W. Visessanguan, T. Nagai, and M. Tanaka, "Characterisation of acid-soluble collagen from skin and bone of bigeye snapper (Priacanthus tayenus)," *Food Chemistry*, vol. 89, pp. 363–372, Feb. 2005.

[228] S. Takahashi, M. Zhao, and C. Eng, "Isolation and characterization of insoluble collagen of dog hearts," *Protein Expression and Purification*, vol. 2, pp. 304–312, Aug. 1991.

[229] J. Dong, Y. Li, and X. Mo, "The study of a new detergent (octyl-glucopyranoside) for decellularizing porcine pericardium as tissue engineering scaffold," *Journal of Surgical Research*, vol. 183, pp. 56–67, July 2013.

[230] H. Ming and A. Callanan, "Comparison of Methods for Whole-Organ Decellularization in Tissue Engineering of Bioartificial Organs," *Tissue Engineering Part B: Reviews*, vol. 19, pp. 194–208, June 2013.

[231] M. Fauzi, Y. Lokanathan, B. Aminuddin, B. Ruszymah, and S. Chowdhury, "Ovine tendon collagen: Extraction, characterisation and fabrication of thin films for tissue engineering applications," *Materials Science and Engineering: C*, vol. 68, pp. 163–171, Nov. 2016.

[232] S. Quereshi, A. Mhaske, D. Raut, R. Singh, A. Mani, and J. Patel, "Extraction and Partial Characterization of Collagen from Different Animal Skins," *Recent Research in Science and Technology*, vol. 2, no. 9, pp. 28–31, 2010.

[233] L. Martínez, "Measuring the Conductivity of Very Dilute Electrolyte Solutions, Drop by Drop," *Química Nova*, vol. 41, no. 7, pp. 814–817, 2018.

[234] Z. Eslek and A. Tulpar, "Solution Preparation and Conductivity Measurements: An Experiment for Introductory Chemistry," *Journal of Chemical Education*, vol. 90, pp. 1665–1667, Dec. 2013.

[235] F. Nyasulu, K. Stevanov, and R. Barlag, "Exploring Fundamental Concepts in Aqueous Solution Conductivity: A General Chemistry Laboratory Exercise," *Journal of Chemical Education*, vol. 87, pp. 1364–1366, Dec. 2010.

[236] W. Geng, W. J. Likos, and C. H. Benson, "Viscosity of Polymer-Modified Bentonite as a Hydraulic Performance Index," in *Geo-Chicago 2016*, (Chicago, Illinois), pp. 498–507, American Society of Civil Engineers, Aug. 2016.

[237] B. Chu, Q. Ying, and A. Y. Grosberg, "Two-Stage Kinetics of Single-Chain Collapse. Polystyrene in Cyclohexane," *Macromolecules*, vol. 28, pp. 180–189, Jan. 1995.

[238] Y. Otsubo, "Relation between bridging conformation and rheology of suspensions," *Advances in Colloid and Interface Science*, vol. 53, pp. 1–32, Sept. 1994.

[239] S. Lages, P. Lindner, P. Sinha, A. Kiriy, M. Stamm, and K. Huber, "Formation of Ca^{2+}-Induced Intermediate Necklace Structures of Polyacrylate Chains," *Macromolecules*, vol. 42, pp. 4288–4299, June 2009.

[240] K. Tian, W. J. Likos, and C. H. Benson, "Polymer Elution and Hydraulic Conductivity of Bentonite–Polymer Composite Geosynthetic Clay Liners," *Journal of Geotechnical and Geoenvironmental Engineering*, vol. 145, p. 04019071, Oct. 2019.

[241] D. Levitt and G. A. Pope, "Selection and Screening of Polymers for Enhanced-Oil Recovery," in *SPE Symposium on Improved Oil Recovery*, (Tulsa, Oklahoma, USA), Society of Petroleum Engineers, 2008.

[242] J. Bella, B. Brodsky, and H. M. Bermanl, "Hydration structure of a collagen peptide," *Structure*, vol. 3, no. 9, pp. 893–906, 1995.

[243] A. V. Persikov, J. A. M. Ramshaw, A. Kirkpatrick, and B. Brodsky, "Electrostatic Interactions Involving Lysine Make Major Contributions to Collagen Triple-Helix Stability †," *Biochemistry*, vol. 44, pp. 1414–1422, Feb. 2005.

[244] N. N. Fathima and A. Dhathathreyan, "Effect of surfactants on the thermal, conformational and rheological properties of collagen," *International Journal of Biological Macromolecules*, vol. 45, pp. 274–278, Oct. 2009.

[245] A. B. Mandal, B. U. Nair, and D. Ramaswamy, "Determination of the critical micelle concentration of surfactants and the partition coefficient of an electrochemical probe by using cyclic voltammetry," *Langmuir*, vol. 4, pp. 736–739, May 1988.

[246] J. Krejčí, "Interaction of mixture of anionic surfactants with collagen," *International Journal of Cosmetic Science*, vol. 29, pp. 121–129, Apr. 2007.

[247] J. J. Lim, "Transition temperature and enthalpy change dependence on stabilizing and destabilizing ions in the helix-coil transition in native tendon collagen," *Biopolymers*, vol. 15, pp. 2371–2383, Dec. 1976.

[248] M. D. Shoulders and R. T. Raines, "Collagen Structure and Stability," *Annual Review of Biochemistry*, vol. 78, pp. 929–958, June 2009.

[249] H. K. Kim, Y. H. Kim, Y. J. Kim, H. J. Park, and N. H. Lee, "Effects of ultrasonic treatment on collagen extraction from skins of the sea bass Lateolabrax japonicus," *Fisheries Science*, vol. 78, pp. 485–490, Mar. 2012.

[250] A. Jouyban, S. Soltanpour, and H.-K. Chan, "A simple relationship between dielectric constant of mixed solvents with solvent composition and temperature," *International Journal of Pharmaceutics*, vol. 269, pp. 353–360, Jan. 2004.

[251] Z. Zhang, Y. Huang, and Z. Jiang, "Electrophoretic Deposition Forming of SiC-TZP Composites in a Nonaqueous Sol Media," *Journal of the American Ceramic Society*, vol. 77, pp. 1946–1949, July 1994.

[252] M. González-Cuenca, P. M. Biesheuvel, and H. Verweij, "Modeling constant voltage electrophoretic deposition from a stirred suspension," *AIChE Journal*, vol. 46, pp. 626–631, Mar. 2000.

[253] A. I. Avgustinik, V. S. Vigdergauz, and G. I. Zhuravlev, "Electrophoretic Deposition of Ceramic Masses from Suspensions and Calculation of Deposit Yields," *Journal of Applied Chemistry USSR*, vol. 35, pp. 2090–2093, 1962.

[254] G. Anné, K. Vanmeensel, J. Vleugels, and O. Van der Biest, "Influence of the suspension composition on the electric field and deposition rate during electrophoretic deposition," *Colloids and Surfaces A: Physicochemical and Engineering Aspects*, vol. 245, pp. 35–39, Sept. 2004.

[255] R. Moreno and B. Ferrari, "Effect of the slurry properties on the homogeneity of alumina deposits obtained by aqueous electrophoretic deposition," *Materials Research Bulletin*, vol. 35, pp. 887–897, Apr. 2000.

[256] B. Ferrari and R. Moreno, "Zirconia Thick Films Deposited on Nickel by Aqueous Electrophoretic Deposition," *Journal of The Electrochemical Society*, vol. 147, no. 8, p. 2987, 2000.

[257] D. E. Clark, W. J. Dalzell, and D. C. Folz, "Electrophoretic Alumina Sol-Gel Coatings on Metallic Substrates," in *Ceramic Engineering and Science Proceedings* (J. B. Wachtman, ed.), vol. 9, pp. 1111–1118, Hoboken, NJ, USA: John Wiley & Sons, Inc., Jan. 1988.

[258] J. Y. Choudhary, H. S. Ray, and K. N. Rai, "Electrophoretic deposition of alumina from aqueous suspensions," *Transactions of the British Ceramic Society*, vol. 81, no. 6, pp. 189–190, 1982.

[259] J.-H. Jean, "Electrophoretic deposition of A1203-SiC composite," *Materials Chemistry and Physics*, vol. 40, no. 4, pp. 285–290, 1995.

[260] J. Ma and W. Cheng, "Electrophoretic Deposition of Lead Zirconate Titanate Ceramics," *Journal of the American Ceramic Society*, vol. 85, no. 7, pp. 1735–1737, 2002.

[261] T. R. Palmer, *Investigation of Electrophoretic Deposition as a Fabrication Technique for High Performance Composites*. Master of Science in Mechanical Engineering, Massachusttes Institute of Technology, 2011.

[262] M. Oddy and J. Santiago, "A method for determining electrophoretic and electroosmotic mobilities using AC and DC electric field particle displacements," *Journal of Colloid and Interface Science*, vol. 269, pp. 192–204, Jan. 2004.

[263] S. M. Lindsay, *Introduction to Nanoscience*. Arizona State University: Oxford University Press, first ed., 2009.

[264] K. Asano, Chang-rag Choi, K. Yatsuzuka, and Duch-Chool Lee, "Acceleration and deceleration of a conductive particle within parallel electrodes in viscous fluid," *Annual Report Conference on Electrical Insulation and Dielectric Phenomena*, vol. 2, pp. 184–187, 2002.

[265] T. L. Jenkins and D. Little, "Synthetic scaffolds for musculoskeletal tissue engineering: Cellular responses to fiber parameters," *npj Regenerative Medicine*, vol. 4, p. 15, Dec. 2019.

[266] B. Neirinck, T. Mattheys, A. Braem, J. Fransaer, O. Van der Biest, and J. Vleugels, "Porous Titanium Coatings Obtained by Electrophoretic Deposition (EPD) of Pickering Emulsions and Microwave Sintering," *Advanced Engineering Materials*, vol. 10, pp. 246–249, Mar. 2008.

[267] A. Miller, "Collagen: The organic matrix of bone," *Philosophical Transactions of the Royal Society*, vol. 304, no. 1121, p. 23, 1984.

[268] J. L. Rigueur, S. A. Hasan, S. V. Mahajan, and J. H. Dickerson, "Buckypaper fabrication by liberation of electrophoretically deposited carbon nanotubes," *Carbon*, vol. 48, pp. 4090–4099, Nov. 2010.

[269] M. Navidirad, B. Raissi, R. Riahifar, M. S. Yaghmaee, and A. Kazemzadeh, "Effect of polyethylenimine on electrophoretic deposition of TiO2 nanoparticles in alternating current electric field," *Journal of Materials Science: Materials in Electronics*, vol. 25, pp. 5041–5050, Nov. 2014.

[270] J. Dong, Z. Yao, T. Yang, L. Jiang, and C. Shen, "Control of Superhydrophilic and Superhydrophobic Graphene Interface," *Scientific Reports*, vol. 3, p. 1733, Dec. 2013.

[271] J. K. Park, I.-H. Do, P. Askeland, and L. T. Drzal, "Electrodeposition of exfoliated graphite nanoplatelets onto carbon fibers and properties of their epoxy composites," *Composites Science and Technology*, vol. 68, pp. 1734–1741, June 2008.

[272] B. Z. Jang and A. Zhamu, "Processing of nanographene platelets (NGPs) and NGP nanocomposites: A review," *Journal of Materials Science*, vol. 43, pp. 5092–5101, Aug. 2008.

[273] A. N. Rider, Q. An, E. T. Thostenson, and N. Brack, "Ultrasonicated-ozone modification of exfoliated graphite for stable aqueous graphitic nanoplatelet dispersions," *Nanotechnology*, vol. 25, p. 495607, Dec. 2014.

[274] W. Zhao, M. Fang, F. Wu, H. Wu, L. Wang, and G. Chen, "Preparation of graphene by exfoliation of graphite using wet ball milling," *Journal of Materials Chemistry*, vol. 20, no. 28, p. 5817, 2010.

[275] J. Biswas, J. S. Rottman-Yang, I. Gonzalo-Juan, and J. H. Dickerson, "Freestanding Carbon Nanotube Films Fabricated by Post-Electrophoretic Deposition Electrochemical Separation," *Journal of The Electrochemical Society*, vol. 159, no. 4, pp. K103–K106, 2012.

[276] J. S. Rottman-Yang, J. Biswas, O. O. Abe, K. L. Campbell, I. Gonzalo-Juan, V. H. Pham, T. Gebre, and J. H. Dickerson, "Post-Electrophoretic Deposition Electrochemical Separation (PEPDECS): Optimization of the Fabrication of Freestanding Carbon Nanotube Films," *ECS Journal of Solid State Science and Technology*, vol. 3, no. 11, pp. M71–M75, 2014.

[277] J. Tabellion and R. Clasen, "Electrophoretic deposition from aqueous suspensions for near-shape manufacturing of advanced ceramics and glasses—applications," *Journal of Materials Science*, vol. 39, pp. 803–811, Feb. 2004.

[278] H. Endo, Y. Kado, M. Mitsuishi, and T. Miyashita, "Fabrication of Free-Standing Hybrid Nanosheets Organized with Polymer Langmuir-Blodgett Films and Gold Nanoparticles," *Macromolecules*, vol. 39, pp. 5559–5563, Aug. 2006.

[279] H. Endo, M. Mitsuishi, and T. Miyashita, "Free-standing ultrathin films with universal thickness from nanometer to micrometer by polymer nanosheet assembly," *Journal of Materials Chemistry*, vol. 18, no. 12, p. 1302, 2008.

[280] S. A. Hasan, D. W. Kavich, and J. H. Dickerson, "Sacrificial layer electrophoretic deposition of free-standing multilayered nanoparticle films," *Chemical Communications*, no. 25, p. 3723, 2009.

[281] C. Jiang, S. Markutsya, Y. Pikus, and V. V. Tsukruk, "Freely suspended nanocomposite membranes as highly sensitive sensors," *Nature Materials*, vol. 3, pp. 721–728, Oct. 2004.

[282] S. A. Hasan, J. L. Rigueur, R. R. Harl, A. J. Krejci, I. Gonzalo-Juan, B. R. Rogers, and J. H. Dickerson, "Transferable Graphene Oxide Films with Tunable Microstructures," *ACS Nano*, vol. 4, pp. 7367–7372, Dec. 2010.

[283] K. M. Song and W. H. Hong, "Dehydration of ethanol and isopropanol using tubular type cellulose acetate membrane with ceramic support in pervaporation process," *Journal of Membrane Science*, vol. 123, pp. 27–33, Jan. 1997.

[284] B. Nandi, R. Uppaluri, and M. Purkait, "Effects of dip coating parameters on the morphology and transport properties of cellulose acetate–ceramic composite membranes," *Journal of Membrane Science*, vol. 330, pp. 246–258, Mar. 2009.

[285] T. Osathanon, K. Bespinyowong, M. Arksornnukit, H. Takahashi, and P. Pavasant, "Human osteoblast-like cell spreading and proliferation on Ti-6Al-7Nb surfaces of varying roughness," *Journal of Oral Science*, vol. 53, no. 1, pp. 23–30, 2011.

[286] D. Brunette, "Spreading and orientation of epithelial cells on grooved substrata," *Experimental Cell Research*, vol. 167, pp. 203–217, Nov. 1986.

[287] M. I. Gariboldi, R. Butler, S. M. Best, and R. E. Cameron, "Engineering vasculature: Architectural effects on microcapillary-like structure self-assembly," *PLOS ONE*, vol. 14, p. e0210390, Jan. 2019.

[288] S. Gogolewski, "Bioresorbable polymers in trauma and bone surgery," *Injury*, vol. 31, pp. D28–D32, Dec. 2000.

[289] R. Cameron and A. Kamvari-Moghaddam, "Synthetic bioresorbable polymers," in *Degradation Rate of Bioresorbable Materials*, pp. 43–66, Elsevier, 2008.

[290] L. Hsu, S.-J. Liu, D. W.-C. Chen, C.-D. Tai, Y.-C. Chou, S. W.-N. Ueng, and E.-C. Chan, "Biodegradable drug-eluting nanofiber-enveloped implants for sustained release of high bactericidal concentrations of vancomycin and ceftazidime: In vitro and in vivo studies," *International Journal of Nanomedicine*, p. 4347, Sept. 2014.

[291] N. Davidenko, C. Schuster, D. Bax, N. Raynal, R. Farndale, S. Best, and R. Cameron, "Control of crosslinking for tailoring collagen-based scaffolds stability and mechanics," *Acta Biomaterialia*, vol. 25, pp. 131–142, Oct. 2015.

[292] L. S. Nair and C. T. Laurencin, "Biodegradable polymers as biomaterials," *Progress in Polymer Science*, vol. 32, pp. 762–798, Aug. 2007.

[293] J. J. Van Tassel and C. A. Randall, "Mechanisms of Electrophoretic Deposition," *Key Engineering Materials*, vol. 314, pp. 167–174, July 2006.

[294] M. Farrokhi-Rad, T. Shahrabi, and S. Khanmohammadi, "Electrophoretic deposition of titania nanoparticles: Wet density of deposits during EPD," *Bulletin of Materials Science*, vol. 37, pp. 1039–1046, Aug. 2014.

[295] M. Milani, S. M. Zahraee, and S. M. Mirkazemi, "Influence of Electrophoretic Deposition Parameters on Pore Size Distribution of Doped Nano Alumina Plates," *Ceramics*, vol. 60, no. 4, pp. 299–307, 2016.

[296] J. Ma and W. Cheng, "Deposition and packing study of sub-micron PZT ceramics using electrophoretic deposition," *Materials Letters*, vol. 56, pp. 721–727, Nov. 2002.

[297] C. Ji, W. Lan, and P. Xiao, "Fabrication of Yttria-Stabilized Zirconia Coatings Using Electrophoretic Deposition: Packing Mechanism During Deposition," *Journal of the American Ceramic Society*, vol. 91, pp. 1102–1109, Apr. 2008.

[298] L. Bi, Z. Cao, Y. Hu, Y. Song, L. Yu, B. Yang, J. Mu, Z. Huang, and Y. Han, "Effects of different cross-linking conditions on the properties of genipin-cross-linked chitosan/collagen scaffolds for cartilage tissue engineering," *Journal of Materials Science: Materials in Medicine*, vol. 22, pp. 51–62, Jan. 2011.

[299] D. V. Shepherd, J. H. Shepherd, S. Ghose, S. J. Kew, R. E. Cameron, and S. M. Best, "The process of EDC-NHS cross-linking of reconstituted collagen fibres increases collagen fibrillar order and alignment," *APL Materials*, vol. 3, p. 014902, Jan. 2015.

[300] C. Chaubaroux, F. Perrin-Schmitt, B. Senger, L. Vidal, J.-C. Voegel, P. Schaaf, Y. Haikel, F. Boulmedais, P. Lavalle, and J. Hemmerlé, "Cell Alignment Driven by Mechanically Induced Collagen Fiber Alignment in Collagen/Alginate Coatings," *Tissue Engineering Part C: Methods*, vol. 21, pp. 881–888, Sept. 2015.

[301] T. S. Girton, N. Dubey, and R. T. Tranquillo, *Magnetic-Induced Alignment of Collagen Fibrils in Tissue Equivalents*, vol. 18, pp. 67–74. New Jersey: Humana Press, Sept. 1998.

[302] J. Torbet and M. C. Ronzière, "Magnetic alignment of collagen during self-assembly," *Biochemical Journal*, vol. 219, pp. 1057–1059, May 1984.

[303] J. Torbet, M. Malbouyres, N. Builles, V. Justin, M. Roulet, O. Damour, A. Oldberg, F. Ruggiero, and D. J. Hulmes, "Orthogonal scaffold of magnetically aligned collagen lamellae for corneal stroma reconstruction," *Biomaterials*, vol. 28, pp. 4268–4276, Oct. 2007.

[304] C. Wu, K. Sassa, K. Iwai, and S. Asai, "Unidirectionally oriented hydroxyapatite/collagen composite fabricated by using a high magnetic field," *Materials Letters*, vol. 61, pp. 1567–1571, Mar. 2007.

[305] E. Verdu, R. O. Labrador, F. J. Rodrıguez, D. Ceballos, J. Fores, and X. Navarro, "Alignment of collagen and laminin-containing gels improve nerve regeneration within silicone tubes," *Restorative Neurology and Neuroscience*, vol. 20, pp. 169–180, 2002.

[306] D. L. Worcester, "Structural origins of diamagnetic anisotropy in proteins.," *Proceedings of the National Academy of Sciences*, vol. 75, pp. 5475–5477, Nov. 1978.

[307] C. Guo and L. J. Kaufman, "Flow and magnetic field induced collagen alignment," *Biomaterials*, vol. 28, pp. 1105–1114, Feb. 2007.

[308] T. K. Jain, M. K. Reddy, M. A. Morales, D. L. Leslie-Pelecky, and V. Labhasetwar, "Biodistribution, Clearance, and Biocompatibility of Iron Oxide Magnetic Nanoparticles in Rats," *Molecular Pharmaceutics*, vol. 5, pp. 316–327, Apr. 2008.

[309] A. J. J. Goffin, J. Rajadas, and G. G. Fuller, "Interfacial Flow Processing of Collagen," *Langmuir*, vol. 26, pp. 3514–3521, Mar. 2010.

[310] D. P. Pope and A. Keller, "A study of the chain extending effect of elongational flow in polymer solutions," *Colloid and Polymer Science*, vol. 256, pp. 751–756, Aug. 1978.

[311] M. Wolman and F. H. Kasten, "Polarized light microscopy in the study of the molecular structure of collagen and reticulin," *Histochemistry*, vol. 85, no. 1, pp. 41–49, 1986.

[312] P. Hlubina and D. Ciprian, "Birefringence dispersion in a quartz crystal retrieved from a channelled spectrum resolved by a fibre-optic spectrometer," *Optics communications.*, vol. 284, no. 12, p. 12, 2011.

[313] J. Klespitz and L. Kovacs, "Peristaltic pumps - A review on working and control possibilities," in *2014 IEEE 12th International Symposium on Applied Machine Intelligence and Informatics (SAMI)*, (Herl'any, Slovakia), pp. 191–194, IEEE, Jan. 2014.

[314] Z. Wu, J. F. Antaki, G. Burgreen, K. Butler, D. Thomas, and B. Griffith, "Fluid Dynamic Characterization of Operating Conditions for Continuous Flow Blood Pumps," *ASAIO Journal*, pp. 442–449, 1999.

[315] M. Noroozi, J. Moghani, J. Mili Monfared, and H. Givi, "An improved direct torque control of brushless DC motors using twelve voltage space vectors," in *2012 3rd Power Electronics and Drive Systems Technology (PEDSTC)*, (Tehran, Iran), pp. 133–138, IEEE, Feb. 2012.

[316] H.-S. Yan and Y.-C. Wu, "A Novel Design of a Brushless DC Motor Integrated With an Embedded Planetary Gear Train," *International Design Engineering*, p. 8, 2005.

[317] E. Camponeschi, B. Florkowski, R. Vance, G. Garrett, H. Garmestani, and R. Tannenbaum, "Uniform Directional Alignment of Single-Walled Carbon Nanotubes in Viscous Polymer Flow," *Langmuir*, vol. 22, pp. 1858–1862, Feb. 2006.

[318] C.-C. Huang, R. G. Winkler, G. Sutmann, and G. Gompper, "Semidilute Polymer Solutions at Equilibrium and under Shear Flow," *Macromolecules*, vol. 43, pp. 10107–10116, Dec. 2010.

[319] J. Xie, M. R. MacEwan, W. Liu, N. Jesuraj, X. Li, D. Hunter, and Y. Xia, "Nerve Guidance Conduits Based on Double-Layered Scaffolds of Electrospun Nanofibers for Repairing the Peripheral Nervous System," *ACS Applied Materials & Interfaces*, vol. 6, pp. 9472–9480, June 2014.

[320] D. E. Smith, "Single-Polymer Dynamics in Steady Shear Flow," *Science*, vol. 283, pp. 1724–1727, Mar. 1999.

[321] R. E. Teixeira, H. P. Babcock, E. S. G. Shaqfeh, and S. Chu, "Shear Thinning and Tumbling Dynamics of Single Polymers in the Flow-Gradient Plane," *Macromolecules*, vol. 38, pp. 581–592, Jan. 2005.

[322] S. Koenen, R. Streubel, J. Jakobi, K. Schwabe, J. K. Krauss, and S. Barcikowski, "Continuous Electrophoretic Deposition and Electrophoretic Mobility of Ligand-Free, Metal Nanoparticles in Liquid Flow," *Journal of The Electrochemical Society*, vol. 162, no. 4, pp. D174–D179, 2015.

[323] A. D. Dillon, L. Le Quoc, M. Goktas, B. Opasanont, S. Dastidar, S. Mengel, J. B. Baxter, and A. T. Fafarman, "Thin films of copper indium selenide fabricated with high atom economy by electrophoretic deposition of nanocrystals under flow," *Chemical Engineering Science*, vol. 154, pp. 128–135, Nov. 2016.

[324] P. Boutouyrie, C. Bussy, P. Lacolley, X. Girerd, B. Laloux, and S. Laurent, "Association Between Local Pulse Pressure, Mean Blood Pressure, and Large-Artery Remodeling," *Circulation*, vol. 100, pp. 1387–1393, Sept. 1999.

[325] K. Aviss, J. Gough, and S. Downes, "Aligned electrospun polymer fibres for skeletal muscle regeneration," *European Cells and Materials*, vol. 19, pp. 193–204, May 2010.

[326] R. D. Cardwell, L. A. Dahlgren, and A. S. Goldstein, "Electrospun fibre diameter, not alignment, affects mesenchymal stem cell differentiation into the tendon/ligament lineage: Ligament differentiation of C3H10T1/2 cells is enhanced on larger fibres," *Journal of Tissue Engineering and Regenerative Medicine*, vol. 8, pp. 937–945, Dec. 2014.

[327] L. Cai, L. Zhang, J. Dong, and S. Wang, "Photocured Biodegradable Polymer Substrates of Varying Stiffness and Microgroove Dimensions for Promoting Nerve Cell Guidance and Differentiation," *Langmuir*, vol. 28, pp. 12557–12568, Aug. 2012.

[328] P. M. Jenkins, M. R. Laughter, D. J. Lee, Y. M. Lee, C. R. Freed, and D. Park, "A nerve guidance conduit with topographical and biochemical cues: Potential application using human neural stem cells," *Nanoscale Research Letters*, vol. 10, p. 264, Dec. 2015.

[329] V. Chiono and C. Tonda-Turo, "Trends in the design of nerve guidance channels in peripheral nerve tissue engineering," *Progress in Neurobiology*, vol. 131, pp. 87–104, Aug. 2015.

Appendix A

Python Code for Pulsed-Current EPD Model

```
#!/usr/bin/env python3
# -*- coding: utf-8 -*-
"""
Author: Matthew Linley

Description: PC-EPD model
"""
import matplotlib
import numpy as np
import matplotlib.pyplot as plt

#%% Initialise the variables

voltage = 10        # The deposition voltage (V)

initial_concentration_wtp = 0.25        # The initial concentration
                                    of collagen in suspension, as
```

```
                                    weight percent of suspension
                                    volume
initial_concentration = initial_concentration_wtp * 1e-2        #
                                    Converet percentage into a unit
                                    interval for collagen
                                    concentration

suspension_volume = 4        # Volume (mL) of collagen suspension in
                                     the EPD cell

initial_mass =  initial_concentration * suspension_volume       #
                                    The initial mass (M0) (g) is
                                    calculated from suspension
                                    concentration and volume, M0 = C0
                                    * V

cell_width = 0.8         # The distance between the electrodes, in
                                    cm

deposition_area = suspension_volume / cell_width         # The
                                    deposition area (S) (cm^2) is
                                    calculated (volume / length = area
                                    )

electric_field = voltage / cell_width        # The electric field (E
                                    ) (V/cm) is calculated

duty_cycle_percent = 40                      # The duty cycle (delta
                                    ) as a percent for pulsed current
                                    EPD
duty_cycle = duty_cycle_percent * 1e-2       # Convert duty cycle
                                    percentage into a unit interval
```

```
pulse_period = 0.05          # The pulse period (lambda) (s) for
                                pulsed current EPD

zeta_potential = 38      # Zeta potential (zeta) (mV) of the
                                suspension at pH 3

viscosity_cP = 0.89      # Viscosity of the suspension media, in
                                centipose (cP)
viscosity = viscosity_cP * 1e-3      # Viscosity (eta) converted to
                                Pa.s for the model

initial_resistivity = 3628.752078        # The initial resistivity (
                                rho 0) (Ohm.m) of the suspension
resistivity_inf = 2813.99335         # The final resistvity (rho inf
                                ) (Ohm.m) of the suspension


################################################
###############      MODEL      ###############
################################################

# calculate the dielectric permittivity of the suspension media
aceticacid_molarity = 0.05       # The acetic acid strength used to
                                hydrate the collagen

volume_percent_ethanol = 50      # The volume percentage of ethanol
                                in the suspension
volume_fraction_ethanol = volume_percent_ethanol / 100
                                                # Convert
                                percentage into a unit interval
                                for ethanol
```

```
aceticacid_molecularweight = 60.05          # Define the molecular
                                    weight of acetic acid
aceticacid_density = 1.049                  # Define the density of
                                     acetic acid

volume_percent_aceticacid_insolution = (aceticacid_molarity *
                                    aceticacid_molecularweight) / (10
                                    * aceticacid_density)
                                    # Calculate the percent acetic
                                    acid in solution from the molarity
                                     in the acetic acid solution
volume_fraction_aceticacid_insolution =
                                    volume_percent_aceticacid_insolution
                                     * 1e-2      # Convert percentage
                                    into a unit interval for acetic
                                    acid solution
volume_fraction_aceticacidsolution = 1 - volume_fraction_ethanol
                                       # Determine acetic acid
                                    solution volume fraction in the
                                    media; the remainder of the
                                    suspension media
volume_fraction_aceticacid = volume_fraction_aceticacidsolution *
                                    volume_fraction_aceticacid_insolution
                                         # Calculate the volume
                                    fraction of acetic acid in
                                    suspension media by multiplying
                                    the fraction of acetic acid
                                    solution by the fraction of acetic
                                     acid in the solution
volume_fraction_water = volume_fraction_aceticacidsolution -
                                    volume_fraction_aceticacid
```

```
                                    # Calculate the volume
                                    fraction of water in the
                                    suspension media; the remaining
                                    liquid in the acetic acid solution
                                     (that is not acetic acid) is
                                    water.


temperature_celcius = 21           # Define the temperature, in
                                    Celcius, within the EPD cell -
                                    room temperature
temperature_kelvin = temperature_celcius + 273      # Convert
                                    Celcius to Kelvin

permittivity_water = 80.1             # The dielectric permittivity
                                    of water
permittivity_aceticacid = 6.15        # The dielectric permittivity
                                    of acetic acid
permittivity_ethanol = 24.5           # The dielectric permittivity
                                    of ethanol

def Sigma(v1,v2,j):                                  # Define a
                                    function to call for the first
                                    sigma notation; v1 = volume
                                    fraction 1, v2 = volume fraction 2
                                    , j = iterations
sigmasum = 0                                         # Initialise
                                    the sumation to be returned
for i in range(j):                                   # Define the
                                    number of iterations, j
sigma = ((v1 - v2)**i) / temperature_kelvin     # The calculation
                                    per iteration
```

```
    sigmasum += sigma                                   # Add each
                                    iteration result to the sum to be
                                    returned
    return sigmasum                                     # Return the
                                    result from the sigma 'sum of'
                                    function


    def SigmaB(V1,V2,V3,j):                                      #
                                    Define a function to call for the
                                    second sigma notation; v1 = volume
                                     fraction 1, v2 = volume fraction
                                    2, v3 = volume fraction 3, j =
                                    iterations
    sigmabsum = 0                                       #
                                    Initialise the sumation to be
                                    returned
    for i in range(j):                                  # Define
                                    the number of iterations, j
    sigmab = ((V1 - V2 - V3)**i) / temperature_kelvin    # The
                                    calculation per iteration
    sigmabsum += sigmab                                 # Add each
                                    iteration result to the sum to be
                                    returned
    return sigmabsum                                    # Return
                                    the result from the sigma 'sum of'
                                     function


    j = 2       # Define the number of iterations for each sigma
                                    function


    # The equation to solve permittivity of a mixture:
```

```
log_permittivity_media = (volume_fraction_water * np.log(
                                permittivity_water)) + (
                                volume_fraction_ethanol * np.log(
                                permittivity_ethanol)) + (
                                volume_fraction_aceticacid * np.
                                log(permittivity_aceticacid))\
+ (volume_fraction_water * volume_fraction_ethanol * Sigma(
                                volume_fraction_water,
                                volume_fraction_ethanol, j))\
+ (volume_fraction_water * volume_fraction_aceticacid * Sigma(
                                volume_fraction_water,
                                volume_fraction_aceticacid, j))\
+ (volume_fraction_ethanol * volume_fraction_aceticacid * Sigma(
                                volume_fraction_ethanol,
                                volume_fraction_aceticacid, j))\
+ (volume_fraction_water * volume_fraction_ethanol *
                                volume_fraction_aceticacid *
                                SigmaB(volume_fraction_water,
                                volume_fraction_ethanol,
                                volume_fraction_aceticacid, j))
# Remove the natural log from the previous equation:
permittivity_media = np.e**(log_permittivity_media)

permittivity_vacuum = 8.854e-12

#%% Generate the electrophoretic mobility (mu) with the calculated
                                variables
electrophoretic_mobility = ((permittivity_media *
                                permittivity_vacuum *
                                zeta_potential) / (viscosity))  #
                                Calculate the electrophoretic
                                mobility of collagen in suspension
```

```
#%% Calculate the pulse factor (kappa)
electrophoretic_velocity = electrophoretic_mobility *
                                    electric_field        # Calculate
                                    the electrophoretic velocity of
                                    collagen in suspension

boltzmann_constant = 1.38e-23

diffusivity = electrophoretic_mobility * temperature_kelvin *
                                    boltzmann_constant

pulse_factor = ((electrophoretic_velocity * duty_cycle *
                                    pulse_period) - np.sqrt(2 *
                                    diffusivity * (1 - duty_cycle) *
                                    pulse_period)) / (
                                    electrophoretic_velocity *
                                    pulse_period)


#%%## Define the characteristic time scale (tau) ###

char_time_scale = suspension_volume / (electrophoretic_mobility *
                                    deposition_area * electric_field *
                                     pulse_factor)


#%%## Calculate model for electrophoretic deposition with all
                                    variables defined ###

# Initialise the variables
```

```
deposited_mass = 0.0              # m = deposited mass [g]
deposition_time = 0.0             # t = deposition time [s]

# Initialise lists to hold values as the model runs
deposited_mass_list = []
deposition_time_list = []

# Run the model for deposited mass over time
while deposited_mass < initial_mass * 0.99:
deposited_mass = initial_mass * (1 - (1 / (1 + ((
                                  initial_resistivity /
                                  resistivity_inf) * (np.e**(
                                  deposition_time / char_time_scale)
                                   -1)))))
deposited_mass_list.append(deposited_mass)
deposition_time_list.append(deposition_time)
deposition_time += 60
deposited_mass_array = np.array(deposited_mass_list)
deposition_time_array = np.array(deposition_time_list)


np.savetxt("EPDmodel.csv", zip(deposition_time_array,
                                  deposited_mass_array), delimiter="
                                  ,")       # Save the output as a .
                                  csv file for visualisation
                                  elsewhere

### Plot the output from the model
plt.plot(deposition_time_array, deposited_mass_array)
plt.title('EPD Model')
plt.xlabel('Time (s)')
plt.ylabel('Deposited Mass (g)')
```

```
plt.show()
```